Department of Precision and Microsystems Engineering

Topology optimization of compliant transmission systems for response minimization under harmonic base excitations

Derek Labaar

Report no	: 2024.038
Coach	: Dr. ir. S. Koppen
Professor	: Dr. D. Farhadi Machekposhti
Specialisation	: Mechatronic System Design
Type of report	: Master Thesis
Date	: June 27, 2024

Delft University of Technology

Precision and Microsystems Engineering

Challenge the future

Topology optimization of compliant transmission systems for response minimization under harmonic base excitations

by

Derek Labaar

to obtain the degree of Master of Science
at the Delft University of Technology,
to be defended publicly on June 27, 2024 at 11:00 AM.

Student number:	4460790	
Project duration:	January 13, 2023 – June 27, 2024	
Thesis committee:	Prof. Dr. ir. M. Langelaar,	TU Delft, chair
	Dr. D. Farhadi Machekposhti,	TU Delft, daily supervisor
	Dr. ir. S. Koppen,	TU Delft, daily supervisor

Abstract

High-precision systems often comprise many individual systems, each operating at its own frequency. However, the vibrations from one system can be transmitted to another, which yields a response. In high-tech applications where precision is crucial, such as compliant transmission systems, these responses are undesired as they result in a loss in precision. Topology optimization can be employed to directly include these unwanted vibrations in the design process of compliant mechanisms. However, the current literature only concerns simple beam structures and suffers from issues such as premature convergence and large intermediate-density areas. This thesis aims to employ topology optimization to design compliant transmission systems whilst simultaneously attenuating the effects of unwanted external vibrations in the form of base excitations. This is done by using an objective function capable of minimizing the displacement response of a structure whilst not suffering from the aforementioned issues. The found objective function relies on the principle of global minimization, which minimizes the largest displacements inside the structure resulting from the applied excitation. An extension of the current research is done by only minimizing a subset of the domain, obtaining a localized minimization whilst other areas of the domain are allowed to exhibit larger responses. These two minimization principles are then applied to the design of a compliant inverter mechanism, with local minimization considering two areas of interest: the entire mechanism area and the regions around the input and output of the mechanism. The results show that global minimization is able to obtain discrete results for a large range of frequencies. Local minimization of the mechanism area yields lower displacement responses and, for higher frequencies, resulting topologies with displacement behaviour similar to the principles of vibration absorption and vibration isolation. Decreasing the response area to be minimized only to cover the input and output regions of the mechanism yields inconclusive results in terms of obtaining lower displacement responses compared to local minimization of the mechanism area. A proof of concept for designing a compliant transmission system whilst minimizing the response to harmonic base excitations is established, demonstrating potential benefits for future research in this domain.

Contents

1

Introduction

This report details the work of my Master of Science thesis. The goal of this research is to utilize topology optimization to design compliant transmission systems that simultaneously mitigate the effects of unwanted external vibrations in the form of harmonic base excitations. First, a background is presented to establish the context and define the problem for this thesis. Next, a short overview of the research gaps in the current literature is provided, which results in the motivation and goals of this thesis. Lastly, an outline is given for the remaining part of this thesis.

Background

In this modern age, almost all equipment in high-tech engineering applications requires an increasing amount of precision to manufacture new technologies at an increasingly smaller scale. The mechanisms employed in these high-precision applications are often compliant mechanisms, such as compliant transmission systems, which rely on elastic deformation to achieve motion or force transmission instead of traditional joints and hinges [1]. This property allows them to provide highly accurate and repeatable motion or force transmission, making them well-suited for precision instrumentation. High-precision systems, which are used in, for example, the semiconductor industry or space applications, are often made up of a large number of individual systems. Each of these individual systems operates at their own specified frequency. These systems, however, are also connected to each other, which means that inevitably, the vibrations from one system can be transmitted to another system. These vibrations can lead to a loss in precision, which is why high-speed machinery sometimes suffers efficiency losses due to the need to wait for vibrations to die out [2]. Mitigating or even eliminating the effects of unwanted vibrations is, therefore, a crucial aspect of the design of mechanisms for high-precision environments. Common methods for mitigating vibrations in such environments include vibration isolation, dynamic balancing, and vibration absorption. Designing compliant transmission systems for these environments often involves problems that have several constraints and might also conflict with each other. A design method for compliant mechanisms capable of handling multiple constraints is that of structural optimization. In this thesis, the method of structural optimization, specifically topology optimization, is employed. Topology optimization is the process of determining the optimal placement of material within a given design domain in order to obtain the best performance given a certain objective function. A common objective function is to optimize the structure to obtain maximum stiffness given a certain load.

Research gaps

Whilst the current literature on topology optimization of compliant transmission systems is extensive, the research on topology optimization of structures in dynamic environments often only concerns simple beam structures. An extension to the design of compliant transmission systems in environments which are disturbed by external vibrations is therefore missing. Furthermore, the research that is done also suffers from several issues. The method of eigenfrequency optimization, for example, is computationally costly and does not take into account the excitation source. Furthermore, objective functions that take into account the excitation source often suffer from issues such as premature convergence when the excitation frequency is higher than the first resonance of the initial domain or have resulting topologies that still contain a large number of intermediate densities.

Motivation and goals

Mitigating or even eliminating the effects of external unwanted vibrations is a crucial aspect of the design of mechanisms for high-precision environments and topology optimization is a promising design method of directly incorporating these external vibrations into the design process.

The goals for this thesis will, therefore, be to utilize topology optimization to design compliant transmission systems that simultaneously mitigate the effects of unwanted external vibrations. The presented issues will, however, have to be overcome first, which will require the introduction of an objective function which does not suffer from excitation frequency issues and has a minimized occurrence of intermediate densities in the final result. For simplification, the external vibrations are applied as a harmonic base excitation, and the problem is defined in a two-dimensional setting.

Outline

The remaining part of this thesis will include a more in-depth discussion of the information introduced in this section, and the outline of this thesis is as follows: Chapter 2 will introduce the working principles of compliant mechanisms, their applications, and their common design methods. To include the attenuation principles directly into the design of compliant mechanisms, topology optimization is employed, the working principles of which are introduced in Chapter 3. Chapter 4 outlines the state of the art of topology optimization of both static and dynamically excited systems, which reveals a gap in the current research. This gap is addressed in Chapter 5, where the scope of this thesis is outlined as well. Chapter 6 covers the objective function employed to fill the research gap, after which several case studies are done in Chapter 7. Lastly, chapters 8 and 9 contain the discussion and conclusion, respectively.

2

Compliant Mechanisms

In this modern age, almost all equipment in high-tech engineering applications requires more and more precision to manufacture new technologies at an increasingly smaller scale. State-of-the-art instruments such as motion stages contain a vast number of moving parts, each of which can cause issues to occur during operation, such as backlash, hysteresis, and unwanted vibrations. This is where compliant mechanisms come in, a term popularized by Howell [1], which describes mechanisms that achieve motion or force transmission by utilizing flexible members such as springs or beams that undergo elastic deformation instead of traditional joints or hinges. In this chapter, the state of the art regarding compliant mechanisms in both static and dynamic applications are introduced, together with their common design methods. The work of Howell et al. [1] already provides several example applications, but as there are hundreds if not thousands of works considering the applications of compliant mechanisms, only several examples will be provided.

Due to the lack of joints and hinges, compliant mechanisms offer several advantages over traditional mechanisms. Firstly, these mechanisms can be designed to be more compact with fewer components, resulting in reduced costs in both assembly and maintenance processes. Secondly, the absence of moving parts eliminates sources of friction and wear, eliminating the need for lubrication and improving reliability and lifespan. Moreover, compliant mechanisms can be designed to provide highly accurate and repeatable motion or force transmission, making them exceptionally well-suited for precision instrumentation [1].

An example of a compliant mechanism is given in figure 2.3 [3], where the image on the left provides the schematics of a displacement amplifier considering a 'classical' design. The term 'classical' denotes that the movement of the joints is facilitated by rotational joints, as represented in the diagram by the circular connections. On the right, the compliant equivalent of this mechanism, which is now a monolithic structure, is given. The motion of the structure is then facilitated by the thin, flexible members located at similar points to the classical mechanism. These members are also called flexures, and the deforming ability of these members allows the mechanism to achieve the desired movement.

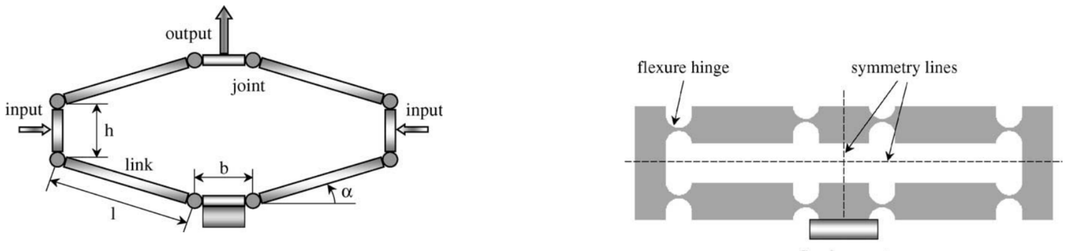

(a) The rigid-body version with rotational joints

(b) The mechanism of figure 2.1a but as a monolithic structure, with flexure hinges instead of rotational joints

Figure 2.1: A mechanism with a fixed support at the bottom, which converts forces or displacements from the input to the output which is in an orthogonal direction [3].

Despite compliant mechanisms offering several advantages over conventional mechanisms, they do, however, also have some disadvantages [1]. In order to provide sufficient motion inside the mechanism, flexure joints are often made as thin as possible. This comes with a drawback, however, of becoming a location of stress concentration, which is not desired as, when a force is applied to the structure, the input energy will be consumed and stored as elastic strain energy, which in turn reduces mechanical efficiency [4].

2.1. Static applications

Compliant mechanisms have found applications in various fields, presenting their versatility and benefits. Examples of these are fields such as adaptable structures, medical applications, tools, transportation components, micro-electro-mechanical systems (MEMS), or robotics [5]. Some notable examples are the applications of compliant mechanisms in soft robotic systems [6], a compliant solar array mechanism that can be packaged using limited space during launch and deployed in space [7], and a six-degree of freedom positioning system capable of micrometer positioning developed by Park and yang [8]. Images of these applications are given in figure 2.2.

(a) A compliant soft robotic gripper [6]

(b) A compliant solar array [7]

(c) A compliant precision positioning system [8]

Figure 2.2: Several examples of static applications of compliant mechanisms found in literature.

2.2. Dynamic applications

The previous examples considered static applications of compliant mechanisms, where the excitation load remains constant in magnitude and does not change over time. Compliant mechanisms have, however, also found applications for problems where a periodic load is applied, where the magnitude remains constant, but the load changes at equal time intervals. Examples of such applications are given in this section.

2.2.1. Dynamic displacement amplification

The displacement amplifier given in figure 2.3 considers an excitation force that is constant, but this load can also be changed to a periodic load. This is exactly what Le Letty et al. [9] did to construct a positioning stage actuated by piezoelectric actuators, an image of which is given in figure 2.3a. Tanksale et al. [10] also considered a compliant mechanism designed to amplify the dynamic input displacement, but used an intermediate mass which was actuated close to or at its natural frequency. This allowed for the use of the vibration absorber effect, which resulted in an amplification of the output displacement. This effect was conventionally used to reduce vibrations in a system [11], but was in this case employed to amplify the input displacement. A schematic of the mechanism designed by Tanksale et al. [10] is given in figure 2.3b.

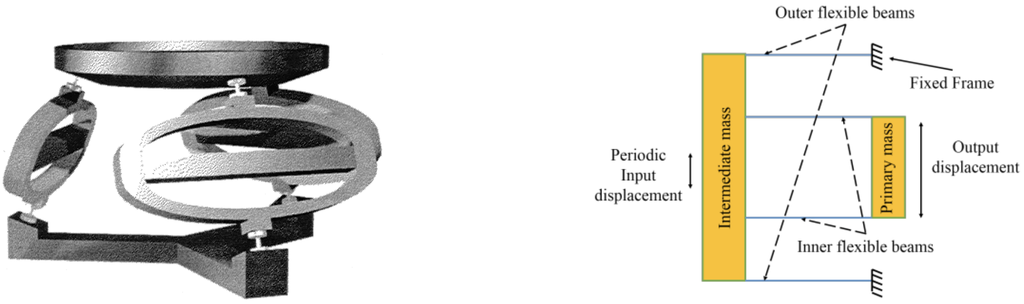

(a) A positioning stage containing three compliant dynamic displacement amplifiers [9]

(b) A compliant dynamic displacement amplifier utilizing an intermediate mass [10]

Figure 2.3: Examples of compliant dynamic displacement amplification found in literature.

2.2.2. Frequency amplification

Besides amplifying input displacements, compliant mechanisms can also be designed to manipulate the relation between input and output frequencies. In Farhadi et al. [12], a compliant transmission mechanism is designed to multiply the frequency of a reciprocating input motion. The obtained design managed to double the input frequency at the output, and the concatenation of this mechanism also provided another doubling in output frequency, yielding a multiplication ratio of four.

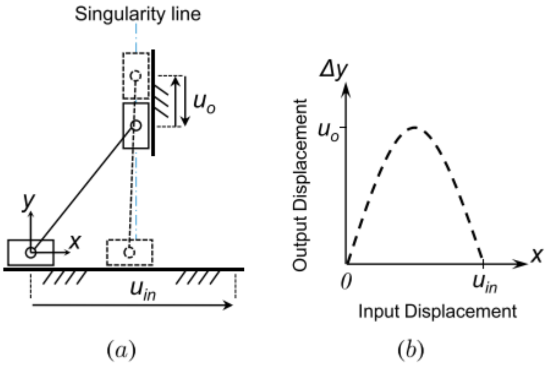

Figure 2.4: A double slider mechanism capable of amplifying the output frequency with respect to the input frequency (a) and the accompanying input-output displacement relationship (b) [12].

The way this mechanism works is by taking advantage of the singularity properties of a double-slider mechanism, an image of which is shown in Figure 2.4. Once the output block reaches its vertical limit, the kinematic chain reaches the boundary of the workspace, the specific configuration of which is called limb singularity [13].

2.2.3. Adjusting eigenfrequencies

The previous sections provided examples of systems that exploited the natural frequencies of the system in order to achieve their desired performance. For a lot of high-performance systems, however, it is actually more important to ensure that the natural frequencies of the system do not coincide or lie too close to the bandwidth at which the system is required to operate. If the natural frequencies of the system align with the operating frequency range, resonance can occur, which could cause the system to fail drastically if the system is not designed for the resulting load intensity.

Designing compliant mechanisms for specific eigenfrequencies or mode shapes can be done during the design process using methods such as the Pseudo Rigid Body Modelling method (PRBM) [14] [15] which will be outlined in section 2.3, or using a Finite Element Analysis (FEA) as a modelling method [16].

Compared to the PRBM method, the FEA method is still the most accurate method, although it does cost more computational effort [17]. FEA is most often used after the mechanism has been developed; however, by utilizing commercially available finite-element software such as ANSYS, the eigenfrequencies of the system can be determined.

2.2.4. Handling disturbances

Chapter 1 mentioned that vibrations produced by one system can be transmitted to another system. Figure 2.5 gives a visualization of this vibration transmission.

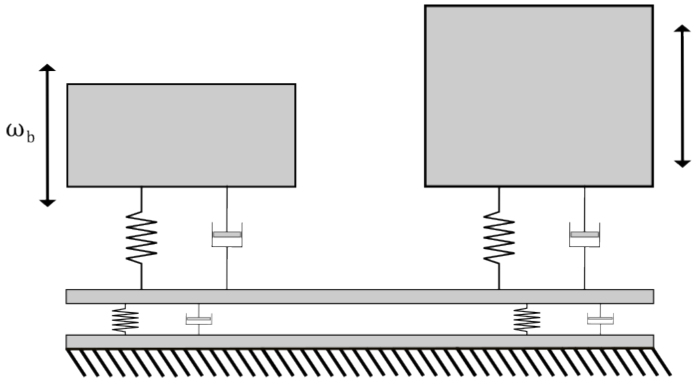

Figure 2.5: An example of how structures in the same system are not rigidly connected but always contain a certain amount of stiffness and damping. This allows for the transmission of vibrations at a frequency ω from one structure to another.

This behaviour can occur when the system is in use or when it is stationary. When the system is in use, a loss in precision will occur. In the worst case, the disturbance frequency matches a resonance of the system, which yields a displacement response that might damage the system. Shifting the resonances of the mechanism, however, does not necessarily minimize the displacement response of the system at a given frequency. The objective of this thesis will, therefore, be to investigate whether a mechanism that transmits forces or displacements can be designed whilst simultaneously optimizing the mechanism against unwanted vibrations in the form of base excitations. Several principles can be applied to mitigate these vibrations, which will be discussed in this section.

Vibration isolation

The principle of vibration isolation can be broadly defined as the process of minimizing the transmission of vibrations from one component to the other. The capability of a system to do this is also often defined as 'transmissibility'. To visualize this, a simple one-degree-of-freedom mass-spring-damper system can be constructed as given in figure 2.6a. This system is excited by a harmonic excitation $y(t)$. The transmissibility is then defined as $\frac{x(t)}{y(t)}$, and its resulting frequency response is given in figure 2.6b.

The initial straight line indicates that all vibrations are transmitted one-to-one to the system. As the frequency approaches a resonance frequency, the transmissibility increases, and these are maximal at the resonance frequency, being only limited by the amount of damping in the system. Next, a sharp decline in transmissibility follows, showing that the transmission of vibrations is minimized for higher frequencies. In order to maximize the effectiveness of the isolation, the resonance frequency of this system is preferred to be as low as possible to minimize the transmissibility over a large frequency range. Given that $\omega_n = \sqrt{\frac{k}{m}}$, this can be achieved by a combination of having a relatively low stiffness k between the mass and the base and a relatively high mass m for the mass itself. The extent to which this resonance frequency can be lowered is often limited for passive vibration isolation systems such as this, but active vibration isolation systems [19], which include actuators which are actuated by a control sequence, can often achieve much better performance. Active vibration isolation is, however, beyond the scope of this thesis.

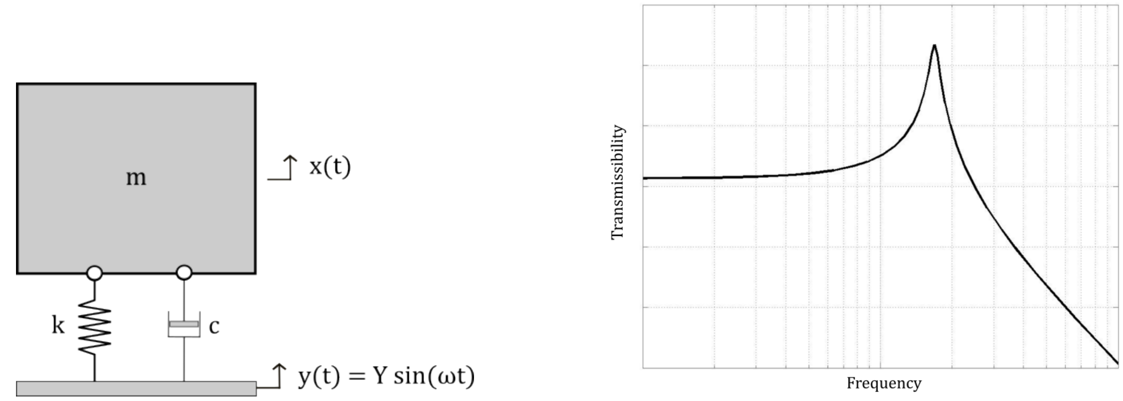

(a) Mass-spring-damper system

(b) Transmissibility plot [18]

Figure 2.6: A mass-spring-damper system and its accompanying transmissibility plot. The decaying response defines the principle of vibration isolation.

Dynamic balancing

Dynamic balancing can be considered the process of designing, or sometimes modifying, a mechanism in such a manner that vibrations caused by an imbalance in rotating components are reduced or eliminated. This imbalance might be created due to the centre of mass of the mechanism not aligning with the axis of rotation, which will result in a centrifugal force that generates vibrations. These unwanted vibrations will then, in turn, affect the accuracy of the system if its application is based on precision.

There are several methods to achieve dynamic balancing in compliant mechanisms. One commonly used approach is the duplicate mechanism principle. This method adds a second mechanism that is identical to the first but rotates in the opposite direction. By connecting these two mechanisms, the shaking forces and moments cancel each other out, resulting in dynamic balancing [20]. An example of this method is shown in figure 2.7, where a double pendulum is dynamically balanced using axial and mirror-symmetric mechanism duplicates. Another method is the principle of the counter mass, where a counter-rotating mass is added to create a counter-inertia effect. This counterbalance helps achieve dynamic balance in the mechanism [21].

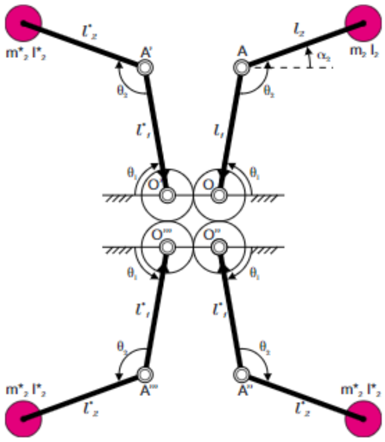

Figure 2.7: A double pendulum system which is dynamically balanced by means of an identical but inverted double pendulum system [20].

Vibration absorption

Whereas dynamic balancing mostly concerns rotating systems, a similar principle to the counter mass method is found for linear motion systems. This principle is known as vibration absorption, which involves an added mass designed to 'absorb' the vibrations of the mass of interest. An example of a vibration absorber is given in figure 2.8a.

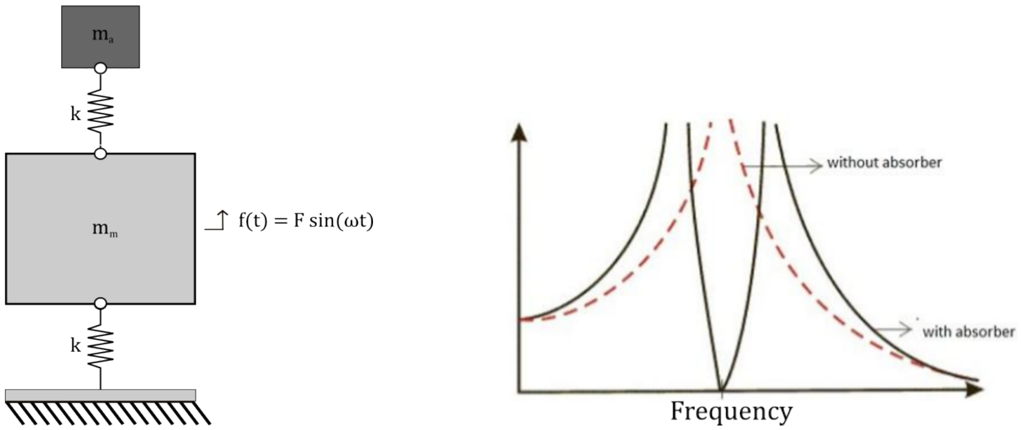

(a) A double mass-spring system containing a main mass of interest and an absorber mass

(b) The frequency response of the system of figure 2.8a with and without the absorber mass [22]

Figure 2.8: An example diagram and frequency response of a vibration absorption system.

In figure 2.8a, the mass of interest is the main mass m_m. This mass contains a resonance which is represented in figure 2.8b by the red dashed line. In order to suppress the vibrations of this mass of interest at this resonance frequency, an absorber mass m_a is added to the system. The mass and stiffness of this absorber are tuned such that the response of the mass of interest produces an anti-resonance at the frequency of interest instead of a resonance. The resulting response is given by the black line in figure 2.8b and shows a zero displacement response at the same resonance frequency. In practical systems, the inclusion of damping will not yield a zero displacement response but will result in minimized displacements.

All of these methods, however, do come with the drawback of adding mass and inertia to the system. This increased mass and inertia will require more power to drive and control the mechanism, as well as increase the material costs [23]. Among these methods, the duplicate mechanism principle generally adds the least mass to the initial system according to Van der Wijk et al. [20]. Van der Wijk et al. [24] attempted to mitigate this drawback by introducing a method of designing a mechanism where all elements contribute to both the motion of the system as well as the dynamic balance. This approach eliminates the need for additional masses or counterbalances and was named the inherently dynamically balanced mechanism method. The common way of designing a dynamically balanced mechanism is to analyze the kinematics of the system first and determine the balancing of the system afterwards. This results in the issue where a part or even the entire design process has to be started anew if the balancing solution is not applicable. In Van der Wijk et al. [24], two methods are derived for the synthesis of inherently dynamically balanced mechanisms. One with the method of linearly independent linear momentum, and one with the method of principal vector linkages.

Considering dynamic balancing compared to vibration isolation, dynamic balancing does have an advantage. According to Weeke et al. [25], the principle of dynamic balancing is considered superior over vibration isolation when considering oscillating systems subjected to environmental disturbances due to being independent of both the frequency and amplitude of the external motion. Vibration isolation, on the other hand, focuses on reducing the transmission of vibrations from one component to another but may not address the inherent unbalance in the system.

2.3. Compliant mechanism design methods

With the applications and advantages of compliant mechanisms presented, the design methods used to construct these mechanisms can be outlined. The process of designing compliant mechanisms can be approached in various ways, depending on the specific goals and requirements of the mechanism. Gallego and Herder [26] summarized the synthesis of compliant mechanisms in three main approaches: the structural optimization approach, the building blocks approach, and the kinematic approach. The structural optimization approach will be discussed further in section 3.

Regarding the other two approaches, the building block approach is a conceptual design procedure that is based on the instant centres [27]. This method concatenates basic building blocks to construct a working mechanism. This does mean, however, that this design becomes quite large relatively fast, as a lot of individual parts are connected together. The kinematic approach can be further divided into the Rigid-Body Replacement method and the Freedom and Constraint (FACT) method. The FACT method is a synthesis method that maps a set of geometric entities in the freedom space into a set of geometric entities in the constraint space to find solutions for the design problem [28]. However, both methods are rarely or never used in the dynamic analysis of compliant mechanisms due to the inability to handle the complexity of dynamics. Therefore, only the Rigid-Body Replacement method will be discussed in this section.

2.3.1. Rigid-Body Replacement method

The Rigid-Body Replacement Method is a procedure that works by, as is evident from the name, constructing a rigid-body mechanism that satisfies the desired functionality and replacing it with its compliant counterpart. This replacement can be done using flexure joints or the Pseudo-Rigid Body Model (PRBM). When considering compliance within compliant mechanisms, there are two types: lumped compliance and distributed compliance. In lumped compliance, the deformation is concentrated in one particular part of the mechanism, and in distributed compliance, the deformation is distributed among a larger part of or even the entire element.

Flexure joints

Lumped compliant flexure joints can be defined as a region in a material that allows for large deflections relative to the other stiffer adjacent regions, normally acquired by geometrical characteristics [26]. Simple flexures consist of notches of various profiles and represent hinges. Figure 2.9a shows an example of different profiles. These notch-type flexure hinges are commonly used for small displacements but can also be designed for large deformations. In distributed compliant flexure joints, the designs can be much more complex, which allows them to behave as other mechanisms such as revolute joints, prismatic joints, or universal joints, as shown in figure 2.9b.

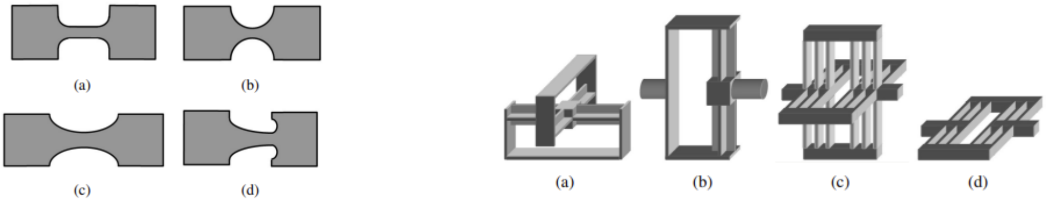

(a) Notch-type flexure hinges: (a) corner fillet, (b) circular, (c) parabolic, (d) hybrid

(b) Complex flexure joints: (a) universal joint, (b) revolute joint, (c) and (d) prismatic joints

Figure 2.9: An overview of flexure joints commonly used in the design of compliant mechanisms [26].

Pseudo-Rigid Body Model (PRBM)

The Pseudo-Rigid-Body Model (PRBM) is a method that emulates the behaviour of a compliant mechanism as a rigid-body mechanism. The kinematics of this rigid-body model can then describe the path of the system, and the force properties can be approximated by a spring, which represents the compliant mechanisms' stiffness. This method provides a quick and easy way to test multiple concepts in the early stages of the design, due to the simpler analysis based on kinematics. While this simplification allows for easier analysis, it does have some disadvantages, such as neglecting local stress concentrations. Furthermore, the accuracy of this method can be limited due to the simplified material behaviour. An example for both lumped compliance and distributed compliance is shown in figure 2.10, where it can be clearly seen that the compliant member is modelled as a combination of a link and a spring.

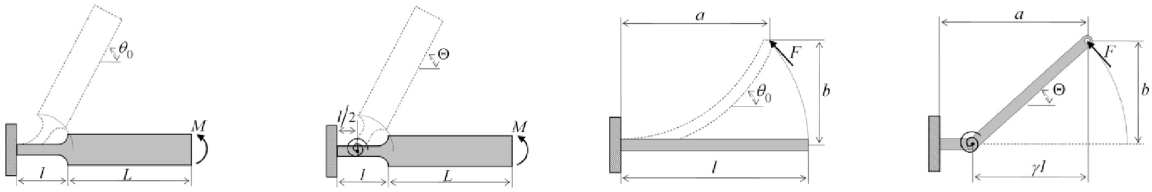

(a) Lumped compliance cantilever (left). PRBM equivalent (right)

(b) Distributed compliance cantilever (left). PRBM equivalent (right)

Figure 2.10: Examples of the Pseudo-Rigid-Body Model (PRBM) equivalents of both lumped and distributed compliant cantilever beams [29].

2.4. Concluding remarks

This chapter presents the properties and applications of compliant mechanisms in static and dynamic environments, together with common design and analysis methods. Compliance mechanisms have a distinct advantage over traditional link and joint systems, especially in precision mechanism applications. Compliant mechanism design is, therefore, highly relevant to this thesis. Despite its advantages, however, their inherent property of being thin and compact allows for local stress concentrations to appear. Using Finite Element Analysis, these issues can be identified and mitigated where necessary. This does, however, add additional steps to the design process.

For the applications in dynamic environments, there seems to be a clear distinction between utilizing and preventing vibrational behaviour. Amplifying the dynamic displacement utilizes resonance behaviour to amplify the output displacement, while vibration isolation attempts to minimize resonance behaviour as much as possible. Frequency amplification, on the other hand, utilizes a specific kinematic relation to achieve its goal. Finally, the dynamic balancing method seems to be more advantageous to vibration isolation.

The PRBM method has been presented as an effective method for designing compliant mechanisms for static applications and for dynamic properties such as eigenfrequencies. This effectiveness comes from the simplification of the material behaviour inside the mechanism. While this greatly reduces computational effort, it is less accurate than finite element methods and will struggle with complex designs that have more intricate layouts or are subjected to more requirements. The mentioned third synthesis method of structural optimization is a technique which is able to overcome these disadvantages for compliant mechanism design, which will be discussed in the following chapter.

3

Topology optimization: formulation

Structures in engineering applications these days are getting more and more complex. There is an increasing demand for performance measures in both static and dynamic environments, on which multiple constraints such as size or weight can be subjected. In the high-tech industry, semiconductors are getting smaller and smaller, thus requiring increased precision of the equipment used to construct them whilst simultaneously increasing in size to increase production efficiency. For these problems with multiple constraints, topology optimization offers a structured method of providing an optimal design.

In the early stages of the design process, the design space and performance requirements of the mechanism are usually known, but coming up with a preliminary design is sometimes difficult. For compliant mechanisms, as explained in section 2.3.1, a kinematic analysis can be done using the PRBM method. This process, however, is often trial and error, which can be time-consuming and increase costs. Also, it may be that some or even several requirements are in conflict with each other. These conflicts might be solvable by a designer, but the problem might be too difficult, for example, when static and complex dynamical requirements start conflicting. Furthermore, assuming these issues do not occur, it might be that a certain constraint is added later in the design process due to a change or overlooked problem. Adding an extra constraint often requires a restart of a large part of or even the entire design process. Topology optimization offers engineers a systematic method to achieve an optimal design for a given problem subjected to constraints in the early stages of the design process. Having this preliminary design can speed up the design process tremendously, increasing efficiency and reducing costs.

In the general sense, topology optimization is the process of determining the optimal distribution of material within a given design space to obtain the maximum desired performance. It was first introduced by Bendsøe and Kickuchi [30] as the homogenization method and was popularized by Bendsøe and Sigmund [31]. Before the introduction of topology optimization, this area of structural optimization was mainly focused on size optimization. Currently, the area of structural optimization can be categorized into three categories: size, shape, and topology optimization. These are visualized in figure 3.1.

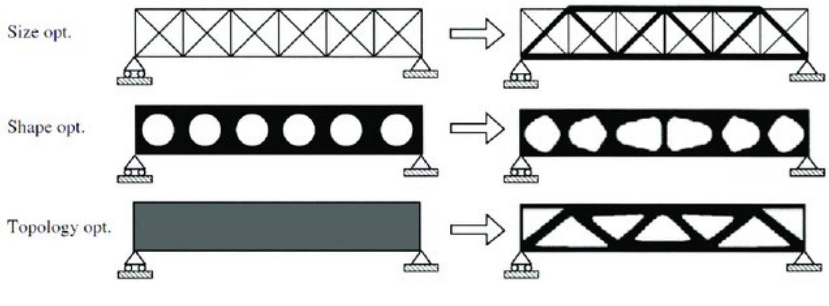

Figure 3.1: The three categories of structural optimization: size optimization, shape optimization and topology optimization for their initial structure (left) and optimized structure (right) [31].

In figure 3.1, size optimization is defined as optimizing the cross-sectional area of the utilized truss members. Shape optimization covers the shape of the holes of the initial structure. These cannot change in number or area, but their shape defines the optimized solution. Shape optimization, therefore, has a fixed topology, but the domain varies. Lastly, there is topology optimization which changes the entire design space to arrive at an optimum topology. In most optimization problems, the structure is not fixed a priori, which means that an optimal topology and shape are often required. Dealing with these constraints during the design process is often challenging, which is where topology optimization comes in.

As for the methods of performing topology optimization, the most prominent design parametrization approaches are density-based topology optimization and level-set-based topology optimization. Density-based topology optimization is a method where the design domain is divided into small cells, and each cell is assigned a density value indicating the material distribution. Level-set-based topology optimization represents structural boundaries using level-set functions, which require careful initialization and manipulation. Considering vibration problems, a recent study done by Keur [32] on minimizing eigenfrequencies of a beam structure suggests that the density-based approach holds the advantage over the level-set approach. While the level-set approach is capable of handling more intricate vibration problems, it requires more time and effort to set up properly. On the other hand, the density-based approach does trade performance, in this case, the capability of achieving lower eigenfrequencies, but offers a reduction in overall time and effort needed to achieve results. On top of that, the density-based approach offers a significant advantage in terms of computational efficiency. Due to these advantages, this thesis will utilize the method of density-based topology optimization.

3.1. Design parametrization

The design parametrization approach of density-based topology optimization method was first introduced by [33], and has gained significant popularity over time. As the name implies, this method revolves around the density of the material and, specifically, the density of each of the individual elements. Figure 3.2 provides a visualization to better understand this method.

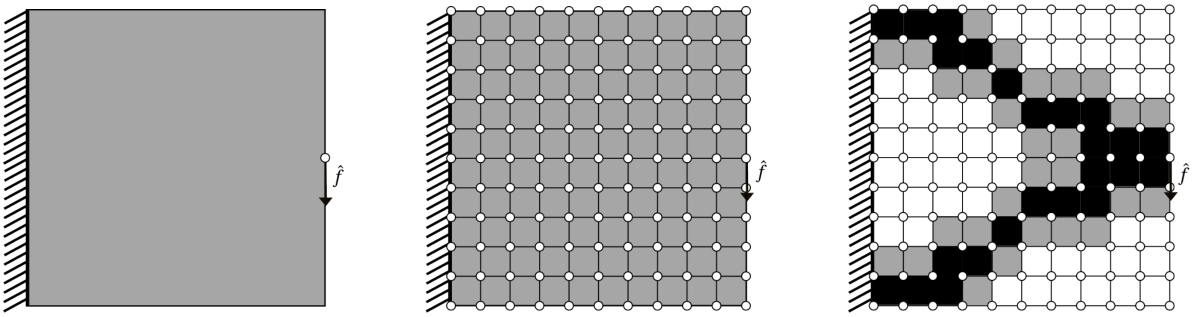

(a) Design domain (b) Finite element grid (c) Final topology

Figure 3.2: Design parametrization using density-based topology optimization. The state of the domain is expressed as a function of the individual element densities within the finite element grid, which allows for the definition of ’solid’ and ’void’ regions.

As an example, an arbitrary design domain is given in figure 3.2a. This domain is constrained at the left boundary and has a force with magnitude $\hat{f}$ applied to it in the middle of the right edge. Next, the domain is discretized into a grid of finite elements as shown in figure 3.2b. Each element can now be given its own density, which can vary between the values 0 and 1, where 0 indicates a void (no material), and 1 represents a fully solid element. The densities between these defined solid and void values however, or the so-called intermediate densities, do not have a direct physical meaning as a material can not have only half density. Therefore, this thesis refers to these pseudo-densities as the design variables x_e. Figure 3.2c shows the resulting topology if the objective is to maximize the stiffness of the structure to support the applied static load. It can be noted that several of these design variables are still at intermediate densities, represented in grey. Preferably, a binary design is obtained, which only contains void or solid elements as these have direct physical meaning, or in other words, an interpretable design is preferably obtained. In the coming sections, however, it will be explained that this is not always obtainable, yet measures can be taken to come close to a binary result.

Furthermore, the white circles visible on the intersections between the elements in figure 3.2b are referred to as nodes. Each node then contains two degrees of freedom, one in the x-direction and one in the y-direction. The displacements of these individual degrees of freedom u_i combined result in the global displacement vector **u**, which describes the displacement of the structure as a whole. Figure 3.3 gives a visualization of these degrees of freedom.

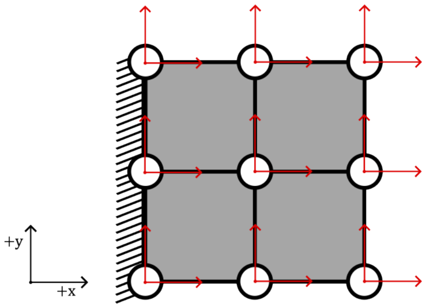

Figure 3.3: An example visualization of the degrees of freedom present for every node in the 2-dimonsional system utilized in this thesis.

3.2. Optimization problem formulation

To solve an optimization problem, the problem must be formulated with an objective function and possibly additional constraints. In engineering and optimization problems, the objective function represents the quantity that needs to be maximized or minimized to achieve the desired optimized result. A typical objective function used commonly in literature for topology optimization of structures subjected to a static force is the objective of minimum compliance. The goal of this objective function is to optimize the topology of a structure to acquire maximum stiffness properties in a specified direction. This higher stiffness will then, in turn, result in smaller displacements of the structure when subjected to the applied static load. This objective function is often used in the minimization sense as the compliance can be seen as the weighted average displacement in the direction of loads [34]. The compliance is a function of the design variables **x** mentioned in section 3.1, and its formulation is given in equation 3.1.

$$\min_{\mathbf{x}} : C(\mathbf{x}) = \mathbf{f}^T \mathbf{u}(\mathbf{x}) \tag{3.1}$$

As can be seen, the force vector **f** is commonly not a function of the design variables. The vector $\mathbf{u}(\mathbf{x})$ represents the displacement vector which contains all displacements of the degrees of freedom of the structure. Another common objective function is that of minimum displacement of a certain single or a set of degrees of freedom u_n. These degrees of freedom are often retrieved from the displacement vector $\mathbf{u}(\mathbf{x})$ by using a selection vector l which is a vector full of zeros and only values of one at the indices of the degrees of freedom of interest. The formulation for this objective function is given in equation 3.2

$$\min_{\mathbf{x}} : u_n(\mathbf{x}) = \mathbf{l}^T \mathbf{u}(\mathbf{x}) \tag{3.2}$$

Note that this objective function is independent of the magnitude of the force that is applied to the structure. The objective function formulation is not limited to single objective functions however, as weighted linear combination functions are often used to combine several functions to obtain a multi-objective optimization [35] [36] [37].

Using only an objective function, however, is not a ’well-defined’ problem definition. Nothing is stopping the optimization from, for example, adding a substantial amount of material to resist deformations or removing all material when the objective is to maximize the displacements. Therefore, there is a need for constraint functions that impose certain limitations on the design problem. The most common constraint that is used in practically all topology optimizations is the volume constraint. This constraint ensures that the design variables, which vary from 0 to 1, do not exceed a certain threshold when added together. In other words, the volume constraint determines the amount of solid material and void space allowed in the design. This is often defined by a volume fraction $\bar{V}$. Furthermore, a minimum value x_{min} is added to ensure that the design variables do not become zero, which will make the system matrices singular. Using the objective of minimum compliance from equation 3.1, a generalized formulation for a topology optimization including these constraints is given in equation 3.3.

$$\begin{aligned} \min_{\mathbf{x}}: \quad & C(\mathbf{x}) = \mathbf{f}^T \mathbf{u}(\mathbf{x}) \\ \text{subject to}: \quad & V(\mathbf{x}) \leq \bar{V} \\ & g(\mathbf{x}) \leq \bar{g(\mathbf{x})} \\ & 0 \leq \mathbf{x}_{\text{min}} \leq \mathbf{x} \leq 1 \\ \\ \text{with } \mathbf{u}(\mathbf{x}) \text{ obtained from}: \quad & \mathbf{K}(\mathbf{x})\mathbf{u}(\mathbf{x}) = \mathbf{f} \end{aligned} \tag{3.3}$$

It can be noted that an extra function $g(\mathbf{x})$ is present in this formulation. This is to represent additional constraints which may come in any form. The mentioned static compliance, for example, can also be implemented as a specific requirement constraint, so as not to exceed a certain value.

3.3. Design regularization

Simply defining a design domain, dividing it into elements and starting the optimization, however, will not necessarily yield properly defined topologies. If the objective is, for instance, to maximize the stiffness of a structure, the optimizer will create regions with alternating solid and void elements, which is also known as 'checkerboarding' due to its checkerboard-like structure [38] [39] [40]. These regions will have artificially high stiffness, which satisfies the goal of the optimizer yet yields designs which would not be feasible to produce. Figure 3.4a shows a topology which exhibits this checkerboarding behaviour.

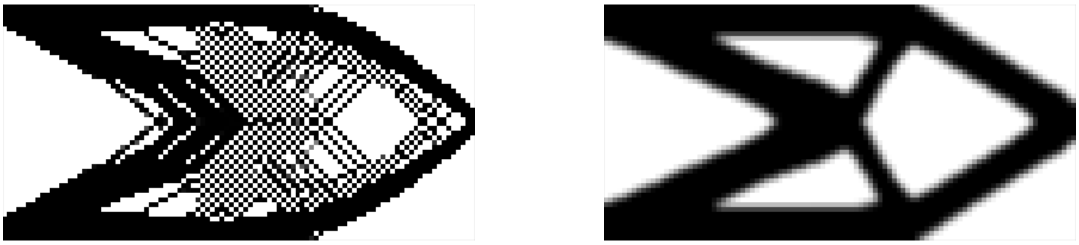

(a) Without density filtering

(b) Including density filtering

Figure 3.4: Topology optimization of a minimum compliance problem with and without density filtering.

In order to remedy this problem, the design variables can be filtered using a density filter. The result of this filter is shown in figure 3.4b, which is the same problem as figure 3.4a but now produces a topology which is feasible to produce. The way the density filter works is similar to the commonly used Gaussian blur used in image processing [41]. The main principle behind this function is to modify the design variables x_e to be a weighted average of the design variables within a certain neighbourhood radius r. This method was first introduced by Bruns and Tortorelli [42] and its formulation is given in equation 3.4. Note that the density filter radius r also defines the minimum member size of the structure.

$$\hat{x}_e = \frac{\sum_{i \in N_e} H_{ei} x_i}{\sum_{i \in N_e} H_{ei}}, \tag{3.4}$$

where H_{ei} is a weight factor given by:

$$H_{ei} = \max(0, r_{\text{min}} - \Delta(e, i)), \tag{3.5}$$

where $\Delta(e, i)$ is the center to center distance from element i to element e and r_{min} the filter radius. From equation 3.5 it is clear that the weighting is linearly decaying. As the elements within the specified radius are further away from element i, the weighting effect becomes smaller. A visualization of this effect for filter radii $r = 2$ and $r = 3$ is given in figure 3.5.

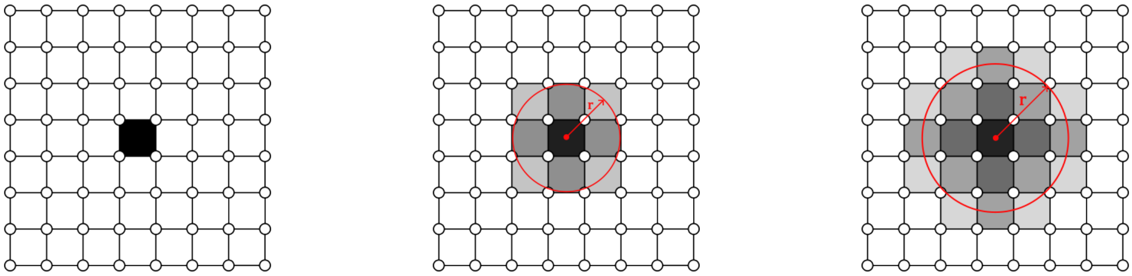

(a) Initial domain (b) Density filtering with $r = 2$ (c) Density filtering with $r = 3$.

Figure 3.5: A visualization of the impact of the density filter radius r on a single element.

From these figures, it is clear that the value of the initial solid design variable gets spread out across the region defined by the filter radius. It can be noted that for both results, the centre element is not fully solid anymore as the total volume fraction in this filter domain is kept similar, and the material is spread out linearly over the filter radius.

The minimum value for the density filter r needed to remedy the checkerboarding behaviour is r=2. In this thesis, it will be desirable to provide the optimizer with as much freedom of design as possible. Therefore, a larger filter radius will not be necessary, as this will also influence the minimum member design which might hinder some interesting intricate design properties. One last important aspect to note is that these obtained 'filtered design variables' are the variables $\hat{x}_e$ for which the optimum is found and are, therefore, also the variables which are plotted to show the obtained topology.

3.4. System matrices

To solve for the objective functions as given in section 3.2, almost every case requires some form of solving for the displacements within the system. To solve for these displacements, the equation of motion can be constructed, of which its most general form is given in equation 3.6. A further explanation of how the second equation is obtained is given in section 4.2.

$$\begin{aligned} \mathbf{K}(\mathbf{x},\omega)\mathbf{u}(\omega) &= \mathbf{f}(\omega) \\ \mathbf{K}(\mathbf{x},\omega) &= \mathbf{K}(\mathbf{x}) + j\omega\mathbf{C}(\mathbf{x}) - \omega^2\mathbf{M}(\mathbf{x}) \end{aligned} \tag{3.6}$$

The matrices $\mathbf{K}(\mathbf{x})$, $\mathbf{C}(\mathbf{x})$ and $\mathbf{M}(\mathbf{x})$ represent the stiffness matrix, damping matrix and mass matrix respectively. For the static case, ω will be equal to zero, and the damping and mass terms will disappear from the equation. Neglecting the damping matrix for now, equation 3.6 reveals that the stiffness and mass matrices are required to solve for the displacements, unless ω=0 where only the stiffness matrix is required. This section will elaborate on the methods used to construct these matrices and how these methods have developed over time.

As stated earlier, the design domain is divided up into a finite element mesh, which conveniently uses identical elements which will have the same material properties such as an element stiffness matrix $\mathbf{K}_e^0$ and element mass matrix $\mathbf{M}_e^0$. What this allows for is to construct the stiffness and mass matrices of the entire design domain as a sum of all the filtered design variables $\hat{x}_e$ from section 3.3 multiplied by the element stiffness matrix and element mass matrix respectively. This formulation is given in equation 3.7.

$$\mathbf{K}(\mathbf{x}) = \sum_{e=1}^{N_E} \hat{x}_e \mathbf{K}_e^0, \qquad \mathbf{M}(\mathbf{x}) = \sum_{e=1}^{N_E} \hat{x}_e \mathbf{M}_e^0, \qquad 0 < \hat{x}_{\min} \leq \hat{x}_e \leq 1, \tag{3.7}$$

The condition $\hat{x}_{\min} \leq \hat{x}_e$ is added to ensure that the design variables do not achieve the value of zero, as this will make the system matrices singular. A typical value of $\hat{x}_{\min}$ is $1e^{-3}$. Using this formulation in topology optimization, however, will yield a large number of design variables, which will remain at a value between 0 and 1, as they are not 'forced' towards a binary 0-1 design. Areas which contain large amounts of these so-called intermediate densities are also known as grey areas. In equation 3.7 the element densities are used in a linear fashion, but they can also be replaced by some arbitrary function $f(\hat{x}_e)$. These functions are called material interpolation functions, and several of them will be discussed in the next section.

3.5. Material interpolation schemes

In order to obtain a binary design which contains only material and void elements, the design variable $\hat{x}_e$ in equation 3.7 can be replaced with some arbitrary function $f(\hat{x}_e)$ which penalizes the design variables in order to force the intermediate densities to either material or void. A generalized version of equation 3.7 is given in equation 3.8.

$$\mathbf{K}(\mathbf{x}) = \sum_{e=1}^{N_E} f(\hat{x}_e)\mathbf{K}_e^0, \qquad \mathbf{M}(\mathbf{x}) = \sum_{e=1}^{N_E} f(\hat{x}_e)\mathbf{M}_e^0, \qquad 0 < \hat{x}_{\text{min}} \leq \hat{x}_e \leq 1, \tag{3.8}$$

Throughout the years, several of these material interpolation functions have been introduced and the most common methods used in topology optimization considering harmonics will be mentioned in the coming subsections. Note that all interpolation functions can be used for either the stiffness interpolation or the mass interpolation and these do not necessarily have to be the same interpolation function.

3.5.1. SIMP method

One of the most popular interpolation methods is the method of Solid Isotropic Material with Penalization (SIMP) method which was introduced by Rozvany et al. [43]. To enforce the binary representation of solid and void, a penalization term p is introduced. This yields the formulation given in equation 3.9, which will be henceforth referred to as 'standard SIMP'.

$$f(\hat{x}_e) = \hat{x}_e^p, \qquad p = 3 \tag{3.9}$$

The most common value for p is also given, which is p=3. If this this function is used for the mass interpolation function, the parameter p is often exchanged for the letter q to create distinction between the two. Without the specification of $\hat{x}_{\text{min}} \leq \hat{x}_e$ however, this method is allowed to reach a value of 0.

3.5.2. Conditional SIMP

As the design variables are penalized and come close to zero, one can note from equation 3.6 that the resulting low stiffness will also yield a resulting high displacement when subjected to the same force excitation magnitude. Pedersen [44] therefore introduced a conditional function for the stiffness interpolation, which limits the design variables once a certain threshold value has been reached. This function is given in equation 3.10.

$$f(\hat{x}_e) = \begin{cases} \hat{x}_e^3 & \text{for } 0.1 \leq \hat{x}_e \leq 1 \\ \hat{x}_e/100 & \text{for } x_{\text{min}} \leq \hat{x}_e \leq 0.1 \end{cases} \tag{3.10}$$

The threshold value for this function is set at 0.1 for this problem, but this value is often chosen by trial and error. This threshold however, also creates a discontinuity at the value of 0.1, which was not found by Pedersen to result in any issues, but other design problems might exist where this discontinuity is not desired. A similar function was adopted by Tcherniak [45] but used for the mass interpolation instead, where the mass of the element was set to zero as the design variable crossed a certain threshold $\hat{x}_{e_{\text{thr}}}$. This function is given in equation 3.11.

$$f(\hat{x}_e) = \begin{cases} \hat{x}_e & \text{for } \hat{x}_e > \hat{x}_{e_{\text{thr}}} \\ 0 & \text{for } \hat{x}_e \leq \hat{x}_{e_{\text{thr}}} \end{cases} \tag{3.11}$$

One last version of the conditional SIMP function which will be introduced is the one from Du and Olhoff [46], who introduced a mass interpolation function based on the version of Tcherniak [45] due to the aforementioned issue of discontinuity present at the threshold value $\hat{x}_{e_{\text{thr}}}$ for the conditional SIMP method. Du and Olhoff, therefore, introduced a function which would provide a continuous interpolation model for these lower values of intermediate densities. This function is given in equation 3.12. Whilst a negligible influence on the final 0-1 design was found for this approach, the discontinuity issue was resolved with this function.

$$f(\hat{x}_e) = \begin{cases} \hat{x}_e & \text{for } \hat{x}_e > 0.1 \\ c_1\hat{x}_e^6 + c_2\hat{x}_e^7 & \text{for } \hat{x}_e \leq 0.1 \end{cases}, \qquad c_1 = 6e^5, \quad c_2 = -5e^6 \tag{3.12}$$

3.5.3. Modified SIMP

In order to address the issue of element density approaching zero in the standard SIMP method, Sigmund [47] proposed a modified version of this method which includes the minimum value $\hat{x}_{\text{min}}$. Including this term ensures that the design variables remain nonzero to avoid a singularity of the system matrix. The formulation is given in equation 3.13.

$$f(\hat{x}_e) = \hat{x}_{\text{min}} + (1 - \hat{x}_{\text{min}})\hat{x}_e^p, \qquad p = 3, \qquad \in [0,1] \tag{3.13}$$

3.5.4. SIMPlin

Another version of SIMP, which is essentially a modification of the modified SIMP version, is the function proposed by Zhu et al. [48], which adds a small linear part to the higher-order SIMP function. For the stiffness interpolation, this ensures that there is still stiffness present as compared to the mass of the same element (given that a linear function is used for the mass interpolation) for very small values of the filtered design variables $\hat{x}_e$. In this thesis, this function is defined as SIMPlin, and the formulation is given in equation 3.14.

$$f(\hat{x}_e) = \hat{x}_{\text{min}} + (1 - \hat{x}_{\text{min}})(0.1\hat{x}_e + 0.9\hat{x}_e^p), \qquad p = 3, \qquad \in [0,1] \tag{3.14}$$

3.5.5. RAMP

The Rational Approximation of Material Properties (RAMP) was introduced by Stolpe and Svanberg [49] as an alternative to the standard SIMP method from equation 3.9. They concluded that the standard SIMP function does not necessarily result in a concave function no matter how large the penalization factor p is chosen. For this reason, a new method was devised, which is given in equation 3.15.

$$f(\hat{x}_e) = \frac{\hat{x}_e}{1 + p(1 - \hat{x}_e)}, \qquad p = 3 \tag{3.15}$$

This function actually contains a non-zero slope for design variables approaching zero. This prevents them from rapidly approaching zero, which could, in turn, lead to numerical instabilities or the same problem mentioned in section 3.5.2.

3.5.6. PIS

One last interpolation scheme which will be introduced is the one presented by Zhu et al. [48], who introduced a Polynomial Interpolation Scheme (PIS). This is a polynomial function which does not rely on a conditional property and, therefore, does not contain any discontinuities. Furthermore, this scheme contains a penalization factor p and an adjustable parameter α which allows for more control over the interpolation model if the penalization factor is increased. In this thesis, the value of α is set at 16, and the resulting function is given in equation 3.16.

$$f(\hat{x}_e) = \frac{\alpha - 1}{\alpha}\hat{x}_e^p + \frac{1}{\alpha}\hat{x}_e \quad = \quad \frac{15}{16}\hat{x}_e^p + \frac{1}{16}\hat{x}_e, \qquad p = 5 \tag{3.16}$$

3.5.7. Comparison of methods

Whilst many more interpolation schemes exist, or can be constructed, the goal of this thesis will not be to provide an in-depth study of the differences between the used material interpolation function and which performs best for the given problem. Furthermore, there is no one ideal material interpolation method which works best for all design problems, and therefore a choice of material interpolation will have to be made. This is especially the case since the final case study proposed in chapter 7 will contain various forms of excitation which not all have been used in combination with all presented functions. This study on which material interpolation function will be used in this thesis is conducted in chapter 6. The performance of each function is measured by its ability to obtain discrete designs for the given design problem. It was found that the combination of PIS (equation B.1) for the stiffness interpolation and Standard SIMP (equation 3.9 are the most appropriate choices for the introduced case study.

3.6. Optimizer

The optimization approach adopted in this thesis is a gradient-based optimization. This means that the rate of change of the objective function is utilized in order to find optima. This works specifically well for topology optimization given that it scales well for many design variables, as often found in topology optimization, and specifically continuous design variables, which are obtained by using the interpolation methods mentioned in the previous section.

Using these gradients, several optimization algorithms exist which can be exploited. The focus of this thesis does, however, not lie in the optimization strategy itself, but more on the optimization problem formulation and, therefore, will make use of the widely adopted Method of Moving Asymptotes (MMA). Introduced by Svanberg [50], the Method of Moving Asymptotes (MMA) is a method which is capable of handling a large number of design variables as well as multiple constraints, making it very suitable for the type of optimization employed in this thesis.

4

Topology optimization: state of the art

With the methodology behind topology optimization outlined, the state of the art of topology optimization applications for both static and dynamic problems can be examined. This chapter will discuss the methodology for statically loaded compliant mechanism design using topology optimization, as well as provide the adaptations needed to solve problems which consider dynamic excitation loads. Furthermore, the types of dynamic excitation problems and their challenges will be outlined as well. By understanding the principles and challenges of topology optimization in both static and dynamic environments, the gaps in the literature, together with the scope of this thesis, can be identified.

4.1. Static applications

Since its introduction, topology optimization has been applied to a wide range of structural design problems. The simplest example, however, is that of the minimization of static compliance. The formulation for this objective was already given in equation 3.3 and the goal is to optimize the topology of a structure in order to acquire maximum stiffness properties in a specified direction by minimizing the static compliance (equation 3.1). This can be done for multiple forms of static excitation loads as shown in figure 4.1.

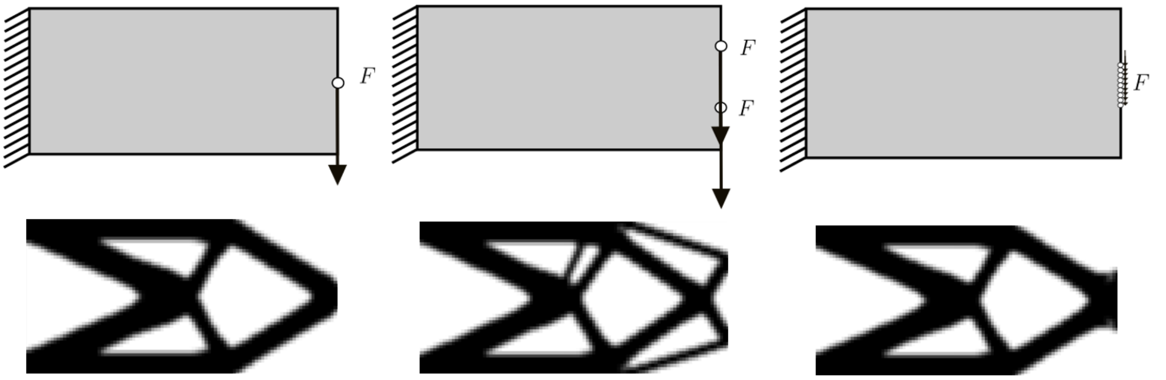

(a) Single force (b) Multiple forces (c) Distributed force

Figure 4.1: Examples of a static compliance minimization under multiple forms of static excitation loads.

These load types show the most basic examples of how topology optimization considering a static load can be used. A real-world application for the distributed force load, for example, is the soft robotics application mentioned in section 2.1. Due to the fragility of the objects, the soft robotic grippers often cannot work with the point loads that are commonly used in topology optimization. A distributed pressure load is therefore required for this optimization problem. Modelling for unknown objects, however, can be challenging [51].

4.1.1. Force-based inverter

The examples of the previous section presented the use of topology optimization for simple clamped beam structures subjected to static loads. In order to construct compliant mechanisms using topology optimization as mentioned in section 2.4, a more complex problem condition needs to be formed. For the final case study in this thesis it will be preferable to have a simple problem which contains all necessary components in terms of load applications and boundary conditions, without much more. The most common example regarding topology optimization of compliant mechanisms which satisfies these criteria is the inverter problem [52] [53] [31].

The inverter problem is characterized by an input excitation, which results in an output motion in the inverse direction. The advantage of this problem specifically is that it contains the most basic requirements for a compliant mechanism, being a fixed boundary, an input excitation point and an output excitation point. These excitations can then be defined in different forms, such as either a displacement or a force. Figure 4.2 gives the design domain for the topology optimization a force-excited inverter mechanism in its most basic form as proposed by Bendsøe and Sigmund [31].

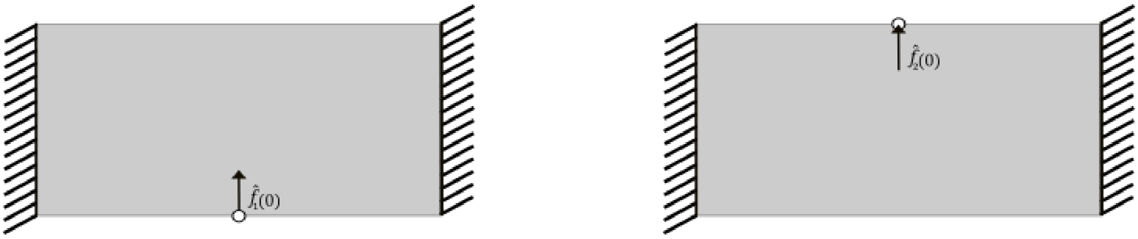

(a) Load case 1

(b) Load case 2

Figure 4.2: The two load cases required for the topology optimization of a force-excited inverter mechanism.

As can be seen from this figure, there are two design domains present, and thus two problems to solve. Each of these individual problems requires a single solve for **Ku**=**f** and contains a description of the boundary conditions, stiffness and loading; they will henceforth be referred to as 'load case' 1 and 2 respectively. Both load cases share the same fixed boundaries, but the first load case only involves the input force, and the second load case only considers the output force. The subscripts 1 and 2 denote the respective load cases 1 and 2. The static excitation force is defined by $\hat{f}_1(0)$, with accompanying displacement u_1. The static output force $\hat{f}_2(0)$ is a pseudo force which represents an equivalent load on the output of the mechanism. The magnitudes of $\hat{f}_1(0)$ and $\hat{f}_2(0)$ are similar for this problem.

Next, the optimization problem can be formulated. In order to obtain an inverter mechanism, the goal is to maximize the output displacement resulting from the input force in the opposite direction as the input displacement. This can also be interpreted as minimizing the negative of the output displacement. Conveniently, the force vector $\mathbf{f}_2$ can be used as a location vector to locate the output displacement in load case 1. Simultaneously, a constraint is placed on both the input and output by means of a limit on static compliance. These compliances are obtained using the forces and accompanying displacements of each individual load case. The optimization formulation is given in equation 4.1, note the subscripts 1 and 2 denoting the load cases 1 and 2.

$$\begin{aligned}
\min_{\mathbf{x}}: &\quad -u_{\text{out}} = -\mathbf{f}_2^T\mathbf{u}_1(\mathbf{x}) \\
\text{subject to}: &\quad \mathbf{f}_1^T\mathbf{u}_1(\mathbf{x}) \leq \bar{C}_1 \\
&\quad \mathbf{f}_2^T\mathbf{u}_2(\mathbf{x}) \leq \bar{C}_2 \\
&\quad V(\mathbf{x}) \leq \bar{V} \\
&\quad 0 \leq \mathbf{x}_{\text{min}} \leq \mathbf{x} \leq 1 \\
\\
\text{with } \mathbf{u}_1(\mathbf{x}) \text{ obtained from}: &\quad \mathbf{K}_1(\mathbf{x})\mathbf{u}_1(\mathbf{x}) = \mathbf{f}_1 \\
\text{and } \mathbf{u}_2(\mathbf{x}) \text{ obtained from}: &\quad \mathbf{K}_2(\mathbf{x})\mathbf{u}_2(\mathbf{x}) = \mathbf{f}_2
\end{aligned} \tag{4.1}$$

Where $\bar{C}_1$ and $\bar{C}_2$ define the maximum allowed static compliance for the input and the output of the mechanism respectively. Using this formulation with the given design domain yields the topology given in figure 4.6. Together with the obtained topology, a visualization done in Paraview of the vertical displacements in the mechanism is given, showing the desired inverting behaviour.

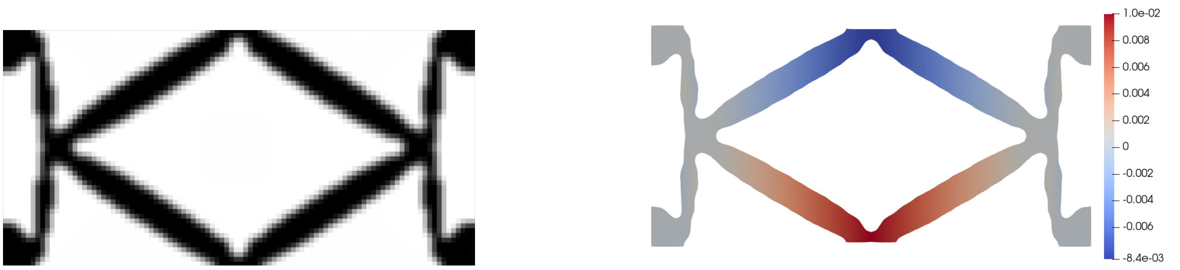

(a) Resulting topology

(b) Static displacements of the mechanism resulting from the applied input force visualized in ParaView

Figure 4.3: The resulting mechanism of the optimization formulation from equation 4.1 and a visualization of its displacements resulting from the applied input load which confirms the working inverting function.

The formulation given in equation 4.1 can also be reversed in order to minimize the sum of the input and output compliances whilst constraining the ratio between the input and output displacements. This does, however, require an additional load case, which is given in figure 4.4.

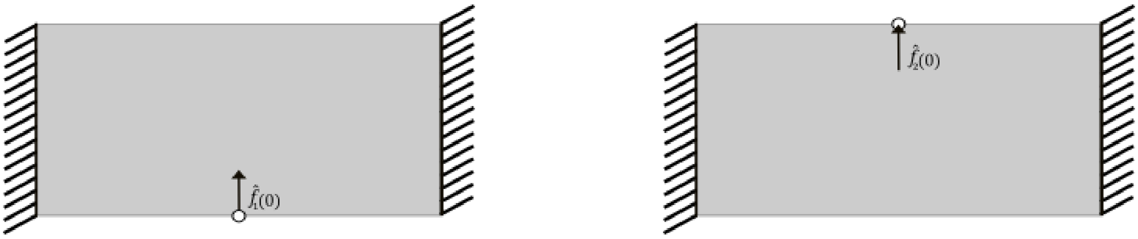

(a) Load case 1

(b) Load case 2

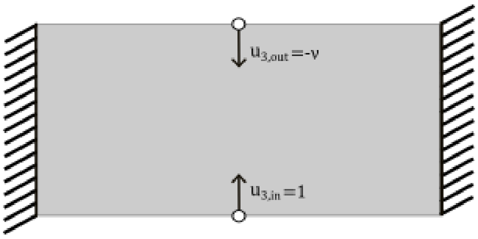

(c) Load case 3

Figure 4.4: The updated load cases required for the topology optimization of a force-excited inverter mechanism which includes a third load case constaining the desired displacement.

This third load case now contains a desired value of the output displacement v. This is typically linked to the input displacement and results in the vector $\boldsymbol{v} = [u_{3,\text{in}},\ u_{3,\text{out}}] = [1,\ \text{-}v]$. As actuating a compliant mechanism with a force will not only yield an output motion but will also store kinetic energy in the structure, the value of v is often set larger than 1. The formulation can then be adapted in order to incorporate this added load case, as given in equation 4.2.

$$\begin{aligned}
\min_{\mathbf{x}}: \quad & C_1 + C_2 = \mathbf{f}_1^T \mathbf{u}_1(\mathbf{x}) + \mathbf{f}_2^T \mathbf{u}_2(\mathbf{x}) \\
\text{subject to}: \quad & C_3 = \boldsymbol{v}^T \mathbf{K} \boldsymbol{v} \leq \bar{C}_v \\
& V(\mathbf{x}) \leq \bar{V} \\
& 0 \leq \mathbf{x}_{\min} \leq \mathbf{x} \leq 1
\end{aligned} \tag{4.2}$$

4.1.2. Displacement-based inverter

As mentioned earlier, this problem can also be defined with a prescribed displacement input as the excitation source. Using a displacement as the excitation source results in the right-hand side of the system equation **Ku**=**f** being set to **0**. To solve for these prescribed displacements, the displacement field needs to be subdivided into free displacements u_f and prescribed displacements u_p [54]. This also yields an accompanying subdivision in the force vector of the applied loads f_f, which are not present in this case, and reaction loads f_p. The resulting system equation from this subdivision is given in equation 4.3.

$$\begin{bmatrix} \mathbf{K}_{ff} & \mathbf{K}_{fp} \\ \mathbf{K}_{pf} & \mathbf{K}_{pp} \end{bmatrix} \begin{bmatrix} \mathbf{u}_f \\ \mathbf{u}_p \end{bmatrix} = \begin{bmatrix} \mathbf{f}_f \\ \mathbf{f}_p \end{bmatrix} = \begin{bmatrix} \mathbf{0} \\ \mathbf{f}_p \end{bmatrix} \tag{4.3}$$

$$\begin{aligned} \mathbf{u}_f &= \mathbf{K}_{ff}^{-1}\left(-\mathbf{K}_{fp}\mathbf{u}_p\right) \\ \mathbf{f}_p &= \mathbf{K}_{pf}\mathbf{u}_f + \mathbf{K}_{pp}\mathbf{u}_p \end{aligned} \tag{4.4}$$

The resulting prescribed displacement vector $\mathbf{u}_p$ can then be filled with the desired excitations, and the resulting free displacement vector $\mathbf{u}_f$ and reaction loads $\mathbf{f}_p$ can be solved for as given by equation 4.4. The design domain for this problem given by Koppen [54] is shown in figure 4.5.

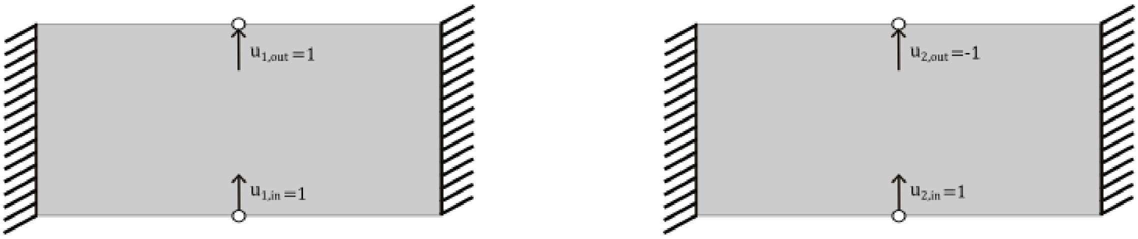

(a) Load case 1

(b) Load case 2

Figure 4.5: The two load cases required for the topology optimization of a displacement-excited inverter mechanism [54].

This design domain now contains a set of prescribed displacements for each load case. In the first load case, both the prescribed displacement on the input and the output are in the same direction, whilst in the second load case, the prescribed displacements are in the desired inverting direction. In order to obtain an inverter with this problem definition, the goal is to achieve a desired limited stiffness between the input and output for the inverted direction (load case 2) whilst simultaneously retaining maximum stiffness between the input, output and ground. This can be achieved by maximizing the compliance values from the first load case, which are calculated with the prescribed displacements and their respective reaction forces, whilst simultaneously limiting the compliance values of the second load case in the desired inverted direction. The formulation for this problem yields an inverter mechanism, and its formulation is given in equation 4.5.

$$\begin{aligned} \max_{\mathbf{x}}: \quad & C_{1,\text{in}} + C_{1,\text{out}} = f_{1,\text{in}} u_{1,\text{in}} + f_{1,\text{out}} u_{1,\text{out}} \\ \text{subject to}: \quad & C_{2,\text{in}} + C_{2,\text{out}} = f_{2,\text{in}} u_{2,\text{in}} + f_{2,\text{out}} u_{2,\text{out}} \leq \bar{C}_2 \\ & V(\mathbf{x}) \leq \bar{V} \\ & 0 \leq \mathbf{x}_{\text{min}} \leq \mathbf{x} \leq 1 \end{aligned} \tag{4.5}$$

$$\begin{aligned} \text{with } f_{1,\text{in}}, f_{1,\text{out}} \text{ obtained from}: \quad & \mathbf{f}_{p,1} = \mathbf{K}_{pf,1}\mathbf{u}_{f,1} + \mathbf{K}_{pp,1}\mathbf{u}_{p,1} \\ \text{and } f_{2,in}, f_{2,\text{out}} \text{ obtained from}: \quad & \mathbf{f}_{p,2} = \mathbf{K}_{pf,2}\mathbf{u}_{f,2} + \mathbf{K}_{pp,2}\mathbf{u}_{p,2} \end{aligned}$$

It can be noted that the previous paragraph mentioned maximizing compliance instead of minimizing compliance, as well as the constraint having a maximum compliance value instead of a minimum compliance value. This is due to the implementation of the prescribed displacements, and for a detailed explanation of why this is necessary, the reader is referred to the work of Koppen [54]. The topology which is obtained when using this formulation is given in figure 4.6 along with a visualization of its vertical displacements. There are some slight differences in topology from the force-excited case, but the same inverting behaviour is achieved.

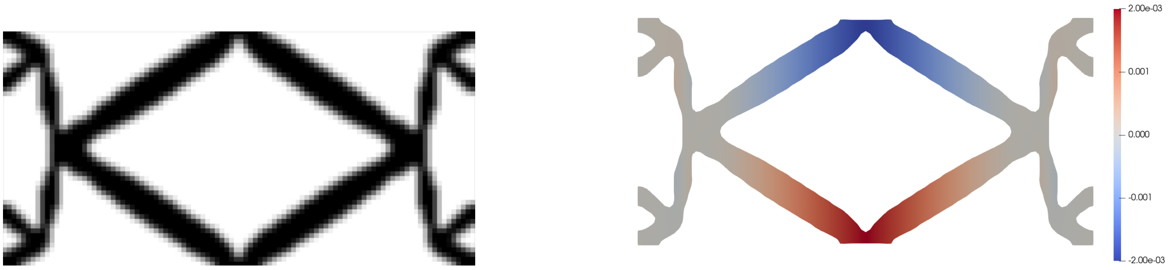

(a) Resulting topology

(b) Static displacements of the mechanism resulting from the applied input force visualized in ParaView

Figure 4.6: The resulting mechanism of the optimization formulation from equation 4.5 and a visualization of its displacements resulting from the applied input load which confirms the working inverting function.

4.1.3. Discussion on inverter formulations

Comparing the formulations given above, there seem to be two general principles: maximizing the displacement given a certain stiffness or maximizing the stiffness given a certain displacement. Of these two, the latter one is considered better conditioned, given that the output displacement of the former will not necessarily be in the negative direction given a large amount of stiffness and will, therefore, not yield an inverter mechanism.

The formulations for obtaining an inverter mechanism are not limited to the formulations introduced in this section, as demonstrated by Cao et al. [55], who provide an overview of a large number of formulations introduced in literature. This thesis will, however, be limited to the formulations introduced here due to the function of the mechanism itself not being the subject of this thesis. For the final case study, the most important aspect will be to have control over the obtained mechanism. This would ensure that all results will obtain an inverter mechanism with similar properties which in turn allows for a fair comparison of the results.

4.2. Harmonics

As mentioned, this thesis will focus on topology optimization considering dynamic problems. Most commonly, dynamic problems can be solved either in the time domain or in the frequency domain. Time domain problems often consider loads which change over time (transient loads) and, as such, require integration over a finite time span[56] [57] [58]. The response which is solved for is then called the transient response and considers the time span over which is integrated. This thesis, however, will consider periodic loading conditions and the accompanying steady-state response, or in other words, harmonic problems. This allows for an easy conversion of the time domain governing equation to the frequency domain, which will be done in this section.

The harmonic governing equation was already presented in equation 3.6, but in this section, the derivation will be provided. For any given system, the general equation of motion can be defined as in equation 4.6.

$$\mathbf{M}(\hat{\mathbf{x}})\ddot{\mathbf{u}}(t)+\mathbf{C}(\hat{\mathbf{x}})\dot{\mathbf{u}}(t)+\mathbf{K}(\hat{\mathbf{x}})\mathbf{u}(t)=\mathbf{f}(t) \tag{4.6}$$

In this equation, $\mathbf{M}(\hat{\mathbf{x}})$, $\mathbf{C}(\hat{\mathbf{x}})$ and $\mathbf{K}(\hat{\mathbf{x}})$ represent the mass matrix, damping matrix and stiffness matrix respectively. Note that these matrices are dependent on the filtered design variables $\hat{\mathbf{x}}$, but this notation will be omitted in the coming section to provide clarity. Consider now a harmonic load written as a set of complex numbers using Euler's formula as given in equation 4.7.

$$\mathbf{f}(t) = \boldsymbol{\lambda}\hat{f}e^{j\omega t} = \boldsymbol{\lambda}\hat{f}\left(\cos\omega t + j\sin\omega t\right) = \boldsymbol{\lambda}(\boldsymbol{\omega})\hat{f} \tag{4.7}$$

Note that the load vector f is now defined in terms of a directional vector $\boldsymbol{\lambda}$ with unit length multiplied by the magnitude of the applied force $\hat{f}$. This notation is chosen in order to provide a better distinction between static and harmonic forces in later sections. The displacements resulting from this harmonic load will have a similar form, which, together with its time derivatives, is given in equation 4.8.

$$\begin{aligned} \mathbf{u}(t) &= \mathbf{u}e^{j\omega t} \\ \dot{\mathbf{u}}(t) &= j\omega\mathbf{u}e^{j\omega t} \\ \ddot{\mathbf{u}}(t) &= -\omega^2\mathbf{u}e^{j\omega t} \end{aligned} \tag{4.8}$$

Both $\boldsymbol{\lambda}$ and $\mathbf{u}$ are arrays with complex numbers, i.e. $\mathbf{u} = \mathrm{Re}(\mathbf{u}) + j\,\mathrm{Im}(\mathbf{u})$ and $\boldsymbol{\lambda} = \mathrm{Re}(\boldsymbol{\lambda}) + j\,\mathrm{Im}(\boldsymbol{\lambda})$ ($\mathrm{Im}(\boldsymbol{\lambda})=\mathbf{0}$). If the results from equation 4.8 and 4.7 are substituted in equation 4.6, the complex system of dynamic equations given in equation 4.9 is obtained.

$$\begin{aligned} -\omega^2\mathbf{u}e^{j\omega t}\mathbf{M} + j\omega\mathbf{u}e^{j\omega t}\mathbf{C} + \mathbf{K}\mathbf{u}e^{j\omega t} &= \boldsymbol{\lambda}\hat{f} \\ \left(\mathbf{K} + j\omega\mathbf{C} - \omega^2\mathbf{M}\right)\mathbf{u}e^{j\omega t} &= \boldsymbol{\lambda}\hat{f}e^{j\omega t}, \end{aligned} \tag{4.9}$$

since $e^{j\omega t} \neq 0$ for all $t \in \Re$. If the dependencies are then inserted again, the final harmonic equation of motion given in equation 4.10 is obtained. The newly defined stiffness matrix $\mathbf{K}(\mathbf{x},\omega)$ is often referred to as the 'dynamic stiffness matrix'. Note also that this equation now solves for the magnitude of the displacements $\mathbf{u}$.

$$\begin{aligned} \mathbf{K}(\mathbf{x},\omega)\mathbf{u}(\omega) &= \boldsymbol{\lambda}(\omega)\hat{f} \\ \mathbf{K}(\mathbf{x},\omega) &= \mathbf{K}(\mathbf{x}) + j\omega\mathbf{C}(\mathbf{x}) - \omega^2\mathbf{M}(\mathbf{x}) \end{aligned} \tag{4.10}$$

For all subsequent sections which cover forced vibration problems, a frequency-dependent harmonic system is considered to which the generalized equation of motion of equation 4.10 applies. Furthermore, the frequency ω, which is used in the computation of the harmonic equations of motion, has the unit of rad/s. In all problem definitions presented in this thesis, however, the excitation frequency ω_{exc} is always presented in Hz. The relation between radians and hertz is given in equation 4.11.

$$\omega = 2\pi[\mathrm{rad/s}] = 1[\mathrm{Hz}] \tag{4.11}$$

Using the harmonic equations, several interesting properties can be exploited. Instead of having only one applied force at one specific frequency, multiple forces at multiple frequencies can be applied to the system through the use of the superposition principle. Due to the linear nature of the harmonic equations of motion, the total displacement $\mathbf{u}_{\mathrm{tot}}$ can be obtained by superposing the solution $\mathbf{u}_i$ for each individual load case k.

$$\mathbf{u}_{\mathrm{tot}} = \sum_{i=1}^{k}\mathbf{u}_i, \tag{4.12}$$

where i represents a single load case of the total load cases k.

4.3. Frequency response

In order to analyze the behaviour of harmonic systems, the frequency response is commonly employed. This response provides the magnitude of the displacement of a chosen degree of freedom for a range of excitation frequencies which allows for the study of the frequency behaviour of the system. If a system is excited close a a resonance frequency, the resulting displacement magnitudes will rise in order of magnitudes rapidly, resulting in behaviour which is defined as resonance. For most structures, this resonance is undesired, which means that having information on the location of these resonance frequencies is crucial. More information on resonance will be provided in later sections.

One of the most influential responses for topology optimization considering harmonic excitations is the response of the initial uniform design domain. This response is often used to obtain the initial resonances of the system and subsequently define one or multiple frequencies of interest which are to be examined. Detailed reasoning behind why this is important will be given in section 4.6. One aspect which is missed or never mentioned in all current literature however, is that the response which is used is often actually not the response of the initial domain but actually the response of the initial domain after material interpolation. What this means exactly is discussed in this section.

The initial uniform design domain such as the grid shown in figure 3.2b is comprised of all design variables x_e. Most commonly, the initial value of these design variables is chosen as x_0=0.5, which is an intermediate density. If a frequency response of the initial uniform design domain is provided, it is implied that this is the domain where all design variables are set to this value of 0.5. However, this is not the case depending on the used material interpolation. Before this response is performed, the design variables are filtered, which will have no influence on the uniform design field but is still important to keep in mind. Next, the filtered design variables $\hat{x}_e$ are inserted into a chosen interpolation function, such as given in section 3.5. Depending on the interpolation function, the penalized filtered design variables $\bar{x}_e$ can become vastly different. The results of the material interpolation functions given in section 3.5 are given in table 4.1. Conditional SIMP (equation 3.10) is left out of this comparison due to the value 0.5 being above the common threshold values.

Interpolation function		$\hat{x}_e$	$\bar{x}_e = f(\hat{x}_e)$
Linear	(equation 3.7)	0.5	0.5000
Standard SIMP	(equation 3.9)	0.5	0.1250
Modified SIMP	(equation 3.13)	0.5	0.1250
SIMPlin	(equation 3.14)	0.5	0.1625
RAMP	(equation 3.15)	0.5	0.2000
PIS	(equation 3.16)	0.5	0.0605

Table 4.1: Filtered design variables after material interpolation

From these results, it is evident that all material interpolation functions have a substantial amount of influence on the filtered design variables. This is important as these penalized filtered design variables $\bar{x}_e$ are used to construct the stiffness matrix $\mathbf{K}(\mathbf{x})$ and mass matrix $\mathbf{M}(\mathbf{x})$, which in turn are used to compute the eigenfrequencies and obtain the undamped frequency response. To visualize the influence of the chosen functions, two frequency responses of the design problem of figure 4.7a are provided in figure 4.8 (the design problem associated with this response is fully defined in section 4.4). Figure 4.8a provides the responses when the mass interpolation function is kept linear and the stiffness interpolation function is varied, and figure 4.8b presents the opposite case.

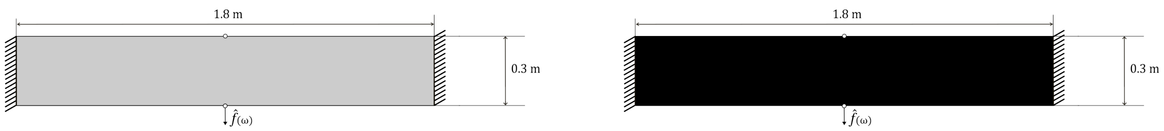

(a) Initial state $\mathbf{x}_0 = 0.5$ (b) Initial state $\mathbf{x}_0 = 1.0$

Figure 4.7: The design domain of the example problem given for two different initial states: the commonly adopted intermediate state $\mathbf{x}_0 = 0.5$ and a fully solid state $\mathbf{x}_0 = 1.0$.

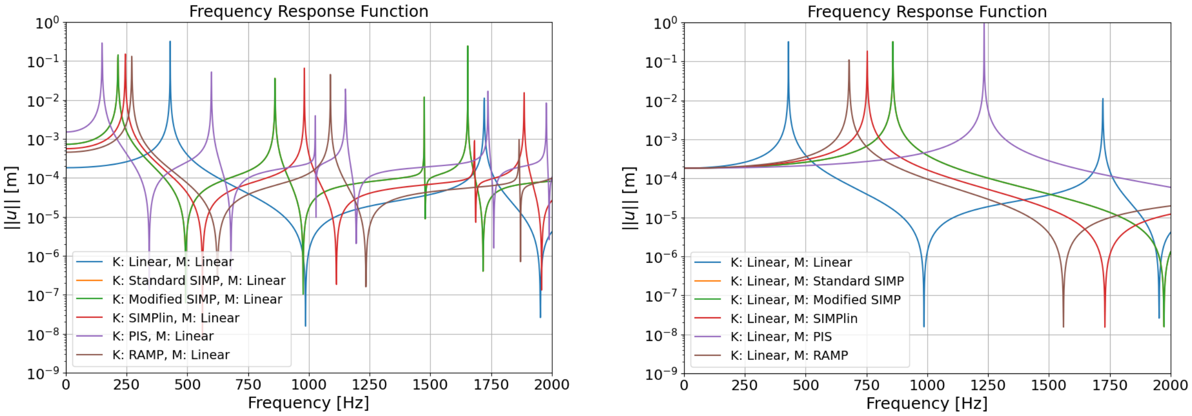

(a) Varying stiffness interpolation function varying, linear mass interpolation function

(b) Linear stiffness interpolation function linear, varying mass interpolation function

Figure 4.8: Frequency response comparison of the initial uniform design domain with an initial state of $\mathbf{x}_0 = 0.5$ after the application of various material interpolation functions for both the stiffness and mass interpolation.

From these responses it is clear that the frequency response is dependent on the used material interpolation functions, with different results for each interpolation function. For the mass interpolation, it seems that the standard SIMP response is not visible, but this yields the same response as modified SIMP. While there is an appropriate material interpolation function for every problem, the response of the initial uniform domain after penalization is highly relevant, as will be explained in section 4.6. One option to circumvent the dependence on the material interpolation function is to set the initial design variables to x_0=1.0. This is shown in figure 4.7b, and the response which is obtained by doing this is given in figure 4.9.

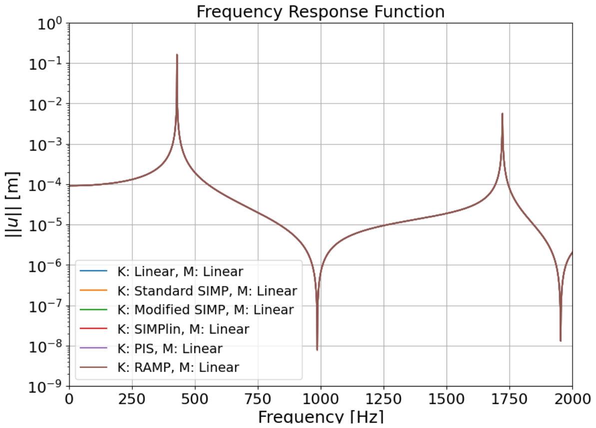

Figure 4.9: Frequency response of the initial uniform design domain after the application of various material interpolation functions for an initial state of x_0=1.0.

This response shows how the obtained response is now independent of the material interpolation functions. Interestingly, the same response is obtained as setting the material interpolation functions for the stiffness and mass interpolation identical to each other for the x_0=0.5 case. This shows that primarily having the same penalization on the filtered design variables gives the same result. In order to have other combinations of interpolation functions however, the choice is made for this thesis to set the initial design domain to x_0=1.0, which should remove all influence from the material interpolation functions. The design domains and load cases given in the coming sections will, however, be presented in grey instead of black for clarity purposes and do not indicate that the initial state of the system is an intermediate density.

4.4. Damping

Whilst the earlier works of topology optimization of structures subjected to harmonic excitations omitted damping for the sake of simplicity [59] [36] [4], all structures exhibit some form of damping in practice. In order to incorporate damping inside the equations of motion, linear viscous damping is often used, which is mathematically convenient due to taking the form of a constant coefficient matrix, which is multiplied by the velocities of the degrees of freedom in a structure.

The effects of damping are simply visualized within the frequency response as it limits the magnitude of the response at the resonance frequencies. The way that these effects of damping are usually quantified is by means of the so-called damping ratio. This ratio represents the factor with which the resonance frequency is damped in terms of response magnitude. A visualization of this effect is given in figure 4.10, which shows an arbitrary response with a single resonance frequency and the effects of different damping ratios. As the damping ratio increases, the resulting magnitude of the response becomes lower.

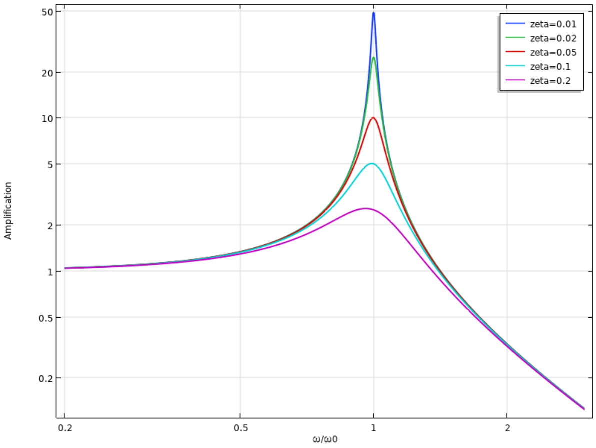

Figure 4.10: A visualization of the effects of different damping ratio's on a resonance frequency [60].

A particular form of damping which is most commonly found for topology optimization problems which include damping is Rayleigh damping. Though often used without argumentation, Rayleigh damping is actually a convenient form of damping due to its linear dependency on the mass and stiffness matrix. The equation for this type of damping is given in equation 4.13.

$$\mathbf{C}(\mathbf{x}) = \alpha\mathbf{M}(\mathbf{x}) + \beta\mathbf{K}(\mathbf{x}) \tag{4.13}$$

As the matrices **K** and **M** used in topology optimization of linear harmonic problems are often sparse, this property is also acquired by the Rayleigh damping matrix due to its simple dependency on these matrices. If a formulation of linear viscous damping is used which does not have this sparse property, the computational effort required to solve the equations of motion will increase drastically [61]. As for the parameters α and β, these are two parameters which specify the proportional influence of the mass and stiffness on the damping characteristics, respectively. To understand the influence of these parameters, the relation between the Rayleigh damping parameters and the damping ratio introduced by Cook et al. [62] can be examined, which is given in equation 4.14.

$$\zeta_n = \frac{\alpha + \beta\omega_n^2}{2\omega_n} = \frac{\alpha}{2\omega_n} + \frac{\beta\omega_n}{2} = \frac{1}{2}\left(\frac{\alpha}{\omega_n} + \beta\omega_n\right) \tag{4.14}$$

From this relation, it is evident that the damping ratio is dependent on the magnitude of the considered eigenfrequency for Rayleigh damping. To visualize this, the resulting damping ratio is plotted in figure 4.11 against the frequency as done by Zerwer et al. [63]. The parameters α and β are represented in this graph by η_1 and η_2 respectively.

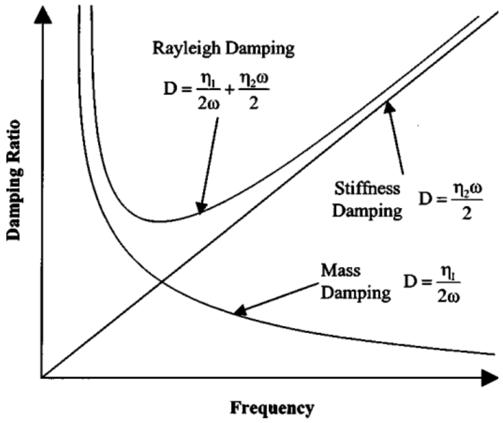

Figure 4.11: The effects of the proportional stiffness damping and mass damping on the damping ratio vs frequency for Rayleigh damping [63].

For lower eigenfrequencies ω_n, the damping ratio is determined more by the parameter α, and for higher order eigenfrequencies, the ratio is determined mostly by the parameter β. As the values of the stiffness matrix $\mathbf{K}(\mathbf{x})$ are often much larger than those of the mass matrix $\mathbf{M}(\mathbf{x})$ the damping ratio is increased for higher order eigenfrequencies. This increase in the damping ratio for higher eigenfrequencies also results in higher damping ratios for higher excitation frequencies ω_{exc}. Given a set of excitation frequencies which are spread out over a certain frequency range, using fixed values for the parameters α and β would yield different amounts of damping for each excitation frequency. In order to compare the results of different excitation frequencies, it is desired to have comparable damping parameters for each of the excitation frequencies of interest. In this thesis, the excitation is considered to be known and of a single frequency, and therefore it is desirable to have this behaviour.

An alternative form of Rayleigh damping was introduced by Silva et al. [64], which approximately imposes a fixed damping ratio ζ during the optimization by introducing an inverse proportionality to the excitation frequency. To derive this damping scheme, the eigenfrequency ω_n is replaced by the excitation frequency ω_{exc} in equation 4.14. Next, the parameter α is set to zero, and the relation is rewritten in terms of β. This derivation is given in equation 4.15.

$$\zeta_n = \frac{1}{2}\beta\omega_{\text{exc}} \qquad \rightarrow \qquad \beta = \frac{2\zeta}{\omega_{\text{exc}}} \tag{4.15}$$

The damping ratio ζ can now be chosen as desired, which will result in an approximately fixed damping ratio at the excitation frequency ω_{exc}. Furthermore, if the optimizer decides on a topology which contains a resonance frequency at the specified excitation frequency, a properly damped system is still guaranteed. For this thesis, a low damping coefficient of 0.05 is used [65]. As for why the parameter α is set to zero, Silva et al. [64] reported that the inclusion of α yielded behaviour where material was removed from the load application region in order to comply with the objective. This thesis will also consider structures subjected to base excitations, and a study was done by Hall [61] on Rayleigh damping which also suggests removing the mass proportional damping contribution for base excited problems and to bound the stiffness proportional damping.

Whilst a choice is made for a specific damping scheme in this section, some of the examples in the coming sections will still include fixed damping parameters in order to provide a better comparison to the given literature. Furthermore, while this investigation into the effects of the damping parameters proposed in literature is concluded here, further research needs to be conducted in order to provide a general approach to choosing appropriate damping parameters which provide the desired influence for a given problem. This is however not within the scope of this thesis.

One last thing to note is the effect that damping has on the eigenfrequencies. Given in figure 4.12 is the undamped frequency response of an arbitrary system which contains an undamped resonance frequency at 429Hz. Together with this undamped response is the damped response which utilizes the proposed damping scheme.

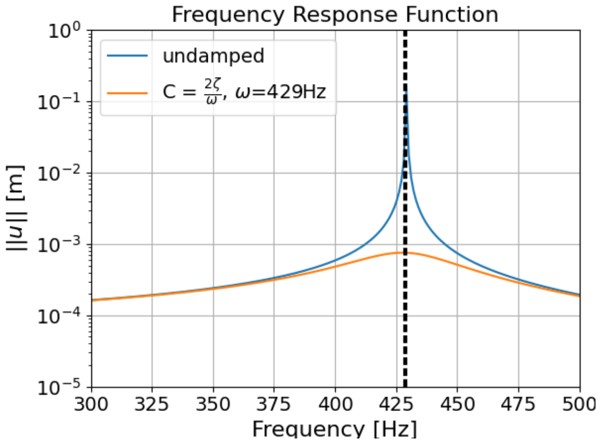

Figure 4.12: A visualization of the effects of damping on the location of the resonance frequency versus the undamped resonance frequency.

While hard to see, the maximum response of the damped response is actually shifted compared to the original undamped resonance frequency. This means that a computation of the eigenfrequencies will not necessarily reveal the actual damped resonance frequency of the system. There are methods to obtain these damped resonance frequencies, such as the one given in equation 4.16 provided by Schmidt et al. [65].

$$\omega_{d,r} = \omega_0 \sqrt{(1 - 2\zeta^2)} \tag{4.16}$$

This formulation will, however, not be used in this thesis, but is important to be aware of. A distinction will, therefore, be made in the eigenfrequencies of the system, which are obtained from the undamped response, and the resonance frequencies of the system, which represent the resonances in the damped response.

4.5. Eigenfrequency optimization

As stated in section 2.2.3, exciting structures near or at their resonance frequencies is not beneficial for most forced vibration problems. Within the realm of topology optimization, these eigenfrequencies of the designed structure can be influenced by incorporating them in the objective function. This was already shown by Diaz and Kikuchi in 1992 [66], who maximized the first eigenvalue λ_1, and thus the first eigenfrequency ω_1 given that $\lambda_n = \omega_n^2$, of a truss structure (figure 4.13a). Du and Olhoff [67] achieved a similar result for a clamped beam problem, but expanded the objective to any eigenvalue of choice λ_n together with being able to maximize the distance between two consecutive eigenvalues λ_n and λ_{n+1} (figure 4.13b). A notable example of targeting the eigenfrequencies to actually induce resonance in the system is the optimization of an atomic force microscope cantilever tip as done by Huigsloot [68] (figure 4.13c). In this section, several versions of the eigenfrequency optimization formulation are given, together with an assessment of the use of eigenfrequency optimization in general.

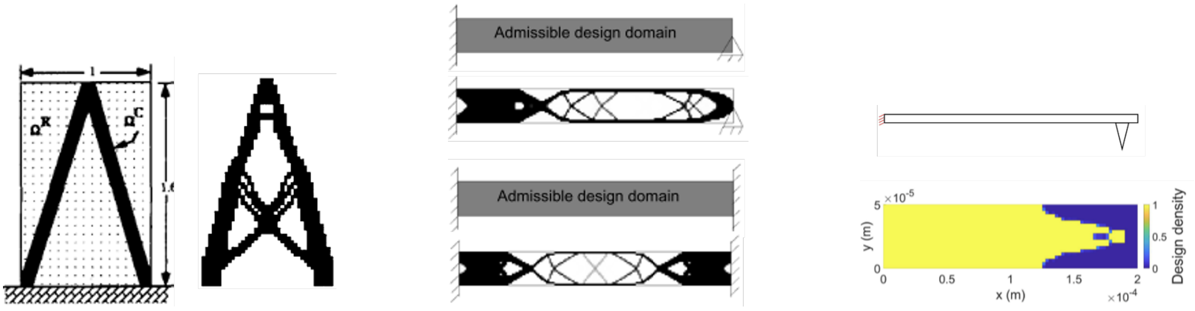

(a) Eigenfrequency optimization of a truss structure [66]

(b) Eigenfrequency optimization of a clamped and double clamped beam structure [67]

(c) Eigenfrequency optimization of an AFM cantilever beam [68]

Figure 4.13: Examples of eigenfrequency optimization found in literature.

4.5.1. Eigenvalue problem

First, however, the eigenvalue problem needs to be defined. The equation of motion given in equation 3.6 will be used as a starting point. Ignoring the damping matrix $\mathbf{C}(\mathbf{x})$ and setting the applied load vector $\mathbf{f}(\omega)$ to $\mathbf{0}$, the equation given in 4.17 is obtained.

$$\begin{aligned}\left(\mathbf{K}(\mathbf{x}) - \omega^2\mathbf{M}(\mathbf{x})\right)\mathbf{u}(\omega) &= \mathbf{0}\\ \left(\mathbf{K}(\mathbf{x}) - \omega_n^2\mathbf{M}(\mathbf{x})\right)\boldsymbol{\phi}_{\boldsymbol{n}}(\omega) &= \mathbf{0}\end{aligned} \tag{4.17}$$

The solution to equation 4.17 yields multiple values for ω_n^2, which is often just used as λ_n ($\lambda_n = \omega_n^2$) and the respective eigenfrequency is represented by ω_n. The accompanying eigenmodes are given by the accompanying eigenvector $\mathbf{u_n}(\omega)$, which is changed in notation to $\boldsymbol{\phi}_{\boldsymbol{n}}(\omega)$ to provide a distinct difference.

4.5.2. Eigenfrequency maximization

In the given example of Díaz and Kikuchi [66], the first eigenvalue λ_1 was optimized for, which was the most common form of eigenfrequency optimization. Du and Olhoff [69] however, expanded on this optimization by formulation a generalized version which would allow for any nth eigenvalue to be optimized for. This formulation is given in equation 4.18.

$$\begin{aligned}\max_{\mathbf{x}}: &\quad \lambda_n\\ \text{subject to}: &\quad V(\mathbf{x}) \leq \bar{V}\\ &\quad 0 \leq \mathbf{x}_{\text{min}} \leq \mathbf{x} \leq 1\\ \\ \text{with } \lambda_n \text{ obtained from}: &\quad \left(\mathbf{K}(\mathbf{x}) - \lambda_n\mathbf{M}(\mathbf{x})\right)\boldsymbol{\phi}_{\boldsymbol{n}}(\omega) = \mathbf{0}\end{aligned} \tag{4.18}$$

In this formulation, λ_n represents the nth eigenvalue and ϕ_n is the nth eigenmode vector.

4.5.3. Eigenfrequency gap optimization

The second mentioned example covered the maximization of the distance between two consecutive eigenvalues λ_n and λ_{n+1}. This was first covered by Bendsøe [70], who put forth the argument that by maximizing this gap resonances and other instabilities in the system may be avoided for a wide range of operating frequencies. The formulation is to that of eigenfrequency maximization and is given in equation 4.19

$$
\begin{aligned}
\max_{\mathbf{x}}: \quad & \lambda_{n+1}^2 - \lambda_n^2 \\
\text{subject to}: \quad & V(\mathbf{x}) \leq \bar{V} \\
& 0 \leq \mathbf{x}_{\min} \leq \mathbf{x} \leq 1 \\
\\
\text{with } \lambda_n \text{ obtained from}: \quad & (\mathbf{K}(\mathbf{x}) - \lambda_n \mathbf{M}(\mathbf{x}))\, \boldsymbol{\phi_n}(\omega) = \mathbf{0}
\end{aligned}
\tag{4.19}
$$

4.5.4. Weighted eigenfrequency optimization

Both of the mentioned methods focus on either a single eigenvalue or a pair of eigenvalues. In practice, however, it is often the case that an optimization needs to be performed for multiple eigenvalues simultaneously. One of the methods capable of handling this is the weighted eigenfrequency optimization method introduced by Ma et al. [71] which is given in equation 4.20.

$$
\begin{aligned}
\max_{\mathbf{x}}: \quad & \bar{\lambda} + \sum_{i=1}^{m} w_n \left(\sum_{n=1}^{m} \frac{w_n}{\lambda_n - \bar{\lambda}} \right)^{-1} \\
\text{subject to}: \quad & V(\mathbf{x}) \leq \bar{V} \\
& 0 \leq \mathbf{x}_{\min} \leq \mathbf{x} \leq 1 \\
\\
\text{with } \lambda_n \text{ obtained from}: \quad & (\mathbf{K}(\mathbf{x}) - \lambda_n \mathbf{M}(\mathbf{x}))\, \boldsymbol{\phi_n}(\omega) = \mathbf{0}
\end{aligned}
\tag{4.20}
$$

In this formulation, w_n are the weights associated with each nth eigenvalue λ_n and $\bar{\lambda}$ is the desired eigenvalue around which is being optimized. For equal weight factors, the eigenvalues closest to $\bar{\lambda}$ will have the most influence on the objective, which results in the eigenvalue closest to $\bar{\lambda}$ being optimized for.

4.5.5. Mean eigenfrequency optimization

A simpler method of optimizing for multiple frequencies was the mean eigenfrequency function introduced by Ma et al. [72]. This objective function optimizes for the harmonic mean of a subset of m eigenvalues. It can be noted that this formulation is one of minimization instead of maximization.

$$
\begin{aligned}
\min_{\mathbf{x}}: \quad & \sum_{n=1}^{m} \frac{1}{\lambda_n} \\
\text{subject to}: \quad & V(\mathbf{x}) \leq \bar{V} \\
& 0 \leq \mathbf{x}_{\min} \leq \mathbf{x} \leq 1 \\
\\
\text{with } \lambda_n \text{ obtained from}: \quad & (\mathbf{K}(\mathbf{x}) - \lambda_n \mathbf{M}(\mathbf{x}))\, \boldsymbol{\phi_n}(\omega) = \mathbf{0}
\end{aligned}
\tag{4.21}
$$

4.5.6. Localized eigenmodes

One issue that can occur when using topology optimization for a performance measure that involves the eigenfrequencies of the structure of interest is the appearance of localized eigenmodes. This happens when there are regions in the domain with elements that have relatively high mass and low stiffness. Pedersen [44] found this to be the case in the void areas (defined by $x_{\min}$) specifically, where the adjacent solid areas would act as a fixed boundary condition. Consequently, the lowest eigenvalues will correspond to eigenmodes involving predominantly motion of the regions that contain void elements, as opposed to the natural frequencies of the solid structure. An example of this behaviour is given in figure 4.14, in which a solid beam structure (black) in a design domain is surrounded by void elements (white).

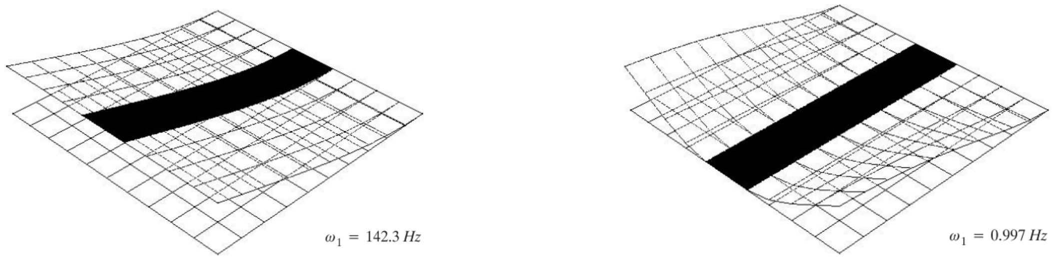

(a) Expected first eigenmode

(b) Computed first (local) eigenmode

Figure 4.14: A comparison of the expected first eigenmode, which is similar to the one found for the clamped beam structure defined by the black solid region, and the actual computed first eigenmode, which is a local eigenmode which only contains displacements in the white void region [44].

Figure 4.14a shows the expected first eigenmode of this domain, that is the eigenmode of the beam structure. If the eigenfrequencies of this domain are computed, however, an eigenfrequency is found at a much lower frequency. The accompanying eigenmode is given in figure 4.14b. This eigenmode occurs at such a low frequency due to the relatively low stiffness and high mass of the void elements. When using an objective function where this first eigenfrequency is incorporated, this eigenmode becomes a problem due to the accompanying eigenfrequency becoming the used eigenfrequency in the objective function instead of the desired first eigenfrequency. The same problem occurs for model order reduction methods, where a set of eigenmodes is used to define the system. If there are local modes present in this subset, inaccurate information is used in the optimization, and more eigenmodes are needed to properly represent the behaviour of the system, which in turn increases computation time.

Most of these issues occurred using the SIMP (equation 3.9) interpolation method, which resulted in the introduction of several of the material interpolation functions introduced in section 3.5 such as conditional SIMP [44], RAMP [49] and PIS [48]. These all aimed to avoid the occurrence of localized eigenmodes by providing a non-zero slope when the design variables approach zero.

For this thesis, the occurrence of localized eigenmodes is, however, not a problem as the eigenfrequencies will not be a part of the objective function. Furthermore, localized displacement behaviour is even encouraged. What is desired however, is that the regions which displace are not made up of intermediate densities but rather solid material. The occurrence of intermediate densities in the resulting topologies in this thesis is, therefore, undesired.

4.5.7. Discussion on the use of eigenfrequency optimization

In this section, several methods of optimizing for the eigenfrequencies of the structure have been presented from literature. As mentioned, controlling the resonances of a structure can be crucial depending on the loading conditions of the structure. If a structure is unintentionally excited at a resonance frequency that it was not designed for, the resulting large displacements might inflict substantial amounts of damage to the structure such that its material properties can no longer be guaranteed. There are, however, also cases where this behaviour is actually desired, as was shown in the AFM cantilever example, but having control of the eigenfrequencies in general is beneficial. Having control of the eigenfrequencies, however, does not necessarily result in a minimization of the vibrations at a given frequency.

Another key issue with eigenfrequency optimization is that it does not fully translate to forced vibration problems. The reasoning behind this was detailed in section 4.4, which introduced the influence of damping on the frequency response of a structure. In the forced vibration problems in this thesis, damping will be taken into account, which means that there will be a difference between the obtained eigenfrequencies of the structure, and the resonance frequencies. While this difference will be small, optimizing for the eigenfrequencies of a structure with damping will result in optimizing for different frequencies than the actual resonance frequencies of the structure.

Furthermore, the occurrence of localized modes might also hinder eigenfrequency optimization or optimizations which make use of the eigenfrequencies in general. Whilst material interpolation functions have been introduced that attempt to mitigate this behaviour, these might still occur. Lastly, the computational costs of an eigenfrequency analysis are often overlooked. To perform an eigenfrequency analysis, meaning obtaining both eigenfrequencies and corresponding eigenvectors, the computational cost is around 10-100 times more expensive than a linear solve as multiple solves are needed per eigen-iteration [73]. The amount of these iterations depends on the number of eigenfrequencies which are to be searched for. Comparing this to the linear solution of evaluating equation 4.9 for a single frequency, the eigenvalue analysis has a much higher computational cost.

4.6. Dynamic compliance

As optimization formulations which include the eigenfrequencies of a system do not seem to translate well to forced vibration problems, a look can be taken at objective functions specifically considering forced vibration. One such objective function is dynamic compliance, which is a concept which was introduced by Ma et al. [72], which focuses on minimizing the structural displacement response to dynamic loads. This may seem familiar, which would be true as the dynamic compliance can be considered as the dynamic equivalent of the static compliance which was presented in section 3.2. By using dynamic compliance as the objective function, the optimized design will result in the stiffest structure which can effectively resist harmonic excitations with specified magnitudes and frequencies [74]. The most common form of objective function formulation for dynamic compliance is given by Olhoff and Du [69] and is shown in equation 4.22.

$$C_\mathrm{d} = |\mathbf{f}(\omega)^T \mathbf{u}(\omega)| \tag{4.22}$$

In this function, $\mathbf{f}(\omega)$ and $\mathbf{u}(\omega)$ represent the global force and displacement vectors respectively, which both depend on the excitation frequency ω. The displacement vector $\mathbf{u}(\omega)$ may be obtained from the equation of motion presented in equation 3.6. One key difference from the static compliance, next to the frequency dependency, is the inclusion of the absolute value in the function. This operation is added in order to avoid the formulation becoming negative during the optimization [75]. In terms of what C_d actually represents, it can be considered as the magnitude of the displacements weighted by the amplitudes of the corresponding time-harmonic loading. It can be noted that as the excitation frequency for the load approaches zero, the dynamic compliance function is reduced to the static compliance function.

4.6.1. Discussion on the use of dynamic compliance

One of the key arguments for using dynamic compliance is its similarity to the frequently used static compliance formulation, together with its capability of optimizing the actual resonance frequencies of the structure. As the excitation frequency approaches one of the resonance frequencies of the structure, the dynamic compliance will drastically increase. This behaviour means that the objective function is able to accurately represent the frequency behaviour of the structure. However, this does come with some drawbacks, which will be presented in this section.

First of all, the behaviour of dynamic compliance can be analyzed with a simple example. Starting with a simple clamped cantilever beam problem, a frequency-dependent problem can be formulated as given in equation 4.23. The initial design domain is given in figure 4.15, together with the domain properties in table 4.2.

$$\begin{aligned}
\min_{\mathbf{x}}: \quad & C_\mathrm{d} = |\mathbf{f}(\omega)^T \mathbf{u}(\omega)| \\
\text{subject to}: \quad & V(\mathbf{x}) \leq \bar{V} \\
& 0 \leq \mathbf{x}_\mathrm{min} \leq \mathbf{x} \leq 1 \\
\\
\text{with } \mathbf{u}(\omega) \text{ obtained from}: \quad & \mathbf{K}(\mathbf{x}, \omega)\mathbf{u}(\omega) = \boldsymbol{\lambda}(\omega)\hat{f}
\end{aligned} \tag{4.23}$$

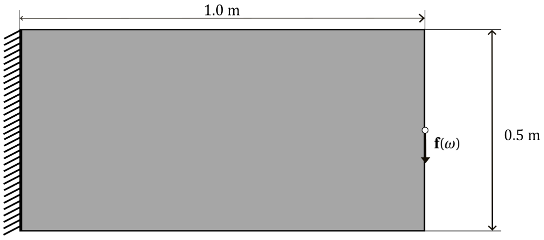

Figure 4.15: Design domain for the dynamic compliance optimization example.

Property	Value	
l_x, l_y, l_z	1.5, 0.5, 1.0	[m]
n_x, n_y	100, 50	[#]
$\hat{f}$	10	[kN]
Filter radius	2	[#]
Volume fraction	0.5	[-]

Table 4.2: Properties of the domain given in figure 4.15.

The magnitude of the applied harmonic force $\mathbf{f}(\omega)$ is $\hat{f}$=10kN. For the damping, Rayleigh damping (equation 4.13) is used with α=1e^{-3} and β=1e^{-8}. As for the material properties, the Young's modulus is set at 200GPa, the density at 7800 kg/m^3 and the Poisson ratio at 0.3. Lastly, the material interpolation functions used are the modified SIMP method (equation 3.13) for both the stiffness interpolation and the mass interpolation. Next, the dynamic compliance can be computed for the frequency interval [0, 2000]Hz with a resolution of 1Hz and plotted in figure 4.16. In this same plot, the resonances and anti-resonances of the structure for this frequency interval are provided.

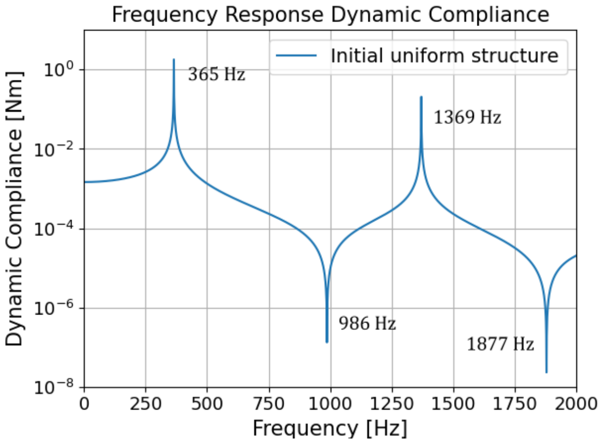

Figure 4.16: The dynamic compliance response of the initial design domain as given in figure 4.15.

To assess the behaviour of the dynamic compliance, the dynamic compliance is first optimized for frequencies below the first resonance. As this resonance is located at 365Hz, the chosen frequencies are 0Hz (the static solution), 200Hz, and 350Hz. These frequencies should cover the behaviour of minimizing the dynamic compliance up until the first resonance. The resulting topologies of these optimizations are given in figure 4.17.

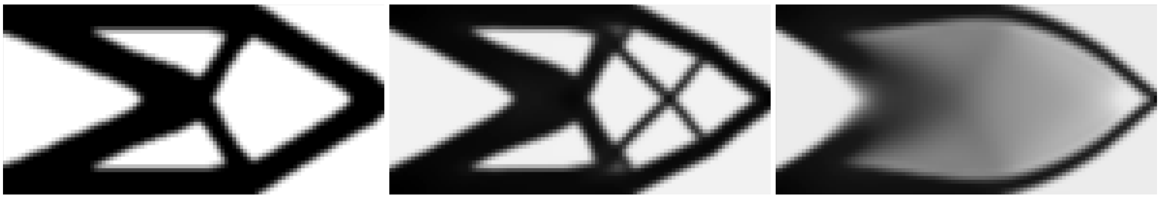

(a) ω_{exc} = 0 Hz (static solution)

(b) ω_{exc} = 200 Hz

(c) ω_{exc} = 350 Hz

Figure 4.17: The obtained topologies for the minimization of the dynamic compliance for the design domain given in figure 4.15 for a set of excitation frequencies below the first resonance of 363Hz.

From the resulting topologies alone, it is not quite clear what the objective function aims to achieve. The topologies themselves however, do show several differences. For a higher frequency than the static solution, it seems that the optimizer chooses to deposit less material near the excitation point. This behaviour is to be expected as less material will result in less mass, which will influence the dynamic stiffness matrix (equation 3.6) less, which in turn leads to smaller displacements at the specified frequency. If the excitation frequency comes very close to the first resonance, however, the optimizer struggles to converge to a binary design, and a lot of intermediate densities remain present in the topology. In order to assess what the objective function actually aims to achieve, the dynamic compliance responses can be assessed for the obtained topologies. These results are given in figure 4.18.

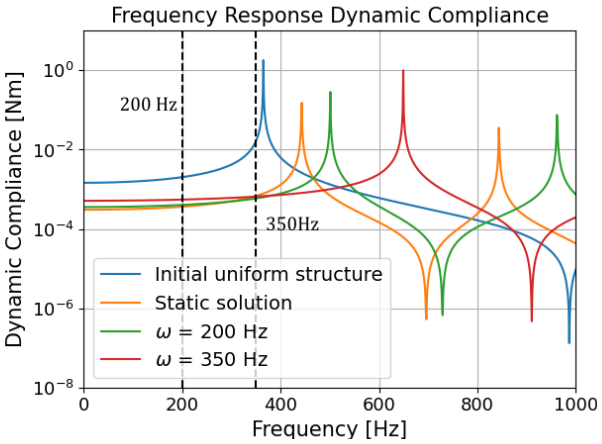

Figure 4.18: Dynamic compliance response comparison of the obtained topologies given in figure 4.17.

From these results, it is clear what the objective function aims to achieve. The static solution seems to already provide an improvement with regards to the initial structure in terms of first resonance location, but increasing the excitation frequency is where the behaviour really comes to light. For higher frequencies, the first resonance is 'pushed' further towards a higher frequency. This behaviour intensifies as the excitation frequency increases, even though the topology still contains a lot of intermediate densities. Comparing this with the eigenfrequency optimization methods given in section 4.5 this objective function does not necessarily control the resonance frequencies directly, but manages to force them away from the excitation frequency, resulting in minimized displacements at the specified frequency. This is highly beneficial as the resonance frequencies can be controlled with an optimization which only requires a linear solution instead of the computationally costly eigenfrequency analysis.

The results from above show the behaviour of the dynamic compliance for excitation frequencies below the first resonance. Above this resonance however, an interesting issue occurs. This issue was first addressed by Silva et al. [76], which presents the problem of the optimization suffering from premature convergence when the excitation frequency is set at a value higher than the first resonance of the initial uniform structure. In order to test this, two frequencies can be chosen from the frequency response in figure 4.16 which are above the first resonance. For this test, the choice is made for 600Hz and 1250Hz, which provide insight into the behaviour just beyond the first resonance and after the first anti-resonance. The resulting topologies for these structures are given in figure 4.19.

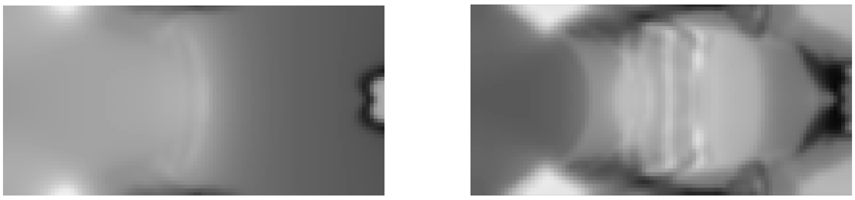

(a) ω_{exc} = 600 Hz (b) ω_{exc} = 1250 Hz

Figure 4.19: The obtained topologies for the minimization of the dynamic compliance for the design domain given in figure 4.15 for a set of excitation frequencies above the first resonance of 363Hz.

These topologies clearly show the inability of the optimizer to converge to a binary design. In this case, however, the optimization did not converge prematurely but was stopped by the maximum amount of 100 iterations being reached. There were, however, large oscillating steps in the objective function observed, which might have been larger than the allowed tolerance between iterations. This would explain why there was no premature convergence. As to why this behaviour occurs, the frequency responses of the obtained topologies can again be examined. These are given in figure 4.20.

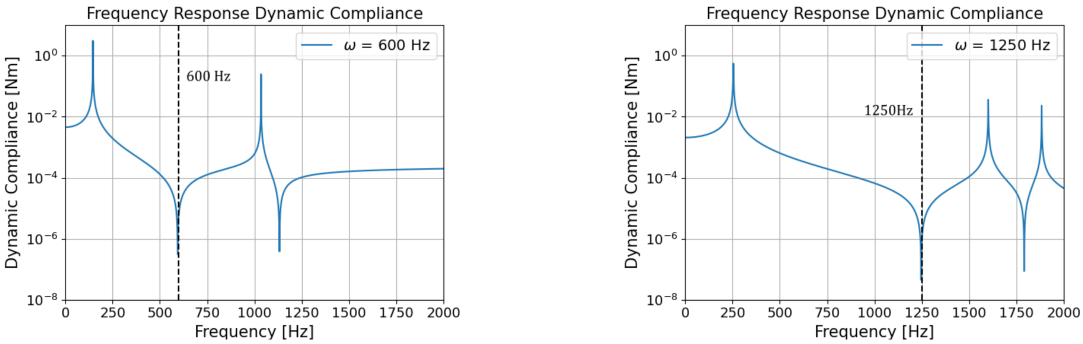

(a) $\omega_{\text{exc}} = 600$ Hz

(b) $\omega_{\text{exc}} = 1250$ Hz

Figure 4.20: The dynamic compliance responses of the obtained topologies from figure 4.19.

By examining the frequency response it becomes evident why the model seems to suffer from premature convergence. When the excitation frequency matches an anti-resonance during the optimization, the resulting displacement response is at its lowest possible point. If the optimizer is not able to determine why this is, it ’thinks’ that it has found the lowest possible value for the dynamic compliance. Therefore, the responses in figure 4.20 both clearly show that there is an anti-resonance located precisely at the excitation frequency. This is the exact behaviour which was described by Silva et al. [76].

It can be concluded from this examination that dynamic compliance works quite well as a way of indirectly influencing the resonance frequencies without having to compute the eigenfrequencies every iteration. However, this behaviour is limited to excitation frequencies below the first resonance of the initial uniform structure, which makes it unsuitable for higher excitation frequencies. One last interesting thing to note is that, as mentioned in 4.3, this initial resonance is not necessarily that of the initial uniform structure, which has the design variables set to the desired volume fraction, but actually the initial design domain after material interpolation. Therefore, the working range of the dynamic compliance can be increased by choosing different material interpolation functions which yield higher first resonances. Choosing material interpolation functions based on this advantage is, however, not recommended as issues like intermediate densities have far more impact on the obtained topologies.

4.7. Harmonic base excitations

Most of the existing literature on topology optimization considering responses under forced harmonic vibrations concerns harmonic force excitations. However, in most practical engineering structures, excitations in the form of base excitations also commonly exist. Up till now, the base to which the structure is connected was considered fixed, but external excitations which may originate from various sources can be conducted to the structure through this connection.

Within the field of compliant mechanisms, this research area is commonly known as vibration isolation, where the goal is to design the system in such a manner as to minimize the influence of the base-induced vibrations. Several examples of this kind of goal being implemented in topology optimization can be found in literature. Vijayan et al. [77] used the principle of vibration isolation with a discrete topology optimization method to design a compliant isolator which was able to cancel undesired disturbances, resulting in attenuated output amplitudes. Allahdadian et al. [78] optimized the bracing system of a multi-story structure under harmonic base excitations. Furthermore, Zhu et al. [79] optimized the relative displacement amplitude at a specified point with added mass along the excitation direction of a structure subjected to harmonic base acceleration excitations. This last example is visualized in figure 4.21

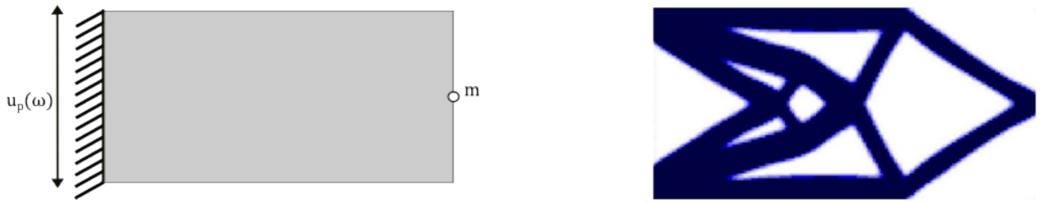

(a) Design domain

(b) An example of the obtained topologies [79]

Figure 4.21: An example from literature as provided by Zhu et al. [79]. The design domain is excited by a harmonic base excitation, and the displacement magnitude of the vertical degree of freedom of the mass node is minimized, yielding the topology shown on the right.

In order to solve for the harmonic base excitations, the general equation of motion of equation 4.10 is insufficient as there are no applied forces present in this problem. The manner in which such a problem can be solved, however, is to directly apply an excitation to the degrees of freedom at the boundaries. A visualization of a vertical excitation is given in figure 4.22.

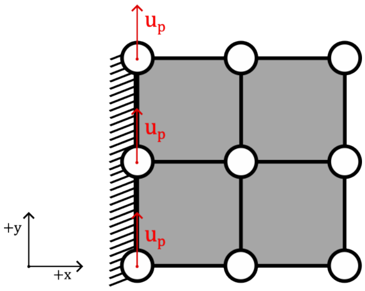

Figure 4.22: A visualization of the base excitation being applied to the vertical degrees of freedom of the base.

This type of excitation is achieved by dividing the degrees of freedom into free degrees of freedom f and prescribed degrees of freedom p, similar to what was done in section 4.1.2. For the subset p, all degrees of freedom of the boundary nodes are then chosen, and for the given examples above, the magnitude of the prescribed displacement is applied to the vertical degrees of freedom whilst constraining the horizontal degrees of freedom to zero. Applying this to equation 4.10 yields the system of equations given in equation 4.24. For a full derivation of this equation, the reader is referred to Appendix A.

$$\begin{bmatrix} \mathbf{K}_{ff}(\omega,\mathbf{x}) & \mathbf{K}_{fp}(\omega,\mathbf{x}) \\ \mathbf{K}_{pf}(\omega,\mathbf{x}) & \mathbf{K}_{pp}(\omega,\mathbf{x}) \end{bmatrix} \begin{bmatrix} \mathbf{u}_f \\ \mathbf{u}_p \end{bmatrix} = \begin{bmatrix} \mathbf{f}_f \\ \mathbf{f}_p \end{bmatrix} \tag{4.24}$$

In this system of equations $\mathbf{u}_f$, $\mathbf{f}_f$ and $\mathbf{u}_p$, $\mathbf{f}_p$ represent the displacements and forces of the free degrees of freedom f and prescribed degrees of freedom p respectively. The matrices $\mathbf{K}(\omega,\mathbf{x})$ represent the same dynamic stiffness matrix from equation 4.10 for the free and prescribed displacements, respectively.

4.7.1. Discussion on harmonic base excitations

Similar to the dynamic compliance objective function for forced excitation, the objective function of minimizing the displacement of a single degree of freedom, which is most commonly used, also suffers from various issues. These will be outlined in this section.

First of all, it can be noted that an extra mass m_b is added to the example problem given in figure 4.21. This mass is added at the node which contains the degree of freedom of interest that is to have its displacements minimized. This mass is an essential addition as it provides initiative for the optimizer to connect this point to the base without resorting to intermediate-density members. The result of the same design problem without the added mass is given in figure 4.23.

Figure 4.23: The resulting topology from the design problem given in figure 4.21a without additional mass added to the response point.

From this result it is clear that a similar topology is obtained, but the members which connect the point of interest to the rest of the structures are made up of intermediate densities. This structure complies most with the objective function as the degree of freedom of interest is able to move freely due to being only very lightly connected to the rest of the structure. A connected topology is, however, desired, which results in the need for mass to be added to this point. In order to provide insight into the effect of the added mass, figure 4.24 provides the result of a sweep over the mass m_b for the values m_b=1kg, 10kg and 100kg.

(a) m_b = 1kg (b) m_b = 10kg (c) m_b = 100kg

Figure 4.24: The resulting topologies from the design problem in figure 4.21a for a parameter sweep over the value of the mass m_b added to the response point.

These results clearly show the effects of the added mass. As the magnitude of m_b increases, the members connecting the point of interest to the rest of the structures become thicker in order to support this mass whilst subjected to the applied base excitations. In this case, if the objective is to maximize frequency behaviour, an added mass of 10kg would be sufficient as it is able to provide a well-connected structure without a large amount of extra material being deposited at the connecting members.

Furthermore, the excitation frequency issue, which is present for the dynamic compliance objective function where an anti-resonance of the system will match the excitation frequency, is also present for the base excited case. It is, however, the case that the initial first anti-resonance is located at a relatively higher frequency than the force excited case. This can be seen by looking at the undamped frequency response given in figure 4.25 of the problem given in figure 4.21a for an initial volume fraction of 1.0.

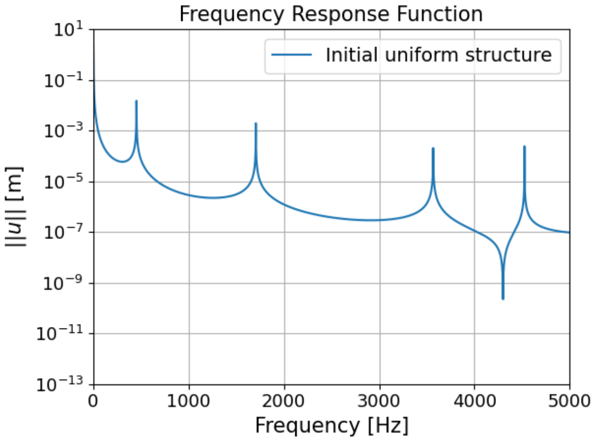

Figure 4.25: Undamped frequency response of the initial design domain given in figure 4.21a

This graph shows that the first resonance is present around 450Hz and the first anti-resonance is only present at around 4300Hz. To see how the optimization performs over a frequency range the resulting topologies of an excitation frequency of 300Hz, 750Hz and 1250Hz are given in figure 4.26.

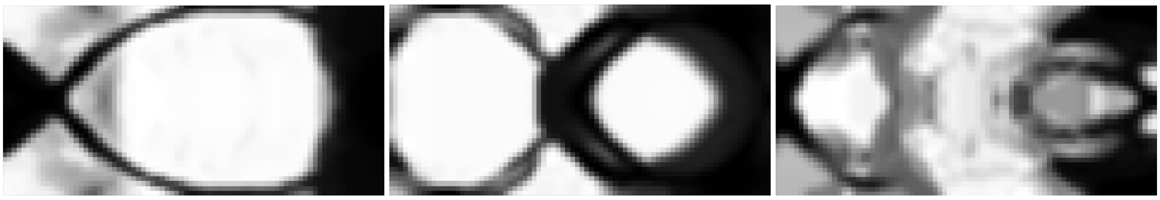

(a) $\omega_{\text{exc}} = 300$Hz

(b) $\omega_{\text{exc}} = 750$Hz

(c) $\omega_{\text{exc}} = 1250$Hz

Figure 4.26: The resulting topologies from the design problem in figure 4.21a of a parameter sweep over the excitation frequency ω_{exc}.

These topologies show that material is mostly being deposited near the point of interest for higher excitation frequencies. The connection to the base, however, becomes decreasingly stiff, and the optimizer resorts to a connection formed with intermediate densities. To see how these obtained structures perform at their respective excitation frequencies, the undamped frequency responses are given in figure 4.27.

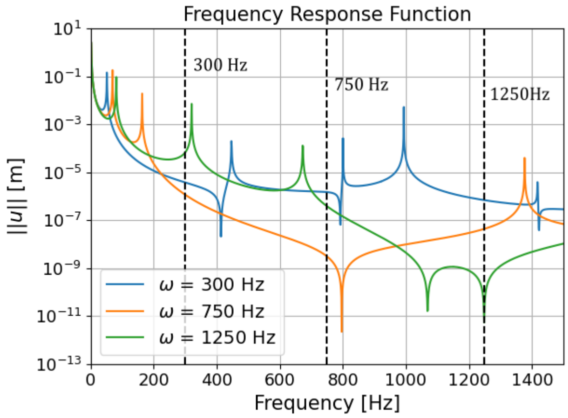

Figure 4.27: The undamped frequency responses for the obtained topologies given in figure 4.26

This response shows that the result of an excitation frequency of 300Hz still performs as expected by moving resonances away from the excitation frequency. This is due to the excitation being below the initial first resonance of 450HZ. At 750Hz, however, an anti-resonance is moved very close to the excitation frequency, and the result of 1250Hz has an anti-resonance present exactly at the excitation frequency. This shows that the same excitation frequency issue is present for the base excitation case.

4.8. Discussion on the state of the art

In this chapter, the state of the art on topology optimization of static mechanism design and structures excited by harmonic excitations is presented. Mechanism design of compliant mechanisms considering static excitation forces has been done quite extensively already, and several principles on how to perform such an optimization were given. As for optimizations regarding frequency behaviour, these are done primarily for clamped beam structures. One of the first optimizations considering frequency behaviour was that of eigenfrequency optimization. While this works as desired, the issue remains that this optimization does not consider an excitation which is applied to the structure. Furthermore, the occurrence of localized eigenmodes can hinder the optimization by replacing the structural modes which are considered in the objective.

An objective function which does consider the response to an applied load is dynamic compliance. This function works by moving the resonances away from the excitation frequency. However, this only works for excitation frequencies which are below the first resonance of the initial uniform structure. For higher excitation frequencies, the structure which is obtained contains a large number of intermediate densities, and when the frequency response is examined, it can be seen that an anti-resonance of the structure has lined up with the excitation frequency. This makes this objective function unsuitable for excitation frequencies higher than the first resonance of the initial uniform structure. For structures considering a harmonic base excitation, which have been studied far less than the dynamic compliance, a similar excitation frequency issue occurs. A new objective function is therefore needed which does not suffer from these excitation frequency issues and is capable of handling both force and base excitations.

5

Addressing the research gaps

Chapter 4 concluded that much research has been done in the individual areas of topology optimization considering transmission systems design and frequency behaviour. Whilst compliant mechanism design using topology optimization has been studied extensively, the study done on the state of the art of topology optimization of eigenfrequencies and harmonically excited structures concluded that research in this area is still lacking. Where eigenfrequency optimization does not consider an applied load and might be hindered by the occurrence of localized eigenmodes, forced vibration problems often only consider clamped beam structures.

Furthermore, the objective functions used for harmonically excited structures appear to suffer from premature convergence issues when the frequency of an anti-resonance in the system matches with the excitation frequency during the optimization. As far as the optimizer is concerned, this is a minimum result which satisfies the objective. The accompanying topology, however, is often still filled with intermediate densities, which is undesired as a discrete design is preferred. A possible solution to this problem would be to incorporate a range of frequencies in the objective function as done by Zhu et al. [79], but solving for this range of frequencies every iteration can become very computationally intensive.

From this research, it can be concluded that the current state of the art on topology optimization is lacking in two areas: a computationally convenient objective function which optimizes a forced vibration response whilst not suffering from premature convergence and the inclusion of externally induced vibrations on compliant transmission systems design using topology optimization. The focus of this thesis will, therefore, be to find an objective function which solves the presented issues and incorporate this function within compliant transmission systems design to minimize the response to externally induced vibrations via harmonic base excitations.

“Utilizing topology optimization to design compliant transmission systems which simultaneously mitigate the effects of external unwanted vibrations.”

An objective function which is computationally convenient and solves the presented issues will be outlined in chapter 6. The case study examined in this thesis will consider the design of a compliant inverter mechanism which is disturbed by a harmonic base excitation, with the objective being to ensure that the displacements within the obtained mechanism resulting from the applied disturbances are minimized. The specific problem will be outlined in chapter 7, and the remaining part of this chapter will outline the scope of this thesis.

Scope

The design problem, which will be defined in chapter 7, is quite complex in nature. To solve this problem, the modular topology optimization framework called pyMOTO [80], developed by Stijn Koppen and Arnoud Delissen, is used. This framework allows for quick and easy changes to an optimization problem, and a more detailed explanation of the working principle of pyMOTO is provided in Appendix E.

The optimization problems which can be solved for, however, are not limitless. A scope, therefore, has to be set to determine what is achievable and what is not. First of all, the case study will be defined as a harmonic problem, and the resulting displacements and their derivatives are defined in the frequency domain. This eliminates the need for computationally costly time integrations, as only the steady-state solution will be considered. For this same reason, the case study will only consider two dimensions, which is sufficient to provide a proof of concept. As for the compliant mechanisms, the focus lies on compliant mechanisms which have a range of motion that is considerably smaller than their respective dimensions, which are also called short stroke compliant mechanisms [54]. These assumptions yield a linear elastic harmonic system with small displacements and rotations and, consequently, small strains. Furthermore, these assumptions also allow for the use of superposition principles mentioned in section 4.2, such that an excitation $f_{\text{tot}}(\omega) = f_1(\omega) + f_2(\omega)$ will result in displacement $x_{\text{tot}}(\omega) = x_1(\omega) + x_2(\omega)$.

Even though the problem is defined harmonically to reduce complexity, the frequency domain also has its limits. The most common material used in literature is steel with a Young's modulus of E=200GPa and density ρ=7800 kgm^3. Given an arbitrary steel plate of dimensions 20x10 cm clamped on two edges, the resulting first three eigenfrequencies for the initial uniform structure become 1718 Hz, 3375 Hz and 3549 Hz, respectively. In literature, however, larger sizes are more commonly used, such as 2x1 m. This results in the first three eigenfrequencies of 172 Hz, 338 Hz and 355 Hz. As the eigenfrequencies of the optimized structures will be lower than the initial structure, the range of frequencies considered in this thesis will, therefore, mostly concern frequencies below $2000 Hz$.

6

Methods to fill the research gap

As was mentioned in chapter 5, a new objective function is needed which is capable of optimizing structures subjected to both force and base excitations whilst also being unaffected by the excitation frequency issues mentioned in chapter 4 which result in structures with a large number of intermediate densities. An objective function which satisfies all of these requirements was introduced by Montero et al. [37]. In this chapter, the proposed advantages of this objective function are given together with its derivation. Next, as this thesis will utilize this objective function in a different manner from Montero et al. [37], a thorough examination is performed of the behaviour of this objective function in order to establish which parameter values are required for the final case study.

6.1. Density-Weighted norm objective formulation

The proposed objective function makes use of the resulting displacements in the structure, which means that the objective function is independent of the applied harmonic excitation. The displacements resulting from the excitation, however, can have both positive and negative values and might switch from iteration to iteration. This is undesired as the optimizer will struggle with continuously switching from positive to negative values. A function which is always positive is the absolute value, which defines the magnitude of a displacement, without its direction. This is also convenient as the resulting displacements of harmonic excited structures, which include damping, are complex values. For an arbitrary degree of freedom j, the absolute value of the complex displacement u_j is given in equation 6.1.

$$|u_j(\omega)| = \sqrt{u_j(\omega)^2_{\text{real}} + u_j(\omega)^2_{\text{imag}}} = (u_j^*(\omega)u_j(\omega))^{\frac{1}{2}} \tag{6.1}$$

where u_j^* denotes the complex conjugate. In a given structure, however, the location of the degree of freedom with maximum displacement at the specified excitation frequency, or in other words, the dominant mode, varies from iteration to iteration. If the objective is to minimize the displacements in the entire structure, the formulation above can be expanded in order to incorporate all the degrees of freedom in the structure with the use of a norm function as given in equation 6.2.

$$\|\mathbf{u}\|_m(\omega) = \left(\sum_{i=1}^{n} |u_j(\omega)|^m\right)^{\frac{1}{m}} \tag{6.2}$$

For a single degree of freedom, this norm function has no influence. When all degrees of freedom of the structure are taken into account, however, the parameter m will influence the outcome of this function based on the magnitude of the displacements of each degree of freedom. If, at a given frequency, there is one degree of freedom u_k, which has the largest displacement, the rest of the displacements will naturally have lower values. If these are taken to the power m, the larger displacement u_k will exponentially rise above the other displacements and eventually for $m \rightarrow \infty$:

$$\|\mathbf{u}\|_\infty(\omega) \approx |u_k(\omega)| \tag{6.3}$$

This way, the objective function accounts for the shifting locations of the degree of freedom of maximum displacement. This function is, however, not limited to only a single degree of freedom or all degrees of freedom in the system, and therefore, a subset S can be defined in order to allow for selection of degrees of freedom. This results in the norm function defined as N_m given in equation 6.4.

$$N_m(\mathbf{u}(\omega)) = \left(\sum_{j \epsilon S} \left(u_j^*(\omega) u_j(\omega) \right)^{\frac{m}{2}} \right)^{\frac{1}{m}} \tag{6.4}$$

In order to visualize how this objective function performs, the frequency response of an arbitrary simple two-degree of freedom system can be examined. Taking the stiffness matrix, mass matrix, damping matrix and force vector as:

$$\mathbf{K} = \begin{bmatrix} 300 & -200 \\ -200 & 200 \end{bmatrix}, \quad \mathbf{M} = \begin{bmatrix} 2 & 0 \\ 0 & 1 \end{bmatrix}, \quad \mathbf{C} = 0.4264\mathbf{K} + 0.004264\mathbf{M}, \quad \mathbf{f} = \begin{bmatrix} 0 \\ 10 \end{bmatrix} \tag{6.5}$$

respectively. In figure 6.1a, the frequency response of the magnitudes of the displacements of both degrees of freedom is plotted, together with the norm function N_m for the value of m=2. In figure 6.1b, the same frequency response is given, this time with the norm function for m=12.

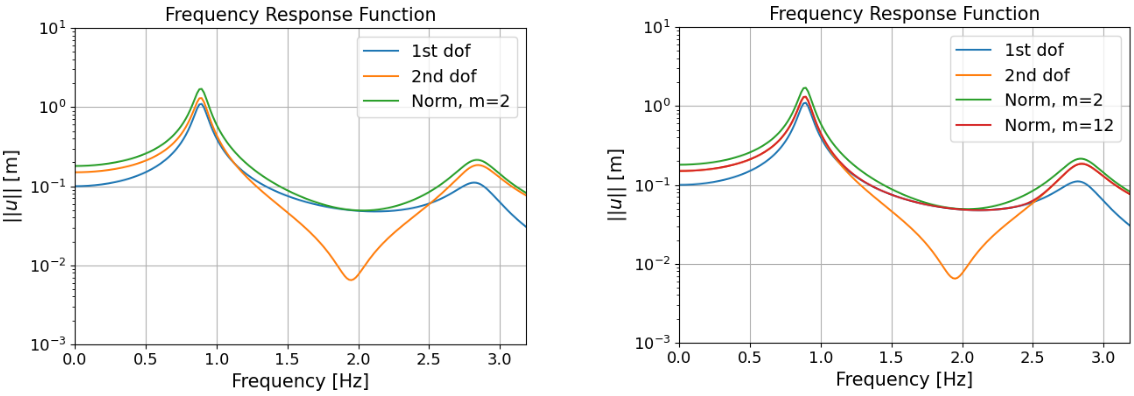

(a) m=2

(b) m=12

Figure 6.1: The frequency responses for the two degrees of freedom of the system given in equation 6.5, together with the norm function response for two different values of the parameter m.

From these responses, one additional benefit of this objective function directly becomes clear: the proposed objective function does not contain any anti-resonances. For every frequency the system is excited at, both degrees of freedom in the system have a displacement response. The magnitude of these responses varies for every frequency, but one of the two always displays a higher magnitude than the other. What the norm function tries to achieve, is to represent the frequency response of the system for each of these dominant magnitude values. This means that where the second degree of freedom presents an anti-resonance, the first degree of freedom does not, and the norm function will follow this response as it is the dominant response at this magnitude. This results in anti-resonances not being present in the frequency response.

Figure 6.1a does, however, show that the norm function does not exactly represent the frequency response and is only an approximation of the true response. Increasing the parameter m to the value of 12, however, gives the resulting function shown in figure 6.1b, which is a much better approximation. The value of the parameter m, therefore, represents the extent to which the true system is approximated. Larger values of m do seem to be advantageous from these results, but this is not necessarily true when this function is used in a topology optimization. These large values of m introduce quite some non-linearity into the system, which may lead to numerical instabilities. These can, in turn, actually decrease accuracy or lead to unwanted topologies, for example, in the form of asymmetric topologies where symmetry is expected. Therefore, for each problem for which this function is utilized, the appropriate value of the parameter m must be determined individually.

For topology optimization considering vibrating structures, a common issue which might occur is found in the behaviour of the void regions. As these regions have almost negligible stiffness, they can present very high displacements. If the goal is to minimize the overall or global displacements of the system, these low-density high-displacement areas could become the focus of the optimizer, which will work to minimize the displacements of these regions by adding material, which then results in less severe displacements. These less severe displacements, however, do not contribute enough to the objective to become relevant and have more material added to the accompanying elements, resulting in a loop where the optimizer gets stuck on choosing which region to optimize for, which in turn results in areas with intermediate densities, also known as 'grey areas'. A similar issue might occur for maximization problems, where the very high displacements might be considered beneficial for the optimizer, and the optimization is ended prematurely.

In order to suppress the displacements of void regions, Montero et al. [37] suggest adding a weight to each of these displacements based on the density values of the surrounding elements. This way, the displacements of the degrees of freedom which are surrounded by void regions, or low-density regions, receive lower weights than those surrounded by regions with material or high-density regions. The formulation given in equation 6.4 can therefore be altered with by incorporating a density weight a_j, as given in equation 6.6.

$$N_{mw}(\mathbf{u}(\omega)) = \left(\sum_{j \epsilon S} \left(u_j^*(\omega) a_j u_j(\omega) \right)^{\frac{m}{2}} \right)^{\frac{1}{m}}, \tag{6.6}$$

where the weight a_j is defined by:

$$a_j = \left(\sum_{v \epsilon S_j} x_v^w \right)^{\frac{1}{w}} \tag{6.7}$$

In equation 6.7, a similar norm function to equation 6.2 can be found, this time being a w-norm function. S_j is a subset which represents the elements surrounding a degree of freedom j. x_v then represents the value of the design variable x_e of one of the surrounding elements. With this function, the weight a_j is defined by the w-norm of the surrounding element densities, or in other words, a density-weighted filter. To provide a better understanding of how this density-weighted filter works, a visual representation is given in figure 6.2.

(a) Surrounded by solid elements

(b) Surrounded by void elements

Figure 6.2: A visualization of the area of elements considered for the density-weighted filter weight a_j. Two examples are given, one where the node is surrounded by solid elements and one where the node is surrounded by void elements.

In figure 6.2a, an arbitrary finite element grid is given, with a diagonal of non-void density elements. If the degree of freedom of interest j is located on the node represented in black, the subset S_j is defined by the yellow region. This region contains the elements directly surrounding the degree of freedom j. As can be noted, the weight for both degrees of freedom of any node will be identical. The resulting weight for this region will be determined by the density of these elements, and as material is present, the weight will be relatively high and the displacement of this degree of freedom will be relevant for the objective function. If the degree of freedom of interest j is surrounded by void elements as shown in figure 6.2b however, the resulting weight a_j will be relatively low due to the low-density values of the surrounding elements, which in turn results in the displacements of this degree of freedom being less relevant for the objective function. What the parameter w in equation 6.2 represents is the penalization factor of these element density values. As the value of w increases, the weights a_j for a degree of freedom j become lower for degrees of freedom surrounded by low-density elements and similarly higher for those in high-density element regions.

The values N_{mw} obtained from equation 6.6, however, can vary tremendously in terms of orders of magnitude during the optimization. This also results in large differences in the orders of magnitude of the sensitivities, which will be difficult for the optimizer to deal with as the differences in sensitivities might become negligible. In order to prevent this behaviour, a logarithmic scaling can be applied to the objective function to allow for these small differences to be manageable. The applied operation to achieve this scaling is given in equation 6.8. For the experiments which will be done later in this chapter, a value of c_0=100 was found to be sufficient.

$$N_{mwdB} = c_0 + 10\log_{10}(N_{mw}) \tag{6.8}$$

As will be seen later in this section, the objective function above allows for a topology which is disconnected from the defined boundaries. Therefore, an additional component is added, which is static compliance. To define static compliance, some generalized system definitions can be set up first. For any system excited by a certain force at a certain frequency ω, the force vector can be defined as:

$$\mathbf{f} = \boldsymbol{\lambda}(\omega)\hat{f}, \tag{6.9}$$

where $\hat{f}$ represents the magnitude of the force, and $\boldsymbol{\lambda}(\omega)$ represents a directional unit vector with accompanying excitation frequency ω. For a static case, or in other words, ω=0, this is represented by $\boldsymbol{\lambda}(0)$. This same principle can be extended to the system matrices, where the stiffness matrix can be given by (section 4.2):

$$\mathbf{K}(\mathbf{x},\omega) = \mathbf{K}(\mathbf{x}) + j\omega\mathbf{C}(\mathbf{x}) - \omega^2\mathbf{M}(\mathbf{x}), \tag{6.10}$$

For any $\omega \neq 0$ the stiffness matrix is equal to the so-called 'dynamic stiffness matrix', and for ω=0, this definition results in the static stiffness matrix $\mathbf{K}(\mathbf{x},0) = \mathbf{K}(\mathbf{x})$. Respectively, these matrices can be used to obtain the dynamic displacements $\mathbf{u}(\omega)$ and static displacements $\mathbf{u}(0)$ With these terms covered, the static compliance can be defined as:

$$C_S = \mathbf{u}^T(0)\mathbf{K}(\mathbf{x},0)\mathbf{u}(0) = \mathbf{u}^T(0)\boldsymbol{\lambda}(0)\hat{f} \tag{6.11}$$

With the static compliance defined, the complete objective function can be formulated. As the order of magnitude of the density-weighted norm function and the static compliance can vary substantially, they are normalized by their initial values N^0_{mwdB} and C^0_s, respectively. Lastly, two weight factors γ_1 and γ_2 are incorporated into the objective formulation. These are used to define the contribution of the static compliance to the objective and satisfy $|\gamma_1| + \gamma_2 = 1$. It can be noted that the absolute value of γ_1 is used for the satisfaction criteria. This is due to the fact that this value can also be negative, which transforms the objective of this formulation entirely. Instead of the norm function being minimized, it will instead be maximized (in other words, the negative will be minimized) whilst still minimizing the static compliance. The full formulation is given by:

$$\begin{aligned}
\min_{\mathbf{x}}: \quad & N_{\text{tot}}(\mathbf{x}) = \gamma_1 \frac{N_{mwdB}(\mathbf{x})}{N^0_{mwdB}(\mathbf{x})} + \gamma_2 \frac{C_S(\mathbf{x})}{C^0_S(\mathbf{x})} \\
\text{subject to}: \quad & V(\mathbf{x}) \leq \bar{V} \\
& 0 \leq \mathbf{x}_{\min} \leq \mathbf{x} \leq 1 \\
\\
\text{with } \mathbf{u}(\omega) \text{ obtained from}: \quad & \mathbf{K}(\mathbf{x},\omega)\mathbf{u}(\omega) = \boldsymbol{\lambda}(\omega)\hat{f}
\end{aligned} \tag{6.12}$$

With the objective function formulated, its behaviour can be examined. Montero et al. [37] studied the cases of global minimization and local maximization for a harmonic force excited system. Local minimization was not covered under the premise of not wanting other regions of the domain to exhibit large displacements in order to minimize displacements in the region of interest. This exact principle, however, covers areas such as vibration isolation and dynamic balancing mentioned in section 2.2.4. The interest of this thesis will, therefore, be to investigate the applications of both global and local minimizations of a compliant mechanism design domain disturbed by harmonic base excitations.

6.2. Parameter study

To determine how the proposed objective function can be used in the final case study, a parameter study will have to be conducted, which expands on the research of Montero et al. [37] in order to study the behaviour of this objective function. The goal will be to first confirm the behaviour found by Montero et al. [37] and then check whether the ability to obtain well-defined topologies for high frequencies without premature convergence or a large number of intermediate densities still persists for local minimization.

As the investigation is quite extensive, the entire study can be found in Appendix B, and this section will only provide a discussion of the results. The load cases which are used for global minimization of the force and base excited case are given in figure 6.3. It can be noted that an additional load case is required for static compliance in both cases.

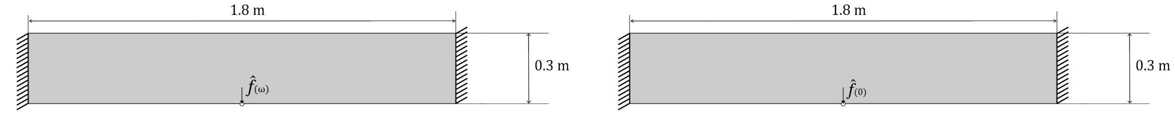

(a) Force excitation load case 1 (b) Force excitation load case 2

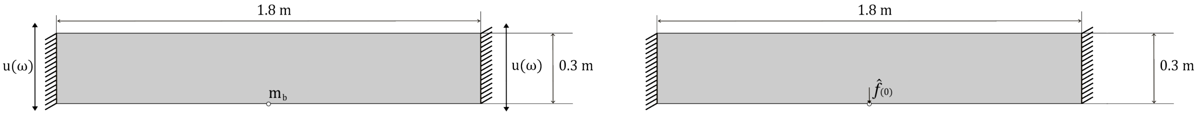

(c) Base excitation load case 1 (d) Base excitation load case 2

Figure 6.3: The load cases required to solve for the global minimization of a double-clamped beam structure under a force and base excitation.

As for the used material interpolation functions, a study was done on what function would perform best in terms of intermediate density occurrence for both the force and base excited case. This study can be found in Appendix C and yielded that the Polynomial Interpolation Scheme (PIS) (equation 3.16) is preferred for the stiffness interpolation, and standard SIMP (equation 3.9) for the mass interpolation.

6.2.1. Global minimization

Global minimization for both the force-excited and base-excited systems yielded well-defined results for a large range of frequencies. It was found that the parameter γ_1, which determines the amount of contribution that the static compliance has to the final result, is a necessary part of the objective function, as was found when setting the value of γ_1 to 1.0, which yielded a structure which was disconnected from the base. The values of γ_1=0.90, 0.95 and 0.99 provided a clear distinction on this influence. For the parameter w, or the density-weighted filter, it was found that its inclusion in global minimization provides the benefits of yielding structures with little to no intermediate densities present for frequencies up to 1721Hz and 2947Hz for the force excited and base excited case, respectively as can be seen in figure 6.4 for γ_1=0.95. As for its appropriate value, it was found that any w is valid, which results in the simplest choice of w=1. One thing which was required however, was a forced symmetry over the y-axis in order to prevent the optimizer from yielding asymmetric designs.

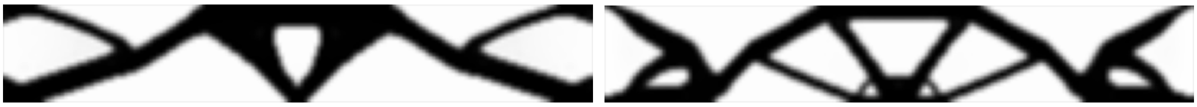

(a) Force excitation, ω_{exc}=1721Hz (b) Base excitation, ω_{exc}=2947Hz

Figure 6.4: The resulting topologies for the global minimization under both force excitation and base excitation of the design domain given in figure 6.3 for their respective highest frequency of interest and γ_1=0.95.

In the previous section, it was determined that a larger value of m would allow for a better approximation of the actual system. In this study, however, contradicting results were found for the force-excited case and the base-excited case. The force excited case did indeed improve for larger values of m, but showed diminishing returns for $m \geq 2$. The base excited case, on the other hand, seemed to show better performance for lower values of m. For global minimization, the parameter m was therefore suggested to be set at m=2.

6.2.2. Local minimization

The influence of the density-weighted norm objective function on local minimization subjected to force and base excitations was explored for two subsets: a single degree of freedom and an area of interest L. The single degree of freedom considers the vertical degree of freedom of the mass point m_b given in figure 6.3c.

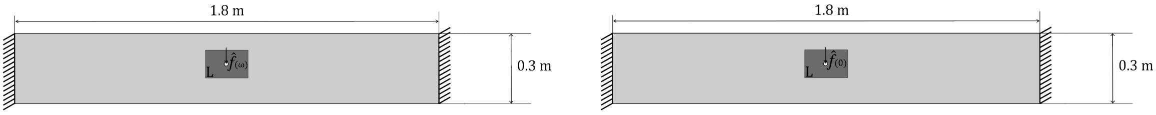

(a) Force excitation load case 1 (b) Force excitation load case 2

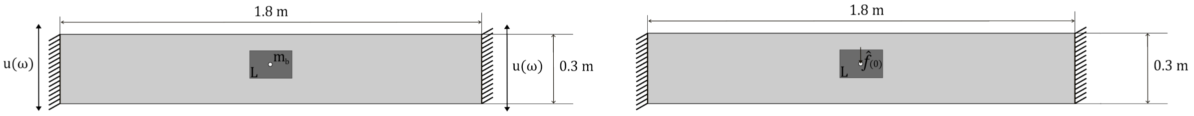

(c) Base excitation load case 1 (d) Base excitation load case 2

Figure 6.5: The load cases required to solve for the local minimization of a double-clamped beam structure under a force and base excitation. The second

For force-based local minimization, the density-weighted filter's impact was found to be negligible for both cases, leading to its removal (w=0) across all experiments. While the density-weighted filter played a significant role in preventing intermediate density regions in global minimization, static compliance contribution seemed more important for force-based local minimization. Specifically, it was observed that a lower static compliance contribution (γ_1=0.99) led to topologies with intermediate density regions. As for the parameter m for force-based local minimization, this had no impact on a single degree of freedom by definition, and its influence on a local area was also limited, resulting in the choice for m=2.

In the case of a single degree of freedom, all results exhibited an anti-resonance present at the excitation point matching the excitation frequency, which is similar behaviour to what was found in section 4.6. In this case, however, all results converged and yielded well-defined topologies due to the static compliance contribution. For an area L, low excitation frequency results exhibited collective anti-resonance behaviour among the degrees of freedom within the area; this effect diminished at higher frequencies, however, due to the modes becoming more complex. Nevertheless, other regions of the domain still displayed larger displacements in order to minimize those of the area of interest.

Similarly, for base excitation-based local minimization, the density-weighted filter (w=0) yielded limited impact, while parameter m exhibited different behaviour compared to the force-excited case. Although response measurements at the point of interest did not vary significantly, higher values of m resulted in the second eigenfrequency ω_2 moving further from the excitation frequency. This behaviour diminished quickly for $m \geq 4$, however, and therefore the choice was made for m=4.

For a single degree of freedom, the resulting topologies contained large amounts of intermediate densities, except at the lowest examined frequency of 340Hz. Surprisingly, increasing the static compliance contribution did not remedy this issue, unlike in the force-excited case. For an area L, the results were a lot more defined but still contained intermediate-density members. Both subsets demonstrated minimized results across all frequencies, however, with higher values of γ_1 correlating with improved frequency performance. Figure 6.6 shows two examples for the minimization of the area of interest L for the highest frequencies of 1721Hz and 2947Hz for force-based and base excitation-based excitations, respectively.

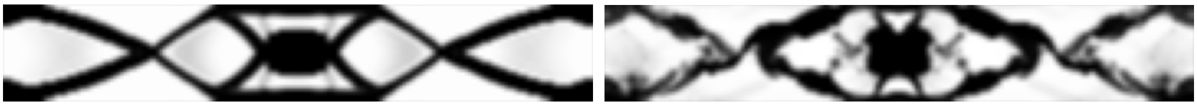

(a) Force excitation, ω_{exc}=1721Hz

(b) Base excitation, ω_{exc}=2947Hz

Figure 6.6: The resulting topologies for the local minimization under both force excitation and base excitation of the design domain given in figure 6.3 for their respective highest frequency of interest and γ_1=0.95.

6.2.3. Conclusions

Overall, the force-excited global minimization case yielded results which were similar to those found in Montero et al. [37], confirming the observations found by Montero et al. Base excited global minimization also showed similar results, only with slightly different behaviour. As for the extension to local minimization, an area of interest appears necessary in order to obtain results which are limited in the number of intermediate densities they present, specifically for the base excited case. To investigate this further, the final case study will include more than one size of the area of interest in order to assess its influence.

7

Case studies

As mentioned in chapter 5, the case study for this thesis will consider the design of a compliant mechanism, specifically an inverter mechanism, which is disturbed by a harmonic base excitation. The aim is to obtain an inverter mechanism which is capable of achieving desired inverting behaviour, whilst presenting a minimized displacement response resulting from an applied harmonic base excitation at a specified frequency.

To achieve this goal, several intermediate steps will be taken, which will allow for a comparison of the resulting topologies. First, an inverter mechanism will be designed within a smaller domain than the proposed case study. The unused part of the full domain for this step can then be used in the next step to design an isolator which minimizes the displacements at the connection points of the obtained mechanism. These two steps consider the process of 'classical' mechanism design, where a mechanism is designed, after which a separate isolator is constructed, which is connected to the design in order to minimize disturbances.

Next, the formulation introduced in chapter 6 will be used to perform a combined optimization, where a mechanism is obtained which contains the inherent property of minimized displacements at a specified frequency. This will be done by first designing a static mechanism for the full-sized domain, which can be used to identify a selection of frequencies of interest. Lastly, the principles of global and local minimization subjected to a base excitation are utilized in order to obtain the final optimized mechanisms to complete this case study.

7.1. Step 1: Stitched mechanism

The first step consists of two intermediate steps, which are the design of the mechanism and the design of the isolator. After these designs are obtained, they can be stitched together to form the full domain mechanism, which can be examined in order to see whether the desired minimized vibration behaviour is achieved.

7.1.1. Step 1a: Mechanism design

Section 4.1 outlined the currently used methods of designing an inverter mechanism using topology optimization, where the presented designs considered a one on one inversion. For this case study, the magnitude of the actual inversion, or in other words, the obtained geometrical advantage, will be a performance indicator but will not be the goal itself. This is due to the fact that the steps, which include the density-weighted norm function, will incorporate a weighted objective function where the static performance of the mechanism might be altered in order to improve dynamic performance. Therefore, the most important aspect is to obtain a mechanism which exhibits an inverted output direction. To outline the problem formulation for this step, the design domain and accompanying load cases are visualized first and provided in figure 7.1. For this visualization and all subsequent visualizations, the threshold is set at a design density of 0.48 unless mentioned otherwise. This will take into account some of the contours created by the density filter.

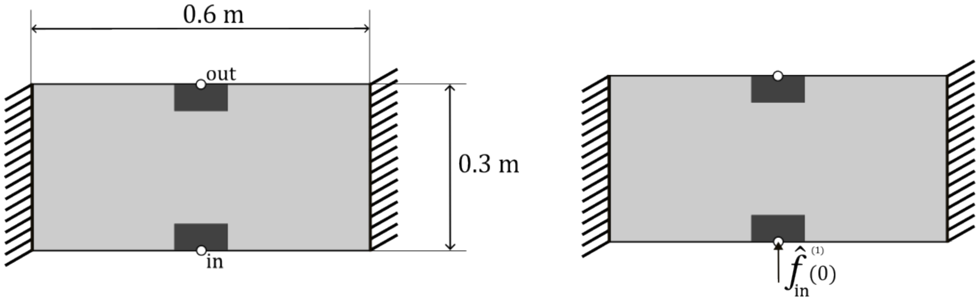

(a) Design domain

(b) Load case 1

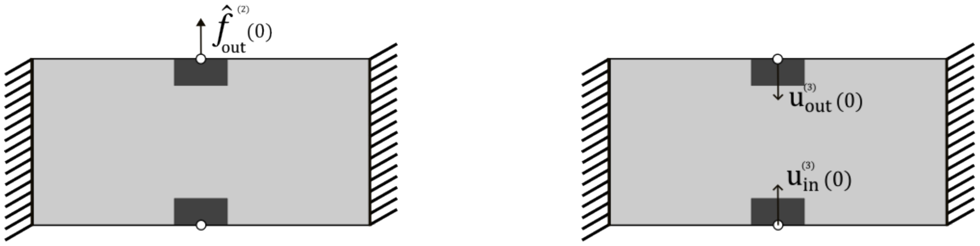

(c) Load case 2

(d) Load case 3

Figure 7.1: The design domain and three load cases required to solve the optimization problem for step 1a of this case study as given in equation 7.1.

The design domain is defined by a rectangle of 0.6 × 0.3m, with the thickness of the domain set at 0.01m. The domain is constrained at both the left and right boundary in all directions, and the input and output locations are marked. The black rectangles represent a non-design domain, which will be needed later once the base excitations are introduced, considering the results of section B.5. The first load case only considers a force on the input of the domain, and the second load case only a force on the output. The magnitudes of these of these forces are set at a similar value of 1kN. The accompanying displacements are also provided in these figures and are not to be confused with prescribed displacements. The third load case specifies the desired displacement directions for this problem, which in this case is set at $\boldsymbol{v} = [u_{\text{in}}^{(3)}, u_{\text{out}}^{(3)}] = [1, -2]$. The value of the output displacement is set higher than the input displacement in order to account for the strain energy stored in the structure when actuated as was also mentioned in section 4.1.1.

With the design domain specified, the optimization formulation can be constructed. The superscripts $^{(1)}$, $^{(2)}$ and $^{(3)}$ represent the first, second and third load cases, respectively, as given in figure 7.1.

$$
\begin{aligned}
\min_{\mathbf{x}}: \quad & C_{\text{in}}^{(1)} + C_{\text{out}}^{(2)} \\
\text{subject to}: \quad & C_{v}^{(3)} \leq \bar{C}_{v} \\
& V(\mathbf{x}) \leq \bar{V} \\
& 0 \leq \mathbf{x}_{\text{min}} \leq \mathbf{x} \leq 1
\end{aligned}
\tag{7.1}
$$

The objective of this minimization is to minimize the force-based compliances $C_{\text{in}}^{(1)}$ and $C_{\text{out}}^{(2)}$ of the input and output respectively, whilst simultaneously constraining the compliance of the motion pattern of the desired geometrical advantage. This formulation allows for the maximization of the stiffness of the input and output locations whilst satisfying the desired geometric advantage and accompanying maximum stiffness of this deformation pattern, all for a given amount of material usage. The definitions of the compliances in equation 7.1 are given in equation 7.2.

$$
\begin{aligned}
C_{\text{in}}^{(1)} &= \mathbf{f}_{\text{in}}^{(1)} \cdot \mathbf{u}_{\text{in}}^{(1)} \\
C_{\text{out}}^{(2)} &= \mathbf{f}_{\text{out}}^{(2)} \cdot \mathbf{u}_{\text{out}}^{(2)} \\
C_{v}^{(3)} &= \boldsymbol{v}^{(3)} \cdot \mathbf{K}^{(3)} \boldsymbol{v}^{(3)}
\end{aligned}
\tag{7.2}
$$

As for further domain properties, the finite element mesh consists of 60×30 4-node quadrilateral elements, the density-filter radius is set at 2 and the desired volume fraction at 2.0. The material interpolation functions which are used are the Polynomial Interpolation Scheme (PIS) from equation B.1 for the stiffness interpolation and the standard SIMP function from equation 3.9 for the mass interpolation. The mass matrix is not used yet in the optimization for this step, but is used to determine the eigenfrequencies and accompanying eigenmodes of the system. The optimizer used is the MMA optimizer, where the tolerance is set at $1e^{-4}$, and the maximum iterations are limited to 100. Lastly, a minimum value for x_{min}=$1e^{-3}$ is implemented in order to avoid the system matrices from becoming singular. Using the formulation given in equation 7.1, the optimization can be performed, and the resulting topology is given together with a visualization of its vertical displacements done in ParaView in figure 7.2.

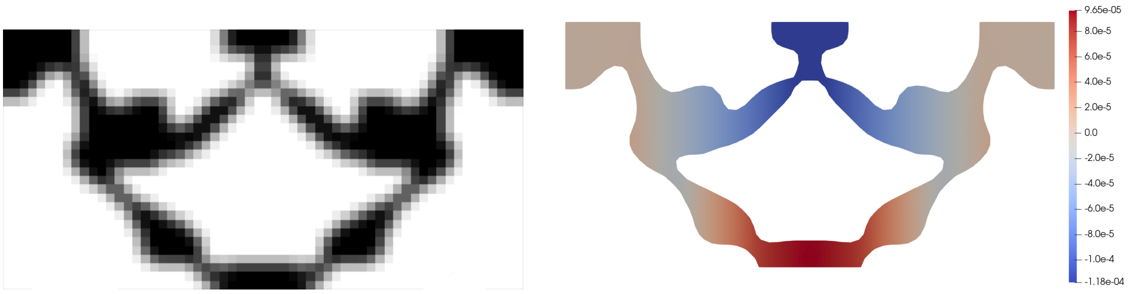

(a) Resulting topology

(b) Vertical displacements of the mechanism visualized in ParaView

Figure 7.2: The resulting topology of the inverter optimization problem given in equation 7.1 together with a visualization done in ParaView of the vertical displacements resulting from the applied static input force which confirms the working inverting function.

As can be seen from these results, a mechanism is obtained that exhibits the desired inverting motion behaviour. Specifically, if a force of 1kN is applied to the input port, the accompanying input displacement and resulting output displacement values in table 7.1 are obtained.

Property	Value	
u_{in}	$9.6473e^{-5}$	[m]
u_{out}	$-1.1745e^{-4}$	[m]
GA	-1.2175	[-]

Table 7.1: An overview of the values of the respective input and output displacements resulting from the applied input force for the topology given in figure 7.2a together with the obtained geometrical advantage.

Next, the eigenmodes of the obtained resulting topology can be analyzed in order to determine its frequency behaviour. If an eigensolve is performed on the resulting structure, the eigenfrequencies can be obtained, of which the first four are given in table 7.2.

Computed Eigenfrequencies	ω_1	ω_2	ω_3	ω_4
	394Hz	397Hz	846Hz	1222Hz

Table 7.2: An overview of the first four computed eigenfrequencies of the resulting topology given in figure 7.2a

As seen in chapter 6, not all eigenmodes will have influence in the direction of interest. In this case, the desired inverting occurs in the vertical direction, and as such, the vertical directions of the eigenmodes are of interest. To visualize the four eigenmodes which accompany the eigenfrequencies given in table 7.2, their vertical displacements are given in figure 7.3.

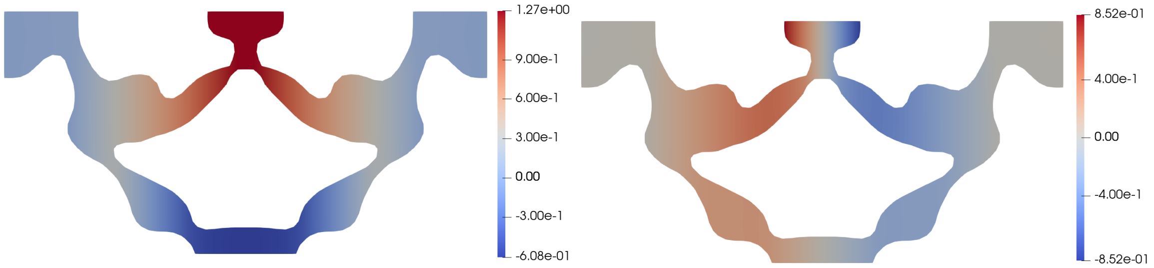

(a) $\omega_1 = 394$Hz (b) $\omega_2 = 397$Hz

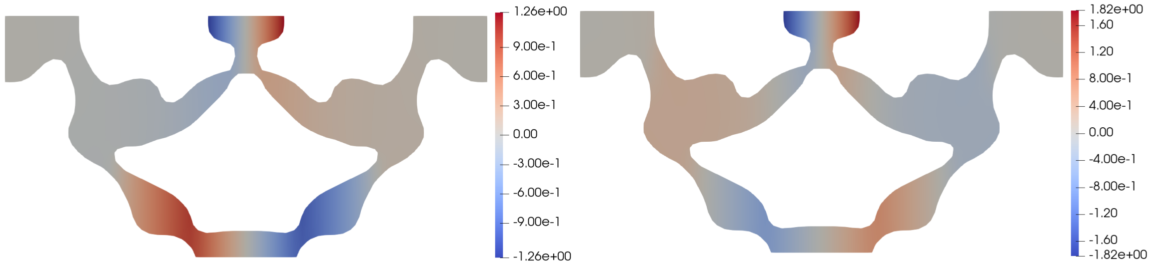

(c) $\omega_3 = 846$Hz (d) $\omega_4 = 1222$Hz

Figure 7.3: A ParaView visualization of the vertical displacements within the obtained structure for the first four eigenmodes of which the respective eigenfrequencies are given in table 7.2.

From this visualization, it is clear that only the first eigenfrequency of this subset affects the vertical displacements of the input and output. This will affect the displacement output of the mechanism, which therefore makes it a frequency of interest. to confirm this, a harmonic base excitation with a magnitude of $100 m/s^2$ is applied to the vertical degrees of freedom of the boundaries. The resulting frequency response of the vertical displacements of the input and output is given in figure 7.4, together with a visualization of the vertical displacements of the mechanism when excited by the base excitations at the first eigenfrequency.

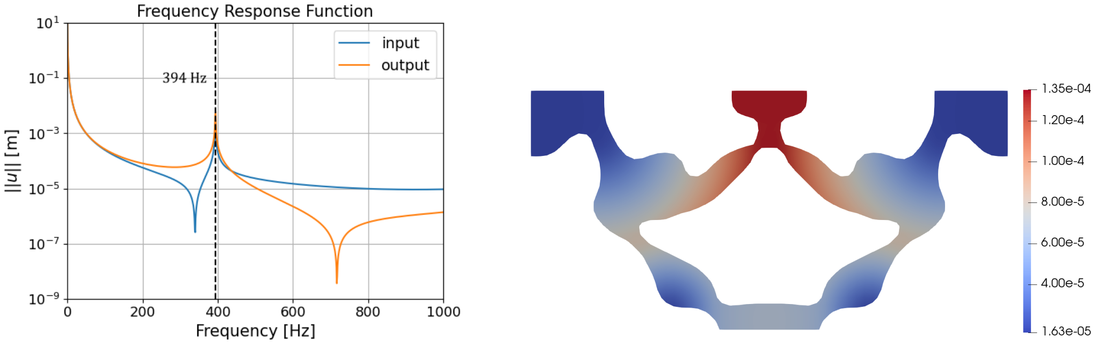

(a) Frequency response of the vertical displacements of the input and output

(b) Vertical displacement response of of the mechanism at the first resonance frequency of 394Hz

Figure 7.4: The frequency response of the respective vertical displacements of the input and output together with a visualization of the displacement response of the structure resulting from the applied base excitation at the first resonance.

From the frequency response, it is clear that the first resonance indeed contains large displacements of the input and output of the mechanism, with the output having larger displacements than the input. This is confirmed by looking at the vertical displacements in figure 7.4b, where the displacements given in table 7.3 are obtained.

For this first step, the objective will, therefore, be to minimize the response to the base excitations at the input and output port by designing for this first resonance of 394Hz specifically. This will be done in the next step by designing an isolator for this frequency of interest.

ω_{exc}=394Hz	Response	
u_{in}	$6.5345e^{-5}$	[m]
u_{out}	$1.3259e^{-4}$	[m]

Table 7.3: An overview of the values of the respective input and output displacements resulting from the applied base excitations.

7.1.2. Step 1b: Isolator design

The next step is to develop an isolator for the mechanism obtained in the previous step. This isolator however, is designed considering only the boundaries to which the mechanism is attached. This means that the isolator which is designed is technically independent of the already-designed mechanism. What will, however, be taken into account is the connection boundary and the mass of the mechanism, which are determined by the dimensions and volume fraction used in the previous step.

The design domain which is used is the same 0.6 × 0.3m rectangle, which results in a 1.8 × 0.3m domain once the isolator is connected to the obtained mechanism at both sides. The left boundary is, therefore, constrained in both directions, while the right boundary is left unconstrained. The domain is provided in figure 7.5, together with the two load cases which are used for this problem. The first load case contains the applied base excitation, which is an acceleration excitation of 100 m/s^2 to the left boundary in the vertical direction. Furthermore, it can be noted that a non-design domain is added to the upper right side of the domain in order to provide a base to which the mechanism from figure 7.2a can connect. This non-design domain is also given a distributed mass m_{m}, which represents the mass of the obtained mechanism. This mass is obtained using the dimensions of the domain of step 1 multiplied by the used density and volume fraction. As the density-weighted norm function from chapter 6 is used for this problem, a static compliance load case is required, and as such the second load case contains two forces added in the upper right corner, which represent the forces exerted by the mechanism when actuated, in order to provide the static stiffness contribution. Lastly, other properties considering material interpolation functions and optimizer settings are kept similar as well.

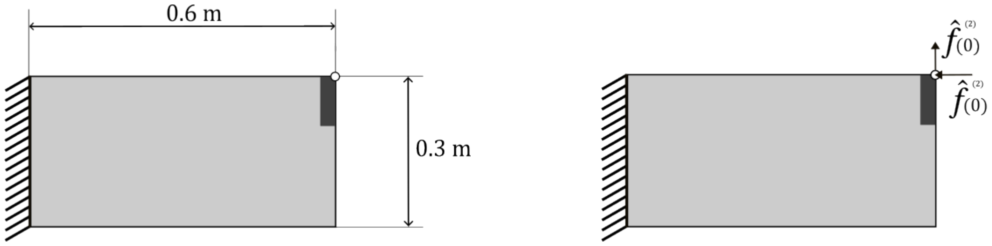

(a) Design domain

(b) Load case 1

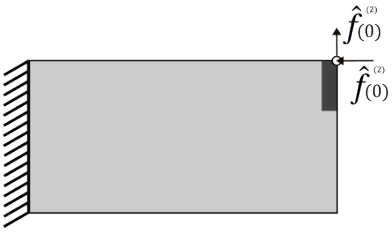

(c) Load case 2

Figure 7.5: The design domain and two load cases required to solve the optimization problem for step 1b of this case study as given in equation 7.3.

As already mentioned, this problem will make use of the density-weighted norm function, specifically in a local minimization sense. The local area to be minimized is the non-design domain shown in figure 7.5. The appropriate parameters w and m for local minimization subjected to a base excitation of an area L were determined in section B.5 to be w=0 and m=4 respectively. For this case study, the static compliance factor γ_1 is set at 0.95, which is adequate for a lower excitation frequency such as 394Hz as examined in section B.5. The formulation for this problem is given in equation 7.3.

$$\begin{aligned} \min_{\mathbf{x}} : \quad & \gamma_1 \frac{N_{mwdBL}(\mathbf{x})}{N^0_{mwdBL}(\mathbf{x})} + \gamma_2 \frac{C_S(\mathbf{x})}{C^0_S(\mathbf{x})} \\ \text{subject to} : \quad & V(\mathbf{x}) \leq \bar{V} \\ & 0 \leq \mathbf{x}_{\min} \leq \mathbf{x} \leq 1 \end{aligned} \tag{7.3}$$

Using this formulation, the optimization can be performed. The previous step determined the frequency at which this isolator is to be designed, which was determined to be 394Hz. Using this frequency, the resulting topology is given together with a visualization of its vertical displacements done in ParaView in figure 7.6.

(a) Resulting topology

(b) Vertical displacements of the obtained isolator visualized in ParaView

Figure 7.6: The resulting topology of the inverter optimization problem given in equation 7.3 together with a visualization done in ParaView of the vertical displacements resulting from the applied base excitations.

The resulting structure exhibits larger displacements in other areas in order to minimize the displacements in the area of interest. This is in line with the results found in section B.5. Specifically, the vertical displacements at the connection point are reduced to $2.0140e^{-6}$ m under the applied base excitation. In the next step, the obtained mechanism and isolator will be combined in order to assess their performance.

7.1.3. Step 1c: Stitched design

Finally, the resulting mechanism from step 1a and the isolator from step 1b can be stitched together in order to form the final structure. The resulting topology of this stitching is given in figure 7.7.

Figure 7.7: The structure obtained when the resulting inverter mechanism and isolator of figure 7.2a and 7.6a respectively are stitched together.

Next, the same base excitation with a magnitude of $100 m/s^2$ at the frequency of interest of 394Hz can be applied to this mechanism. A visualization of the resulting vertical displacements is given in figure 7.8.

From the resulting visualization in figure 7.8, it might seem that there are still large displacements present due to the applied base excitations. This is, however, due to the scaling of the colour scale, and the actual results of the displacements of the input and output due to the applied base excitations are given in table 7.4 together with the results of step 1a.

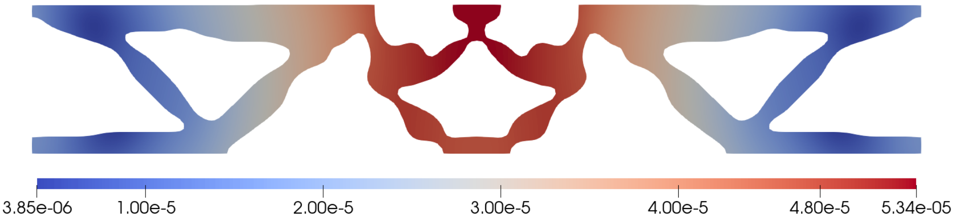

Figure 7.8: A visualization of the resulting vertical displacement magnitudes within the obtained structure under the applied base excitations.

ω_{exc}=394Hz	Step 1a	Stitched	
u_{in}	$6.5345e^{-5}$	$4.6855e^{-5}$	[m]
u_{out}	$1.3259e^{-4}$	$5.3237e^{-5}$	[m]

Table 7.4: A comparison of the values of the respective input and output displacement magnitudes resulting from the applied base excitations for the mechanisms given in figure 7.2a and 7.7 respectively.

It can be seen that there is indeed a minimization of the displacements in the mechanism. It can be argued, however, whether these results are actually comparable, considering the difference in the design domain. As the base excitation is not provided at a similar location, the comparison might be unfair. This is, however, not the largest discussion point for this stitched mechanism. If the same input force of 1kN is applied to this combined mechanism, the inverter property is actually lost. The static displacements resulting from this input force are visualized in figure 7.9.

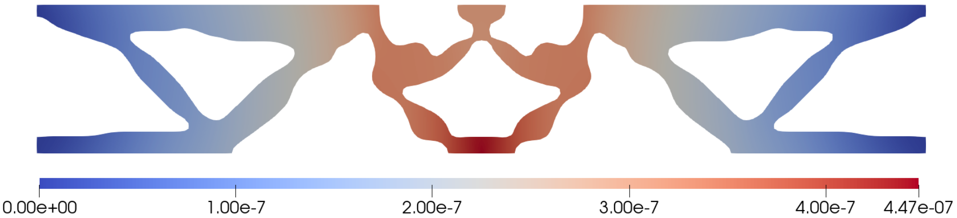

Figure 7.9: A visualization of the displacements within the stitched structure resulting from the same applied static input force as in step 1a.

From this visualization, it seems that the entire mechanism now moves in the positive vertical direction, with no visible inverting direction of the output of the mechanism. This can be confirmed by looking at the resulting vertical displacements of the input and output, which are provided together with the results of step 1a in table 7.5. It can again be argued whether these values are comparable, but the most important part is the lack of negative direction for the output displacement, which indicates a loss in inverter function.

	Step 1a	Stitched	
u_{in}	$9.6473e^{-5}$	$4.4697e^{-7}$	[m]
u_{out}	$-1.1745e^{-4}$	$3.0925e^{-7}$	[m]
GA	-1.2175	0.6919	[-]

Table 7.5: The displacement values of the vertical input and output degrees of freedom resulting from the applied static input force together with the obtained geometrical advantage for both the resulting topology found in step 1a as well as the stitched mechanism of step 1c.

These results show that the method of separately designing an inverter mechanism and an isolator does not necessarily yield the desired results. Whilst the resulting displacements from the applied base excitations might be minimized, the inverting function of the mechanism is lost in the process. A combined formulation is therefore needed, which takes both optimizations into account concurrently. This will be done in the coming steps.

7.2. Step 2: Static mechanism in a larger design domain

In order to provide a comparative basis for the upcoming optimizations, a new static inverter mechanism which spans the full design domain has to be designed. The frequency behaviour of this mechanism will be analyzed, and several frequencies of interest will be chosen which this mechanism will be optimized for. First, the same design domain and load cases from step 1a are modified to accommodate this problem and are given in figure 7.10.

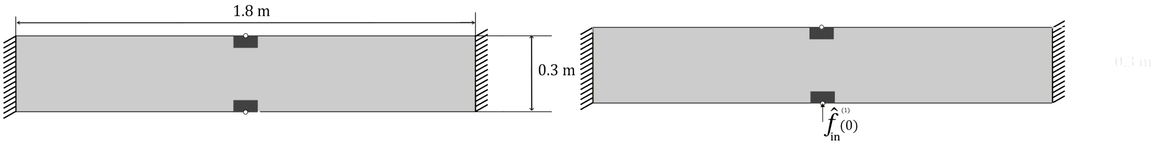

(a) Design domain

(b) Load case 1

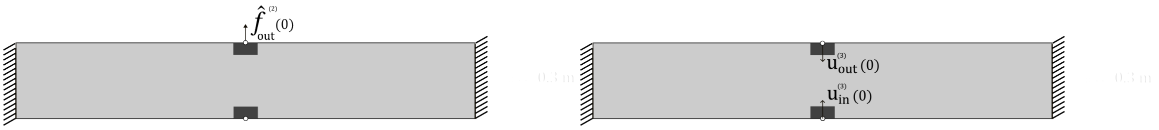

(c) Load case 2

(d) Load case 3

Figure 7.10: The design domain and three load cases required to solve the inverter optimization problem for step 2 of this case study as given in equation 7.4.

This design domain considers the full domain, which is defined by a rectangle of 1.8 × 0.3m, with the thickness of the domain set at 0.01m. The same boundary constraints at both edges are present, and the loads are applied at similar respective locations. Furthermore, the magnitude the applied load is the same 1kN, and the desired displacements directions are again set at $\boldsymbol{v} = [u^{(3)}_{\text{in}}, u^{(3)}_{\text{out}}] = [1, -2]$. The formulation is similar to the one given in 7.1, but this time two extra constraints are added to the input and output compliance. This may seem counter-intuitive given that both these values are minimized, but this will allow for each of the inverters in the coming steps to be comparable as they will all contain similar compliance values. The updated formulation is given in equation 7.4.

$$\begin{aligned}
\min_{\mathbf{x}}: \quad & C^{(1)}_{\text{in}} + C^{(2)}_{\text{out}} \\
\text{subject to}: \quad & C^{(3)}_{v} \leq \bar{C}_{v} \\
& C^{(1)}_{\text{in}} \leq \bar{C}_{\text{in}} \\
& C^{(2)}_{\text{out}} \leq \bar{C}_{\text{out}} \\
& V(\mathbf{x}) \leq \bar{V} \\
& 0 \leq \mathbf{x}_{\min} \leq \mathbf{x} \leq 1
\end{aligned} \tag{7.4}$$

For the mechanism compliance constraint, the value $\bar{C}_v$ is used as in step 1a. Considering now that the design domain is much larger, it is expected that the resulting geometrical advantage will be lower as the larger structure is able to store more strain energy. The definitions of the compliances are again given by:

$$\begin{aligned}
C^{(1)}_{\text{in}} &= \mathbf{f}^{(1)}_{\text{in}} \cdot \mathbf{u}^{(1)}_{\text{in}} \\
C^{(2)}_{\text{out}} &= \mathbf{f}^{(2)}_{\text{out}} \cdot \mathbf{u}^{(2)}_{\text{out}} \\
C^{(3)}_{v} &= \boldsymbol{v}^{(3)} \cdot \mathbf{K}^{(3)} \boldsymbol{v}^{(3)}
\end{aligned} \tag{7.5}$$

Lastly, all optimization properties are kept similar to step 1a except for the maximum amount of iterations, which is increased to 300, and the same material interpolation functions are used. The resulting topology, together with a visualization of its vertical displacements resulting from the applied static input load done in Paraview, is given in figure 7.11.

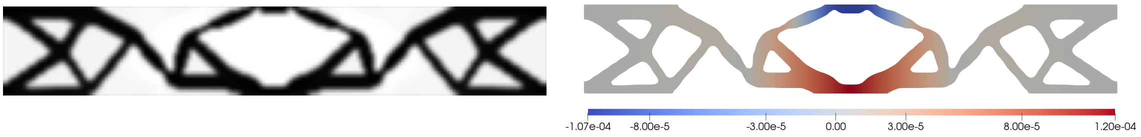

(a) Resulting topology

(b) Resulting static displacements visualized ParaView

Figure 7.11: The resulting topology of the inverter optimization problem given in equation 7.4 together with a visualization done in ParaView of the vertical displacements resulting from the applied static input force confirming the working inverting function.

The resulting topology presents an inverter mechanism which differs substantially from the mechanism found in step 1. However, this was to be expected for the larger design domain, given the same mechanism compliance constraint. For this larger domain, the mechanism is located in the centre of the domain and is connected to the boundaries through an intermediate structure. This connecting structure appears to consist of a structure similar to what would be obtained from a simple clamped cantilever static compliance optimization and a flexure which connects to the mechanism itself. The visualization given in figure 7.11b shows that the mechanism exhibits the desired inverting behaviour. The resulting displacement values of the input and output, together with the obtained geometrical advantage, are given in table 7.6.

Property	Value	
u_{in}	$1.2000e^{-4}$	[m]
u_{out}	$-1.0667e^{-4}$	[m]
GA	-0.8889	[-]

Table 7.6: The displacement values of the vertical input and output degrees of freedom resulting from the applied static input force together with the obtained geometrical advantage for both the resulting topology given in figure 7.11a.

Compared to step 1a, a higher input displacement is achieved and a lower output displacement. The resulting geometrical advantage is, therefore, drastically lower given its definition. This was to be expected however, and the magnitude of the inverting behaviour is less relevant for this case study. The important part is that similar inverter performance is yielded such that the results obtained from the upcoming optimizations are comparable.

Next, the frequency behaviour of the obtained structure can be examined. An eigensolve can be performed on the topology of figure 7.11a, but as was already found in chapter 6, the eigenmode accompanying a given eigenfrequency does not necessarily have to show displacements in the regions of interest, which in this case are the input and output regions, specifically in the vertical direction. To see which modes will contribute the most to the displacements of these points of interest, the undamped frequency response of the vertical displacements of the input and output for the structure subjected to the applied base excitation with a magnitude of 100 m/s^2 can be examined. This response is given in figure 7.12.

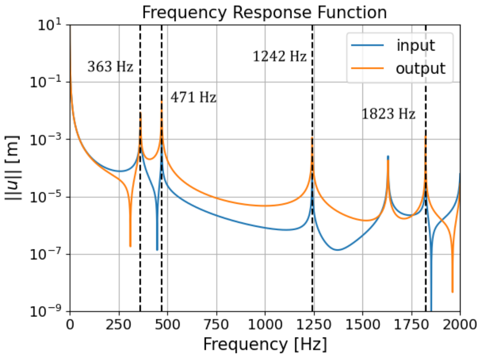

Figure 7.12: The frequency response of the respective vertical displacements of the input and output under the applied base excitation.

In this response the eigenfrequencies ω_2, ω_3, ω_7 and ω_{10} are plotted as well, as the input and output of the mechanism appear to exhibit the largest displacements at these resonance frequencies. The resonance appearing at ω_8=1630Hz could be included as well, but the higher frequency resonance will be of more interest in this case to provide a broader picture of the frequency behaviour. For each of these chosen resonances, it differs whether the input or output has a larger displacement, but both are affected. A visualization of the resonance which occurs when the structure is excited by the applied base excitations at these frequencies is given in figure 7.13.

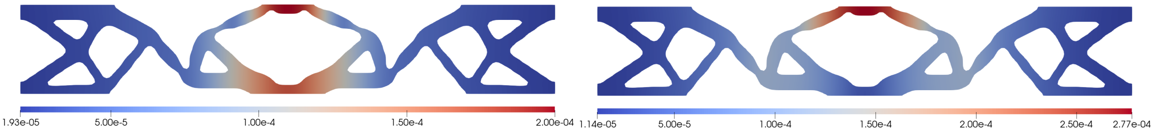

(a) ω_{exc} = 363Hz

(b) ω_{exc} = 471Hz

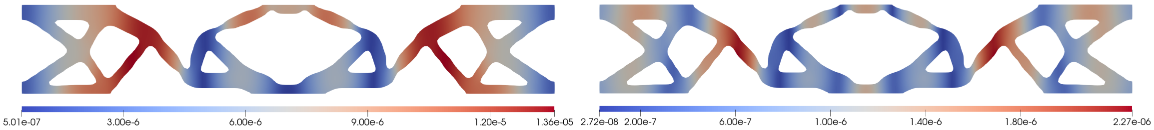

(c) ω_{exc} = 1242Hz

(d) ω_{exc} = 1823Hz

Figure 7.13: A visualization of the vertical displacement magnitudes within the structure resulting from the applied base excitation at the four respective frequencies of interest visualized in ParaView.

These results clearly show how either the input or the output exhibits a larger displacement than the input for a given resonance. For the results of the higher frequencies 1242Hz and 1823Hz, relatively large displacements are also present in other parts of the mechanism. The specific displacements of the input and output at these four frequencies are given in table 7.7.

Property	ω_2=363Hz	ω_3=471Hz	ω_7=1242Hz	ω_8=1823Hz	
u_{in}	$1.7763e^{-4}$	$2.6846e^{-5}$	$5.0102e^{-7}$	$1.3258e^{-6}$	[m]
u_{out}	$1.9988e^{-4}$	$2.7723e^{-4}$	$8.2329e^{-6}$	$1.4209e^{-6}$	[m]

Table 7.7: An overview of the values of the respective input and output displacement magnitudes resulting from the applied base excitations for the four respective frequencies of interest as given in figure 7.13.

These four frequencies will serve as the frequencies of interest for the upcoming steps, where the goal will be to apply the proposed minimization principles in order to minimize the large displacements in the structure occurring due to the applied base excitations at these frequencies. It is to be noted, however, that this case study represents a worst-case scenario, where the mechanism is excited at a resonance frequency. Practically, this would not necessarily be the case, but this scenario will provide a good insight into how the proposed objective function performs in the hardest optimization scenario.

7.2.1. Defining the design domain and load cases for global and local minimization

In the coming sections, a similar inverter to the one obtained in this step will be optimized for the applied base excitations at the frequencies of interest. As the inverter mechanism formulation remains identical, the required load cases for each of these optimizations are also identical. Figure 7.14 therefore defines the design domain and load cases for steps 3, 4 and 5. Note that these are the same as those in figure 7.10, only with different numbering.

Figure 7.14a defines the design domain, which is the same 1.8m × 0.3m domain as defined in step 2. Figures 7.14b, 7.14c and 7.14d then provide load cases 2, 3 and 4 respectively. Note that the first load case is left out, as this is the only load case differing for the coming steps. This load case will be defined separately for each step, whilst the rest of the load cases remain the same as those given in figure 7.14.

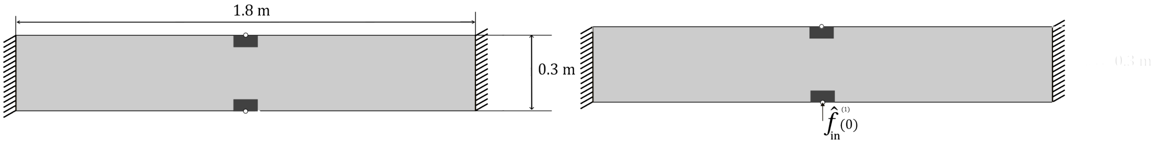

(a) Design domain (b) Load case 2

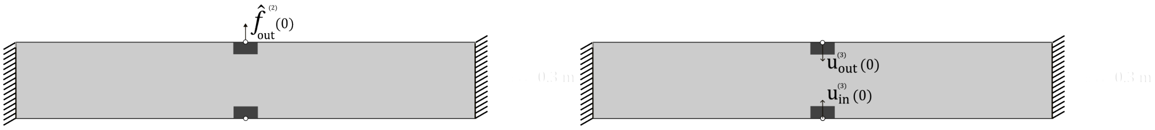

(c) Load case 3 (d) Load case 4

Figure 7.14: The design domain and three of the four load cases required to solve the inverter optimization problem for step 3, 4 and 5.

7.3. Step 3: Global minimization

In order to minimize the displacements at the resonance frequencies found in the previous step, the density-weighted norm objective function from chapter 6 will be utilized. First, the principle of global minimization is applied. given that the global minimization principle targets the largest displacements present in the design domain, it is expected that topologies are obtained which minimize or do not display the large input and output displacements found in figure 7.13 at the specified excitation frequency. As the base excitations are now included in the problem formulation, an extra load case containing these excitations needs to be added. Given that the design domain and inverter load cases were already defined in section 7.2.1, only the first load case, containing the base excitations, is given in figure 7.15.

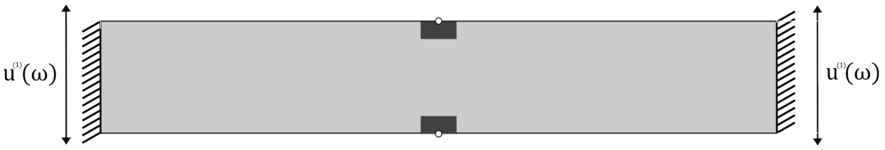

Figure 7.15: Load case 1 used for global minimization. Note that the other load cases which are required for this optimization problem were defined in section 7.2.1

All domain properties, optimizer properties and mechanism properties are kept similar to those defined in step 2. The static compliance contribution needed for the density-weighted norm function is conveniently covered by the compliance minimization already present for the mechanism optimization. Furthermore, while a non-design domain is added at the input and output, which has mass, no additional masses are added to this problem. The formulation for this problem is given in equation 7.6, where the the superscripts $^{(1)}$, $^{(2)}$, $^{(3)}$ and $^{(4)}$ represent the respective load cases.

$$\begin{aligned}
\min_{\mathbf{x}}: \quad & \gamma_1 \frac{N^{(1)}_{mwdB}(\mathbf{x})}{{N^{(1)}_{mwdB}}^{0}(\mathbf{x})} + \gamma_2 \left(\frac{C^{(2)}_{\text{in}}(\mathbf{x})}{{C^{(2)}_{\text{in}}}^{0}(\mathbf{x})} + \frac{C^{(3)}_{\text{out}}(\mathbf{x})}{{C^{(3)}_{\text{out}}}^{0}(\mathbf{x})} \right) \\
\text{subject to}: \quad & C^{(4)}_{v}(\mathbf{x}) \leq \bar{C}_{v} \\
& C^{(2)}_{\text{in}} \geq \bar{C}_{\text{in}} \\
& C^{(3)}_{\text{out}} \geq \bar{C}_{\text{out}} \\
& V(\mathbf{x}) \leq \bar{V} \\
& 0 \leq \mathbf{x}_{\min} \leq \mathbf{x} \leq 1
\end{aligned} \tag{7.6}$$

As for the properties of the norm function, it was determined in section B.2 that the density-weighted filter is to be included with a value of w=1 and the parameter m set at 2. Furthermore, the same constraint values for $\bar{C}_v$, $\bar{C}_{\text{in}}$ and $\bar{C}_{\text{out}}$ from step 2 are used.

The only parameter of the objective function which then remains is the parameter γ_1. Its definition specifies the contribution of static compliance to the objective function. In this case study, however, the input and output compliances are also constrained to a minimum value, which would make this parameter redundant. The optimizations conducted for this case study, however, showed otherwise. It seems that the influence of this parameter is present during the optimization, where it leans more towards the norm function or the static compliance as the optimization progresses. While similar compliance values are found for different values of γ_1, these are all considered different local minima with varying frequency performance. The parameter γ_1 is therefore also taken into account in this case study and examined for the same values of γ_1=0.90, 0.95 and 0.99 as was done in chapter 6.

Using this formulation, the harmonic base excitation with a magnitude of 100 m/s^2 can be added with the excitation frequencies of interest of 363Hz, 471Hz, 1242Hz and 1823Hz, as determined in the previous section. The topologies which result from these optimizations for the different values of γ_1 are given in figure 7.16.

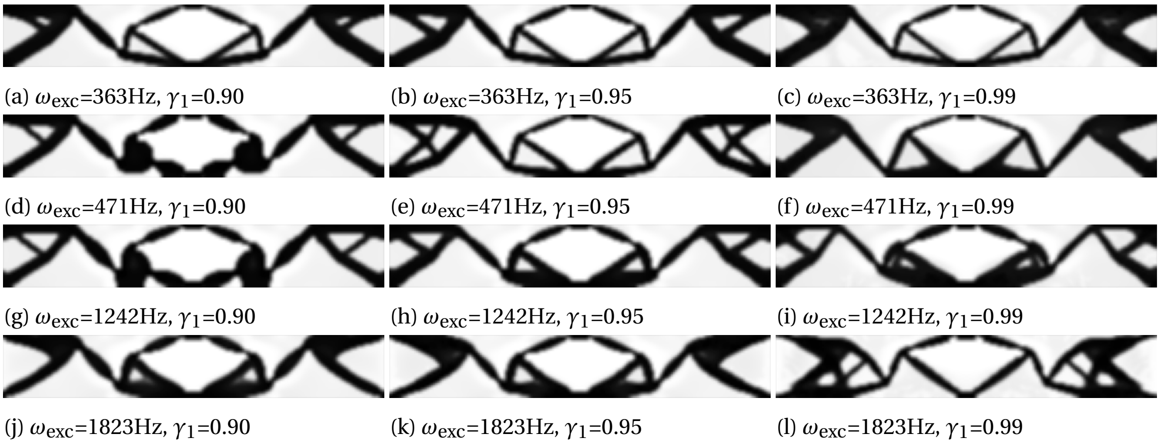

(a) ω_{exc}=363Hz, γ_1=0.90 (b) ω_{exc}=363Hz, γ_1=0.95 (c) ω_{exc}=363Hz, γ_1=0.99

(d) ω_{exc}=471Hz, γ_1=0.90 (e) ω_{exc}=471Hz, γ_1=0.95 (f) ω_{exc}=471Hz, γ_1=0.99

(g) ω_{exc}=1242Hz, γ_1=0.90 (h) ω_{exc}=1242Hz, γ_1=0.95 (i) ω_{exc}=1242Hz, γ_1=0.99

(j) ω_{exc}=1823Hz, γ_1=0.90 (k) ω_{exc}=1823Hz, γ_1=0.95 (l) ω_{exc}=1823Hz, γ_1=0.99

Figure 7.16: The topologies obtained with the global minimization formulation given in equation 7.6 for the four respective frequencies of interest as well as the three values of interest for the parameter γ_1.

Whilst all results appear to have obtained an inverter mechanism, their topologies are vastly different. One important thing to confirm is that the obtained inverters still actually provide an inverted displacement and that this function is not lost as it was for the stitched design in Step 1. A visualization of the displacements resulting from the applied static input load can be found in Appendix D.1, which confirms that the inverter function is still present for all obtained topologies. As for the resulting topologies, a behavioural pattern can be observed. For lower values of γ_1, more material is deposited in the centre part of the domain, often being added to the members of the inverter mechanism. This does not seem to influence the mechanism itself as the compliant joints still seem to be of similar thickness for different values of γ_1. Comparing the lowest frequency of 363Hz with the highest frequency of 1823Hz, the main difference can be found in the connection to the base, which is quite slender for the high frequency and a lot thicker for the low frequency. In between these frequencies there is a gradual shift in material being deposited away from the boundaries, with the only exception being the result of γ_1=0.99 for 1823Hz. Why this might be can be determined by looking at both the inverter performance, as well as the frequency performance. The quantitative analysis will be done in section 7.6, but a visualization of the frequency performance is given in figure 7.17.

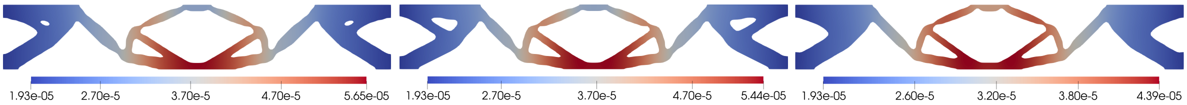

(a) ω_{exc}=363Hz, γ_1=0.90 (b) ω_{exc}=363Hz, γ_1=0.95 (c) ω_{exc}=363Hz, γ_1=0.99

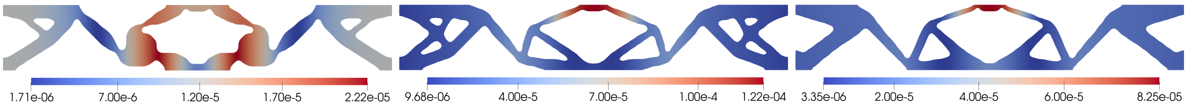

(d) ω_{exc}=471Hz, γ_1=0.90 (e) ω_{exc}=471Hz, γ_1=0.95 (f) ω_{exc}=471Hz, γ_1=0.99

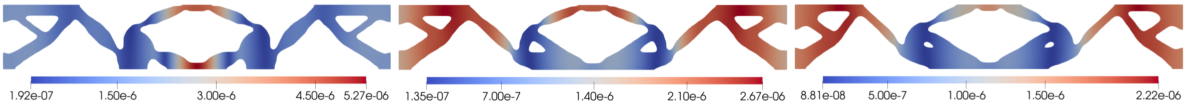

(g) ω_{exc}=1242Hz, γ_1=0.90 (h) ω_{exc}=1242Hz, γ_1=0.95 (i) ω_{exc}=1242Hz, γ_1=0.99

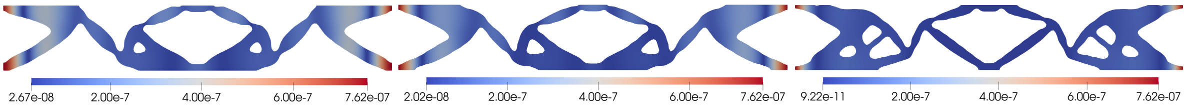

(j) ω_{exc}=1823Hz, γ_1=0.90 (k) ω_{exc}=1823Hz, γ_1=0.95 (l) ω_{exc}=1823Hz, γ_1=0.99

Figure 7.17: The vertical displacement magnitudes resulting from the applied base excitations for each of the respective topologies given in figure 7.16 visualized in ParaView.

For the excitation frequency of 363Hz, it seems that a large part of the mechanism still exhibits substantial displacements. The magnitudes of these displacements, however, are much lower than those found for the eigenmode, which was present at this frequency for the statically optimized inverter. For the result of γ_1=0.90 for 471Hz, the patches of material which were added to the mechanism appear to contain the largest displacements. Overall, for all frequencies except the highest excitation frequency of 1823Hz, the largest displacements are still present at the input or output regions, albeit with much lower displacement magnitudes than for the statically optimized inverter. For the excitation frequency of 1823Hz, however, the largest displacements are found at the previously mentioned slender members connecting the structure to the base. This is similar behaviour to what was found in chapter 6 for high excitation frequencies, and yields minimized displacements in the rest of the structure. Overall, the resulting displacement fields found in figure 7.17 appear to minimize the displacements in a seemingly random sense, which is to be expected considering the objective function targets the maximum displacements present in the structure at a given iteration.

7.4. Step 4: Local minimization of the mechanism area

The next step will consider the principle of local minimization to investigate whether lower displacement magnitude responses can be obtained compared to global minimization. Chapter 6 already showed that this principle allows for higher displacements in other regions of the domain than the specified area of interest. For local minimization, a point of interest or an area L has to be specified, which is to be minimized. For this case study, two different areas of interest will be examined, of which one will be used in this step, and the other in the last step. This step will consider the entire mechanism area as it was defined in Step 1, being the middle third of the domain. From this minimization, it is expected that the resulting topologies display a more even minimization of the mechanism area and larger displacements outside this area, whereas global minimization still had the largest displacements present within the mechanism. The design domain and inverter load cases are the same as defined in section 7.2.1, and the modified first load case, which includes the area of interest, is given in figure 7.18.

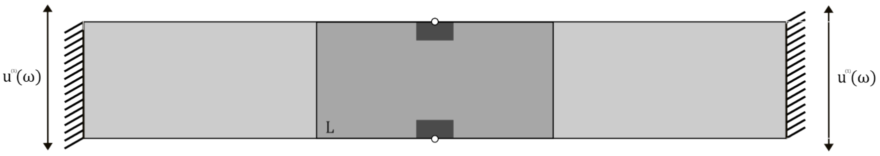

Figure 7.18: Load case 1 used for local minimization of the mechanism area. Note that the other load cases which are required for this optimization problem were defined in section 7.2.1

The non-design domain areas for the input and output are still present, and again no mass is added to the area of interest. Furthermore, all domain properties, optimizer properties and mechanism properties are kept similar to those defined in step 3. Only the optimization formulation is altered slightly in order to now denote the use of an area of interest L. This formulation is given in equation 7.7.

$$\begin{aligned} \min_{\mathbf{x}}: \quad & \gamma_1 \frac{N^{(1)}_{mwdBL}(\mathbf{x})}{N^{(1)}_{mwdBL}{}^{0}(\mathbf{x})} + \gamma_2 \left(\frac{C^{(2)}_{\text{in}}(\mathbf{x})}{C^{(2)}_{\text{in}}{}^{0}(\mathbf{x})} + \frac{C^{(3)}_{\text{out}}(\mathbf{x})}{C^{(3)}_{\text{out}}{}^{0}(\mathbf{x})} \right) \\ \text{subject to}: \quad & C^{(4)}_{v}(\mathbf{x}) \leq \bar{C}_v \\ & C^{(2)}_{\text{in}} \geq \bar{C}_{\text{in}} \\ & C^{(3)}_{\text{out}} \geq \bar{C}_{\text{out}} \\ & V(\mathbf{x}) \leq \bar{V} \\ & 0 \leq \mathbf{x}_{\min} \leq \mathbf{x} \leq 1 \end{aligned} \tag{7.7}$$

In section B.5 it was determined that the density-weighted filter is to be removed for this kind of optimization (w=0), and the parameter m is set at a value of 4. The topologies which are obtained with this formulation for the respective frequencies of interest and values of the parameter γ_1 are given in figure 7.19.

(a) ω_{exc}=363Hz, γ_1=0.90 (b) ω_{exc}=363Hz, γ_1=0.95 (c) ω_{exc}=363Hz, γ_1=0.99

(d) ω_{exc}=471Hz, γ_1=0.90 (e) ω_{exc}=471Hz, γ_1=0.95 (f) ω_{exc}=471Hz, γ_1=0.99

(g) ω_{exc}=1242Hz, γ_1=0.90 (h) ω_{exc}=1242Hz, γ_1=0.95 (i) ω_{exc}=1242Hz, γ_1=0.99

(j) ω_{exc}=1823Hz, γ_1=0.90 (k) ω_{exc}=1823Hz, γ_1=0.95 (l) ω_{exc}=1823Hz, γ_1=0.99

Figure 7.19: The topologies obtained with the local minimization formulation considering the mechanism area as given in equation 7.7 for the four respective frequencies of interest as well as the three values of interest for the parameter γ_1.

The obtained topologies all exhibit the desired inverting function, as can be seen by looking at the vertical displacements resulting from the applied input load is given in Appendix D.2. The resulting topologies for the excitation frequency of 363Hz, together with the γ_1=0.90 and 0.95 results for 471Hz, are very similar to those found for global minimization. This is likely due to most of the contribution of the norm function in global minimization considering this same area. The resulting topologies of γ_1=0.90 and 0.95 for 1242Hz and 1823Hz appear to construct connecting structures with some intricate members. For the high value of

γ_1=0.99 the connecting members seem to become very slender and the mechanism itself is given a relatively large amount of mass. This is similar to the vibration isolation behaviour found in chapter 6. The results of γ_1=0.95 and 0.99 for 1823Hz do, however, seem to contain some intermediate densities. To examine the frequency behaviour, the vertical displacement magnitudes resulting from the applied base excitations are given for each topology in figure 7.20.

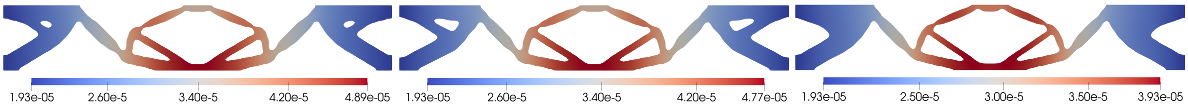

(a) ω_{exc}=363Hz, γ_1=0.90 (b) ω_{exc}=363Hz, γ_1=0.95 (c) ω_{exc}=363Hz, γ_1=0.99

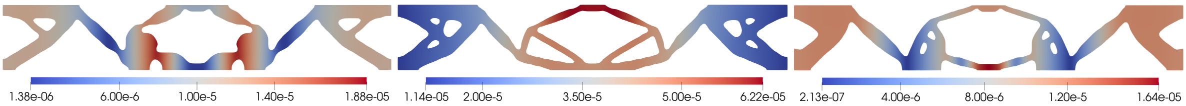

(d) ω_{exc}=471Hz, γ_1=0.90 (e) ω_{exc}=471Hz, γ_1=0.95 (f) ω_{exc}=471Hz, γ_1=0.99

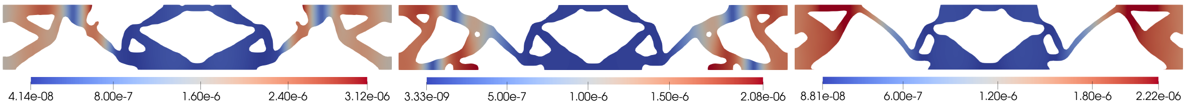

(g) ω_{exc}=1242Hz, γ_1=0.90 (h) ω_{exc}=1242Hz, γ_1=0.95 (i) ω_{exc}=1242Hz, γ_1=0.99

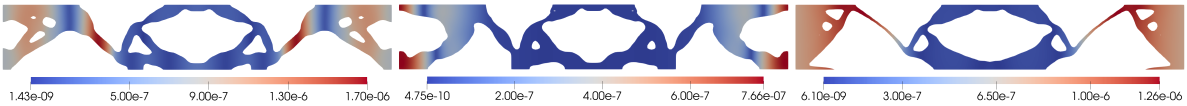

(j) ω_{exc}=1823Hz, γ_1=0.90 (k) ω_{exc}=1823Hz, γ_1=0.95 (l) ω_{exc}=1823Hz, γ_1=0.99

Figure 7.20: The vertical displacement magnitudes resulting from the applied base excitations for each of the respective topologies given in figure 7.19 visualized in ParaView.

For the lower frequencies of 363Hz and 471Hz, similar behaviour is found for global minimization, where displacements of the input and output regions are still present but with lower magnitudes. For the higher excitation frequencies of 1242Hz and 1823Hz however, some interesting behaviour is found. It appears that for all values of γ_1, the displacements of the mechanism area specifically are minimized. This is exactly what was desired from this objective function formulation. The manner in which this is achieved differs for each value of γ_1, however. For γ_1=0.90, the member which connects the mechanism to the base structure seems to exhibit the largest displacements, whereas for γ_1=0.99 this same member is very slender and the entire base structure exhibits the largest displacements. The result of γ_1=0.95 for 1242Hz shows the most interesting behaviour, however. It appears that the two lobes of material which are added to the structure exhibit the largest displacements in order to minimize the displacements of the mechanism area. This can be seen as the vibration absorption principle explained in section 2.2.4.

7.5. Step 5: Local minimization of the input and output area

For the last step of this case study, the area of interest is reduced to only the input and output area. Compared to the previous step, having even smaller specified areas of interest will give the optimizer more room inside the design domain to come up with designs that minimize the input and output area specifically. Section B.5 determined that a local minimization subjected to a base excitation presents topologies containing large amounts of intermediate densities for single degrees of freedom of interest at higher excitation frequencies. Therefore, a local area L is needed, which will conveniently be the non-design areas added to the input and output earlier. The updated first load case is given in figure 7.21.

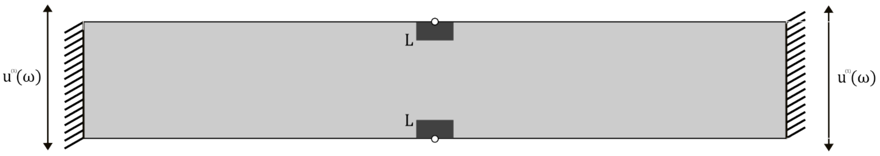

Figure 7.21: Load case 1 used for local minimization of the input and output area. Note that the other load cases which are required for this optimization problem were defined in section 7.2.1

In this case, no additional mass is again added to the system, and all domain, optimizer and mechanism properties remain identical to those of previous steps. The same formulation given in equation 7.7 is used, only considering the now different area of interest L. As for the parameters w and m, the density-weighted filter is again removed for local area minimization (w=0) and the parameter m is set at m=4. The topologies which are obtained for the respective frequencies of interest and parameter values for γ_1 are given in figure 7.22.


(a) ω_{exc}=363Hz, γ_1=0.90 (b) ω_{exc}=363Hz, γ_1=0.95 (c) ω_{exc}=363Hz, γ_1=0.99


(d) ω_{exc}=471Hz, γ_1=0.90 (e) ω_{exc}=471Hz, γ_1=0.95 (f) ω_{exc}=471Hz, γ_1=0.99


(g) ω_{exc}=1242Hz, γ_1=0.90 (h) ω_{exc}=1242Hz, γ_1=0.95 (i) ω_{exc}=1242Hz, γ_1=0.99


(j) ω_{exc}=1823Hz, γ_1=0.90 (k) ω_{exc}=1823Hz, γ_1=0.95 (l) ω_{exc}=1823Hz, γ_1=0.99

Figure 7.22: The topologies obtained with the local minimization formulation considering the input and output area for the four respective frequencies of interest as well as the three values of interest for the parameter γ_1.

The resulting topologies for the excitation frequency of 363Hz for all values of γ_1 and the results of 471Hz for γ_1=0.90 and 0.95 again show similar resulting topologies to the previous global and local minimizations with only slight differences. The results of higher frequencies also seem similar, with the difference being primarily in the material deposition on the mechanism. The resulting topologies of γ_1=0.99 however, do seem to contain large amounts of intermediate densities for higher frequencies, and as can be seen in the resulting static displacements in Appendix D.3, the inverter function is lost for the result of γ_1=0.99 at 1823Hz. As for the frequency behaviour, the vertical displacement magnitude fields resulting from the applied base excitations are given in figure 7.23. The results for γ_1=0.99 at 1823Hz had their threshold value lowered in order to visualize the displacements of the intermediate density fields.

Given that the topologies for 363Hz showed similar results compared to the minimizations of the previous steps, it is to be expected that the displacement field looks similar as well. For 471Hz, the results of γ_1=0.90 and 0.99 show similar results to the previous step, but with much more focus on the minimized displacements of the areas of interest. For the results of γ_1=0.90 and 0.95 for higher frequencies, similar results to those in the previous step are found as well, but also with the same added behaviour of parts within the mechanism being allowed to displace in order to minimize the displacements of the areas of interest. For 1242Hz and 1823Hz, similar mass lobes are also formed, which contain large displacements, but these are connected to the rest of the structure via very low-density members. The results of γ_1=0.99 show the desired behaviour of displacing other parts of the structure in order to minimize the displacements in the area of interest, but these large displacements are mainly found in the large intermediate-density areas.

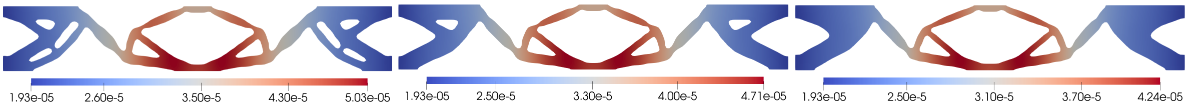

(a) ω_{exc}=363Hz, γ_1=0.90 (b) ω_{exc}=363Hz, γ_1=0.95 (c) ω_{exc}=363Hz, γ_1=0.99

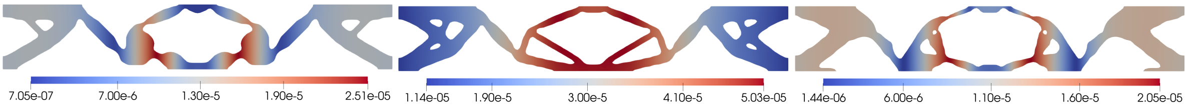

(d) ω_{exc}=471Hz, γ_1=0.90 (e) ω_{exc}=471Hz, γ_1=0.95 (f) ω_{exc}=471Hz, γ_1=0.99

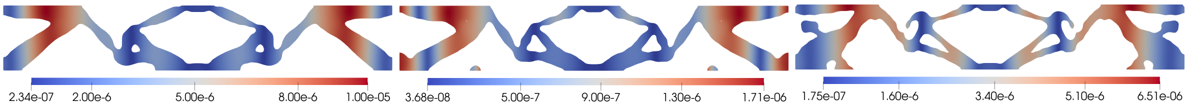

(g) ω_{exc}=1242Hz, γ_1=0.90 (h) ω_{exc}=1242Hz, γ_1=0.95 (i) ω_{exc}=1242Hz, γ_1=0.99

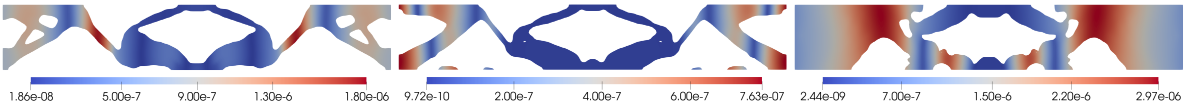

(j) ω_{exc}=1823Hz, γ_1=0.90 (k) ω_{exc}=1823Hz, γ_1=0.95 (l) ω_{exc}=1823Hz, γ_1=0.99

Figure 7.23: The vertical displacement magnitudes resulting from the applied base excitations for each of the respective topologies given in figure 7.22 visualized in ParaView.

To clearly see the difference between the results of the local minimization conducted in this step compared to global minimization, figure 7.24 provides a comparison of the results of the excitation frequency at 471Hz for γ_1=0.90. The result of global minimization is coloured in blue, and the result of the local minimization of the input and output regions is coloured in black.

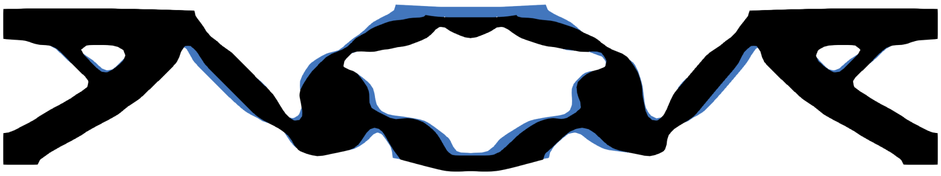

Figure 7.24: A visualization of the difference between the displacement magnitudes of the topologies obtained for global minimization (blue) and local minimization of the input and output area (black) for the excitation frequency ω_{exc}=471Hz and γ_1=0.90.

The structure obtained with global minimization aimed to achieve minimized displacements in a global sense, which can be seen by the connecting members showing smaller displacements than the local result. The displacement of the input is quite similar, but the displacement of the output is indeed minimized for the local result.

7.6. Quantitative comparison

Next, the displacement performance resulting from the applied base excitations can be examined. First, however, the inverter performance of each obtained structure must be assessed. Table 7.8 provides the geometrical advantage values for each of the topologies given in figure 7.16, 7.19 and 7.22. As several values do not match the desired geometrical advantage, a colour scheme is applied where the values within a 5% margin are marked orange, and values beyond this margin are marked red.

Geometrical Advantage	363Hz	471Hz	1242Hz	1823Hz
γ_1=0.90				
Global	-0.8889	-0.8889	-0.8889	-0.8889
Local mechanism	-0.8889	-0.8889	-0.8888	-0.8857
Local input output	-0.8889	-0.8889	-0.8888	-0.8668
γ_1=0.95				
Global	-0.8888	-0.8885	-0.8888	-0.8888
Local mechanism	-0.8889	-0.8873	-0.8153	-0.7236
Local input output	-0.8889	-0.8888	-0.8699	-0.7654
γ_1=0.99				
Global	-0.8110	-0.7134	-0.7889	-0.6506
Local mechanism	-0.8243	-0.5814	-0.4505	-0.2874
Local input output	-0.8358	-0.2600	-0.3776	0.1087

Table 7.8: The values of the geometrical advantages of the obtained structures of figure 7.16, 7.19 and 7.22. Values within the range of 5% of the geometrical advantage found in step 2 are marked orange, and values beyond this margin are marked red.

These results show that not all obtained topologies contain the same geometrical advantage, and the result of the last step for γ_1=0.99 at 1823Hz even lost its inverting function. It is, therefore, debatable whether these results are comparable, given that a different inverter is obtained, which will also impact the frequency performance. This impact could be beneficial or even hindering, but it will have an influence nonetheless. The results which will be compared in this section will therefore primarily consider the γ_1=0.90 results and the γ_1=0.95 results will be examined keeping these static results in mind.

Figure 7.25 contains the displacement magnitudes for the input and output, respectively, resulting from the applied base excitations for each of the obtained topologies for γ_1=0.90 compared with the displacements of the original structure from step 2. The results are split into the input and output displacements due to the results found in figure 7.13, which displayed the displacement magnitudes of the original structure at the chosen resonance frequencies. For most results, mainly the output contained high displacements, and the input contained high or similar displacements only for 363Hz and 1823Hz. The optimized results could, therefore, contain input displacements which are higher than the original structure but improved on the displacements of the output.

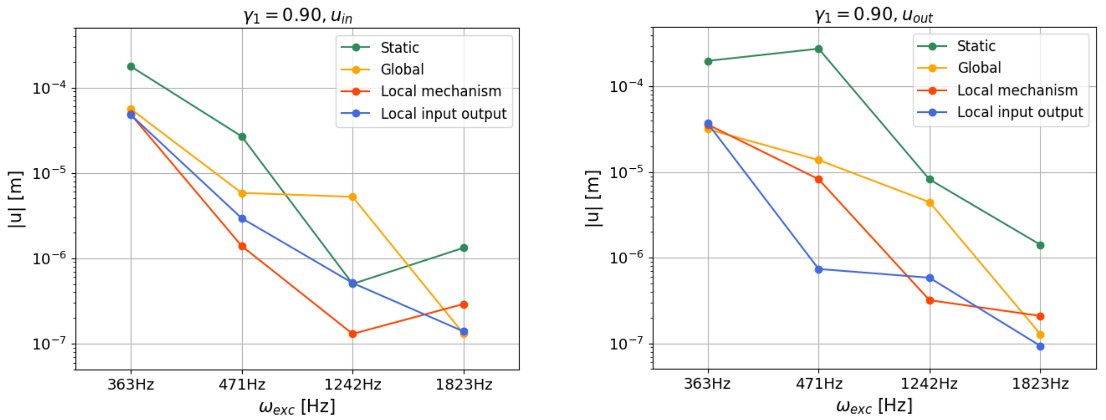

(a) γ_1=0.90, u_{in}

(b) γ_1=0.90, u_{out}

Figure 7.25: A graphical representation of the vertical displacement responses under the applied base excitations at each of the frequencies of interest for both the input and the output given γ_1=0.90.

What stands out immediately from these results is that almost all optimized structures have lower displacement values than those found for the original structure. The only time this is not the case is the input displacement at 1242Hz of the global and local mechanism optimizations. As mentioned, however, the input displacement of the original structure was comparatively low. It is hard to see the 363Hz results, but it appears that the method of local minimization achieves lower displacement magnitudes than those found for global minimization, except for the highest frequency of 1823Hz. Looking at the result of figure 7.17j, this might be explained by the fact that the highest displacements are present near the edges of the structure. Comparing both methods of local minimization, however, yields inconclusive results as the results vary from frequency to frequency. To see whether this also holds for other values of γ_1, the results of γ_1=0.95 are given in figure 7.26.

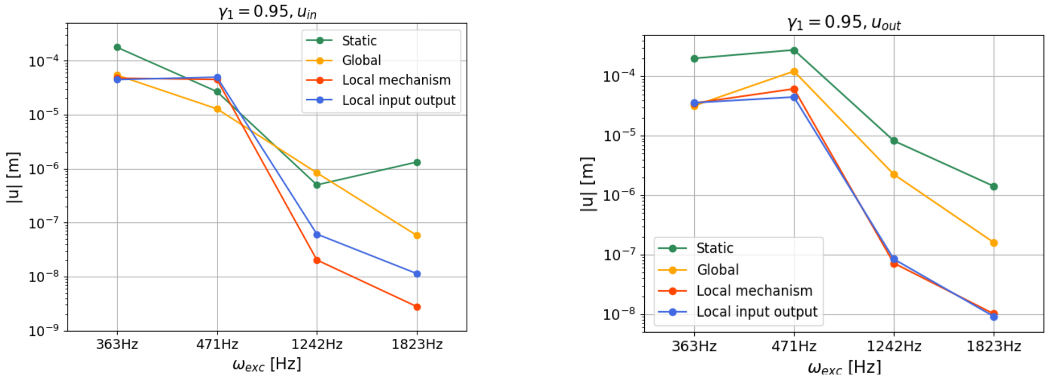

(a) γ_1=0.95, u_{in}

(b) γ_1=0.95, u_{out}

Figure 7.26: A graphical representation of the vertical displacement responses under the applied base excitations at each of the frequencies of interest for both the input and the output given γ_1=0.95.

These results show that local minimization of the input and output areas does indeed yield lower displacement magnitudes for the output displacements but achieves this at the cost of higher input displacements. The results of global minimization however, do show consistent improvement of the results, apart from the expected difference in input displacement at 1242Hz. The higher frequency results for local minimization also show lower displacement magnitudes, but these results are not comparable due to the resulting different geometrical advantages as given in table 7.8. For the same reason, the results of γ_1=0.99 will not be compared.

7.7. Discussion

Comparing global and local minimization, the local minimization problem formulation generates designs in which the areas of interest have a lower displacement magnitude than global minimization. This is also exactly where an argument can be made whether this comparison is justified, given that global minimization did not specifically target the input and output regions. This same argument applies to the comparison of the frequency response values. Given that global minimization considers all the degrees of freedom inside the structure, *n* frequency responses would have to be examined in order to assess the full behaviour. Such a comparison, however, would be impossible to perform. The frequencies of interest were chosen by examining the frequency response of the vertical degrees of freedom of the input and output of an inverter mechanism which did not consider the applied base excitations. Four frequencies that presented resonances were then chosen as the frequencies of interest in order to simulate a worst-case scenario. It is, therefore, to be expected that global minimization would yield a topology that at least has minimized displacements compared to the original structure, but without prejudice for a specific area, simply the overall minimized result. This same argument holds for local minimization, which is, in turn, expected to yield a lower displacement magnitude response compared to global minimization due to specifically targeting these areas. Comparing the results of local minimization of the two considered areas of interest, it appeared that decreasing the area of interest only to cover the input and output regions resulted in improved displacement responses in some cases but also showed decreased performance in other results. Whether the minimization of a smaller area of interest yields better performance, therefore, remains inconclusive.

For the case study where the area of interest considers the mechanism area, the results show behaviour that could be considered similar to the principles of vibration absorption and vibration isolation. The resulting topology of γ_1=0.95 for 1242Hz contains lumps of mass with high displacement magnitudes in order to minimize the displacements in the mechanism area. This could be considered an example of vibration absorption, where the lumps of mass act as an absorber mass. This mass was, however, located at the boundary of the design domain, begging the question of whether the same problem definition in a larger design domain would allow for more room to create these counter masses. For the higher value of γ_1=0.99, the resulting topology contains a large amount of material added to the mechanism members and very thin flexures which connect the mechanism to the base. This is in line with the principle of vibration isolation given the thin flexures allow for a low stiffness connection between the large mass to the base. Why this behaviour is only found for high excitation frequencies is also quite logical. In section 2.2.4, it was determined that effective vibration isolation can be accomplished by having a large amount of mass and a low amount of stiffness in order to obtain a low eigenfrequency. For the design domain considered in this case study, this mass and stiffness is limited however, and therefore, this behaviour is obtained more easily for higher excitation frequencies. While the geometrical advantage of these results is lower than the rest of the results, the inverter function is still present for these topologies. This does, however, yield incomparable results.

8

Discussion

This thesis focuses on utilizing topology optimization to design compliant transmission systems whilst simultaneously designing them against unwanted vibrations in the form of base excitations. This is achieved in two ways: minimizing the overall vibrations in the structure and minimizing the vibrations in one area of the structure by allowing other areas in the structure to vibrate instead. In the results of this thesis, similar principles to the currently used methods of attenuating unwanted vibrations, such as vibration isolation and vibration absorption, are found.

Chapters 2, 3 and 4 contain a literature study on the current state of the art of compliant mechanisms and topology optimization of compliant mechanisms and dynamic environments. Specifically, the topology optimization of structures in dynamic environments presented several issues. Eigenfrequency optimizations do not fully translate to forced vibration problems due to the influence of damping and require a significant amount of computational effort. Furthermore, eigenfrequency optimization only moves the eigenfrequency to a desired value but does not necessarily minimize the vibrations for a certain frequency. A better alternative would be the principle of dynamic compliance, which does take into account the excitation source, but this objective function is unable to optimize for excitation frequencies above the first resonance of the initial structure without suffering from premature convergence and containing large amounts of intermediate density areas. This same issue occurs for base excited problems, which presents the need for a new objective function which can minimize vibrations for a large range of excitation frequencies.

The density-weighted norm objective function, introduced by Montero et al. [37], is presented in Chapter 6 to remedy these issues. The original work, however, only considers a force-excited global minimization problem, and therefore, a parameter study is done with an extension to base excited problems, which yielded similar results to the force-excited case. Comparing the global minimization results to the work of Montero et al., however, does not show similar performance, especially in terms of the impact of the density-weighted filter. Originally introduced to prevent the occurrence of localized modes, the density-weighted filter appears to minimize the occurrence of intermediate density areas, which could result in such localized modes, but with a much less defined impact as found in the original work. The influence that is present, however, has a positive impact, and as such, the density weights are still included. The resulting intermediate densities for local minimization can, therefore, not be fully allocated to the absence of the density-weighted filter. Appendix C presents a study done one the use of different interpolation functions for the example problem used in the parameter study on the density-weighted norm function. Several of the resulting topologies in this appendix presented large amounts of intermediate-density areas, therefore suggesting that the material interpolation functions have the largest influence on the occurrence of intermediate densities. It does, however, not appear that there is a one-size-fits-all function. Therefore, the recommendation is to assess each design problem individually to determine the appropriate interpolation function.

On top of an expansion of the original work done on global minimization to base excitations, an extension was also made to local minimization, where only a selection of degrees of freedom of interest is minimized, and the rest of the domain is allowed to portray higher displacements. The parameter study shows that this optimization problem, especially when considering a single degree of freedom for the base excited case, yields a large number of intermediate densities present in the final topology. The density-weighted filter was excluded for local minimization due to not showing a significant influence on local minimization problems, but as mentioned, the occurrence of intermediate densities cannot fully be accredited to its removal. Increasing the size of the area of interest to be minimized, however, does seem to aid in minimizing the occurrence of intermediate densities. This might be due to the added mass of the non-design domain being more distributed over the domain, given that the added mass of the area of interest was equal to the one added to the single degree of freedom case, but this influence was not examined further due to the parameter values needed for the final case studies being established.

In the case studies, the principles of global and local minimization using the density-weighted norm objective function are applied to the design of a compliant inverter mechanism. The goal of minimizing the displacement response of the mechanism as a result of the applied harmonic base excitations for a set of excitation frequencies is achieved for both minimization principles. As for the displacement behaviour of the obtained topologies, the global minimization and both local minimization principles perform as expected. Where global minimization yields minimized displacement results without prejudice, the local minimization principles clearly target the chosen areas of interest and allow parts of the structure outside these areas to displace to minimize displacements in the area of interest. Global minimization appears to obtain topologies for all excitation frequencies and values of γ_1, which display little to no presence of intermediate densities. Local minimization, however, shows an increase in the amount of intermediate densities present in the final topology, especially for the smaller areas of interest when only the input and output regions are considered. This is in line with the results found in the parameter study and shows that a smaller area of interest is undesired. For the lowest excitation frequency of 363Hz, the results of both global and local minimization yield a similar topology. This is expected due to the more complex local modes needed for local minimization being present at higher frequencies.

To obtain comparable results for each minimization principle, it is important for the static compliance values of the input and output to be similar. The input and output compliance can conveniently be used in the density-weighted norm objective function for the static compliance contribution, but this leads to a lack of control. These compliances are, therefore, also constrained, which is a bit counterintuitive, and it can, therefore, be argued whether another formulation would be more adequate given that lower contributions of the static compliance and higher excitation frequencies yield a loss in geometrical advantage or, in other words, the inability to conform to these constraints and yielding incomparable results. Whilst the other inverter formulation introduced in section 4.1.1 would be more advantageous due to its benefit of already including static compliance constraints, testing found that this formulation could not be implemented in the density-weighted norm function.

Another discussion point in this thesis is the assumption of a single disturbance frequency. To make the system more robust, however, it would be better to consider a range of frequencies, as it will make the system more capable of withstanding a larger range of disturbance frequencies. Incorporating this range of frequencies does, however, increase the computational effort, which the inclusion of reduced-order modelling methods could partly alleviate. However, including these reduced order model methods would allow issues with localized modes to occur.

Due to the assumptions of a linear harmonic system as given in section 5, the resulting mechanism acts as an inverter for a static input load and as an isolator for the applied base excitation. Given the assumption of linearity and superposition, the inverter will still work when excited with a static force at this frequency. However, this is not necessarily the case for larger deformations, as the resulting deformations within the structure will affect the performance of the mechanism. If the mechanism is actuated and a base excitation is applied to this deformed structure, it might behave very differently from the results presented in this case study. Optimizing the mechanism for its deformed state would, however, require a more complex optimization, which includes non-linear physics.

9

Conclusions & recommendations

The objective of this thesis was to utilize topology optimization to design compliant transmission systems whilst simultaneously designing them to minimize their response to unwanted external vibrations. The research on the state of the art of topology optimization showed the shortcomings of the current methods of minimizing forced vibrations which resulted in the introduction of the density-weighted norm objective function.

This thesis showed that this objective function can be used in conjunction with the design formulations of compliant mechanisms to simultaneously minimize them for their response to harmonic base excitations at a specified frequency. Two principles for the objective function were examined: global minimization and local minimization. Global minimization considers all degrees of freedom in the design domain and minimizes the maximum displacement response inside the structure. Local minimization, on the other hand, only minimizes a specified area of the design domain. It is shown that global minimization is capable of obtaining topologies for a large range of frequencies, even higher excitation frequencies than those found in literature. The inclusion of the density-weighted filter aids in preventing the occurrence of intermediate densities, but the largest contributor to this occurrence is the chosen set of material interpolation functions for the stiffness and mass interpolation, respectively. Local minimization allowed for an improvement in the displacement response for both considered areas of interest. If the mechanism area is considered, the obtained results display displacement responses similar to the principles of vibration absorption and vibration isolation for high excitation frequencies.

In general, it can be concluded that the density-weighted norm objective function can be effectively used to design a compliant transmission system whilst simultaneously minimizing the response to harmonic base excitations. A proof of concept has been provided in this thesis, but further research is required. The following section will provide some research directions and recommendations.

Recommendations

As mentioned, several research directions can be determined from the research gaps that arose during the writing of this thesis.

- Change the mechanism optimization formulation. This might again consider an inverter mechanism, but it could also be any other mechanism, such as a resonator or an amplification mechanism. Having a formulation that provides more control over the desired mechanism might limit the performance of the norm function but will allow for better insights into its influence and behaviour. One option might be to use the geometrical advantage in the objective function, which would yield $\gamma_1\ N_{mwdB}$+γ_2 (GA-$\bar{GA}$), where $\bar{GA}$ is the desired geometrical advantage. The stiffness of the input and output could then, in turn, be added as constraints.
- One aspect that was included in the original goal of this thesis was the examination of this objective function for mechanisms that were excited by a harmonic excitation instead of a static excitation. Due to time constraints, this was not included, but the density-weighted norm parameter study also contains force-based excitations for this reason. Future research could, therefore, adapt this research to harmonically excited mechanisms, which might, for example, act as a resonator for the excitation frequency and as an isolator for the specified disturbance frequency.

- The current designed mechanism has been optimized for a single disturbance frequency. In order to make the system more robust, however, it is preferable to have a minimized response for a range of frequencies. This thesis showed a proof of concept that can be expanded in order to include a range of frequencies. This does, however, require more computational effort, and a study will have to be done on model order reduction methods to alleviate this.

- Another aspect is the size of the design domain. Some results of local minimization portrayed material distributions at the edges of the domain. Therefore, the design domain might be increased in order to see whether local minimization can benefit from this extra space. This will, however, increase the computational cost, given the increase in grid size required.

- Lastly, the expansion can be made to experimental testing. However, this requires some extra steps. First, the problem must be modelled in three dimensions rather than two in order to capture a more accurate representation. Furthermore, incorporating manufacturing principles becomes essential, especially in the context of 3D printing. This transition to 3D would also allow for an analysis of stress concentrations in the obtained mechanism.

A

Derivation of the system of equations for harmonic base excitations

To solve for systems subjected to harmonic base excitations, the original forced vibration equation of motion given in equation A.1 is insufficient. The base excitations cannot be represented by a force vector and, therefore, have to be directly inserted into the equation of motion.

$$\left(\mathbf{K}(\mathbf{x}) + j\omega\mathbf{C}(\mathbf{x}) - \omega^2\mathbf{M}(\mathbf{x})\right)\mathbf{u}(\omega) = \mathbf{f}(\omega) \tag{A.1}$$

To achieve this, the degrees of freedom in the systems can be divided into free degrees of freedom f and prescribed degrees of freedom p. The subset p of the displacements of the degrees of freedom can then be filled with the desired magnitudes of the prescribed displacements. This is done by taking the original time domain equation of motion from equation 4.6 and describing it in terms of the free and prescribed degrees of freedom, which yields the system of equation given in equation A.2.

$$\begin{bmatrix}\mathbf{M}^*_{ff} & \mathbf{M}^*_{fp}\\ \mathbf{M}^*_{pf} & \mathbf{M}_{pp}\end{bmatrix}\begin{bmatrix}\ddot{\mathbf{u}}_f\\ \ddot{\mathbf{u}}_p\end{bmatrix} + \begin{bmatrix}\mathbf{C}_{ff} & \mathbf{C}_{fp}\\ \mathbf{C}_{pf} & \mathbf{C}_{pp}\end{bmatrix}\begin{bmatrix}\dot{\mathbf{u}}_f\\ \dot{\mathbf{u}}_p\end{bmatrix} + \begin{bmatrix}\mathbf{K}_{ff} & \mathbf{K}_{fp}\\ \mathbf{K}_{pf} & \mathbf{K}_{pp}\end{bmatrix}\begin{bmatrix}\mathbf{u}_f\\ \mathbf{u}_p\end{bmatrix} = \begin{bmatrix}\mathbf{f}_f\\ \mathbf{f}_p\end{bmatrix} \tag{A.2}$$

In all literature on harmonic base excitations [79] [81] [82], a certain amount of mass m is added to a specific node of interest in the system. The superscripts * shown on the mass matrices concerning the free degrees of freedom denote that the matrices may be augmented by the additional mass. Next, the same harmonic load and displacement solution from equations 4.7 and 4.8 can be inserted into equation A.2, which results in the frequency-dependent system of equations in equation A.3. The dependencies are omitted for this derivation.

$$\left(-\omega^2\begin{bmatrix}\mathbf{M}^*_{ff} & \mathbf{M}^*_{fp}\\ \mathbf{M}^*_{pf} & \mathbf{M}_{pp}\end{bmatrix} + j\omega\begin{bmatrix}\mathbf{C}_{ff} & \mathbf{C}_{fp}\\ \mathbf{C}_{pf} & \mathbf{C}_{pp}\end{bmatrix} + \begin{bmatrix}\mathbf{K}_{ff} & \mathbf{K}_{fp}\\ \mathbf{K}_{pf} & \mathbf{K}_{pp}\end{bmatrix}\right)\begin{bmatrix}\mathbf{u}_f\\ \mathbf{u}_p\end{bmatrix}e^{j\omega t} = \begin{bmatrix}\mathbf{f}_f\\ \mathbf{f}_p\end{bmatrix}e^{j\omega t} \tag{A.3}$$

Rewriting equation A.3 yields:

$$\begin{bmatrix}-\omega^2\mathbf{M}^*_{ff} + i\omega\mathbf{C}_{ff} + \mathbf{K}_{ff} & -\omega^2\mathbf{M}^*_{fp} + i\omega\mathbf{C}_{fp} + \mathbf{K}_{fp}\\ -\omega^2\mathbf{M}^*_{pf} + i\omega\mathbf{C}_{pf} + \mathbf{K}_{pf} & -\omega^2\mathbf{M}_{pp} + i\omega\mathbf{C}_{pp} + \mathbf{K}_{pp}\end{bmatrix}\begin{bmatrix}\mathbf{u}_f\\ \mathbf{u}_p\end{bmatrix} = \begin{bmatrix}\mathbf{f}_f\\ \mathbf{f}_p\end{bmatrix}, \tag{A.4}$$

Which finally yields the simplified system of equations, including dependencies given in equation A.5.

$$\begin{bmatrix}\mathbf{K}^*_{ff}(\omega,\mathbf{x}) & \mathbf{K}^*_{fp}(\omega,\mathbf{x})\\ \mathbf{K}^*_{pf}(\omega,\mathbf{x}) & \mathbf{K}_{pp}(\omega,\mathbf{x})\end{bmatrix}\begin{bmatrix}\mathbf{u}_f(\omega,\mathbf{x})\\ \mathbf{u}_p(\omega,\mathbf{x})\end{bmatrix} = \begin{bmatrix}\mathbf{f}_f(\omega)\\ \mathbf{f}_p(\omega)\end{bmatrix} \tag{A.5}$$

Lastly, the system of equations above can also be written out as:

$$\begin{aligned}\mathbf{K}^*_{ff}(\omega,\mathbf{x})\mathbf{u}_p(\omega,\mathbf{x}) + \mathbf{K}^*_{fp}(\omega,\mathbf{x})\mathbf{u}_p(\omega,\mathbf{x}) &= \mathbf{f}_f(\omega)\\ \mathbf{K}^*_{pf}(\omega,\mathbf{x})\mathbf{u}_f(\omega,\mathbf{x}) + \mathbf{K}_{pp}(\omega,\mathbf{x})\mathbf{u}_p(\omega,\mathbf{x}) &= \mathbf{f}_p(\omega)\end{aligned} \tag{A.6}$$

B

Density Weighted norm objective function parameter study

This appendix contains the extensive study done on the behaviour of the density-weighted norm function proposed in chapter 6 for its use case in both global and local minimization problems. Furthermore, both a system excited by a force excitation and a base excitation are considered. The goal of this study is to study the behaviour of the objective function and determine the parameters required to minimize the amount of intermediate densities present in the obtained topology such that it can be implemented in the case study done in chapter 7. As mentioned, the parameter study is structured as follows: Global minimization subjected to a force excitation, global minimization subjected to a base excitation, local minimization subjected to a force excitation, and lastly, local minimization subjected to a base excitation.

B.1. Global minimization subjected to a force excitation

First, the behaviour of global minimization subjected to a force excitation is examined. As this is also done by Montero et al. [37], the results can be compared to confirm the objective function behaves similarly. A direct comparison will not be made; however, to study this behaviour in a relevant manner for the final case study, a different design problem will be tackled.

B.1.1. Problem definition

The chosen problem is a simple double-clamped cantilever beam problem. The design domain is defined by a 1.8 x 0.3 m rectangle, with the domain thickness set at 0.01 m. The finite element mesh consists of 180x30 4-node quadrilateral elements. A visual representation is given in figure B.2. Both the left and right boundaries are constrained in all directions, and a force with a magnitude of 10kN is added at the middle bottom node in the negative y-direction.

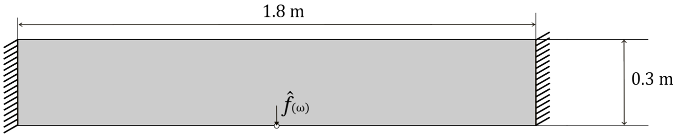

(a) Load case 1

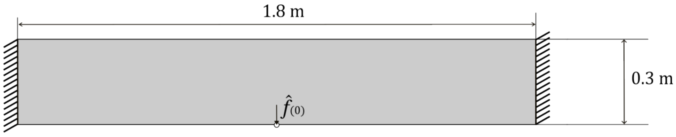

(b) Load case 2

Figure B.2: The two load cases required for global minimization subjected to a force excitation including the used dimensions.

Property	Value	
l_x, l_y, l_z	1.8, 0.3, 0.01	[m]
n_x, n_y	180, 30	[#]
$\hat{f}$	10	[kN]
Filter radius	2	[#]
Volume fraction	0.4	[-]

Table B.1: An overview of the properties of the used design domain.

An overview of the used dimensions is given in table B.1, together with the filter radius used for the density filter and the desired volume fraction. The reasoning behind the filter radius was provided in section 3.3, and as for the choice of volume fraction, a look can be taken at some arbitrary results from the coming section. Given in figure B.3 are the results for the same problem for the volume fractions 0.3, 0.35, 0.4 and 0.5. Comparing the results based on the material distribution, it is evident that the volume fraction impacts the obtained topology substantially. For a small volume fraction such as 0.3, however, the extent to which the topology can vary will be limited due to the relatively small amount of material that can be used. This would shift the focus of the optimization from being on the objective function to being a volume minimization, which is unwanted. For a large volume fraction such as 0.5, there seems to be an excess of material spread evenly throughout the domain. This excess material could have been added arbitrarily as floating material, but in this case, it will introduce extra stiffness, which might, in turn, hinder some dynamic properties which the topology otherwise could achieve. Looking at the intermediate values for the volume fractions, 0.35 and 0.4, two different results are presented. The result of 0.3, however, does show some gaps within the structure, whereas the result of 0.4 presents a structure with well-defined yet intricate members. Therefore, the volume fraction used for this problem will be set at 0.4.

(a) Volume fraction 0.3 (b) Volume fraction 0.35

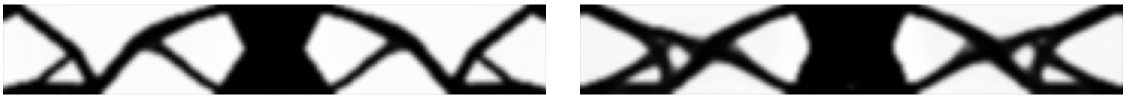

(c) Volume fraction 0.4 (d) Volume fraction 0.5

Figure B.3: Example topologies of the design problem given in figure B.2 for a parameter sweep over the desired volume fraction.

As for the material properties used for this problem, these are given in table B.2. The optimizer which will be used is the Method of Moving Asymptotes (MMA), where the tolerance is set at the most common value of $1e^{-4}$. This means that the stopping criteria for the optimization will be met if the difference in objective function from one iteration to the next is smaller than this tolerance value. If this stopping criterion is not met after 300 iterations, however, the optimization will be terminated as well. Lastly, a minimum value for x_{min} is introduced to avoid the system matrices becoming singular if one of the design variables achieves a value of 0. These optimizer properties are summarized in table B.3.

Property	Value	
Young's modulus	200	[GPa]
Density	7800	[kg/m^3]
Poisson ratio	0.3	[-]

Table B.2: The material properties used for this parameter study.

Property	Value	
Maximum iterations	300	[-]
Tolerance	$1e^{-4}$	[-]
x_{min}	$1e^{-3}$	[-]

Table B.3: Properties of the MMA optimizer used for this parameter study.

Regarding material interpolation functions, Montero et al. [37] utilized a standard SIMP function (equation 3.9) for the stiffness interpolation, together with a mass interpolation scheme introduced by Du and Olhoff [46]. For this parameter study, however, two different interpolation schemes are used to obtain proper results for both the force excited and the base excited case. For a more detailed description of the reasoning behind this choice, the reader is referred to appendix C. For the stiffness interpolation, the scheme suggested by Zhu et al. [48] is utilized (equation 3.16):

$$f(x_e) = \frac{15}{16}x_e^p + \frac{x_e}{16}, \qquad p = 5 \tag{B.1}$$

For the mass interpolation function, a standard SIMP model (equation 3.9) is used and defined by:

$$f(x_e) = x_e^q, \qquad q = 3 \tag{B.2}$$

With the interpolation functions for the mass and stiffness matrices defined, only the damping is left to be defined. As mentioned in section 4.4, stiffness proportional Rayleigh damping will be used. The Rayleigh damping scheme is given in equation 4.13, and the damping parameters used are:

$$\alpha = 0, \qquad \beta = \frac{2\zeta}{\omega_{\text{exc}}}, \tag{B.3}$$

where ω_{exc} represents the excitation frequency, and the imposed constant damping coefficient is ζ=0.05.

B.1.2. Initial uniform design domain

In order to examine the influence of the excitation frequency ω_{exc} on the proposed objective function, a set of frequencies of interest can be defined which will best represent its behaviour. As mentioned in 4.6, the dynamic compliance given equation 4.22, which is commonly used for topology optimization of harmonic force excited structures, suffers from premature convergence problems caused by an anti-resonance matching the excitation frequency [76]. The frequency response normally used for dynamic compliance can, therefore, be used to determine the frequencies of interest. Figure B.4a shows the undamped frequency response of the initial design domain, together with the norm function response N_m for the values m=2, m=4, m=8, m=12 and m=20. Figure B.4b shows the same response, only including the mentioned stiffness proportional damping, which varies with the excitation frequency. The degree of freedom of interest is chosen to be at the force excitation point.

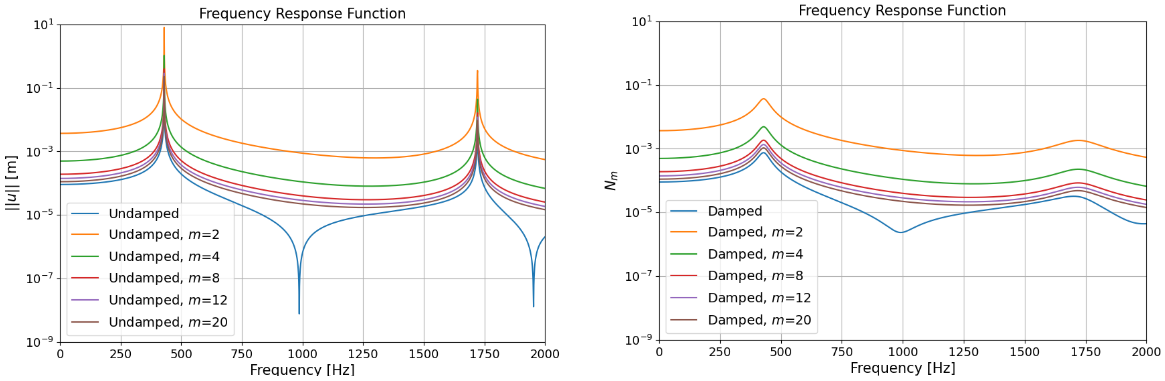

(a) Undamped frequency response

(b) Damped frequency response

Figure B.4: The undamped and damped frequency response of the initial design domain given in figure B.1b for the displacement response as well as the norm function response N_{mw} for a sweep over the parameter m.

From figure B.4b it is evident that even in a damped case, the system still has anti-resonances. Considering now the response of the global norm function N_m for both the undamped and the damped case, it is clear that the response does not show any anti-resonances as was explained in section 6.1. Furthermore, it is evident that the norm function approximates the original frequency response, achieving a better representation as m increases. For low values of m it can also be noted that the resulting graph is substantially higher in magnitude than the other graphs. This is due to the nature of the norm function, and this should not influence the resulting performance as it is only a scaling of the response. It seems that the norm function approximates the original response best as m->∞. The appropriate value of this parameter for each problem, however, will be examined later.

From figure B.4 several frequencies of interest can be extracted. These frequencies will be determined by any frequency leading to convergence issues for an objective function such as dynamic compliance. First and foremost, the first resonance frequency is chosen as this is the classical 'boundary' frequency at which the dynamic compliance will fail to converge. Next, the first anti-resonance frequency is chosen, which for the dynamic compliance would yield a fast convergence as the starting point would be close to a local minimum. To cover the behaviour between these two frequencies, a frequency halfway between these frequencies is chosen. Lastly, the second resonance frequency is chosen to examine whether the same performance of optimizing for the first resonance can be found at higher frequencies. The values of these frequencies are 429Hz, 700Hz, 986Hz and 1721Hz, respectively and are plotted in figure B.5.

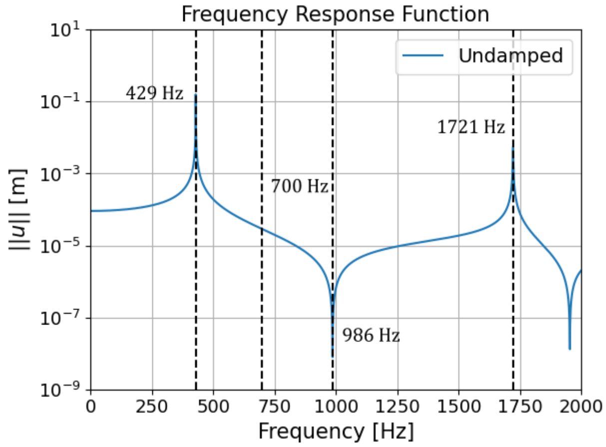

Figure B.5: The chosen frequencies of interest for the parameter study on global minimization subjected to a force excitation.

One last thing to note, however, is that whilst the frequencies of interest have been extracted from the frequency response concerning the force excitation point, these are not the actual eigenfrequencies of the system. The computed eigenfrequencies are given in table B.4, and it is immediately clear that the second and third eigenfrequency ω_2 and ω_3 are not present in the frequency response in figure B.4a. Further inspection, however, reveals the reason why this is the case. In figure B.6, the vertical displacements of the eigenmodes corresponding to these eigenfrequencies are visualized using ParaView. From these figures, it is clear that the force excitation point exhibits no movement in the vertical direction at these eigenfrequencies, and these frequencies are, therefore, not present in the obtained frequency response.

Computed Eigenfrequencies	ω_1	ω_2	ω_3	ω_4
	429Hz	1013Hz	1483Hz	1721Hz

Table B.4: An overview of the first four eigenfrequencies computed for the initial uniform design domain given in figure figure B.1b.

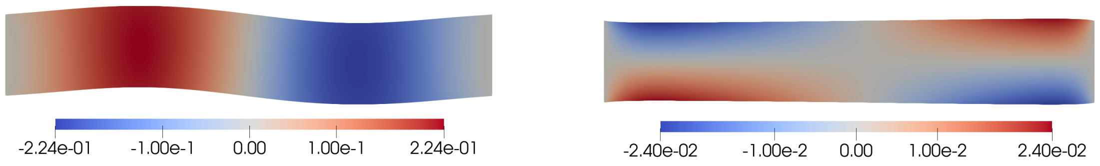

(a) Eigenfrequency w_2

(b) Eigenfrequency w_3

Figure B.6: A visualization of the vertical displacements present for the eigenmodes accompanying the second and third eigenfrequency of the initial design domain.

This begs the question of whether the chosen degree of freedom of interest is an appropriate choice for representing the behaviour of the system. As one of the main goals of this objective function is to overcome the shortcomings of an objective function such as dynamic compliance, it is reasonable to compare the same responses which would be used if this function was employed. Furthermore, the degree of freedom of interest is also the force application point, which is the point where maximum deformation is expected. However, it has to be kept in mind that orthogonal modes such as those mentioned above can present themselves.

B.1.3. Influence of γ_1 on global minimization

For a global minimization, all degrees of freedom are used in the computation of the norm function of equation 6.6. This means that the overall response of the structure to the applied force will be minimized, or in other words, the global response will be minimized. This subsection will examine the influence of the static compliance contribution γ_1 and determine its value for the subsequent optimizations.

The parameter γ_1 determines the extent to which the static compliance contributes to the objective function. For low values of γ_1, the parameter γ_2 ($|\gamma_1| + \gamma_2 = 1$) has a high value which results in the optimization being more focused on incorporating the minimization of the static compliance and vice versa for higher values of γ_1. Setting the excitation frequency at the first frequency of interest of 429Hz, the results for the values γ_1=0.0 (static compliance minimization), γ_1=0.95, γ_1=0.99 and γ_1=1.0 are given in figure B.7. As the values of the parameters w and m will be examined later, these are set at w=1 and m=2, respectively.

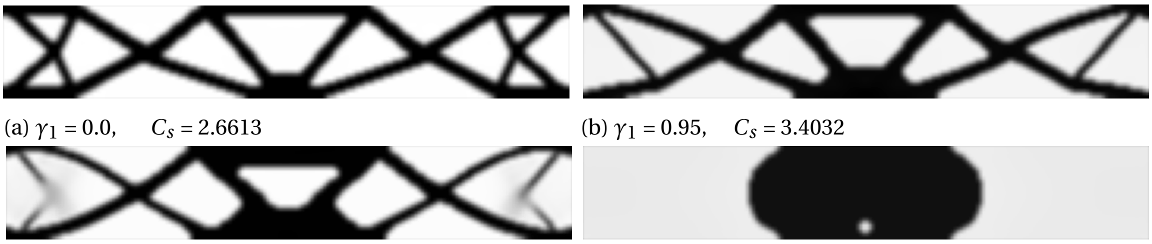

(a) $\gamma_1 = 0.0, \quad C_s = 2.6613$

(b) $\gamma_1 = 0.95, \quad C_s = 3.4032$

(c) $\gamma_1 = 0.99, \quad C_s = 4.5239$

(d) $\gamma_1 = 1.0, \quad C_s = 0.9136$

Figure B.7: The topologies found for a parameter sweep over the parameter γ_1 for global minimization subjected to a force excitation together with the accompanying static compliance values.

One thing that immediately stands out from these results is the result from γ_1=1.0, which yields a disconnected topology. This shows that the inclusion of the static compliance factor remains a necessary component of this objective function in order to obtain connected results. Comparing the static compliance values C_s for all structures, this value decreases as γ_1 decreases, as is to be expected. This is not the case for γ_1=1.0, but this can be explained by the disconnected topology. In order to comply with the minimization of the global norm part of the objective function, it seems the goal is to construct more flexible connecting structures which connect the middle section to the boundaries. For the value γ_1=0.99, the optimization does seem to suffer with the occurrence of intermediate densities, however. A more in-depth analysis can be taken by examining the frequency response of the obtained structures. The undamped frequency response of the force excitation point is given in figure B.8.

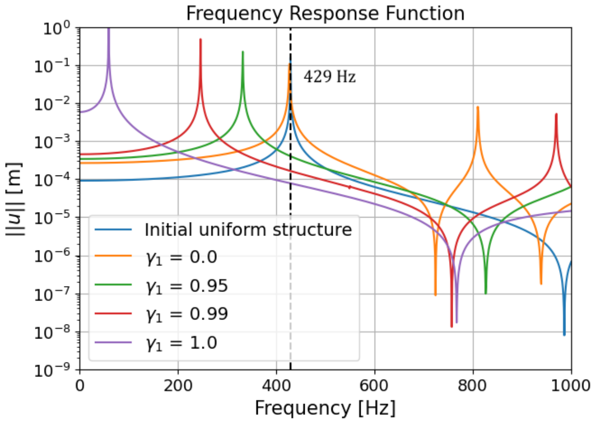

Figure B.8: The undamped frequency response comparison of the resulting topologies given in figure B.7 and the initial uniform domain, showcasing the influence of the parameter γ_1 on global minimization subjected to a force excitation.

This graph clearly shows that as the parameter γ_1 increases, the first eigenfrequency and first anti-resonance is moved further away from the excitation frequency of 429Hz. For the static minimization γ_1=0.0, this behaviour does not occur at all, showing the direct influence of the global norm function. It should also be noted that the resulting topology for γ_1=0.99 contains an eigenmode at 408Hz, which is close to the excitation frequency. Further inspection revealed a similar mode as was found in figure B.6a. This reveals that, even though the global minimization takes into account all degrees of freedom, the force application point is prioritized, and as such even a mode which contains displacements at all degrees of freedom except this point is considered complying with the objective function. This prioritization could be explained by the fact that the excitation point presents the highest displacements, which then become the priority for the norm function.

B.1.4. Discussion on the influence of γ_1 on global minimization

From these results it can be concluded that the static compliance factor is still required in the formulation of the objective function. Increasing this contribution, however, limits the frequency response properties of the obtained structures. Even though the optimizer appears to allow eigenmodes to be present at the excitation frequency for $\gamma_1 = 0.99$, this behaviour is interesting to observe and therefore, the parameter γ_1 will be set at $\gamma_1 = 0.99$ for optimizations where this parameter is fixed. This will allow for the observation of the global norm function without much influence from the static compliance factor. For optimizations where a set of γ_1 values is examined, the subset is shifted towards γ_1=0.99, γ_1=0.95 γ_1=0.90 as γ_1=1.0 yields a disconnected topology.

B.1.5. Influence of the parameter w on global minimization

Next, the influence of the parameter w on a global minimization can be examined. As w has a direct influence on the weighting factor assigned to each degree of freedom (equation 6.7), and all degrees of freedom are taken into account, this parameter is expected to have a visible influence.

For these optimizations, the excitation frequency is again set at 429Hz, the parameter m at 2 and γ_1 at 0.99 so as not to hinder dynamic properties whilst still obtaining connected topologies. The parameter values of interest will be w=0, w=2, w=4 and w=8. This first value of w=0 is, however, technically not possible due to $1/w = 1/0$ in equation 6.7 being undefined. Therefore, w=0 refers to the use of the original norm objective function without the added density weights as given in equation 6.4. The results are given in figure B.9.

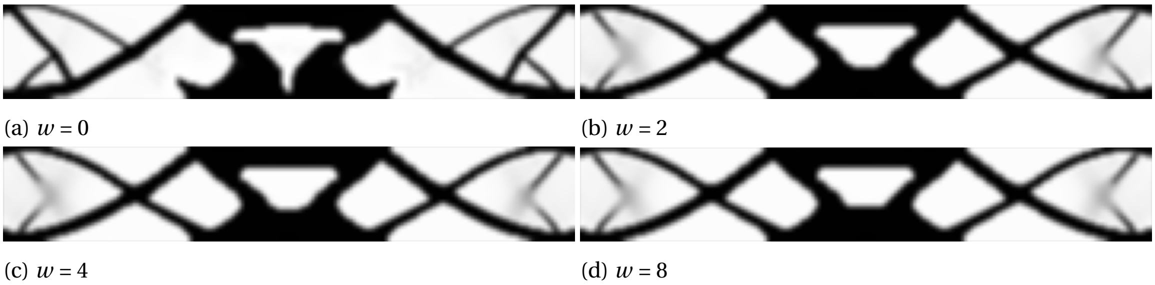
(a) $w = 0$
(b) $w = 2$
(c) $w = 4$
(d) $w = 8$

Figure B.9: The topologies found for a parameter sweep over the parameter w for global minimization subjected to a force excitation.

From the obtained topologies, it does not appear that the parameter w has much influence on the topology apart from the result of w=0. This is similar to the results presented by Montero et al. [37], which also showed only subtle differences apart from w=0. What is interesting is the fact that the density weights were introduced to prevent intermediate densities from appearing, yet these results show the exact opposite, with fewer intermediate densities being present when the density weights are not utilized. Further analysis can be done by examining the frequency response, the undamped version of which is given in figure B.10. This figure also includes the response for an extreme case of w=20, the topology of which is not given due to showing no visible difference to the results from lower values of w.

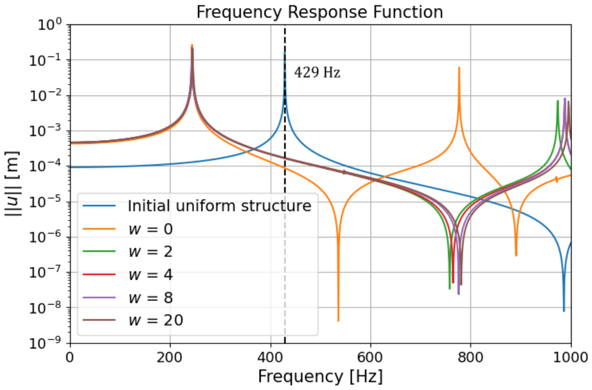

Figure B.10: The undamped frequency response comparison of the resulting topologies given in figure B.9 and the initial uniform domain, showcasing the influence of the parameter w on global minimization subjected to a force excitation.

The frequency response presents the same result, showing very little difference between the performance of the obtained topologies for different values of w. Only the result of w=0 seems to be vastly different. Upon further inspection, however, it seems that there is a slight asymmetry visible near the force excitation point. To confirm this, the magnitudes of the displacements can be examined in ParaView, a visualization of which is given in figure B.11.

(a) The resulting topology for $w = 0$

(b) A visualization of the displacement magnitudes resulting from the applied force excitation done in ParaView

Figure B.11: The resulting topology and displacement magnitudes for w=0, showing an asymmetry present in the resulting topology and displacement magnitudes where symmetry is expected.

This clearly shows that asymmetry is present within the obtained topology. The cause of this asymmetry might be numerical errors occurring during the optimization. As the used MMA optimizer (section 3.6) works with a specified tolerance, all values below this tolerance might sustain rounding errors, which could introduce asymmetry. To prevent this from happening, the optimization is performed again, but this time with a forced symmetry added on the y-axis. This is a valid operation as the problem formulation for this optimization is symmetric, which is expected to yield a symmetric result. This result is given in figure B.12.

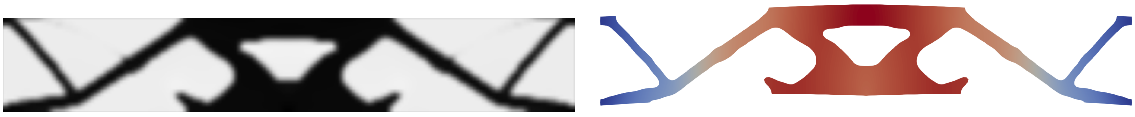

(a) The resulting topology for $w = 0$ including a forced symmetry over the y-axis

(b) A visualization of the displacement magnitudes resulting from the applied force excitation done in ParaView

Figure B.12: The resulting topology and displacement magnitudes for w=0 including a forced symmetry over the y-axis.

The optimization now yields an expected symmetric result. The frequency response comparison from figure B.10 can, therefore, be plotted again with the results from this newly obtained topology. This comparison is given in figure B.13.

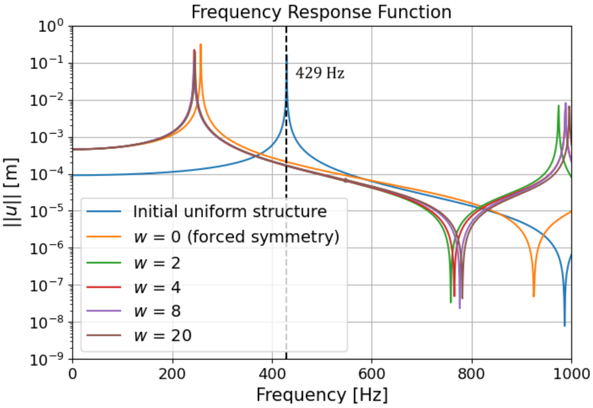

Figure B.13: The undamped frequency response comparison of the resulting topologies given in figure B.9, the forced symmetry result given in figure B.12a and the initial uniform domain.

The performance of the result, including forced symmetry, is now vastly different and more in line with the other results. However, when comparing them, there seems to be little difference in the inclusion of the parameter w for the first resonance. If the goal is to 'push' the resonance frequencies as far away from the excitation frequency as possible, then the inclusion of the parameter w is favourable comparing the location of the first resonance. The opposite appears to be true for the first anti-resonance, but given that the objective function does not measure the anti-resonance, this is likely coincidental. The inclusion of the density weights, therefore, seems problem-dependent but, overall, does not seem to have a large influence.

B.1.6. Discussion on the influence of w on global minimization

From the results found, the impact of the parameter w seems minimal. Including the density-weighted filter does seem to increase performance in terms of moving the first resonance further away from the excitation frequency, yet only slightly. When removing the density-weighted filter (w=0) it seems that a forced symmetry is necessary to prevent the optimizer from obtaining asymmetrical designs. In the coming sections, the use of forced symmetry will be assessed on a case-by-case basis, and it will be mentioned when this is necessary. For the examination of the influence of the parameter m however, the parameter w will be included to study the influence of m combined with the density-weighted filter. Considering the results, the value of w chosen does not seem to make a difference, so therefore, the choice is made for simply w=1.

B.1.7. Influence of the parameter m on global minimization

With the influence of the parameter w established, the influence of the parameter m can be examined. In order to ensure that the derivative of the complex norm function from equation 6.4 remains defined, the parameter m must remain even. Therefore, the values m=2, m=4, m=8 and m=12 are chosen to be examined. For these experiments, the excitation frequency is again set at 429Hz, the parameter w at 1 and γ_1 at 0.99. The results are given in figure B.9.

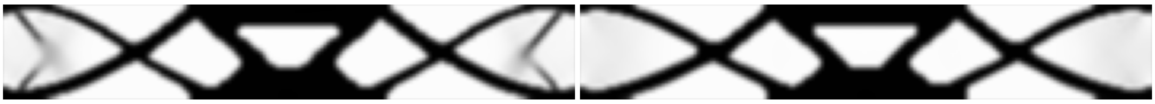

(a) $m = 2$, $M_{nd} = 27.70\%$ (b) $m = 4$, $M_{nd} = 25.26\%$

(c) $m = 8$, $M_{nd} = 25.67\%$ (d) $m = 12$, $M_{nd} = 21.11\%$

Figure B.14: The topologies found for a parameter sweep over the parameter m for global minimization subjected to a force excitation without forced symmetry together with the accompanying measure of non-discreteness values.

Comparing these results to those from the parameter sweep of parameter w, the parameter m seems much more pronounced. Particularly, this influence is found in the connecting structure between the boundary and the larger centre structure. For $m \geq 2$, the intermediate structure within this connecting structure disappears and changes completely for m=12. The result for m=8, however, does seem to present some asymmetry, which might be caused by the sensitivities becoming very small when the power operation $1/m$ is performed. Interestingly, this behaviour does not occur for the even higher values of m=12. Comparing the measure of non-discreteness values, it is clear that a larger value of m yields better black-and-white designs, which are traded for numerical stability. The undamped frequency response of these topologies is given in figure B.15, which also contains the response for m=20, which showed little topological difference to the m=12 result.

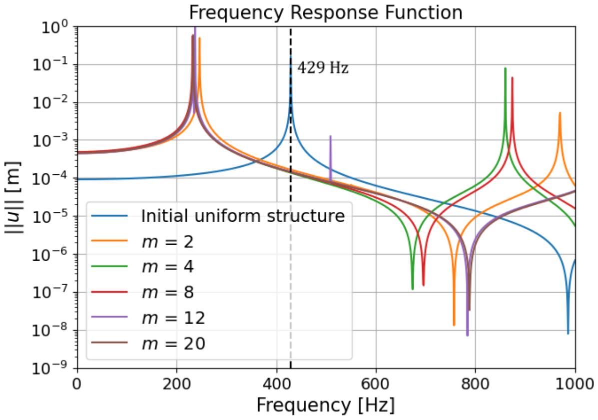

Figure B.15: The undamped frequency response comparison of the resulting topologies given in figure B.14 and the initial uniform domain, showcasing the influence of the parameter m on global minimization subjected to a force excitation without forced symmetry.

One thing that immediately stands out is the little resonance spike from m=12 at around 509Hz. This can probably be explained by the clearly different topology of this design. Comparing the responses, yields that the distance between the resonance, anti-resonance and excitation frequency increases as m increases. For m=2 however, the behaviour is vastly different. To assess whether this is due to an asymmetry being present, forced symmetry can be added to the design problem, and the same parameter sweep can be performed again. The resulting topologies are given in figure B.16.

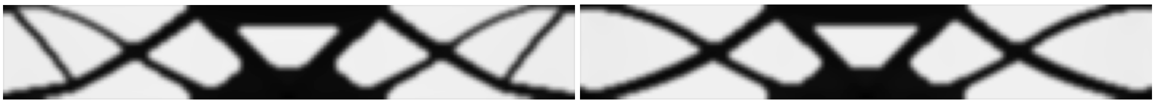

(a) $m = 2$ (b) $m = 4$

(c) $m = 8$ (d) $m = 12$

Figure B.16: The topologies found for a parameter sweep over the parameter m for global minimization subjected to a force excitation including forced symmetry over the y-axis.

Interestingly, these results show little differences in topology between each other apart from m=2 when compared to the results from figure B.14. The inner structures that were semi-present or contained intermediate densities in the previous case are now either not present or fully defined. This shows that the added symmetry yielded an improvement in the obtained topology. To see how the frequency response has changed due to the forced symmetry, the undamped frequency response is given in figure B.17.

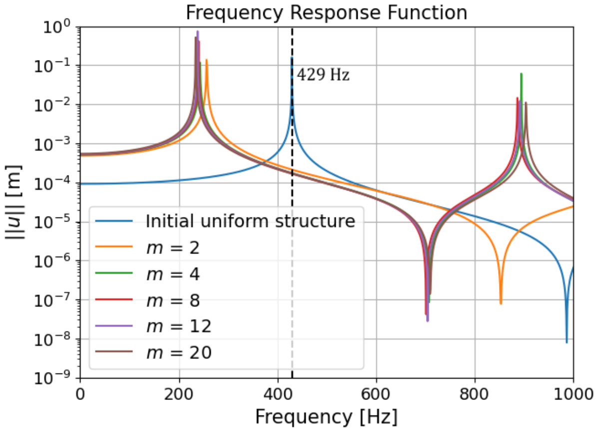

Figure B.17: The undamped frequency response comparison of the resulting topologies given in figure B.16 and the initial uniform domain, showcasing the influence of the parameter m on global minimization subjected to a force excitation including forced symmetry over the y-axis.

These results show very different behaviour compared to what was found in figure B.17. There is now little difference in response to be found apart from the result from m=2. This result, however, is also in line with the response found for the initial design domain in figure B.4. Therefore, it seems that any value of $m \geq 2$ is sufficient. One other aspect that proves this is the location of the second eigenfrequency. It was already established that an eigenmode could occur near the excitation frequency, which contains no displacements at the force excitation point as given in figure B.6. The values of these second eigenfrequencies ω_2 for the structures of figure B.16 are given in table B.5. These show that as the parameter m increases, this eigenmode is also moved further away from the excitation frequency, showing that a value of $m \geq 2$ is beneficial.

Second eigenfrequency ω_2	m=2	m=4	m=8	m=12	m=20
ω_{exc} = 429Hz	412Hz	386Hz	383Hz	379Hz	363Hz

Table B.5: An overview of the second eigenfrequencies computed for the topologies given in figure B.16.

Lastly, to also fully define the influence of the parameters w and m together, the forced symmetry results can be obtained again, but this time without the inclusion of the density weights (w=0). These results are given in figure B.18.

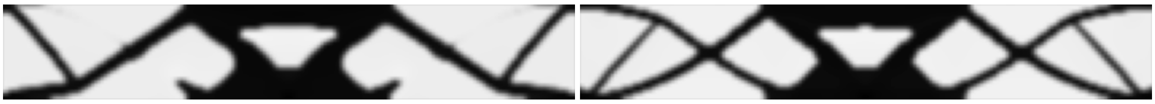

(a) $m = 2$ (b) $m = 4$

(c) $m = 8$ (d) $m = 12$

Figure B.18: The topologies found for a parameter sweep over the parameter m for global minimization subjected to a force excitation including forced symmetry over the y-axis and excluding the density-weighted filter (w=0).

Without the density-weighted filter, it seems that the occurrence of ill-defined members with intermediate densities has returned. This shows that even though the influence of the density weights seemed minimal in section B.1.4, it has a defined influence on these results. The undamped frequency response is given in figure B.19 for further analysis.

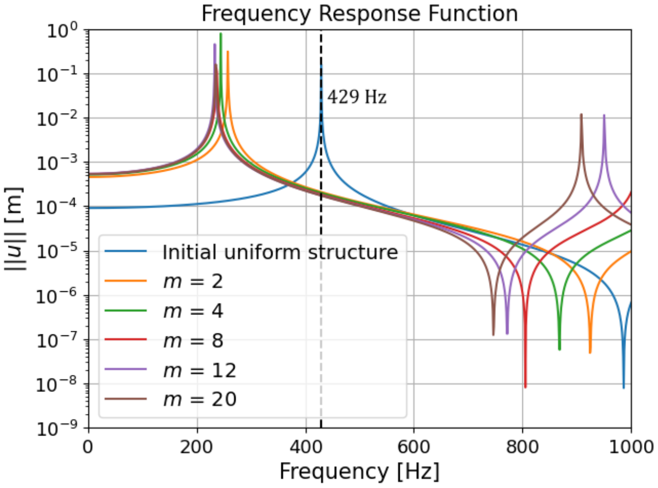

Figure B.19: The undamped frequency response comparison of the resulting topologies given in figure B.18 and the initial uniform domain, showcasing the influence of the parameter m on global minimization subjected to a force excitation including forced symmetry over the y-axis and excluding the density-weighted filter (w=0).

The resulting frequency response now shows quite some differences from the response found in figure B.17. The difference seems to be mainly in the location of the first anti-resonance of the structure, which is likely due to the absence of the density-weighted filter, which results in an increase in intermediate densities. As the parameter m increases, however, these intermediate densities seem to diminish, and the resulting response seems to represent the one found in figure B.17. Lastly, looking at the second eigenfrequency ω_2 of the obtained structures as given in table B.6, it seems that an increase in the parameter m yields a second eigenfrequency which is closer to the excitation frequency of 429Hz. This is the opposite behaviour of what was found in table B.5, which included the density-weighted filter.

Second eigenfrequency ω_2	m=2	m=4	m=8	m=12	m=20
ω_{exc} = 429Hz	258Hz	490Hz	441Hz	417Hz	408Hz

Table B.6: An overview of the second eigenfrequencies computed for the topologies given in figure B.18.

B.1.8. Discussion on the influence of m on global minimization

The previous section provided insight into both the parameter m as well as the parameter w and yielded some interesting results. It seems that without the inclusion of a forced symmetry over the y-axis, the response of the obtained structures varies drastically without a clear trend. Including forced symmetry, however, the parameter m does not seem to have a large influence for $m \geq 2$, which is beneficial as a higher value of m increases the nonlinearity of the system. A larger value of m does, however, increase the distance between the second eigenfrequency and the excitation frequency. If the density-weighted filter is removed, however, the occurrence of intermediate densities increases, and the responses vary drastically. The second eigenfrequency behaviour also inverts, which is interesting.

Given the obtained results, it seems that an appropriate value of m is any $m \geq 2$, and to limit the nonlinearity of the system, the value of m=4 is chosen for subsequent optimizations of global minimization subjected to a force. As for the density-weighted filter, its inclusion seems to improve performance in terms of the occurrence of intermediate densities, which then leads to the final parameter choice of w=1 and m=4. As for the forced symmetry, it appears it has to be included in the optimization.

B.1.9. Influence of the density-weighted filter radius R_{DW} on global minimization

Another study which can be done for global minimization is to assess the influence of the filter radius of the density-weighted filter. The filter definition of Montero et al. [37] given in equation 6.7 considers a subset S_j which only contains the elements directly surrounding jth the degree of freedom. However, this radius can also be increased to incorporate a larger or smaller area for the weight calculation. To compare the differences of these filter radii, however, a new density-weighted filter has to be created, which is given in equation B.4.

$$a_j = \left(\frac{\sum_{v\epsilon S_j} x_v^w}{\#S} \right)^{\frac{1}{w}} \tag{B.4}$$

The only difference between this filter and the original is that the sum of the penalized surrounding elements is now normalized by the number of elements which are taken into account. This allows for the results of different filter radii to be compared to each other. The radii which will be assessed are the original R_{DW}=1, R_{DW}=2, R_{DW}=3 and R_{DW}=6. The parameters w and m are set at w=1 and m=4, γ_1 is set at 0.99, the excitation frequency at 429Hz and the results are given in figure B.20.

(a) $R_{\mathrm{DW}} = 1$ (b) $R_{\mathrm{DW}} = 2$

(c) $R_{\mathrm{DW}} = 3$ (d) $R_{\mathrm{DW}} = 6$

Figure B.20: The topologies found for a parameter sweep over the density-weighted filter radius R_{DW} for global minimization subjected to a force excitation including forced symmetry over the y-axis and the parameter values w=1 and m=2.

The obtained topologies seem to show little difference difference in topology apart from R_{DW}=6, which only differs slightly. A deeper delve can be done by comparing the frequency responses of the obtained topologies. In figure B.21, the undamped frequency response is given, which also includes the results for R_{DW}=4. The topology of this value was not included as the topology showed no visible difference from R_{DW}=3.

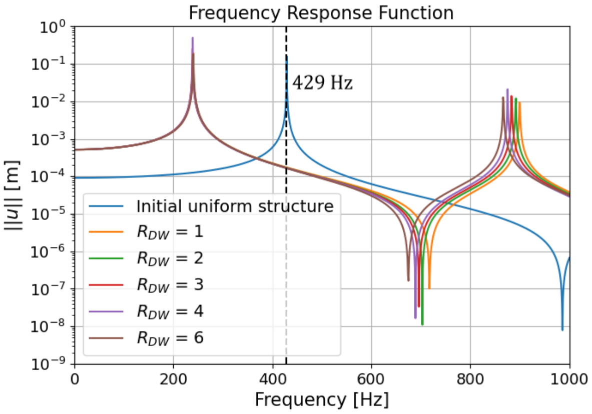

Figure B.21: The undamped frequency response comparison of the resulting topologies given in figure B.20 and the initial uniform domain, showcasing the influence of the density-weighted filter radius R_{DW} on global minimization subjected to a force excitation including forced symmetry over the y-axis and parameter values w=1 and m=2.

Comparing the results also shows little difference in the location of the first resonance. For the first anti-resonance, however, it could be argued that an increase in R_{DW} yields a decrease in performance as the anti-resonance moves closer towards the excitation frequency. Furthermore, the computation time required to obtain the topologies of figure B.20 increases by 20% from R_{DW}=1 to R_{DW}=6, which shows a further decrease in performance when the density-weighted filter radius is increased. The initial R_{DW}=1 is therefore sufficient.

B.1.10. Influence of the excitation frequency ω_{exc} on global minimization

The last study, considering global minimization subjected to a force excitation, examines the influence of the excitation frequency ω_{exc}. In the previous sections, the excitation frequency was fixed at the first frequency of interest of 429Hz. In this section, however, all frequencies of interest given in figure B.5 are examined. This frequency sweep is performed together with a sweep over the static compliance factor γ_1 to assess its influence at higher frequencies. The parameters w and m are set at w=1 and m=4, forced symmetry is added over the y-axis, and the results of this two-sided sweep are given in figure B.22.

(a) γ_1 = 0.90, ω_{exc}=429Hz (b) γ_1 = 0.95, ω_{exc}=429Hz (c) γ_1 = 0.99, ω_{exc}=429Hz

(d) γ_1 = 0.90, ω_{exc}=700Hz (e) γ_1 = 0.95, ω_{exc}=700Hz (f) γ_1 = 0.99, ω_{exc}=700Hz

(g) γ_1 = 0.90, ω_{exc}=986Hz (h) γ_1 = 0.95, ω_{exc}=986Hz (i) γ_1 = 0.99, ω_{exc}=986Hz

(j) γ_1 = 0.90, ω_{exc}=1721Hz (k) γ_1 = 0.95, ω_{exc}=1721Hz (l) γ_1 = 0.99, ω_{exc}=1721Hz

Figure B.22: The topologies found for a two-sided parameter sweep over both the parameter γ_1 and the excitation frequency ω_{exc} for the frequencies of interest defined in section B.1.2 showcasing their influence on global minimization subjected to a force excitation including forced symmetry over the y-axis and the parameter values w=1 and m=4.

Whilst the influence of the parameter γ_1 was already examined for 429Hz, its influence at higher frequencies is clearly visible. For γ_1=0.90, meaning quite substantial static compliance contribution, the excitation frequency has limited influence on the obtained topology until the frequency is raised to 1721Hz. For higher excitation frequencies in general, more focus is laid on distributing material in the centre structure. This allows for more slender connecting structures, providing lowered stiffness. This lower stiffness then allows the system to minimize the response at higher frequencies. As γ_1 decreases for these higher frequencies, however, more material is deposited on the connecting structure to provide more stiffness to resist the applied static force. One last thing to note is that all obtained topologies contain almost no intermediate densities, showing that the settings obtained from the studies of the previous sections are appropriate for this set of frequencies. To observe the change in response of the obtained structures as compared to the initial uniform domain, the undamped frequency response is given in figure B.23.

The result for 429Hz shows similar behaviour to the behaviour found in figure B.8 as is to be expected. For 700Hz, the first resonance seems to be moved away from the excitation frequency, which comes at the cost of also moving the first anti-resonance closer. An increase in γ_1 then yields a first resonance, which is further away, and an anti-resonance, which is also relatively further away. For 986Hz, which initially contained an anti-resonance, the optimizer seems to move the anti-resonance further away from the excitation frequency. This is beneficial behaviour as this shows that the proposed objective function works well, even directly at an anti-resonance. A consequence, however, is that higher order modes are 'pulled' towards the excitation frequency, but this behaviour seems to decrease as γ_1 increases. Lastly, at 1721Hz, the influence of γ_1 diminishes as there is hardly any difference between the lower resonance nearest to the excitation frequency. For the first higher resonance however, tough γ_1=0.90 and γ_1=0.95 show similar behaviour, γ_1=0.99 seems to have a resonance present further away from the excitation frequency.

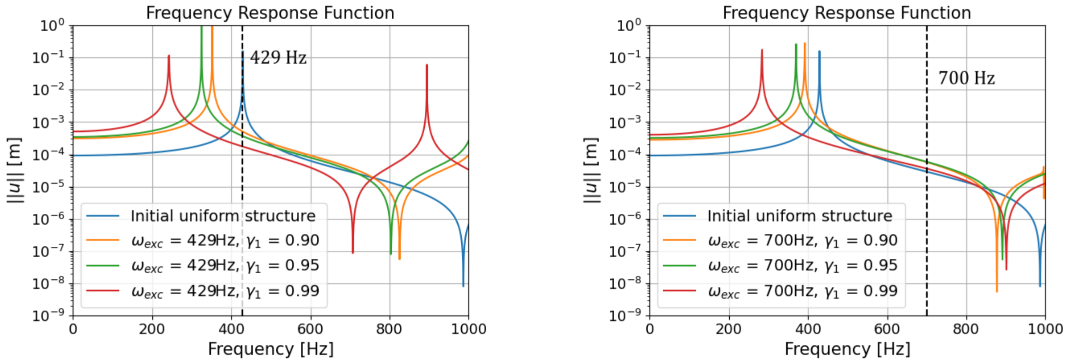

(a) ω_{exc}=429Hz

(b) ω_{exc}=700Hz

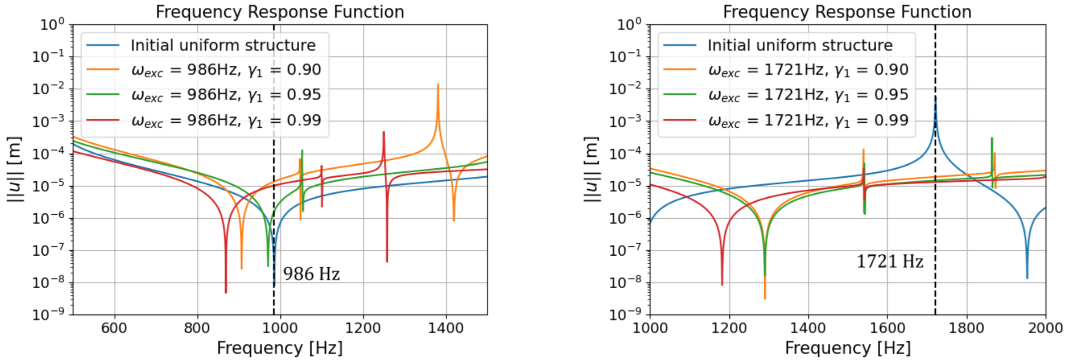

(c) ω_{exc}=986Hz

(d) ω_{exc}=1721Hz

Figure B.23: The undamped frequency response comparison of the resulting topologies given in figure B.22 and the initial uniform domain, showcasing the influence of the parameter γ_1 for each of the four respective excitation frequencies of interest ω_{exc} on global minimization subjected to a force excitation including forced symmetry over the y-axis and parameter values w=1 and m=4.

B.1.11. Discussion on the influence of ω_{exc} on global minimization

First of all, it is evident that the proposed objective function works very well at all frequencies of interest, showing almost no intermediate densities within all obtained results. This shows that the chosen values of the parameters w and m are also appropriate for all excitation frequencies of interest. Furthermore, the influence of γ_1 remains similar over all frequencies, where an increase in the static compliance contribution (or a decrease in γ_1) limits the frequency response performance to increase the static compliance.

B.2. Global minimization subjected to a base excitation

With the behaviour of the global minimization function examined for a force excitation, the same study can be performed considering a base excitation. For these studies, the same clamped beam problem with dimensions 1.8 × 0.3 × 0.01m from figure B.2 will be utilized. For the static compliance contribution, the same load case as for the force excited case will be used.

The first load case is shown in figure B.24a. The main difference is found in the boundary conditions. Where these were fixed in both directions for the force excited case, both boundaries are now only fixed in the x-direction. On the y-directional boundary degrees of freedom, the harmonic base excitation $u(\omega)$ with a magnitude of 100 m/s^2 is applied as explained in section 4.7.1. Furthermore, an additional mass m_b is added to the bottom middle node. Considering the mass of the total structure is 42.1kg ($l_x \times l_y \times l_z \times \rho$), the magnitude of this added mass is set at 10kg.

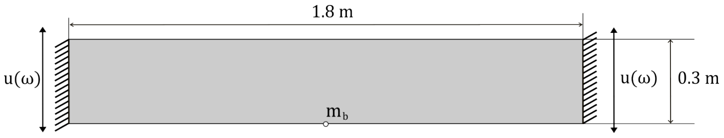

(a) Load case 1

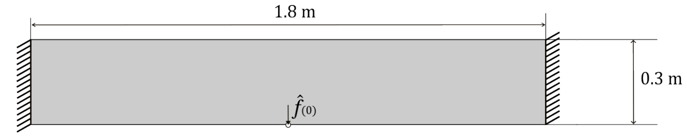

(b) Load case 2

Figure B.25: The two load cases required for global minimization subjected to a base excitation including the used dimensions.

Property	Value	
l_x, l_y, l_z	1.8, 0.3, 0.01	[m]
n_x, n_y	180, 30	[#]
$\hat{f}$	10	[kN]
$\hat{u}$	100	$[m/s^2]$
m_b	10	[kg]
Filter radius	2	[#]
Volume fraction	0.4	[-]

Table B.7: An overview of the properties of the used design domain.

The second load case contains the design domain for static compliance. In this case, the boundaries remain fixed in both directions and a static force $\mathbf{f}(0)$ with the same magnitude as the force excited case $\hat{f}$=10kN is applied. Regarding the material properties of the structure and the settings for the MMA optimizer, these are similar as well and the same material interpolation functions are used, with PIS (equation 3.16) for the stiffness interpolation and standard SIMP (equation 3.9) for the mass interpolation as was determined in appendix C. Lastly, the same Rayleigh damping parameters given in equation B.3 are used.

B.2.1. Initial uniform design domain

Whilst the design domain is similar to the force excited case, it can be noted that an extra mass m_b is now added to the system, which will result in vastly different eigenfrequencies of the initial uniform design domain. The frequency response of this domain is therefore examined again for the same vertical degree of freedom of the bottom middle node as this node also contains the added mass. Figure B.26 shows the undamped frequency response of the initial design domain, together with the norm function response N_m for the values m=2, m=4, m=8, m=12 and m=20.

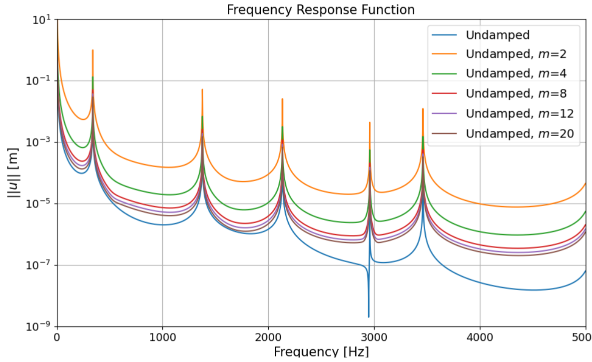

Figure B.26: The undamped frequency response of the initial design domain given in figure B.25 for the displacement response as well as the norm function response N_{mw} for a sweep over the parameter m.

The location of the mass is chosen as the response point as the harmonic base excitation examples given in section 4.7 endured excitation frequency problems limited by the resonance at the mass node. If the frequency response would be examined for global minimization n of these graphs would have to be analyzed, but this examination will only cover the vertical degree of freedom of the mass node. As can be seen from the frequency axis, the response is given up till a frequency of 5000Hz. This is due to the fact that no anti-resonances are present for this point of interest up until a frequency of 2947Hz.

From figure B.26, several frequencies of interest can be extracted. As mentioned in section 4.7, the harmonic base excitation problem also suffers from convergence issues when optimizing for frequencies above the first resonance. Therefore, the first resonance is again chosen as the first frequency of interest.

Secondly, the first anti-resonance is chosen, together with the location of the second eigenfrequency, which is not visible in the frequency response but is provided in table B.8. Lastly, a frequency is chosen such that a broad frequency spectrum is covered. The resulting values of these frequencies of interest are 340Hz, 880Hz, 1377Hz and 2947Hz, and these are given together with the undamped frequency response in figure B.27.

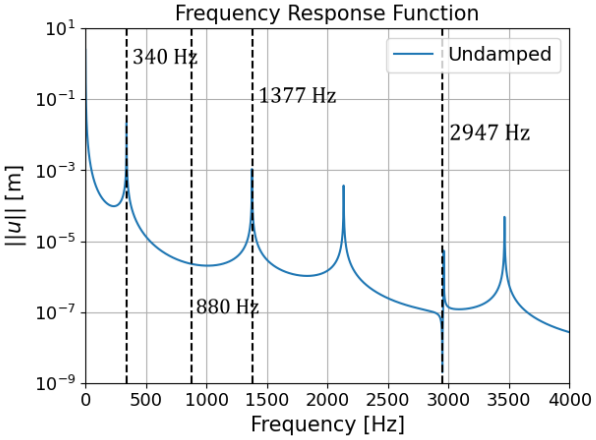

Figure B.27: The chosen frequencies of interest for the parameter study on global minimization subjected to a base excitation.

Computed Eigenfrequencies	ω_1	ω_2	ω_3	ω_4
	340Hz	880Hz	1155Hz	1377Hz

Table B.8: An overview of the first four eigenfrequencies computed for the initial uniform design domain given in figure B.25.

B.2.2. Influence of γ_1 on global minimization

The influence of the parameter γ_1 can now be examined again for the base excited case. As this design problem contains two load cases, the value of γ_1=0 explored in section B.1.3 is not relevant due to the base excitations being ignored entirely in this case. Therefore, the subset of values is shifted to γ_1=0.90, γ_1=0.95, γ_1=0.99 and γ_1=1.0. The outcome of γ_1=1.0 is also expected to produce a similar disconnected result as observed in figure B.7d, but this will still be confirmed for this excitation case. The values of parameters w and m are reverted back to w=1 and m=2, the excitation frequency is set at 340Hz, and the results are given in figure B.28.

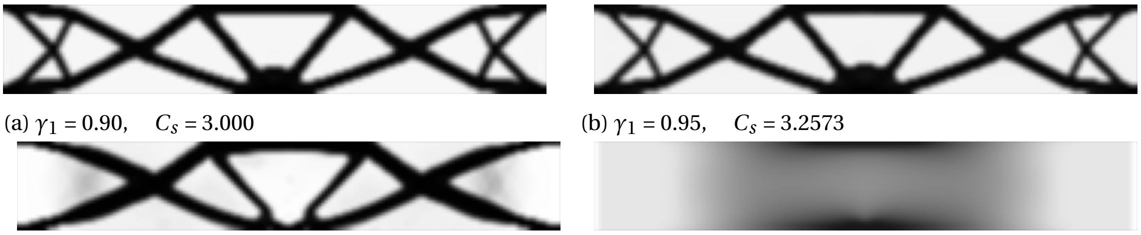

(a) $\gamma_1 = 0.90$, $C_s = 3.000$

(b) $\gamma_1 = 0.95$, $C_s = 3.2573$

(c) $\gamma_1 = 0.99$, $C_s = 5.4479$

(d) $\gamma_1 = 1.0$, $C_s = 33071342.14$

Figure B.28: The topologies found for a parameter sweep over the parameter γ_1 for global minimization subjected to a base excitation together with the accompanying static compliance values.

As was expected, the result of γ_1=1.0 yielded a disconnected result. Furthermore, the static compliance again decreases as the parameter γ_1 decreases, and the topology obtained for γ_1=0.99 again yields a topology which contains some intermediate density areas. These results are very similar to those found in section

B.1.3, and to confirm this, the undamped frequency response of the obtained topologies is given in figure B.29.

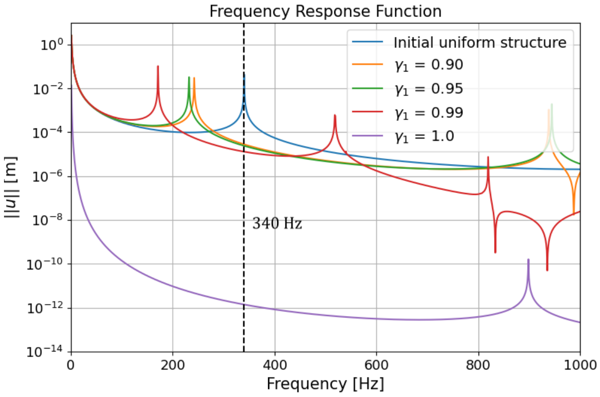

Figure B.29: The undamped frequency response comparison of the resulting topologies given in figure B.28 and the initial uniform domain, showcasing the influence of the parameter γ_1 on global minimization subjected to a base excitation.

These results show similar behaviour to those observed in figure B.8, where the first resonance is 'pushed' away from the excitation frequency. This effect becomes more pronounced as γ_1 increases, and is maximal for γ_1=1.0. A consequence of this effect, however, is that higher-order resonances are 'pulled' towards the excitation frequency. Furthermore, the first resonance of γ_1=1.0 is hardly visible due to it being located at 0.073Hz. Another thing to note is that the behaviour of the second eigenfrequency being close to the excitation frequency in the force-excited case was not found here.

B.2.3. Discussion on the influence of γ_1 on global minimization

The results shown above show that, similar to the force excited case, the static compliance factor remains a necessary contribution to the objective function. The influence of the parameter γ_1, however, is a lot more pronounced for γ_1=0.99, where higher order modes seemed to be 'pulled' towards the excitation frequency substantially more than for lower values of γ_1. For the coming optimizations, the parameter γ_1 will still be set at 0.99 to limit the influence of the static compliance. If a set of γ_1 values is examined, the subset will consist of γ_1=0.99, γ_1=0.95 γ_1=0.90 as γ_1=1.0 again yielded a disconnected topology.

B.2.4. Influence of the parameter w on global minimization

In section B.1.5, it was concluded that the influence of the parameter w was minimal, yet section B.1.7 showed it still had a positive influence. This parameter is, therefore, examined again for the base excited case. Setting γ_1 at 0.99, parameter m at 2 and the excitation frequency at 429Hz, the results in figure B.30 are obtained for the parameter values w=0, w=2, w=4 and w=8. The value w=0 again refers to the case where the density-weighted filter is removed.

(a) $w = 0$ (b) $w = 2$

(c) $w = 4$ (d) $w = 8$

Figure B.30: The topologies found for a parameter sweep over the parameter w for global minimization subjected to a base excitation.

These results again show that an asymmetric result is obtained for w=0. Furthermore, quite some intermediate densities are present for the results of higher values of w, which also occurred in the force excited case. These effects of these intermediate densities are also visible in the undamped frequency response given in figure B.31. This response also includes the result of w=20, which had little visible difference in topology form w=8.

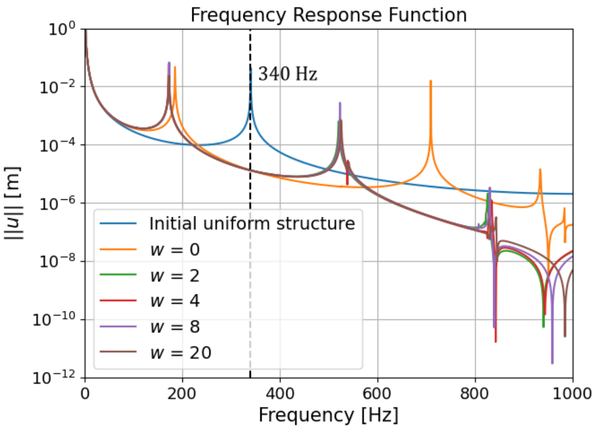

Figure B.31: The undamped frequency response comparison of the resulting topologies given in figure B.30 and the initial uniform domain, showcasing the influence of the parameter w on global minimization subjected to a base excitation.

The frequency response shows how higher order modes are ’pulled’ towards the excitation frequency for all values of w. The solution in section B.1.5 was to include a forced symmetry over the y-axis. As the base excited problem is symmetrical, this principle can also be applied here. The same results, including the forced symmetry, are given in figure B.32.

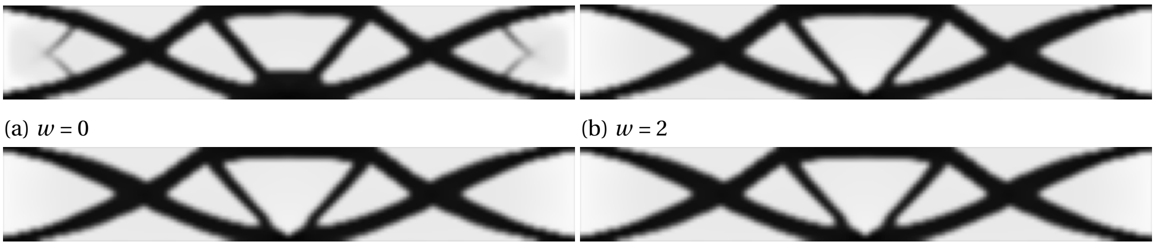

(a) $w = 0$

(b) $w = 2$

(c) $w = 4$

(d) $w = 8$

Figure B.32: The topologies found for a parameter sweep over the parameter w for global minimization subjected to a base excitation including forced symmetry over the y-axis.

With the added forced symmetry, the result for w=0 still contains some intermediate densities. The other results, however, show no intermediate densities in the design. This differs from the results found in the force-excited case, which showed the opposite behaviour. It would seem, therefore, that the addition of the density-weighted filter has the positive benefit of removing intermediate densities for a base excited problem. Furthermore, it seems that without the density-weighted filter, more material is distributed near the mass node, and with the density-weighted filter, mass seems to be removed from the mass node. Increasing the value of the parameter w however, appears to hardly affect the topology. The undamped frequency response of these results is given in figure B.33.

The issue of higher-order modes being ’pulled’ seems to have disappeared, showing that the included forced symmetry is beneficial. Apart from the result of w=0, there seems to be little difference in response, however. For higher-order resonances, the increase of w does seem to move the resonance further away from the excitation frequency, but only slightly.

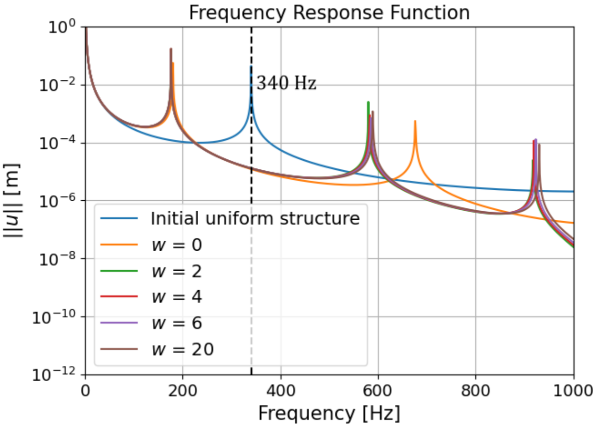

Figure B.33: The undamped frequency response comparison of the resulting topologies given in figure B.32 and the initial uniform domain, showcasing the influence of the parameter w on global minimization subjected to a base excitation including forced symmetry.

B.2.5. Discussion on the influence of w on global minimization

Similar to the results from section B.1.5, the influence of the parameter w is minimal. Its inclusion, however, meaning $w \geq 0$, is still necessary to suppress the occurrence of intermediate densities in the obtained result. On top of this, forced symmetry also seems required for the base excited problem. In the coming sections, the value of the parameter w will, therefore, be set at w=1, and forced symmetry over the y-axis will be included.

B.2.6. Influence of the parameter m on global minimization

Next, the influence of the parameter m is examined. For the force excited case, it was determined that any value higher than $m \geq 2$ was sufficient and that the inclusion of the density-weighted filter improved the results. In this section, however, the same parameter sweep will be performed again to establish whether this same behaviour occurs in the force-excited case. A sweep will, therefore, also be done for the case where the density-weighted filter is removed (w=0). Setting the parameter γ_1 at 0.99, the excitation frequency at 340Hz, the parameter w at 1 and including forced symmetry over the y-axis, the results for m=2, m=4, m=8 and m=12 are given in figure B.34.

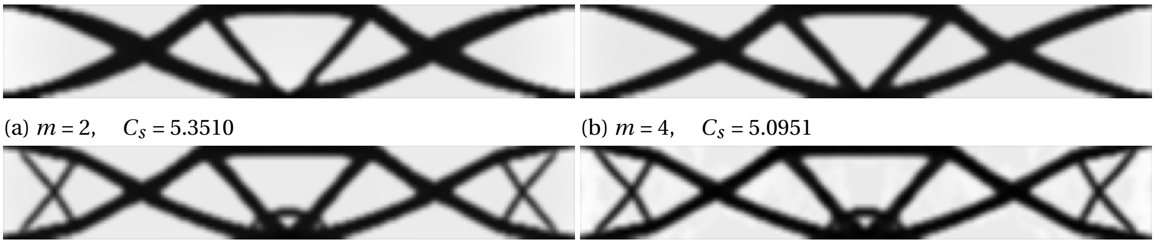

(a) $m = 2$, $C_s = 5.3510$

(b) $m = 4$, $C_s = 5.0951$

(c) $m = 8$, $C_s = 4.7244$

(d) $m = 12$, $C_s = 4.5522$

Figure B.34: The topologies found for a parameter sweep over the parameter m for global minimization subjected to a base excitation including forced symmetry over the y-axis, together with their accompanying static compliance values.

The resulting topologies show very different behaviour compared to the force-excited case, which had little influence. For the base excited case, it seems to have a significant influence, however. As m increases, the connecting structures which connect the centre structure to the base seem to get more material distributed towards them, which yields a connecting structure with added inner members. It seems that the heavier penalization yields structures which limit the displacements near the edges where the excitation takes place. This yields stiffer structures, as noted from the lower static compliance values C_s given in figure B.34. The result for m=8, however, yields added inner members, which are comprised of intermediate densities, when compared to the result of m=12, which contains the same members but with higher density values. For this case, a larger value of m is therefore not necessarily desired. Looking at the location of the second eigenmode

ω_2 given in table B.9 reveals that the result of m=4 yields a mode close to the excitation frequency. Next, the frequency response, of which the undamped version is given in figure B.35, can be examined.

Second eigenfrequency ω_2	m=2	m=4	m=8	m=12	m=20
ω_{exc} = 340Hz	308Hz	321Hz	369Hz	366Hz	370Hz

Table B.9: An overview of the second eigenfrequencies computed for the obtained topologies as given in figure B.34.

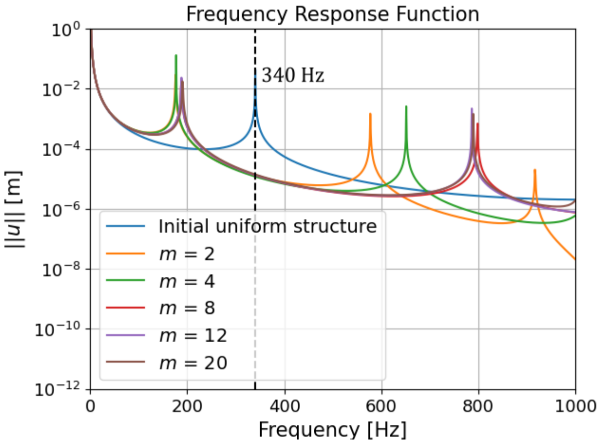

Figure B.35: The undamped frequency response comparison of the resulting topologies given in figure B.34 and the initial uniform domain, showcasing the influence of the parameter m on global minimization subjected to a base excitation including forced symmetry.

The frequency response shows a distinct pattern where higher order modes are pushed away from the excitation frequency as m increases. This suggests that higher values of m are preferred, though it comes at the cost of the first resonance moving slightly closer to the excitation frequency. It is hard to see in the graph, but the lower values of m yield lower displacement magnitudes of the vertical displacement of the mass for lower values of m. These improvements are, however, slight when compared to the fact that higher-order modes are now much closer to the excitation frequency. combined with the observations from the resulting topologies, it, therefore, seems that a high value of m such as m=12 is preferred as the result of m=20 differs only slightly from the result of m=12. As mentioned, however, the influence of the parameter w will also be examined again. The resulting topologies of the same parameter sweep but without the density-weighted filter (w=0) are given in figure B.36.

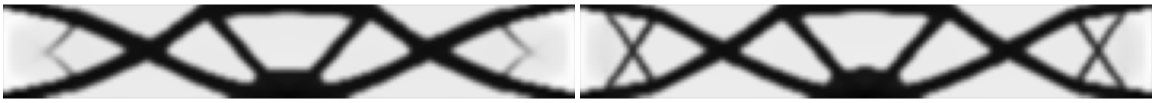

(a) $m = 2$, $C_s = 4.8730$

(b) $m = 4$, $C_s = 4.4411$

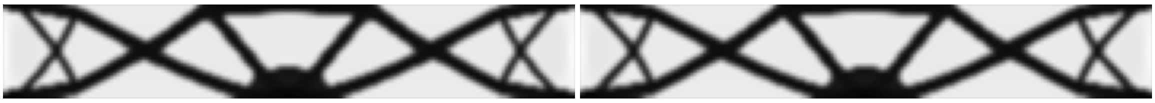

(c) $m = 8$, $C_s = 4.0291$

(d) $m = 12$, $C_s = 3.8687$

Figure B.36: The topologies found for a parameter sweep over the parameter m for global minimization subjected to a base excitation including forced symmetry over the y-axis and excluding the density-weighted filter (w=0), together with their accompanying static compliance values.

Without the density-weighted filter, the results of $m \geq 2$ seem more in line with each other. The intermediate densities also seem to only be present for m=2 and disappear for higher values of m. The same effect of the static compliance decreasing, however, also appears in this case but with an even greater effect given the lower values of C_s. This would suggest that the frequency performance is expected to show higher displacement magnitudes as more emphasis is put on static compliance. To verify this, the undamped frequency response is given in figure B.37.

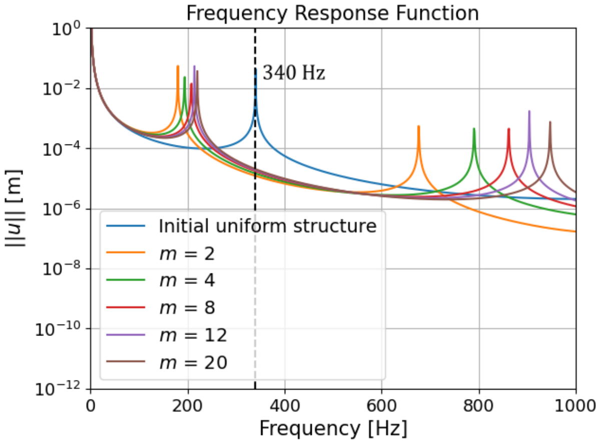

Figure B.37: Undamped frequency response comparison influence of m on global minimization subjected to a base excitation including forced symmetry

The resulting response now shows an even more distinctive pattern when compared to the result with the density-weighted filter included. As the parameter m increases, the first resonance moves closer to the excitation frequency, but the second resonance moves further from the excitation frequency. The choice of the parameter m would, therefore, seem to depend on whether the first or second resonance has priority. The magnitudes of the displacements at the excitation frequency, however, are much higher than in the case where the density-weighted filter was included. This is likely due to the added emphasis on static compliance, and it would therefore seem that the inclusion of the density-weighted filter is still preferred.

B.2.7. Discussion on the influence of m on global minimization

From these results, it seems that the inclusion of the density-weighted filter is still desired. As for the appropriate value of the parameter m, this is still inconclusive as a lower value, such as m=2, provides a lower displacement magnitude response at the excitation frequency but moves the second resonance closer to the excitation frequency, and a higher value, such as m=12 does the exact opposite. Furthermore, the intermediate values of m=4 and m=8 are not desired because they have a second eigenfrequency near the excitation frequency and contain intermediate densities. The coming section will, therefore, examine the results for both m=2 and m=12.

B.2.8. Influence of the excitation frequency ω_{exc} on global minimization

Lastly, the influence of the excitation frequency ω_{exc} is examined for global minimization subjected to a base excitation. The frequencies of interest were already provided in figure B.27 and will, as mentioned, be examined for both m=2 and m=12. The density-weighted filter will be applied with w=1, and symmetry is forced over the y-axis. The frequency sweep for m=2 over the frequency of interest and over the values γ_1=0.99, γ_1=0.95 and γ_1=0.90 is given in figure B.38.

(a) γ_1 = 0.90, ω_{exc}=340Hz (b) γ_1 = 0.95, ω_{exc}=340Hz (c) γ_1 = 0.99, ω_{exc}=340Hz

(d) γ_1 = 0.90, ω_{exc}=880Hz (e) γ_1 = 0.95, ω_{exc}=880Hz (f) γ_1 = 0.99, ω_{exc}=880Hz

(g) γ_1 = 0.90, ω_{exc}=1377Hz (h) γ_1 = 0.95, ω_{exc}=1377Hz (i) γ_1 = 0.99, ω_{exc}=1377Hz

(j) γ_1 = 0.90, ω_{exc}=2947Hz (k) γ_1 = 0.95, ω_{exc}=2947Hz (l) γ_1 = 0.99, ω_{exc}=2947Hz

Figure B.38: The topologies found for a two-sided parameter sweep over both the parameter γ_1 and the excitation frequency ω_{exc} for the frequencies of interest defined in section B.2.1 showcasing their influence on global minimization subjected to a force excitation including forced symmetry over the y-axis and the parameter values w=1 and m=2.

What immediately stands out is that there are almost no intermediate densities present apart from the result of figure B.38i. This shows that the chosen parameters for w and m are appropriate choices. As for the obtained topologies, the same behaviour as for the force excited case is visible, where more emphasis is put on the structures which connect the centre structure to the base as γ_1 decreases. One topology which stands out, however, is the result from 2947Hz at γ_1=0.99 in figure B.38l. It is hard to see that its connection to the base is only defined by four single elements at the four corners, and on top of that, these elements consist of an intermediate density. For this excitation frequency, it, therefore, seems that a certain amount of static compliance contribution is still needed to yield a connected topology. For a more in-depth view into the frequency performance, the undamped frequency for all topologies respective for each excitation frequency of interest is given in figure B.39.

The effects of higher order modes being pulled towards the excitation frequency at high values of γ_1 were already established for 340Hz. For 880Hz, it seems this behaviour is present as well, with the second resonance and first anti-resonance even being moved below the excitation frequency for γ_1=0.99. It does appear that γ_1 provides the lowest displacement magnitude by a margin, at the cost of resonances being very close to the excitation frequency. At the excitation frequency of 1377Hz, something interesting happens. Though γ_1=0.99 again yields the lowest displacement magnitude, it has a resonance extremely close to this frequency at 1392Hz, which is very undesirable behaviour. This might also explain the presence of intermediate densities in this topology. For γ_1=0.95 and γ_1=0.90, it seems that this same resonance is moved in front of the excitation frequency. Lastly, the result of 2947Hz shows all values of γ_1 performing well in terms of moving the resonances away from the excitation frequency, but as was already established, the result of γ_1=0.99 yields a not fully connected topology. As mentioned, the same sweep would be performed for m=12, the results of which are given in figure B.40.

From these results, similar behaviour is found as for m=2, but there are some differences. The not fully connected behaviour which was found for one topology of m=2 is now present for γ_1=0.99 at 880Hz and γ_1=0.95 at 2947Hz, given in figure B.40f and B.40k respectively. The most interesting result, however, is that of γ_1=0.99 at 2947Hz given in figure B.40l, which is almost fully disconnected. This is hard to see in these images, but the four corner elements have very low-density values for these cases, with the latter having the lowest density. It would, therefore, seem that the higher value of m is not suitable for all excitation frequencies when

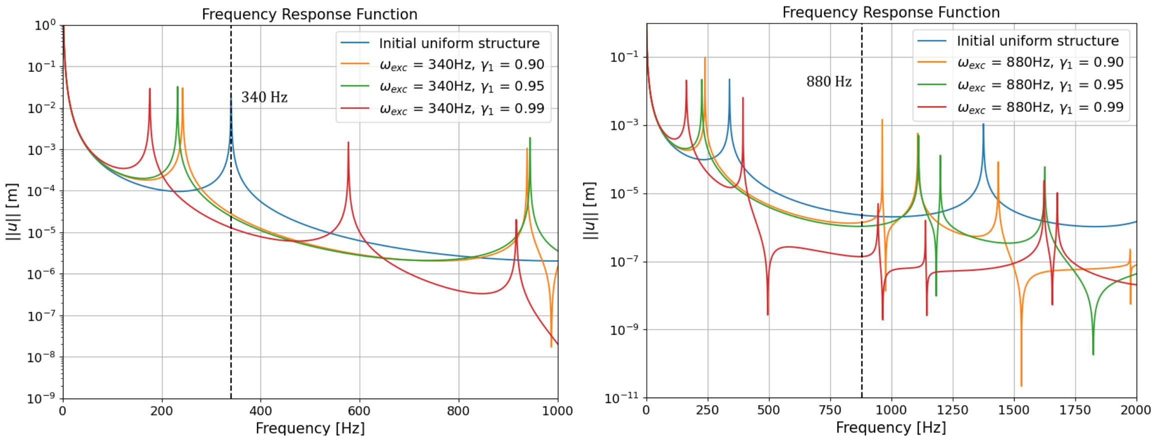

(a) ω_{exc}=340Hz

(b) ω_{exc}=880Hz

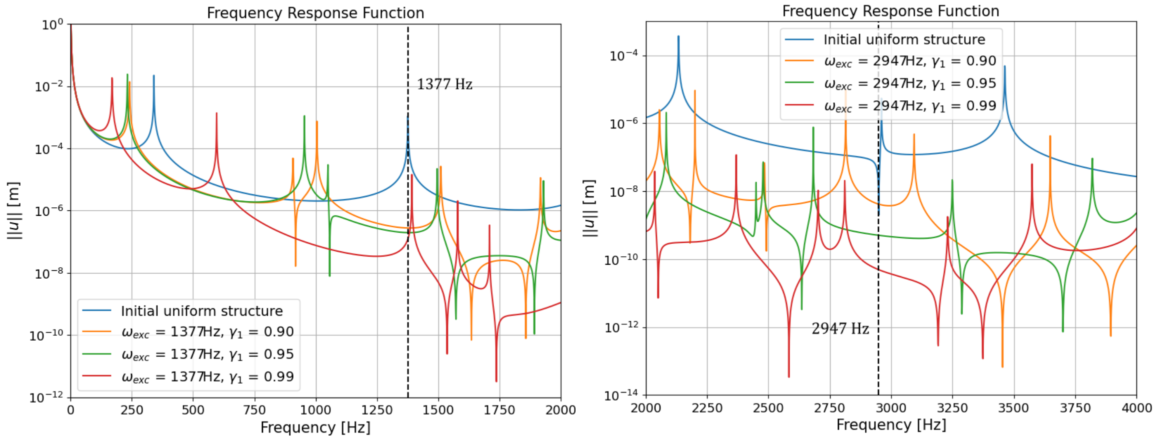

(c) ω_{exc}=1377Hz

(d) ω_{exc}=2947Hz

Figure B.39: The undamped frequency response comparison of the resulting topologies given in figure B.38 and the initial uniform domain, showcasing the influence of the parameter γ_1 for each of the four respective excitation frequencies of interest ω_{exc} on global minimization subjected to a force excitation including forced symmetry over the y-axis and parameter values w=1 and m=2.

(a) $\gamma_1 = 0.90$, ω_{exc}=340Hz (b) $\gamma_1 = 0.95$, ω_{exc}=340Hz (c) $\gamma_1 = 0.99$, ω_{exc}=340Hz

(d) $\gamma_1 = 0.90$, ω_{exc}=880Hz (e) $\gamma_1 = 0.95$, ω_{exc}=880Hz (f) $\gamma_1 = 0.99$, ω_{exc}=880Hz

(g) $\gamma_1 = 0.90$, ω_{exc}=1377Hz (h) $\gamma_1 = 0.95$, ω_{exc}=1377Hz (i) $\gamma_1 = 0.99$, ω_{exc}=1377Hz

(j) $\gamma_1 = 0.90$, ω_{exc}=2947Hz (k) $\gamma_1 = 0.95$, ω_{exc}=2947Hz (l) $\gamma_1 = 0.99$, ω_{exc}=2947Hz

Figure B.40: The topologies found for a two-sided parameter sweep over both the parameter γ_1 and the excitation frequency ω_{exc} for the frequencies of interest defined in section B.2.1 showcasing their influence on global minimization subjected to a force excitation including forced symmetry over the y-axis and the parameter values w=1 and m=12.

compared to the results of m=2. The frequency response can still be examined to confirm this, however, and the undamped version is given in figure B.41.

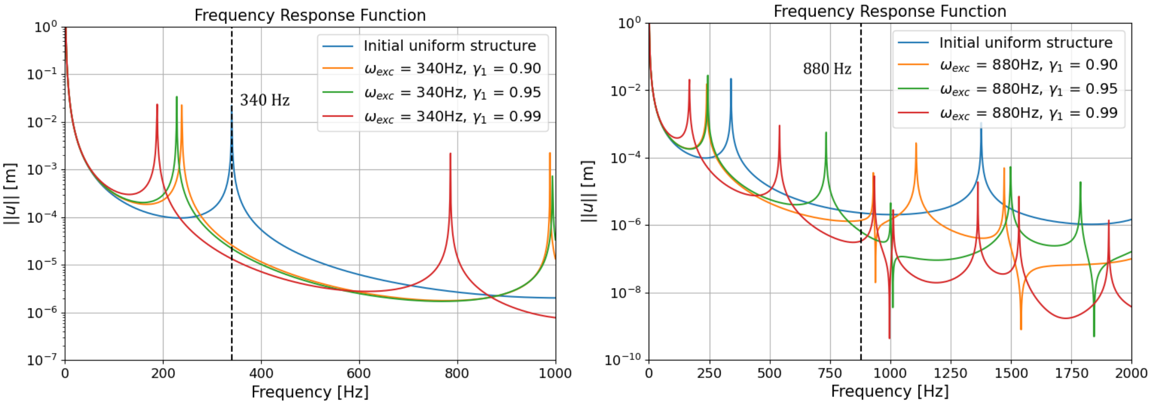

(a) ω_{exc}=340Hz (b) ω_{exc}=880Hz

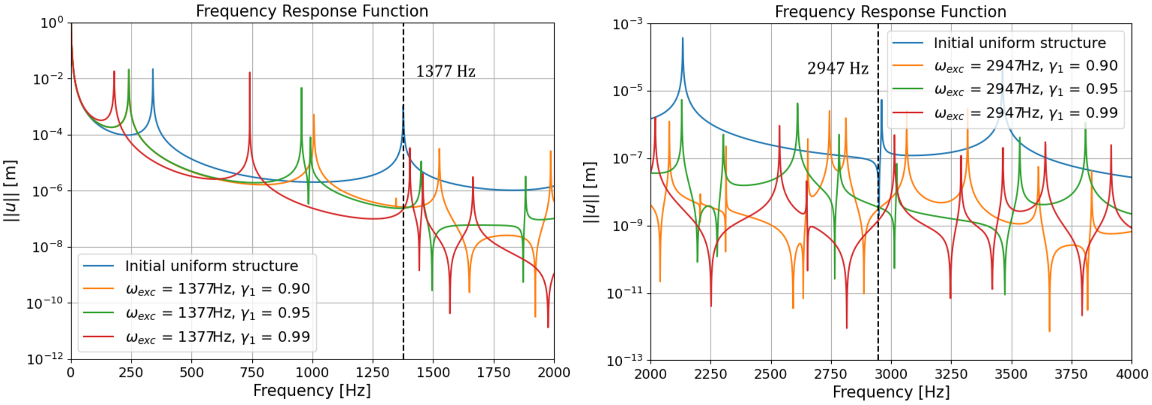

(c) ω_{exc}=1377Hz (d) ω_{exc}=2947Hz

Figure B.41: The undamped frequency response comparison of the resulting topologies given in figure B.40 and the initial uniform domain, showcasing the influence of the parameter γ_1 for each of the four respective excitation frequencies of interest ω_{exc} on global minimization subjected to a force excitation including forced symmetry over the y-axis and parameter values w=1 and m=12.

The frequency response also shows worse performing behaviour when compared to the results of m=2. Whilst the result of 340Hz seems better, with the result of γ_1=0.99 showing only one higher resonance in the same frequency range, the results of the three other frequencies all show resonances being very close to the excitation frequency. It would, therefore, seem that the value of m=12 is not an appropriate value.

B.2.9. Discussion on the influence of the excitation frequency ω_{exc} on global minimization

Combining the result from this examination with the previous results, it would seem that, first of all, the density-weighted filter still is a positive addition to the optimization problem together with forced symmetry over the y-axis. As for the value of m, a higher value might seem preferable for lower excitation frequencies, but for higher excitation frequencies, the lower value of m=2 showed more beneficial results.

B.3. Discussion on global minimization

From this study, it would seem that global minimization of both force-excited and base-excited problems requires symmetry to be forced over the y-axis in order to prevent obtaining asymmetric topologies. Furthermore, though it first seemed that the density-weighted filter had little effect, its inclusion greatly influences the occurrence of intermediate densities, which is similar to what Montero et al. [37] found. As for the appropriate value, any w is valid, and therefore, the lowest value of w=1 is the simplest choice. As for the parameter m, it seems that any value $m \geq 2$ is desired for the force excited case, whereas the higher values of m are actually undesired for the base excited case. One thing that is to be noted, however, is that the proposed objective function yielded topologies with very few intermediate densities present for a wide range of frequencies.

B.4. Local minimization subjected to a force excitation

With the behaviour of the density-weighted norm objective function established for global minimization problems, the behaviour of its use in local minimization can be examined. Montero et al. [37] did consider a local optimization, but this was a maximization case and as such the behaviour of this objective function for local minimization is still unknown. If the displacements of only a specific area within the domain are minimized, nothing is stopping the optimizer from choosing to promote very high displacements in other areas within the domain in order to compensate for the displacements of the region of interest. In Montero et al. [37], this possible behaviour is labelled as 'unwanted effects', but this thesis aims to investigate whether this is something which can be taken advantage of. In this section, the influence of the density-weighted filter, the parameter γ_1 and the parameter m are therefore examined again, which is all done for various sizes of the local area of interest L. As for the problem definition, the same design domain, parameters and frequencies of interest are used as outlined in section B.1.

B.4.1. A single degree of freedom

For the first case, only a single degree of freedom is considered, the bottom centre vertical degree of freedom, which is also the location of the applied force excitation. In contrast to the global minimization case, the frequency response of this single degree of freedom will now be directly comparable.

For a single degree of freedom, the parameter w will only affect the surrounding elements, which, considering that the considered degree of freedom is at the edge of the domain, is, in this case, only two elements. Adding the density weights in this case would not benefit the optimization, and therefore, the density-weighted filter is removed (w=0) for this case. As for the influence of the parameter m, this can be derived from equation 6.6. For a subset L containing a single degree of freedom, this equation simplifies to equation B.5.

$$\begin{aligned} N_{mw}(\mathbf{u}(\omega)) &= \left(\sum_{j \epsilon S} \left(u_j^*(\omega) a_j u_j(\omega) \right)^{\frac{m}{2}} \right)^{\frac{1}{m}} = \left(\left(u_L^*(\omega) a_L u_L(\omega) \right)^{\frac{m}{2}} \right)^{\frac{1}{m}} \\ &= \left(\left(u_L^*(\omega) a_L u_L(\omega) \right)^{\frac{m}{2}} \right)^{\frac{1}{m}} = \left((a_L^{\frac{m}{2}}) \right)^{\frac{1}{m}} \left(\| u_L(\omega) \|^m \right)^{\frac{1}{m}} = a_L^{\frac{1}{2}} \| u_L(\omega) \| \end{aligned} \tag{B.5}$$

This shows that the parameter m disappears from the objective function and will, therefore, have no influence on the optimization. What can also be noted is that without the density weights, the norm function reverts to the magnitude of a single response point. Given how the norm function follows the maximum response, this objective function will now contain anti-resonances due to only containing the response of a single degree of freedom. This section will, therefore, determine whether the addition of static compliance aids in avoiding premature convergence.

With the influence of the parameters w and m established, a sweep can be done over the frequencies of interest to see whether the found behaviour is consistent over a range of frequencies. For this sweep, the density-weighted filter is removed (w=0), the parameter m set at its lowest value of m=2, symmetry is forced over the y-axis, and the two elements which contain the degree of freedom of interest have their density set as a non-design domain with a value of 1. The resulting sweep over the frequencies of interest and γ_1 are given in figure B.42.

(a) $\gamma_1 = 0.90$, ω_{exc}=429Hz (b) $\gamma_1 = 0.95$, ω_{exc}=429Hz (c) $\gamma_1 = 0.99$, ω_{exc}=429Hz

(d) $\gamma_1 = 0.90$, ω_{exc}=700Hz (e) $\gamma_1 = 0.95$, ω_{exc}=700Hz (f) $\gamma_1 = 0.99$, ω_{exc}=700Hz

(g) $\gamma_1 = 0.90$, ω_{exc}=986Hz (h) $\gamma_1 = 0.95$, ω_{exc}=986Hz (i) $\gamma_1 = 0.99$, ω_{exc}=986Hz

(j) $\gamma_1 = 0.90$, ω_{exc}=1721Hz (k) $\gamma_1 = 0.95$, ω_{exc}=1721Hz (l) $\gamma_1 = 0.99$, ω_{exc}=1721Hz

Figure B.42: The topologies found for a two-sided parameter sweep over both the parameter γ_1 and the excitation frequency ω_{exc} for the frequencies of interest defined in section B.1.2 showcasing their influence on local minimization of a single degree of freedom subjected to a force excitation including forced symmetry over the y-axis and the parameter values w=0 and m=2.

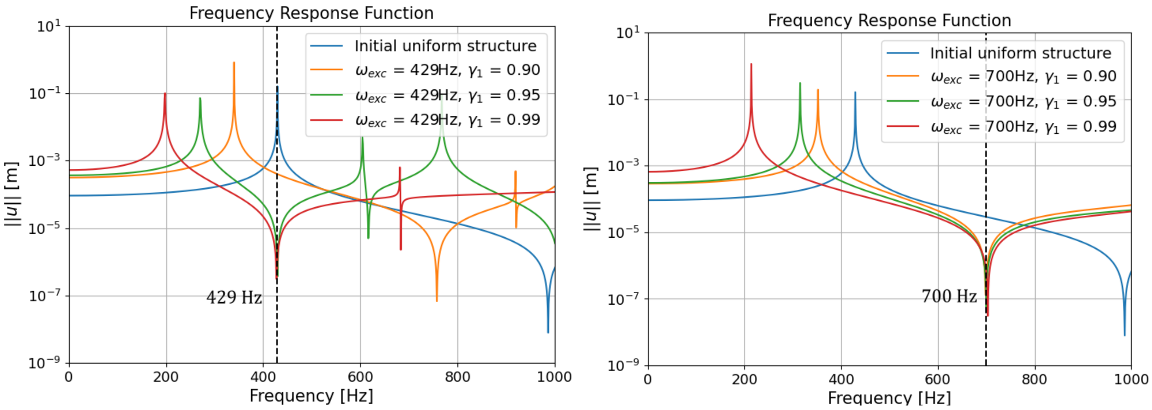

(a) ω_{exc}=429Hz (b) ω_{exc}=700Hz

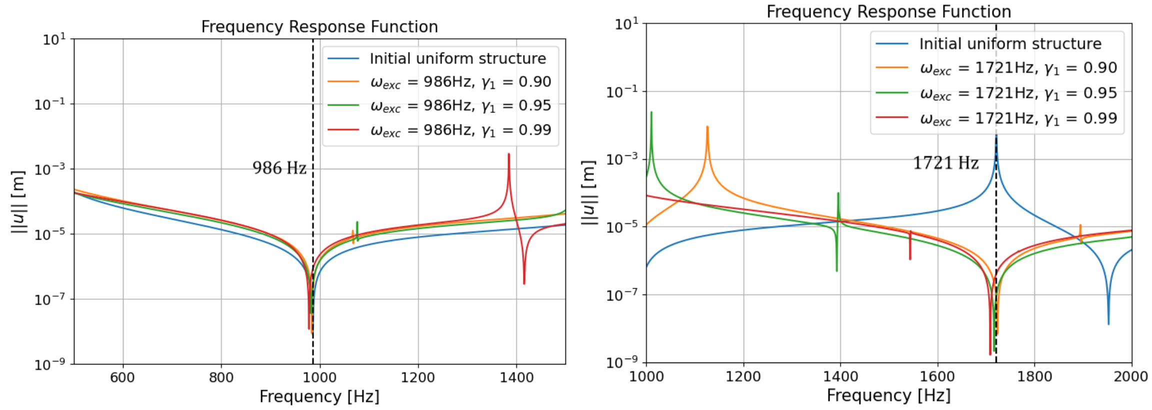

(c) ω_{exc}=986Hz (d) ω_{exc}=1721Hz

Figure B.43: The undamped frequency response comparison of the resulting topologies given in figure B.42 and the initial uniform domain, showcasing the influence of the parameter γ_1 for each of the four respective excitation frequencies of interest ω_{exc} on local minimization of a single degree of freedom subjected to a force excitation including forced symmetry over the y-axis and the parameter values w=0 and m=2.

The influence of γ_1 is clearly visible for γ_1=0.99. Whilst a black and white topology is obtained for the lowest frequency of 429Hz, all higher frequency results contain intermediate density regions. Increasing the static compliance contribution aids in the removal of these intermediate densities, with γ_1=0.95 already being sufficient, given that it provides topologies with limited to no intermediate densities present in the obtained topology. To check whether the same anti-resonance behaviour is present at all frequencies, the undamped frequency response for the obtained topologies respective of frequency are given in figure B.43.

As expected, all obtained topologies contain the same behaviour of an anti-resonance matching the excitation frequency. Given that the resulting topologies showed intermediate density regions primarily for high values of γ_1, it seems that the contribution of the static compliance is the main factor for obtaining well-defined topologies even though the objective function contains anti-resonances for local minimization of a single degree of freedom subjected to a force excitation.

B.4.2. An area of interest L

Local minimization of a single degree of freedom yielded topologies which contained an anti-resonance at the degree of freedom of interest. For a larger area of interest L, more degrees of freedom are taken into account, which would provide the norm function with a maximum response to a selection of responses. Whether this is the case for an area of interest which also contains a non-design domain remains to be seen. The chosen area of interest is shown in the updated design domain given in figure B.44. All other parameters are kept similar to those mentioned in section B.1.

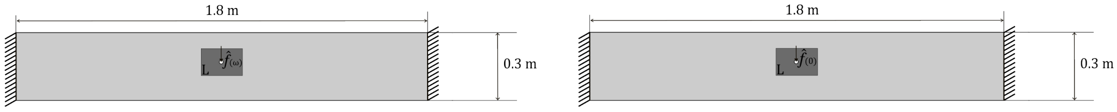

(a) Load case 1

(b) Load case 2

Figure B.44: The two load cases required for local minimization of an area of interest L subjected to a force excitation including the used dimensions.

This area of interest spans a rectangular 10% l_x by 30% l_y area in the centre of the design domain in order to keep the same ratio as the design domain. It can be noted that the force application point has been changed to be in the centre of the area L. This ensures that the applied force has no effects on the boundaries of the area of interest. The static force with similar magnitude $\hat{f}$ is also applied at the same location. In order to avoid the issue of the optimizer removing material from the area of interest in order to improve its frequency behaviour, a non-design domain is added. To visualize the relation between the non-design domain and area of interest, an arbitrary example finite element grid is provided in figure B.45.

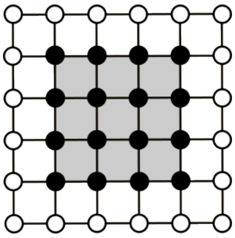

Figure B.45: An example visualization of the nodes of the area of interest (black) encapsulating the non-design domain marked by the grey elements.

The grey elements represent the elements which are part of the non-design domain. The nodes which are black contain the degrees of freedom considered in the subset L. It can be seen that the area of interest encapsulates the non-design domain in this case. For this problem, both the x- and y-directional degrees of freedom are considered as the degrees of freedom of interest. Whilst there are more degrees of freedom considered here, the addition of the non-design domain could also ensure similar behaviour of all of the degrees of freedom in this domain. This means that an anti-resonance can still appear in the frequency response as long as all degrees of freedom portray the same behaviour. The parameter sweep of γ_1 is given in figure B.46, which includes the results of γ_1=0.0, γ_1=0.90, γ_1=0.95 and γ_1=0.99. The result of γ_1=0.0 is included due to the new problem definition, and the result of γ_1=1.0 is not examined due to leading to a disconnected result.

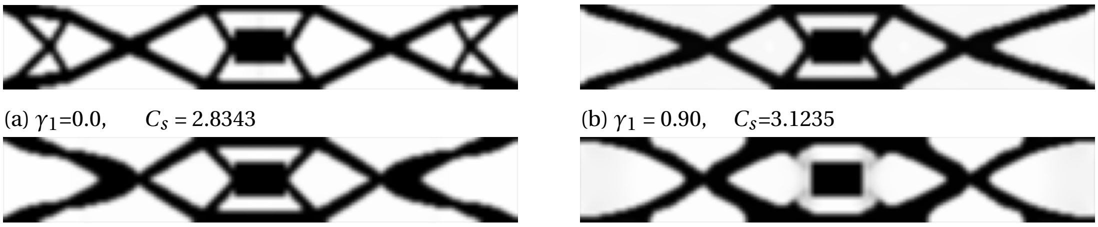

(a) γ_1=0.0, C_s = 2.8343

(b) γ_1 = 0.90, C_s=3.1235

(c) γ_1 = 0.95, C_s=3.5276

(d) γ_1 = 0.99, C_s=7.0934

Figure B.46: The topologies found for a parameter sweep over the parameter γ_1 for local minimization of an area of interest L subjected to a force excitation together with the accompanying static compliance values.

As expected, the parameter γ_1 has the same influence on the static compliance. The interesting result, however, is that of γ_1=0.99, where it seems that the optimizer chose a topology which connects the area of interest with the rest of the structure with members comprised of intermediate densities. This shows that a higher amount of static compliance contribution is necessary for this problem, given that the result of γ_1=0.95 gives a well-connected result. As for the difference between γ_1=0.90 and γ_1=0.95, it seems that the former contains a second eigenfrequency ω_2 at 434Hz, which is close to the excitation frequency of 429Hz, while the latter contains this same eigenfrequency at 323Hz. This is likely a mode which only contains displacements in the x-direction, and as such, it is a valid choice from the perspective of the optimizer. This is interesting as the x-directional degrees of freedom of the area of interest are also included in the subset L. For a deeper delve into the frequency behaviour, the undamped frequency response of the vertical degree of freedom of the centre of the area of interest (which is also the force application point) is given in figure B.47.

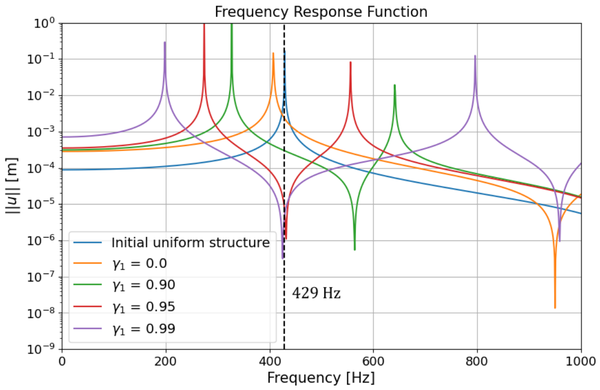

Figure B.47: The undamped frequency response comparison of the resulting topologies given in figure B.46 and the initial uniform domain, showcasing the influence of the parameter γ_1 on local minimization of an area of interest L subjected to a force excitation.

The resulting response shows an anti-resonance present at the excitation frequency for the results of γ_1=0.95 and γ_1 0.99. This means that the hypothesis from earlier was correct, where all degrees of freedom inside the area of interest obtain the same behaviour and collectively contain an anti-resonance at the excitation frequency. The resulting topology of γ_1=0.90 does not contain this behaviour but does maximize the distance between the first resonance and first anti-resonance, being located exactly between them. The added static compliance contribution then ensures a connected result, as can be seen from the γ_1=0.99 result, but may limit the anti-resonance behaviour, as can be seen from the γ_1=0.90 result. To visualize this anti-resonance behaviour, the magnitudes of the displacements are visualized in ParaView, the output of which is given in figure B.48.

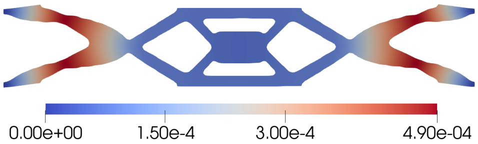

Figure B.48: A visualization done in ParaView of the displacement magnitudes resulting from the applied force excitation for the result of γ_1=0.95 at 429Hz showcasing the minimization of the displacements in the area of interest.

The resulting displacement field exactly encapsulates the behaviour which was expected from local minimization, where other parts of the domain are allowed to have higher displacement magnitudes in order to minimize displacements of the area of interest. In this case, specifically, the area of interest L, and seemingly an even larger area, contains an anti-resonance at the excitation frequency, which allows for this minimization behaviour whilst the static compliance contribution aids in obtaining a well-connected result. Considering that this study aimed to achieve compensating behaviour without the presence of intermediate densities, this is beneficial behaviour.

Next, the influence of the parameter w can be examined. Given that the area of interest covers the non-design domain (figure B.44), the weights a_j should not change much due to most of the design variables which are incorporated in the weight determination being fixed. Setting the parameter γ_1 at 0.95 obtain a connected result, the parameter m at 2 and the excitation frequency at 429Hz, the resulting topologies for w=0, w=2, w=4, and w=8. Similar to the global case, w=0 refers to the density-weighted filter being removed.

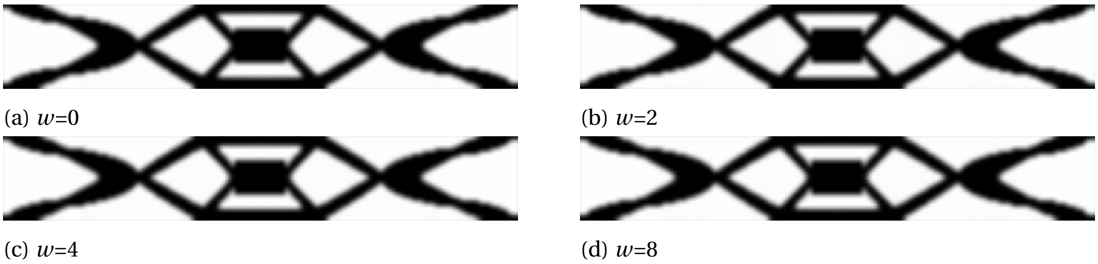
(a) w=0
(b) w=2
(c) w=4
(d) w=8

Figure B.49: The topologies found for a parameter sweep over the parameter w for local minimization of an area of interest L subjected to a force excitation.

These results confirm that the parameter w has little visible influence on local minimization considering an area L. To see whether the frequency response shows a distinct difference, the undamped frequency response is given in figure B.50. This response also includes the result of w=20.

Even though there are small differences, these are so small they can be considered negligible. A change in parameter w, therefore, has no positive or negative impact, but it still has a small impact. There is, therefore, no reason to add the density weights to this optimization problem, and thus, the density-weighted filter will be removed (w=0) for local minimization of an area of interest L.

Next, the influence of the parameter m is examined. Setting w=0, the excitation frequency at 429Hz and the parameter γ_1 at 0.95, the resulting topologies for m=2, m=4, m=8 and m=12 are given in figure B.51.

Again, no significant visible differences are found in the obtained topologies. This is to be expected as it was already shown that the parameter m had no influence when the subset L contains one degree of freedom, and, therefore, is expected to only have little influence if the subset L contains only a small set of degrees of freedom, specifically when it was already shown that the area of interest portrays a collective response. A deeper delve can be done by looking at the undamped frequency response given in figure B.52, which also includes the result of m=20.

The resulting frequency response also shows only small differences. The first resonance seems to be moved further from the excitation frequency as m increases at the cost of the second resonance moving closer. This is irrelevant, however, as the behaviour is mainly characterized by the first anti-resonance matching

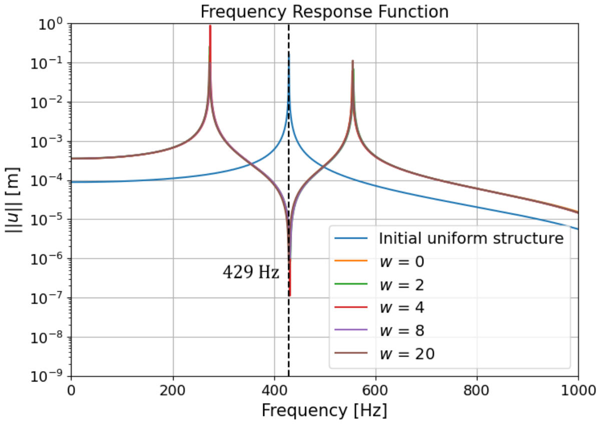

Figure B.50: The undamped frequency response comparison of the resulting topologies given in figure B.49 and the initial uniform domain, showcasing the influence of the parameter w on local minimization of an area of interest L subjected to a force excitation.

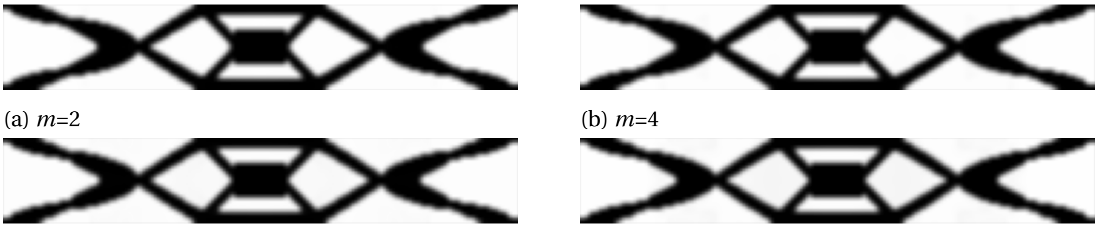
(a) m=2

(b) m=4

(c) m=8

(d) m=12

Figure B.51: The topologies found for a parameter sweep over the parameter m for local minimization of an area of interest L subjected to a force excitation.

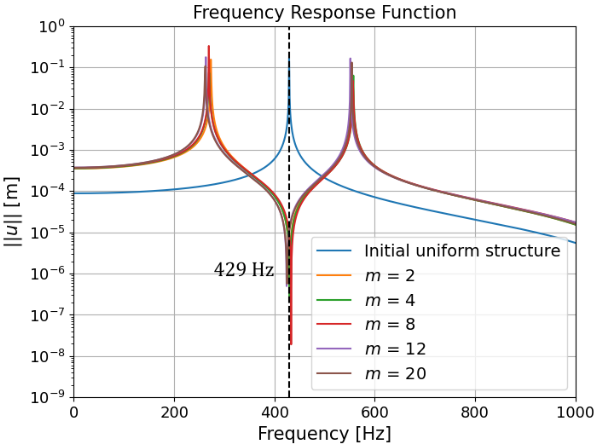

Figure B.52: The undamped frequency response comparison of the resulting topologies given in figure B.49 and the initial uniform domain, showcasing the influence of the parameter m on local minimization of an area of interest L subjected to a force excitation.

the excitation frequency. For this behaviour, the parameter m has influence, but without a distinguishable pattern. The result of whether a larger or smaller m is desired for local minimization of an area L is therefore inconclusive.

To investigate the influence of the excitation frequency, the density-weighted filter will be removed (w=0), and the parameter m will be set at the lowest value of m=2. Symmetry is forced over the y-axis, the degrees of freedom in the subset L cover the non-design domain and the results of the sweep over both the frequencies of interest and the parameter γ_1 is given in figure B.53.

(a) $\gamma_1 = 0.90$, ω_{exc}=429Hz (b) $\gamma_1 = 0.95$, ω_{exc}=429Hz (c) $\gamma_1 = 0.99$, ω_{exc}=429Hz

(d) $\gamma_1 = 0.90$, ω_{exc}=700Hz (e) $\gamma_1 = 0.95$, ω_{exc}=700Hz (f) $\gamma_1 = 0.99$, ω_{exc}=700Hz

(g) $\gamma_1 = 0.90$, ω_{exc}=986Hz (h) $\gamma_1 = 0.95$, ω_{exc}=986Hz (i) $\gamma_1 = 0.99$, ω_{exc}=986Hz

(j) $\gamma_1 = 0.90$, ω_{exc}=1721Hz (k) $\gamma_1 = 0.95$, ω_{exc}=1721Hz (l) $\gamma_1 = 0.99$, ω_{exc}=1721Hz

Figure B.53: The topologies found for a two-sided parameter sweep over both the parameter γ_1 and the excitation frequency ω_{exc} for the frequencies of interest defined in section B.1.2 showcasing their influence on local minimization of an area of interest L subjected to a force excitation including forced symmetry over the y-axis and the parameter values w=0 and m=2.

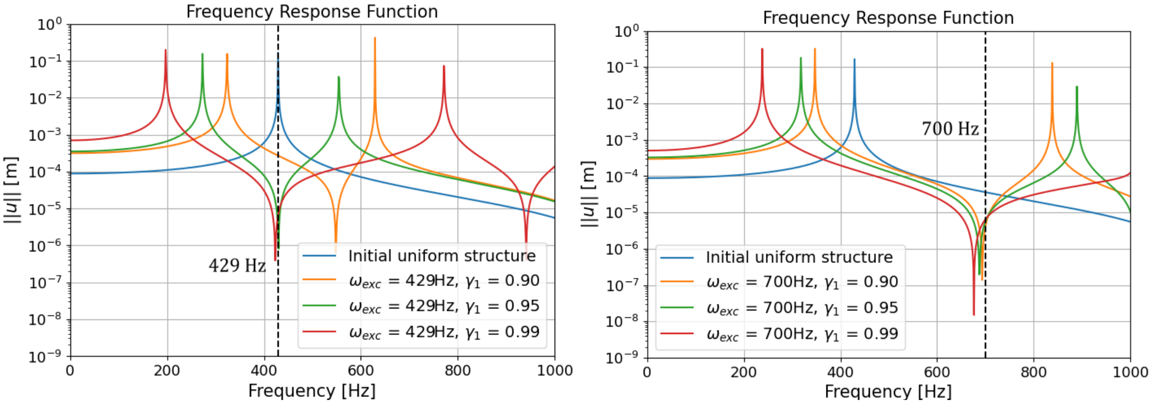

(a) ω_{exc}=429Hz (b) ω_{exc}=700Hz

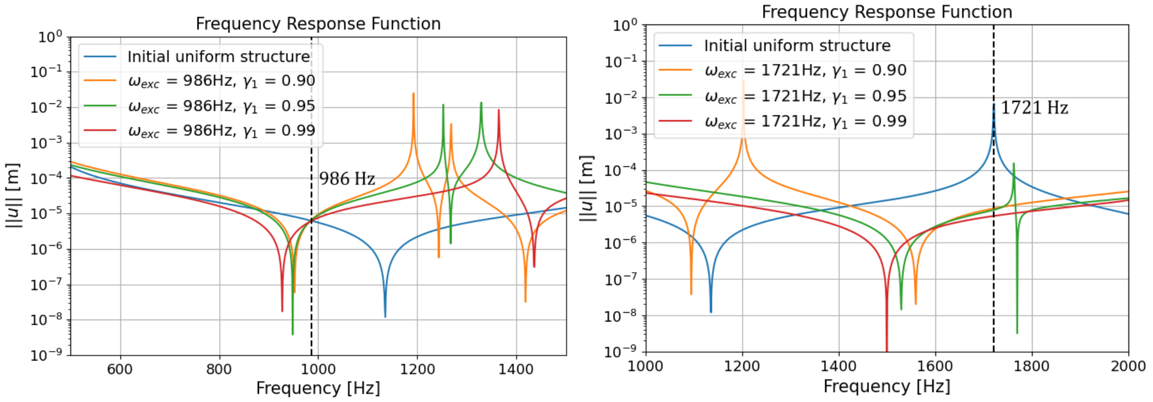

(c) ω_{exc}=986Hz (d) ω_{exc}=1721Hz

Figure B.54: The undamped frequency response comparison of the resulting topologies given in figure B.53 and the initial uniform domain, showcasing the influence of the parameter γ_1 for each of the four respective excitation frequencies of interest ω_{exc} on local minimization of an area of interest L subjected to a force excitation including forced symmetry over the y-axis and the parameter values w=0 and m=2.

For the value of γ_1=0.99, the same behaviour is found where the area of interest is connected to the rest of the structure via intermediate densities. This indicates that a larger static compliance contribution is necessary for local minimization of an area of interest L subjected to a force excitation. As for the other results, it seems that little to no intermediate densities are present except for the γ_1=0.95 result for 1721Hz. To see how the resulting topologies compare with each other in terms of displacement performance near and at the respective frequencies of interest, the undamped frequency responses are given in figure B.54.

The frequency responses of the obtained topologies show quite different behaviour, of which the result of 429Hz was already discussed. It appears that, as the excitation frequency increases, the anti-resonance seems to move further away from the excitation frequency for all values of γ_1. What this means is that the degrees of freedom in the area of interest portray other displacements which dominate the response in the norm function. The resulting displacements are still minimized but are not fully represented by only the frequency response of the force excitation point. To visualize the displacements at this frequency, the resulting displacement magnitudes of the result of γ_1=0.90 at 1721Hz are plotted with ParaView and given in figure B.55.

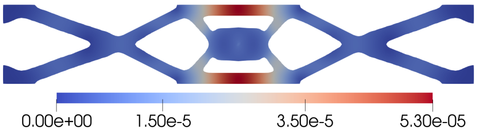

Figure B.55: A visualization done in ParaView of the displacement magnitudes resulting from the applied force excitation for the result of γ_1=0.90 at 1721Hz showcasing the minimization of the displacements in the area of interest.

The resulting displacement field shows that the displacement magnitudes of the degrees of freedom in the area of interest are still minimized, but not exactly with an anti-resonance. There is, however, similar behaviour where other parts of the structure display larger displacements to ensure that the area of interest has minimized displacement magnitudes at the excitation frequency.

B.4.3. Discussion on the local minimization subjected to a force excitation

In this section, the influence of the density-weighted norm objective function is examined for its behaviour considering local minimization subjected to a force excitation for two subsets: a single degree of freedom and an area of interest L. It was determined that for both of these subsets, the influence of the density-weighted filter became negligible, and it was removed (w=0) for all optimizations. Where the density-weighted filter aided in preventing the occurrence of intermediate density regions for global minimization, it seems that the static compliance contribution is of greater importance for local minimization as it was found that the value of γ_1=0.99, or in other words the lowest static compliance contribution, yielded topologies which contained intermediate density regions. A similar result was found for the parameter m, which was therefore set at m=2.

When only a single degree of freedom was chosen, the results all showed how an anti-resonance in the structure matched the excitation frequency. Considering the results found in section 4.7, it appears that the premature convergence and excitation frequency issues were solved primarily by adding the static compliance in the objective function. For an area of interest L, similar behaviour was found for low excitation frequencies where the degrees of freedom inside the area of interest collectively obtained an anti-resonance at the excitation frequency. This did not translate to higher frequencies, however, where more complex modes are present, which limit this behaviour. What was found, however, is that other regions of the domain were still given larger displacements in order to minimize the displacements of the area of interest.

B.5. Local minimization subjected to a base excitation

Lastly, the local minimization behaviour subjected to a base excitation can be examined. In contrast to the force excited case, this problem is non-collocated, given that the response and excitation points do not share the same location. The same behaviour is to be expected, however, where certain regions of the domain will be allowed to have higher displacement magnitudes in order to minimize the displacement magnitudes of the region of interest. To examine this behaviour, the same single degree of freedom and area of interest L will be examined as in the previous section. The single degree of freedom problem will determine whether the excitation frequency issues present for harmonic base excitations can again be solved with the inclusion of static compliance. The problem definition which is used is the same design domain, parameters and frequencies of interest which are outlined for the global minimization case in section B.2.

B.5.1. A single degree of freedom

First, a single degree of freedom is considered again to determine whether the static compliance contribution aids in obtaining well-connected results over a wide range of frequencies. The point of interest chosen is the vertical degree of freedom of the node, which contains the added mass m_b. This is also the same degree of freedom where the force is applied for the static load case. As the parameter m was already shown to have a negligible effect on the local minimization subjected to a force excitation of a single degree of freedom, the parameters w and m are set to similar values of w=0 and m=2. Next, a parameter sweep over both the frequencies of interest and the parameter γ_1 can be done. Figure B.56 shows the resulting topologies from this sweep.

(a) $\gamma_1 = 0.99$, ω_{exc}=340Hz (b) $\gamma_1 = 0.95$, ω_{exc}=340Hz (c) $\gamma_1 = 0.90$, ω_{exc}=340Hz

(d) $\gamma_1 = 0.99$, ω_{exc}=880Hz (e) $\gamma_1 = 0.95$, ω_{exc}=880Hz (f) $\gamma_1 = 0.90$, ω_{exc}=880Hz

(g) $\gamma_1 = 0.99$, ω_{exc}=1377Hz (h) $\gamma_1 = 0.95$, ω_{exc}=1377Hz (i) $\gamma_1 = 0.90$, ω_{exc}=1377Hz

(j) $\gamma_1 = 0.99$, ω_{exc}=2947Hz (k) $\gamma_1 = 0.95$, ω_{exc}=2947Hz (l) $\gamma_1 = 0.90$, ω_{exc}=2947Hz

Figure B.56: The topologies found for a two-sided parameter sweep over both the parameter γ_1 and the excitation frequency ω_{exc} for the frequencies of interest defined in section B.1.2 showcasing their influence on local minimization of a single degree of freedom subjected to a base excitation including forced symmetry over the y-axis and the parameter values w=0 and m=2.

The resulting topologies seem to contain a large amount of intermediate densities. Only the results of the lowest frequency of 340Hz and the γ_1=0.90 result of 800Hz appear to be free of intermediate densities. The same behaviour of obtaining better-connected topologies when the static compliance contribution is increased seems to be present but to a much lesser extent. For a more in-depth analysis, the response of each of these topologies can be compared, and the undamped frequency responses are given in figure B.57.

These responses show that a minimized result is indeed obtained, with increased performance as the static compliance contribution decreases. The resulting topologies, however, are still largely filled with intermediate densities.

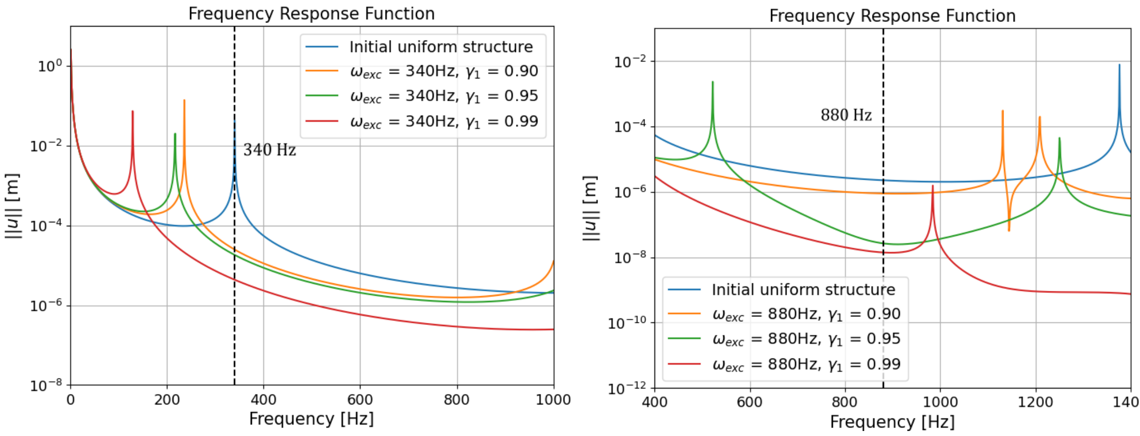

(a) ω_{exc}=340Hz (b) ω_{exc}=880Hz

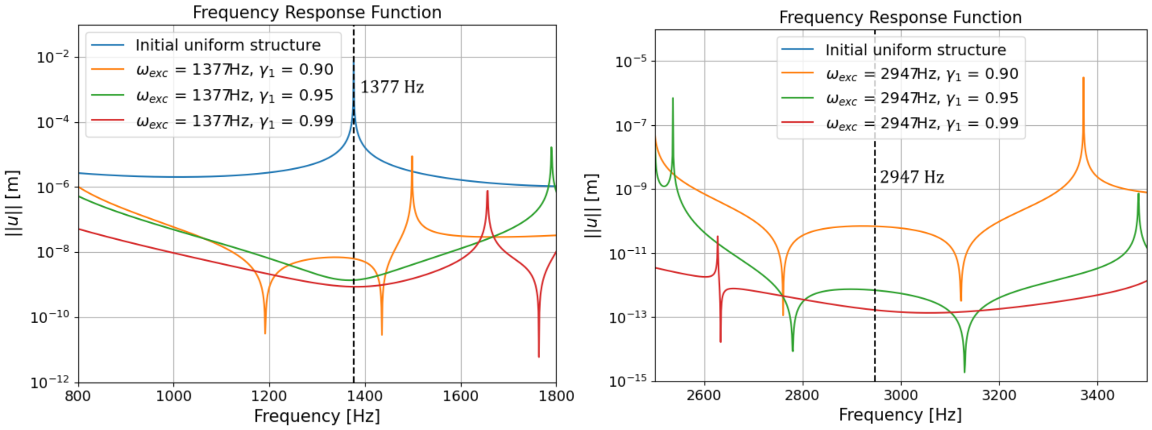

(c) ω_{exc}=1377Hz (d) ω_{exc}=2947Hz

Figure B.57: The undamped frequency response comparison of the resulting topologies given in figure B.56 and the initial uniform domain, showcasing the influence of the parameter γ_1 for each of the four respective excitation frequencies of interest ω_{exc} on local minimization of a single degree of freedom subjected to a base excitation including forced symmetry over the y-axis and the parameter values w=0 and m=2.

B.5.2. An area of interest L

The minimization of a single degree of freedom yielded topologies that contained large amounts of intermediate densities, some of which were not even connected to the base. The subset L is therefore enlarged to examine the influence of a larger subset of degrees of freedom L. The same area is used as in the force excited local minimization case, and visualization is given in figure B.58. The rest of the parameters are similar to the global minimization problem.

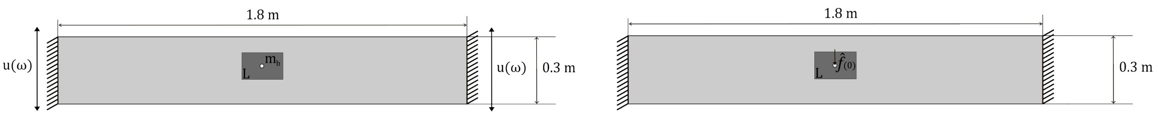

(a) Load case 1 (b) Load case 2

Figure B.58: The two load cases required for local minimization of an area of interest L subjected to a base excitation including the used dimensions.

The area of interest is again centred in the middle of the domain, with the static force applied in the middle of this domain for the second load case. The added mass m_b is also added to the centre of this domain in the first load case. Furthermore, a non-design domain is added to the area of interest and is encapsulated by the degrees of freedom considered by the subset L. The density-weighted filter will not be included (w=0) in this examination as it was already determined in the force excited case that it has little influence on this design problem. Firstly, the influence of the parameter γ_1 is examined, and the results for γ_1=0.90, γ_1=0.95, γ_1=0.99 and γ_1=1.0 for an excitation frequency of 340Hz and m=2 are given in figure B.59.

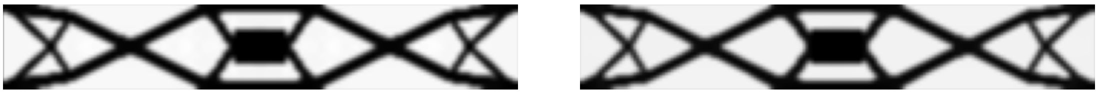

(a) γ_1=0.90, $C_s = 3.1113$ (b) γ_1=0.95, $C_s = 3.4802$

(c) γ_1=0.99, $C_s = 7.1763$ (d) γ_1=1.0, $C_s = 3423.47$

Figure B.59: The topologies found for a parameter sweep over the parameter γ_1 for local minimization of an area of interest L subjected to a base excitation together with the accompanying static compliance values.

From these results, it is clear that the result of γ_1=1.0 yields a disconnected topology, and γ_1=0.99 yields a topology with some members which consist of intermediate densities. The results of γ_1=0.90 and γ_1=0.95 do not appear to contain much visible differences, but their respective static compliance values show otherwise. To see how these topologies compare at the excitation frequency, the undamped frequency response of the mass point is given in figure B.60.

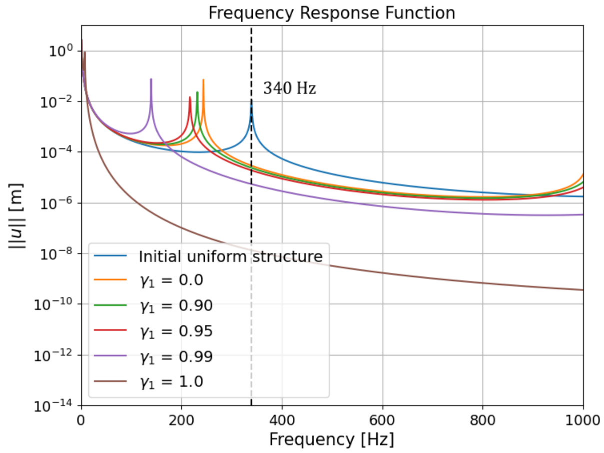

Figure B.60: The undamped frequency response comparison of the resulting topologies given in figure B.59 and the initial uniform domain, showcasing the influence of the parameter γ_1 on local minimization of an area of interest L subjected to a base excitation.

The resulting frequency response shows the expected result of the displacement magnitude response decreasing as the static compliance contribution decreases. For the extreme case of γ_1, where the stiffness between the base and the obtained centre mass is very low, similar behaviour to the principle of vibration isolation explained in section 2.2.4 can be seen. This effect is limited for larger values of γ_1, but the same principle of obtaining a large centre mass which is connected to the base with minimized stiffness can be seen in the obtained topology of γ_1=0.99 in figure B.59. This same result, however, does contain some intermediate densities, and therefore, the examination of the influence of the parameter m on this problem will be performed using γ_1=0.95. Keeping the same excitation frequency of 340Hz, the resulting topologies of the parameter sweep for m=2, m=4, m=8 and m=12 are given in figure B.61.

The differences in the obtained topologies are slight, but there are differences. For larger values of m it seems that the four members connecting the area of interest L to the rest of the structure are connected with slightly thicker members. To see how this difference performs at the excitation frequency, the undamped frequency response of these topologies is given in figure B.62. This also includes the result of m=20, the topology of which showed no visible difference to the result of m=12.

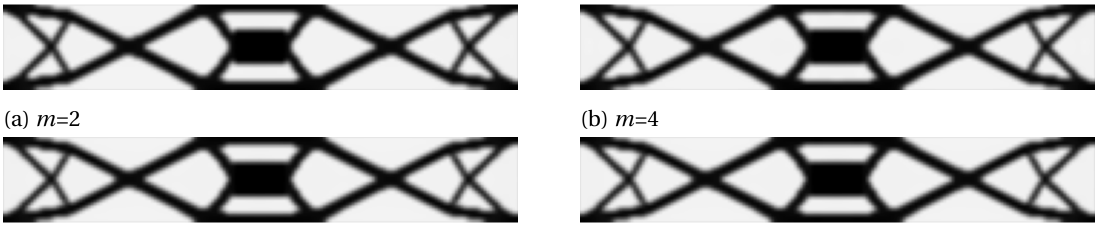

(a) m=2

(b) m=4

(c) m=8

(d) m=12

Figure B.61: The topologies found for a parameter sweep over the parameter m for local minimization of an area of interest L subjected to a base excitation.

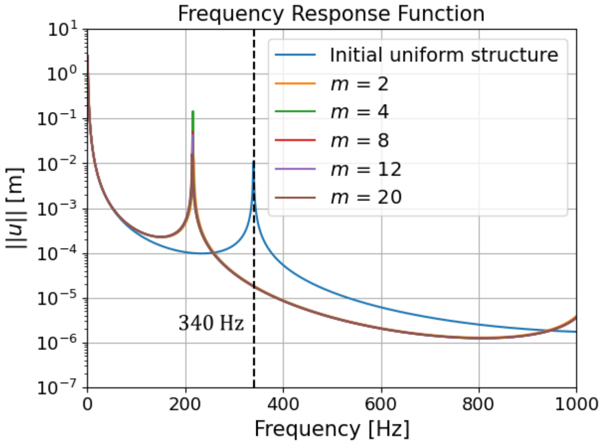

Figure B.62: The undamped frequency response comparison of the resulting topologies given in figure B.61 and the initial uniform domain, showcasing the influence of the parameter m on local minimization of an area of interest L subjected to a base excitation.

The resulting frequency response also shows little difference, but there is a slight decrease in displacement magnitude as the parameter m increases. The largest difference, however, is found in the second eigenfrequency ω_2. The respective second eigenfrequencies of the obtained topologies are given in table B.10.

Second eigenfrequency ω_2	m=2	m=4	m=8	m=12	m=20
ω_{exc} = 340Hz	367Hz	375Hz	378Hz	378Hz	380Hz

Table B.10: An overview of the second eigenfrequencies computed for the obtained topologies as given in figure B.61.

As m increases, this eigenfrequency seems to be moved further away from the excitation frequency, which is beneficial. The largest increase in this movement is found for m=4, and higher values yield diminishing returns. Therefore, for the parameter sweep of the excitation frequency ω_{exc}, the parameter m will be set at m=4. Figure B.63 provides this frequency sweep over both the excitation frequencies of interest and the parameter γ_1.

Compared with the results of the local minimization of a single degree of freedom, the minimization of an area L does seem to yield only slightly fewer topologies which contain intermediate densities. The results are, however, a lot more defined, with the intermediate density regions consisting of rather clear members instead of seemingly random regions of material. For larger values of γ_1, the same vibration isolation principles can be found, where more mass is added to the centre of the domain, and the connection to the base contains little stiffness due to the connecting members being made up of intermediate densities. For higher frequencies, the main differences are found in the connecting structures, which seem to change

(a) $\gamma_1 = 0.90$, ω_{exc}=340Hz (b) $\gamma_1 = 0.95$, ω_{exc}=340Hz (c) $\gamma_1 = 0.99$, ω_{exc}=340Hz

(d) $\gamma_1 = 0.90$, ω_{exc}=880Hz (e) $\gamma_1 = 0.95$, ω_{exc}=880Hz (f) $\gamma_1 = 0.99$, ω_{exc}=880Hz

(g) $\gamma_1 = 0.90$, ω_{exc}=1377Hz (h) $\gamma_1 = 0.95$, ω_{exc}=1377Hz (i) $\gamma_1 = 0.99$, ω_{exc}=1377Hz

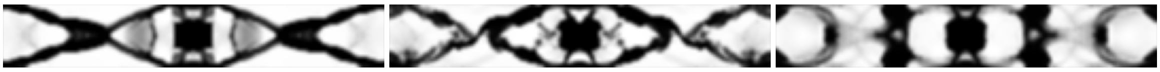

(j) $\gamma_1 = 0.90$, ω_{exc}=2947Hz (k) $\gamma_1 = 0.95$, ω_{exc}=2947Hz (l) $\gamma_1 = 0.99$, ω_{exc}=2947Hz

Figure B.63: The topologies found for a two-sided parameter sweep over both the parameter γ_1 and the excitation frequency ω_{exc} for the frequencies of interest defined in section B.1.2 showcasing their influence on local minimization of an area of interest L subjected to a base excitation including forced symmetry over the y-axis and the parameter values w=0 and m=4.

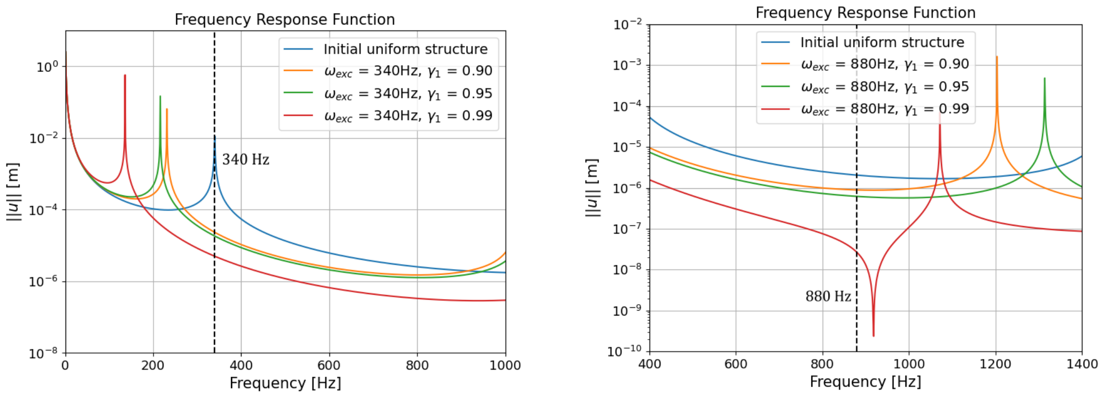

(a) ω_{exc}=340Hz (b) ω_{exc}=880Hz

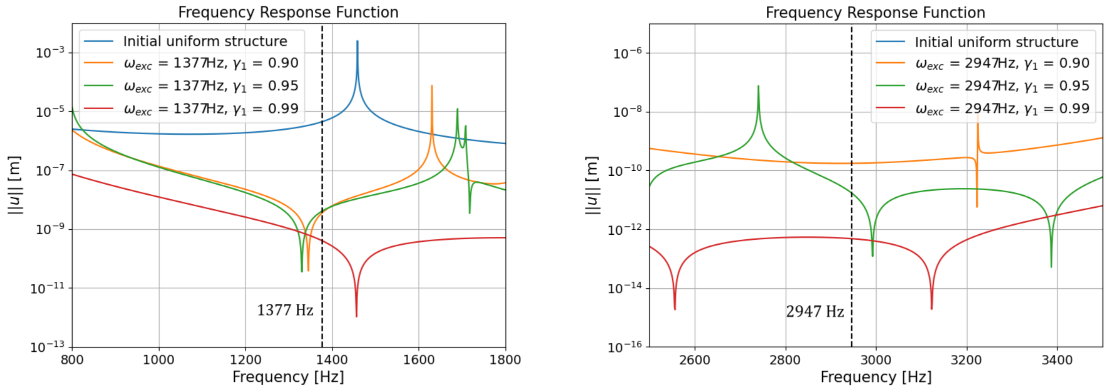

(c) ω_{exc}=1377Hz (d) ω_{exc}=2947Hz

Figure B.64: The undamped frequency response comparison of the resulting topologies given in figure B.63 and the initial uniform domain, showcasing the influence of the parameter γ_1 for each of the four respective excitation frequencies of interest ω_{exc} on local minimization of an area of interest L subjected to a base excitation including forced symmetry over the y-axis and the parameter values w=0 and m=4.

into structures with less stiffness. To assess the performance of these topologies, the undamped frequency response of the vertical degree of freedom of the mass node is provided in figure B.64.

It should be noted that these responses do not capture the full behaviour of the response now that an area of interest is considered. It was, however, shown for local minimization under a force excitation that the area of interest portrayed collective behaviour. For all responses, it seems that the resonances are moved far away from the excitation frequency. For higher frequencies, an anti-resonance is still present near the excitation frequency, but it does not necessarily seem like the optimizer is actively trying to place this anti-resonance near the excitation frequency.

B.5.3. Discussion on the local minimization subjected to a base excitation

In this section, the influence of the density-weighted norm objective function is examined for its behaviour considering local minimization subjected to a base excitation for the same subsets as for a force excitation: a single degree of freedom and an area of interest L. The density-weighted filter was again removed (w=0), but the parameter m showed different behaviour to the force excited case. Whilst the response measured at the point of interest did not display much difference, the second eigenfrequency ω_2 was moved further away from the excitation frequency for higher values of m. This behaviour diminished quickly however for larger m and as such this parameter value was set at m=4.

For a single degree of freedom, it was found that a large amount of intermediate densities were still present in the system. Only the lowest examined frequency of 340Hz did not portray this issue, and an increase in static compliance contribution did not solve this issue either. This is also different from the results found for the force excited case, where an increase in static compliance contribution was beneficial for suppressing intermediate densities. For an area of interest L, the results were much more defined, yet still contained intermediate densities. Both subsets did show minimized results, however, for all frequencies, with an increase in γ_1 also yielding an increase in frequency performance.

C

Material interpolation functions

In this appendix, the different material interpolation functions presented in section 3.5 will be examined. As was mentioned in this same section, there is no one 'best' interpolation function for every problem. Therefore, one can arbitrarily choose a material interpolation function, or a comparison can be made for a sample problem. For the parameter study concerning the density-weighted norm function, the latter is chosen.

To quantify which material interpolation scheme is the optimal choice for this problem, a measure can be used, which was introduced by Sigmund [47]. This measure can determine the amount of 'black- and whiteness' of a topology. In other words, a topology scores better if it contains fewer intermediate densities. For topology optimization considering dynamic excitations such as the frequency-dependent problem presented in section B.1.1, the occurrence of intermediate densities is undesired as these low-density areas might result in localized modes being formed as mentioned in section 4.5.6. This measure, which is called the measure of non-discreteness, is given in equation C.1.

$$M_{\text{nd}} = \frac{\sum_{e=1}^{n} 4x_e(1-x_e)}{n} \times 100\% \tag{C.1}$$

The used problems are the force excited global minimization problem in section B.1.1 and the base excited global minimization problem outlined in section B.2. Both of these problems are used in order to obtain a combination of interpolation functions which will be able to cover both problems. The excitation frequency is set at 429Hz, γ_1 at 0.99 for maximum frequency influence, w at 1 and m at 2. Using the naming conventions presented together with the different interpolation functions, the first results are given in figure C.1 and C.2, which show the same interpolation function combinations for the force excited case and base excited case respectively.

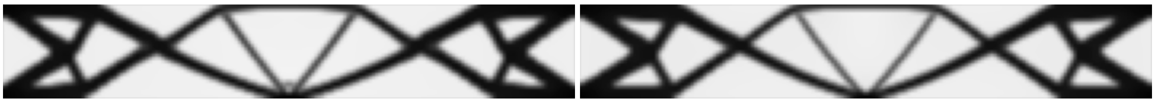

(a) Stiffness: Standard SIMP (equation 3.9),
Mass: Standard SIMP (equation 3.9), M_{nd}=42.37%

(b) Stiffness: SIMPlin (equation 3.14),
Mass: Standard SIMP (equation 3.9), M_{nd}=44.45%

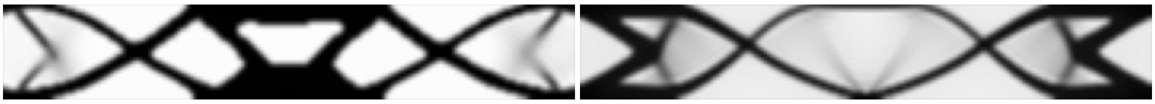

(c) Stiffness: PIS (equation 3.16),
Mass: Standard SIMP (equation 3.9), M_{nd}=29.20%

(d) Stiffness: RAMP (equation 3.15),
Mass: Standard SIMP (equation 3.9), M_{nd}=50.90%

Figure C.1: Resulting topologies of the defined force-excited global minimization problem at an excitation frequency of ω_{exc}=429Hz for a range of stiffness interpolation functions and constant mass interpolation function, together with their accompanying measure of non-discreteness value.

(a) Stiffness: Standard SIMP (equation 3.9),
Mass: Standard SIMP (equation 3.9), M_{nd}=33.10%

(b) Stiffness: SIMPlin (equation 3.14),
Mass: Standard SIMP (equation 3.9), M_{nd}=58.60%

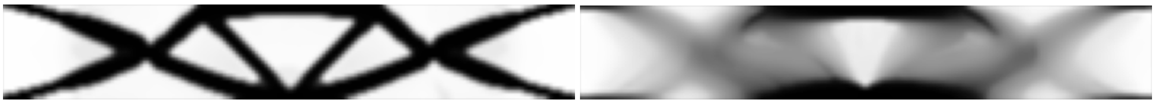

(c) Stiffness: PIS (equation 3.16),
Mass: Standard SIMP (equation 3.9), M_{nd}=26.84%

(d) Stiffness: RAMP (equation 3.15),
Mass: Standard SIMP (equation 3.9), M_{nd}=63.54%

Figure C.2: Resulting topologies of the defined base-excited global minimization problem at an excitation frequency of ω_{exc}=429Hz for a range of stiffness interpolation functions and constant mass interpolation function, together with their accompanying measure of non-discreteness value.

Comparing the results, it is found that not all interpolation functions will work for both excitation forms. While both RAMP and SIMPlin work for the excited case, they both contain many intermediate densities for the base excited case. Standard SIMP and PIS, on the other hand, work very well in both cases, but PIS does have a much lower non-discreteness score M_{nd}, which makes it the optimal interpolation function for this case. These examples, however, all have the same mass interpolation function, which is standard SIMP. Therefore, the functions Standard SIMP and PIS are examined again for stiffness interpolation, but this time, they are examined with linear interpolation for mass interpolation. These results are given in figure C.3.

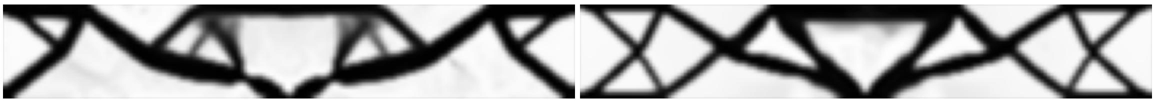

(a) Force excitation, M_{nd}=32.64%,
Stiffness: Standard SIMP (equation 3.9),
Density: Linear (equation 3.7)

(b) Force excitation, M_{nd}=34.57%,
Stiffness: PIS (equation 3.16),
Density: Linear (equation 3.7)

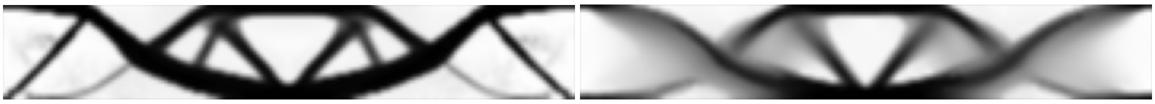

(c) Base excitation, M_{nd}=34.75%,
Stiffness: Standard SIMP (equation 3.9),
Density: Linear (equation 3.7)

(d) Base excitation, M_{nd}=35.10%,
Stiffness: PIS (equation 3.16),
Density: Linear (equation 3.7)

Figure C.3: Resulting topologies of the defined force-excited and base-excited global minimization problem at an excitation frequency of ω_{exc}=429Hz for Standard SIMP and PIS as stiffness interpolation functions and a linear mass interpolation function, together with their accompanying measure of non-discreteness value.

This result should lead to a less complex problem, as there is no extra penalization present in the mass interpolation. Without this penalization, however, it seems that the base excited case yields some extra intermediate densities. This shows that penalization for mass interpolation benefits optimization in this case. Comparing Standard SIMP and PIS again, however, now results in Standard SIMP being the optimal interpolation function. Comparing this result with the previous result of PIS in combination with Standard SIMP is still the optimal choice.

As removing complexity from the mass interpolation function does not seem beneficial, the mass interpolation method used by Montero et al. [37] can be checked. This is the conditional SIMP function from Du and Olhoff [46], which was given in equation 3.12, and the results are given in figure C.4.

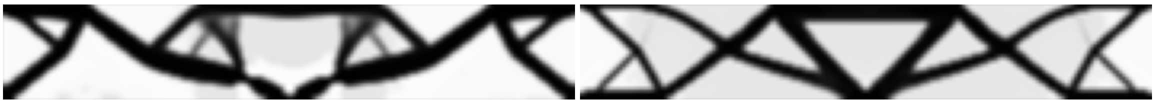

(a) Force excitation, M_{nd}=31.51%,
Stiffness: Standard SIMP (equation 3.9),
Density: Conditional SIMP (equation 3.12)

(b) Force excitation, M_{nd}=41.57%,
Stiffness: PIS (equation 3.16),
Density: Conditional SIMP (equation 3.12)

(c) Base excitation, M_{nd}=31.08%,
Stiffness: Standard SIMP (equation 3.9),
Density: Conditional SIMP (equation 3.12)

(d) Base excitation, M_{nd}=37.45%,
Stiffness: PIS (equation 3.16),
Density: Conditional SIMP (equation 3.12)

Figure C.4: Resulting topologies of the defined force-excited and base-excited global minimization problem at an excitation frequency of ω_{exc}=429Hz for Standard SIMP and PIS as stiffness interpolation functions and the Conditional SIMP mass interpolation function, together with their accompanying measure of non-discreteness value.

With this mass interpolation function, the Standard SIMP combination again seems to perform better in terms of M_{nd}, but the optimal choice for this problem does still appear to be the PIS/Standard SIMP combination for stiffness/mass interpolation. Whilst the different frequencies which are examined during the experiments might yield other optimal material interpolation functions, it is important to remain consistent, so a comparison for one of the frequencies of interest should be sufficient as most experiments will be performed at this lowest frequency.

D

Case study static displacement results

This appendix contains a visualization of the displacements of the obtained topologies from sections 7.3, 7.4 and 7.5 resulting from the applied static input force.

D.1. Step 3: Global minimization

In figure D.1 a visualization of the vertical displacements resulting from the applied input force for the topologies of figure 7.16 is given, confirming the working inverting function of the obtained mechanisms.

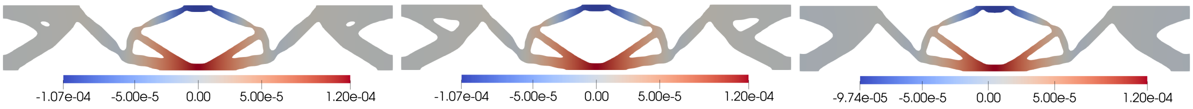

(a) ω_{exc}=363Hz, γ_1=0.90 (b) ω_{exc}=363Hz, γ_1=0.95 (c) ω_{exc}=363Hz, γ_1=0.99

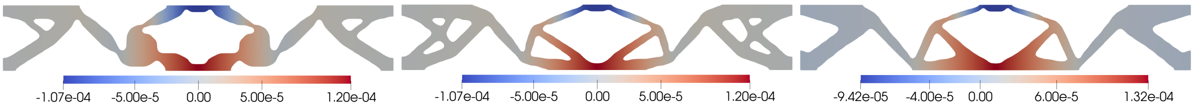

(d) ω_{exc}=471Hz, γ_1=0.90 (e) ω_{exc}=471Hz, γ_1=0.95 (f) ω_{exc}=471Hz, γ_1=0.99

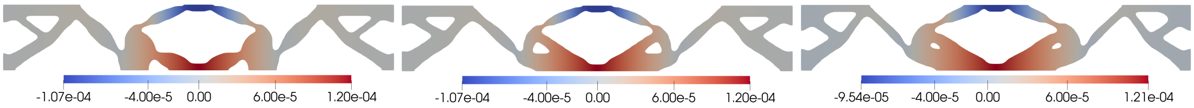

(g) ω_{exc}=1242Hz, γ_1=0.90 (h) ω_{exc}=1242Hz, γ_1=0.95 (i) ω_{exc}=1242Hz, γ_1=0.99

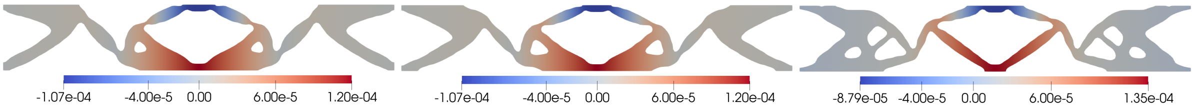

(j) ω_{exc}=1823Hz, γ_1=0.90 (k) ω_{exc}=1823Hz, γ_1=0.95 (l) ω_{exc}=1823Hz, γ_1=0.99

Figure D.1: A visualization done in Paraview of the vertical displacements resulting from the applied static input force for the topologies found for a two-sided parameter sweep over both the parameter γ_1 and the excitation frequency ω_{exc} for the frequencies of interest as given in figure 7.16.

D.2. Step 4: Local minimization of the mechanism area

In figure D.2 a visualization of the vertical displacements resulting from the applied input force for the topologies of figure 7.19 is given, confirming the working inverting function of the obtained mechanisms.

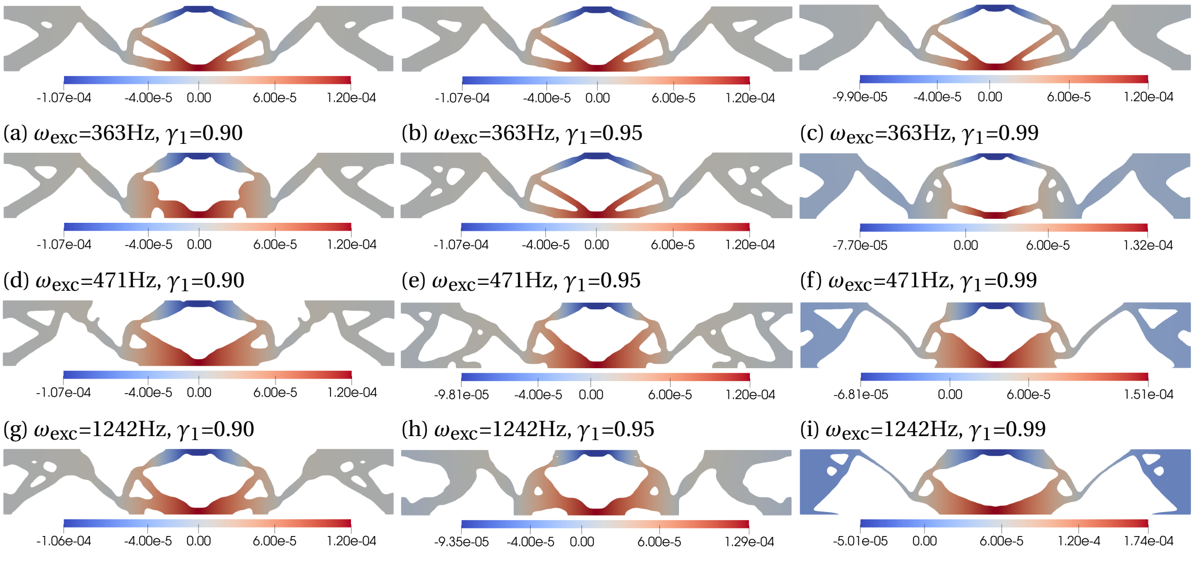

(a) ω_{exc}=363Hz, γ_1=0.90 (b) ω_{exc}=363Hz, γ_1=0.95 (c) ω_{exc}=363Hz, γ_1=0.99

(d) ω_{exc}=471Hz, γ_1=0.90 (e) ω_{exc}=471Hz, γ_1=0.95 (f) ω_{exc}=471Hz, γ_1=0.99

(g) ω_{exc}=1242Hz, γ_1=0.90 (h) ω_{exc}=1242Hz, γ_1=0.95 (i) ω_{exc}=1242Hz, γ_1=0.99

(j) ω_{exc}=1823Hz, γ_1=0.90 (k) ω_{exc}=1823Hz, γ_1=0.95 (l) ω_{exc}=1823Hz, γ_1=0.99

Figure D.2: A visualization done in Paraview of the vertical displacements resulting from the applied static input force for the topologies found for a two-sided parameter sweep over both the parameter γ_1 and the excitation frequency ω_{exc} for the frequencies of interest as given in figure 7.19.

D.3. Step 5: Local minimization of the input and output area

In figure D.3 a visualization of the vertical displacements resulting from the applied input force for the topologies of figure 7.22 is given, confirming the working inverting function of the obtained mechanisms except for the result of γ_1=0.99 at 1823Hz.

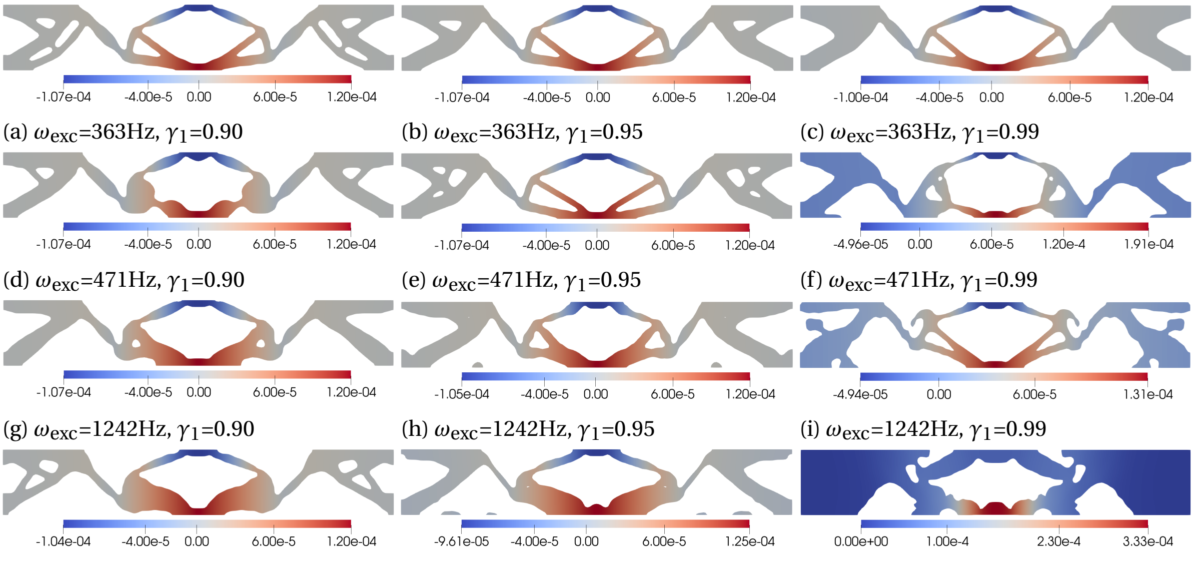

(a) ω_{exc}=363Hz, γ_1=0.90 (b) ω_{exc}=363Hz, γ_1=0.95 (c) ω_{exc}=363Hz, γ_1=0.99

(d) ω_{exc}=471Hz, γ_1=0.90 (e) ω_{exc}=471Hz, γ_1=0.95 (f) ω_{exc}=471Hz, γ_1=0.99

(g) ω_{exc}=1242Hz, γ_1=0.90 (h) ω_{exc}=1242Hz, γ_1=0.95 (i) ω_{exc}=1242Hz, γ_1=0.99

(j) ω_{exc}=1823Hz, γ_1=0.90 (k) ω_{exc}=1823Hz, γ_1=0.95 (l) ω_{exc}=1823Hz, γ_1=0.99

Figure D.3: A visualization done in Paraview of the vertical displacements resulting from the applied static input force for the topologies found for a two-sided parameter sweep over both the parameter γ_1 and the excitation frequency ω_{exc} for the frequencies of interest as given in figure 7.22.

E

pyMOTO

For the topology optimizations done in this thesis, the modular framework known as pyMOTO, which was developed by Arnoud Delissen and Stijn Koppen, is employed. This framework makes use of so-called 'Signals', which allow for the storage of data on both the variables and sensitivity information. These signals can then be routed through so-called 'Modules', which provide functionality and sensitivity formulations. This appendix will provide a simple example to understand the basic working principles, but for a more detailed explanation, the reader is referred to the original repository on GitHub (https://doi.org/10.5281/zenodo.10600313) [80].

A simple example module can be constructed to explain the working principle of pyMOTO. The chosen example is a module which constructs the Rayleigh damping matrix $\mathbf{C}(\mathbf{x})$ using the stiffness matrix $\mathbf{K}(\mathbf{x})$ and the mass matrix $\mathbf{M}(\mathbf{x})$. A visualization of this module is given in figure E.1.

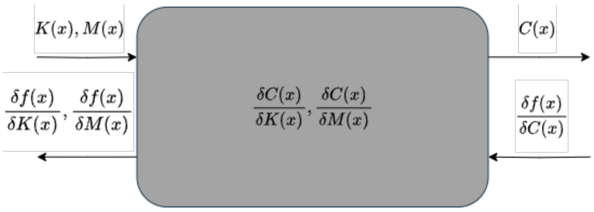

Figure E.1: A schematic of an example module which constructs the Rayleigh damping matrix, showing the variables and sensitivities entering and exiting this module.

The entries of this module comprise of the stiffness matrix $\mathbf{K}(\mathbf{x})$ and mass matrix $\mathbf{M}(\mathbf{x})$, which are then converted according to:

$$\mathbf{C}(\mathbf{x}) = \alpha\mathbf{M}(\mathbf{x}) + \beta\mathbf{K}(\mathbf{x}) \tag{E.1}$$

For a given final desired objective $f(\mathbf{x})$, the sensitivity with respect to the design variables $\frac{\delta f(\mathbf{x})}{\delta \mathbf{x}}$ is required. This is done in pyMOTO by applying the chain rule for each module, which means that for every module, only the sensitivity of the desired objective with respect to the input signals of the module is required. This allows for the order of each module to be changed without having to worry about the sensitivity calculations. The sensitivity derivation, which is then yielded, is given in equation E.2.

$$\begin{gathered}\frac{\delta f(\mathbf{x})}{\delta \mathbf{K}(\mathbf{x})} = \frac{\delta \mathbf{C}(\mathbf{x})}{\delta \mathbf{K}(\mathbf{x})}\frac{\delta f(\mathbf{x})}{\delta \mathbf{C}(\mathbf{x})} \\ \frac{\delta f(\mathbf{x})}{\delta \mathbf{M}(\mathbf{x})} = \frac{\delta \mathbf{C}(\mathbf{x})}{\delta \mathbf{M}(\mathbf{x})}\frac{\delta f(\mathbf{x})}{\delta \mathbf{C}(\mathbf{x})}\end{gathered} \tag{E.2}$$

The second term now present in equation E.2 is the sensitivity input of the module, which means that only $\frac{\delta \mathbf{C}(\mathbf{x})}{\delta \mathbf{K}(\mathbf{x})}$ and $\frac{\delta \mathbf{C}(\mathbf{x})}{\delta \mathbf{M}(\mathbf{x})}$ have to be implemented inside the module.

Given in figure E.2 is an example of the implementation of a static compliance minimization (section 3.2) using the pyMOTO framework. Each grey block represents a module, and its given name aligns with the naming conventions present in the pyMOTO framework. The notation 'pym.' represents the pyMOTO package, which is commonly imported as 'pym' in a Python environment. The notations on each connecting arrow represent each signal which enters or exits a module.

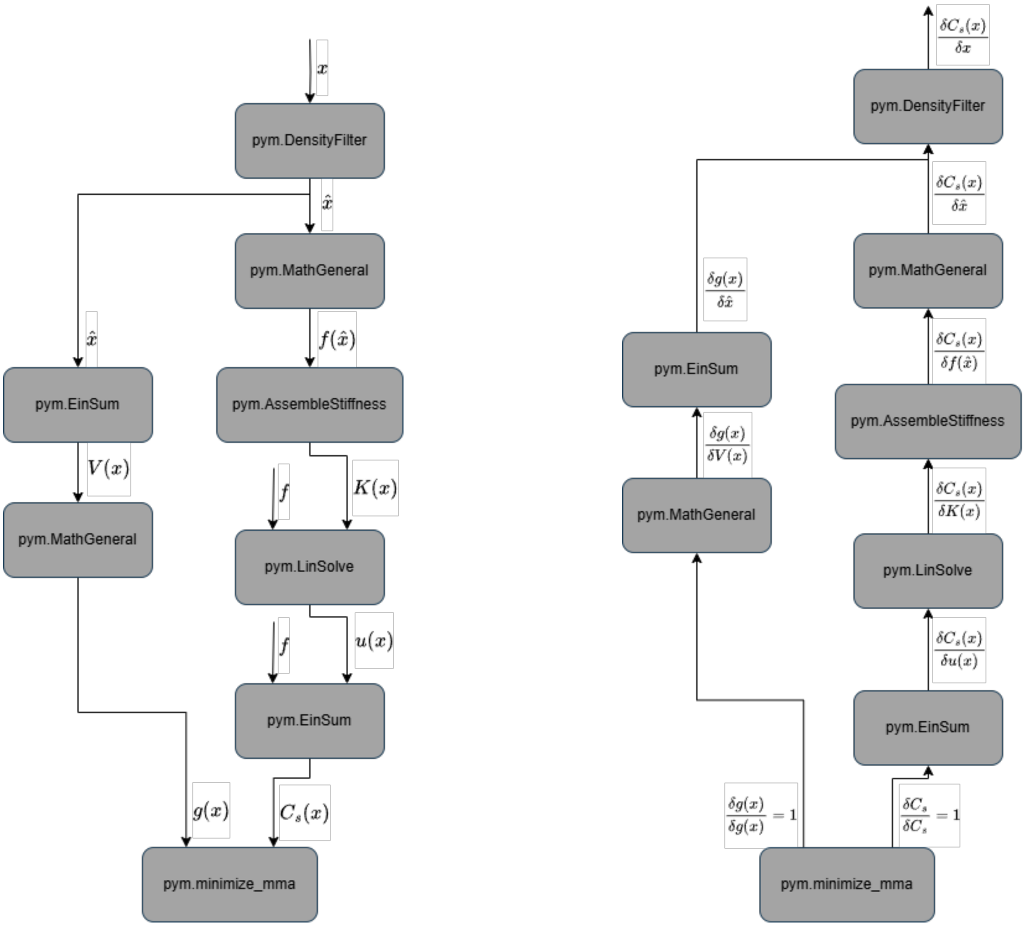

(a) Forwards (b) Backwards

Figure E.2: An example schematic of a static compliance minimization showing both the forward calculation from the design variables to the static compliance and the backward calculation of the sensitivity of the static compliance with respect to the design variables.

Figure E.2a provides the forward calculation of the static compliance. The final result is the desired value of the static compliance, which enters the MMA module together with the volume constraint. The sensitivities of these values with respect to the design variables can then be calculated using backpropagation, an image of which is provided in figure E.2b. This is done in the same network, only backwards. The final value is seeded with a value of 1, after which the modules are executed in reverse order. This is possible due to the use of the chain rule, as mentioned earlier.

Bibliography

[1] L.L. Howell. *Compliant Mechanisms.* A Wiley-Interscience publication. Wiley, 2001.

[2] R. Raaijmakers. Besi zoekt snelheidslimiet pakken en plaatsen op. *Mechatronica Nieuws*, pages 26–31, 2007.

[3] N. Lobontiu and E. Garcia. Analytical model of displacement amplification and stiffness optimization for a class of flexure-based compliant mechanisms. *Computers and Structures*, 81:2797–2810, 12 2003.

[4] H. Du, G.K. Lau, M.K. Lim, and J. Qui. Topological optimization of mechanical amplifiers for piezoelectric actuators under dynamic motion. *Smart Materials and Structures*, 9:788–800, 12 2000.

[5] S. Shuib, M.I.Z. Ridzwan, and A.H. Kadarman. Methodology of compliant mechanisms and its current developments in applications: A review. *American Journal of Applied Sciences*, 4:160–167, 3 2007.

[6] C.H. Liu, C.H. Chiu, T.L. Chen, T.Y. Pai, Y. Chen, and M.C. Hsu. A soft robotic gripper module with 3d printed compliant fingers for grasping fruits. pages 736–741. IEEE, 7 2018.

[7] S.A. Zirbel and S. Alisa. Compliant mechanisms for deployable space systems, 2014.

[8] S.R. Park and S.H. Yang. A mathematical approach for analyzing ultra precision positioning system with compliant mechanism. *Journal of Materials Processing Technology*, 164-165:1584–1589, 5 2005.

[9] R. Le Letty, F. Claeyssen, N. Lhermet, and P. Bouchilloux. New amplified piezoelectric actuator for precision positioning and active damping. pages 496–504, 6 1997.

[10] A.A. Tanksale and P.S. Gandhi. On novel dynamic displacement amplification using compliant mechanisms, 2018.

[11] N. Olgac and N. Jalili. Modal analysis of flexible beams with delayed resonator vibration absorber: theory and experiments. *Journal of Sound and Vibration*, 218:307–331, 11 1998.

[12] D. Farhadi MacHekposhti, J.L. Herder, G. Semon, and N. Tolou. A compliant micro frequency quadrupler transmission utilizing singularity. *Journal of Microelectromechanical Systems*, 27:506–512, 6 2018.

[13] G. Hao. A framework of designing compliant mechanisms with nonlinear stiffness characteristics. *Microsystem Technologies*, 24:1795–1802, 4 2018.

[14] S.M. Lyon, P.A. Erickson, M.S. Evans, and L.L. Howell. Prediction of the first modal frequency of compliant mechanisms using the pseudo-rigid-body model. *Journal of Mechanical Design*, 121:309–313, 6 1999.

[15] Vedant and J.T. Allison. Pseudo-rigid body dynamic modeling of compliant members for design. American Society of Mechanical Engineers, 8 2019.

[16] W. Wang and Y. Yu. Analysis of frequency characteristics of compliant mechanisms. *Frontiers of Mechanical Engineering in China*, 2:267–271, 7 2007.

[17] V. Platl and L. Zentner. An analytical method for calculating the natural frequencies of spatial compliant mechanisms. *Mechanism and Machine Theory*, 175, 9 2022.

[18] F.J. Darsivan, W. Martono, and W.F. Faris. Active engine mounting control algorithm using neural network. *Shock and Vibration*, 16:417–437, 2009.

[19] T. Tantanawat, Z. Li, and S. Kota. Application of compliant mechanisms to active vibration isolation systems. pages 1165–1172. ASMEDC, 1 2004.

[20] V. van der Wijk, J.L. Herder, and B. Demeulenaere. Comparison of various dynamic balancing principles regarding additional mass and additional inertia. *Journal of Mechanisms and Robotics*, 1:1–9, 11 2009.

[21] H. Hilpert. Weight balancing of precision mechanical instruments. *Journal of Mechanisms*, 3:289–302, 12 1968.

[22] VirtualLabs. Dynamic vibration absorber. `https://mdmv-nitk.vlabs.ac.in/exp/exp-dynamic-vibration-absorber-nitk/theory.html`, 2024. Accessed: 2024-06-07.

[23] I.S. Kochev. General theory of complete shaking moment balancing of planar linkages: a critical review. *Mechanism and Machine Theory*, 35:1501–1514, 11 2000.

[24] V. van der Wijk. Methodology for analysis and synthesis of inherently force and moment-balanced mechanisms: theory and applications, 4 2014.

[25] S.L. Weeke, N. Tolou, G. Semon, and J.L. Herder. A fully compliant force balanced oscillator, 2016.

[26] J.A. Gallego and J.L. Herder. Synthesis methods in compliant mechanisms: an overview, 2009.

[27] C.J. Kim, S. Kota, and Y.M. Moon. An instant center approach toward the conceptual design of compliant mechanisms. *Journal of Mechanical Design, Transactions of the ASME*, 128:542–550, 5 2006.

[28] J. Hopkins. *Design of parallel flexure systems via freedom and constraint topologies (FACT)*. PhD thesis, Massachusetts Institute of Technology, 2007.

[29] J.L. Herder. ME46115 compliant mechanisms. 2020.

[30] M.P. Bendsøe and N. Kikuchi. Generating optimal topologies in structural design using a homogenization method, 1988.

[31] M.P. Bendsøe and O. Sigmund. *Topology Optimization - Theory, Methods and Applications*. Springer Berlin Heidelberg, 2004.

[32] J. Keur. Density and level-set based topology optimization for structural vibration problems: A comparative study, 2022.

[33] M.P. Bendsøe. Optimal shape design as a material distribution problem. *Structural Optimization*, 1:193–202, 01 1989.

[34] M. Langelaar. ME46060 engineering optimization: Concepts and applications. 2021.

[35] S. Nishiwaki, M.I. Frecker, S. Min, and N. Kikuchi. Topology optimization of compliant mechanisms using the homogenization method, 1998.

[36] Nishiwaki S., Saitou K., Min S., and Kikuchi N. Topological design considering flexibility under periodic loads. *Structural and Multidisciplinary Optimization*, 19:4–16, 3 2000.

[37] D.S. Montero, O.M. Silva, and E.L. Cardoso. Topology optimization for harmonic vibration problems using a density-weighted norm objective function. *Structural and Multidisciplinary Optimization*, 62:3301–3327, 12 2020.

[38] A.R. Díaz and O. Sigmund. Checkerboard patterns in layout optimization. *Structural Optimization*, 10:40–45, 8 1995.

[39] R.B. Haber, C.S. Jog, and M.P. Bendsøe. A new approach to variable-topology shape design using a constraint on perimeter. *Structural Optimization*, 11:1–12, 2 1996.

[40] O. Sigmund and J. Petersson. Numerical instabilities in topology optimization: A survey on procedures dealing with checkerboards, mesh-dependencies and local minima. *Structural Optimization*, 16:68–75, 8 1998.

[41] W.K. Pratt. *Digital Image Processing*. Wiley, 1991.

[42] T.E. Bruns and D.A. Tortorelli. Topology optimization of non-linear elastic structures and compliant mechanisms. *Computer Methods in Applied Mechanics and Engineering*, 190:3443–3459, 3 2001.

[43] G.I.N Rozvany, M. Zhou, and T. Birker. Structure optimization generalized shape optimization without homogenization, 1992.

[44] N.L. Pedersen. Maximization of eigenvalues using topology optimization. *Structural and Multidisciplinary Optimization*, 20:2–11, 8 2000.

[45] D. Tcherniak. Topology optimization of resonating structures using simp method. *International Journal for Numerical Methods in Engineering*, 54:1605–1622, 8 2002.

[46] J. Du and N. Olhoff. Topological design of freely vibrating continuum structures for maximum values of simple and multiple eigenfrequencies and frequency gaps. *Structural and Multidisciplinary Optimization*, 34:91–110, 2007.

[47] O. Sigmund. Morphology-based black and white filters for topology optimization. *Structural and Multidisciplinary Optimization*, 33:401–424, 4 2007.

[48] J. Zhu, W. Zhang, and P. Beckers. Integrated layout design of multi-component system. *International Journal for Numerical Methods in Engineering*, 78:631–651, 5 2009.

[49] M. Stolpe and K. Svanberg. An alternative interpolation scheme for minimum compliance topology optimization, 2001.

[50] K. Svanberg. The method of moving asymptotes—a new method for structural optimization. *International Journal for Numerical Methods in Engineering*, 24:359–373, 2 1987.

[51] F. Chen, W. Xu, H. Zhang, Y. Wang, J. Cao, M.Y. Wang, H. Ren, J. Zhu, and Y.F. Zhang. Topology optimized design, fabrication, and characterization of a soft cable-driven gripper. *IEEE Robotics and Automation Letters*, 3:2463–2470, 7 2018.

[52] U.D Larsen, O. Signund, and S. Bouwsta. Design and fabrication of compliant micromechanisms and structures with negative poisson's ratio. *Journal of Microelectromechanical Systems*, 6:99–106, 6 1997.

[53] O. Sigmund. On the design of compliant mechanisms using topology optimization. *Mechanics of Structures and Machines*, 25:493–524, 1997.

[54] S. Koppen. Topology optimization of compliant mechanisms with multiple degrees of freedom. 11 2022.

[55] L. Cao, A. Dolovich, and W.J. Zhang. On understanding of design problem formulation for compliant mechanisms through topology optimization. *Mechanical Sciences*, 4:357–369, 2013.

[56] B.S. Kang, G.J. Park, and J.S. Arora. A review of optimization of structures subjected to transient loads. *Structural and Multidisciplinary Optimization*, 31:81–95, 2 2006.

[57] X. Zhang and Z. Kang. Dynamic topology optimization of piezoelectric structures with active control for reducing transient response. *Computer Methods in Applied Mechanics and Engineering*, 281:200–219, 11 2014.

[58] R. Behrou and J.K. Guest. Topology optimization for transient response of structures subjected to dynamic loads. American Institute of Aeronautics and Astronautics Inc, AIAA, 2017.

[59] Z.D. Ma, N. Kikuchi, and I. Hagiwara. Structural topology and shape optimization for a frequency response problem, 1993.

[60] Henrik Sönnerlind. Damping in structural dynamics: Theory and sources. `https://www.comsol.com/blogs/damping-in-structural-dynamics-theory-and-sources/`, 2019. Accessed: 2024-05-08.

[61] J.F. Hall. Problems encountered from the use (or misuse) of rayleigh damping, 2007.

[62] R.D. Cook, D.S. Malkus, M.E. Plesha, and R.J. Witt. *Concepts and Applications of FInite Element Analysis - 4th edition.* 10 2001.

[63] A. Zerwer, G. Cascante, and J. Hutchinson. Parameter estimation in finite element simulations of rayleigh waves. *Journal of Geotechnical and Geoenvironmental Engineering*, 128:250–261, 3 2002.

[64] O.M. Silva, M.M. Neves, and A. Lenzi. On the use of active and reactive input power in topology optimization of one-material structures considering steady-state forced vibration problems. *Journal of Sound and Vibration*, 464, 1 2020.

[65] R.M. Schmidt, G. Schitter, A. Rankers, and J. van Eijk. *The Design of High Performance Mechatronics*. Delft University Press, 3rd edition, 2014.

[66] A.R. Díaz and N. Kikuchi. Solutions to shape and topology eigenvalue optimization problems using a homogenization method. *International Journal for Numerical Methods in Engineering*, 35:1487–1502, 10 1992.

[67] J. Du and N. Olhoff. Topology optimization of continuum structures with respect to simple and multiple eigenfrequencies. *6 th World Congresses of Structural and Multidisciplinary Optimization*, 2005.

[68] M. Huigsloot. Topology optimization of constrained eigenfrequencies, 2018.

[69] N. Olhoff and J. Du. Topological design of continuum structures subjected to forced vibration, 2005.

[70] M.P. Bendsøe and N. Olhoff. A method of design against vibration resonance of beams and shafts. *Optimal Control Applications and Methods*, 6:191–200, 7 1985.

[71] Z.D. Ma, H.C. Cheng, and N. Kikuchi. Structural design for obtaining desired eigenfrequencies by using the topology and shape optimization method, 1994.

[72] Z.D. Ma, N. Kikuchi, and H.C. Cheng. Topological design for vibrating structures, 1995.

[73] J. Lee, V. Balakrishnan, C. Koh, and D. Jiao. From $o(k^2 n)$ to $o(n)$: A fast complex-valued eigenvalue solver for large-scale on-chip interconnect analysis. *2009 IEEE MTT-S International Microwave Symposium Digest*, pages 181–184, 6 2009.

[74] H. Liu, W. Zhang, and T. Gao. A comparative study of dynamic analysis methods for structural topology optimization under harmonic force excitations. *Structural and Multidisciplinary Optimization*, 51:1321–1333, 6 2015.

[75] C.S. Jog. Topology design of structures subjected to periodic loading. *Journal of Sound and Vibration*, 253:687–709, 6 2002.

[76] O.M. Silva, M.M. Neves, and A. Lenzi. A critical analysis of using the dynamic compliance as objective function in topology optimization of one-material structures considering steady-state forced vibration problems. *Journal of Sound and Vibration*, 444:1–20, 3 2019.

[77] V. Vijayan, M. Udayakumar, and K. Chellamuthu. Passive vibration isolation by compliant mechanism using topology optimization, 2014.

[78] S. Allahdadian, B. Boroomand, and A.R. Barekatein. Towards optimal design of bracing system of multi-story structures under harmonic base excitation through a topology optimization scheme. *Finite Elements in Analysis and Design*, 61:60–74, 11 2012.

[79] J.H. Zhu, F. He, T. Liu, W.H. Zhang, Q. Liu, and C. Yang. Structural topology optimization under harmonic base acceleration excitations. *Structural and Multidisciplinary Optimization*, 57:1061–1078, 3 2017.

[80] A. Delissen. aatmdelissen/pymoto: v1.3.0 (v1.3.0). zenodo, 2024.

[81] T. Liu, J.H. Zhu, W.H. Zhang, H. Zhao, J. Kong, and T. Gao. Integrated layout and topology optimization design of multi-component systems under harmonic base acceleration excitations. *Structural and Multidisciplinary Optimization*, 59:1053–1073, 4 2019.

[82] F. He, H. Liao, J. Zhu, and Z. Fuo. Structural topology optimization under stationary random base acceleration excitations. *Chinese Journal of Aeronautics*, 32:1416–1427, 6 2019.